CHEMISTRY OF *N*-HETEROCYCLIC CARBENES WITH SELECTED FLUORIDE COMPOUNDS

Blaž Ališ

Doctoral Dissertation
Jožef Stefan International Postgraduate School
Ljubljana, Slovenia

Supervisor: Asst. Prof. Dr. Gašper Tavčar, JSIPS and Jožef Stefan Institute, Ljubljana, Slovenia

Evaluation Board:
Prof. Dr. Boris Žemva, Chair, IPS and Jožef Stefan Institute, Ljubljana, Slovenia
Prof. Dr. Janez Plavec, Member, National Institute of Chemistry, Ljubljana, Slovenia
Asst. Prof. Dr. Uroš Grošelj, Member, Faculty of Chemistry and Chemical Technology, University of Ljubljana, Ljubljana, Slovenia

MEDNARODNA PODIPLOMSKA ŠOLA JOŽEFA STEFANA
JOŽEF STEFAN INTERNATIONAL POSTGRADUATE SCHOOL



Blaž Alič

CHEMISTRY OF *N*-HETEROCYCLIC CARBENES WITH SELECTED FLUORIDE COMPOUNDS

Doctoral Dissertation

KEMIJA *N*-HETEROCIKLIČNIH KARBENOV Z IZBRANIMI FLUORIDI

Doktorska disertacija

Supervisor: Asst. Prof. Dr. Gašper Tavčar

Ljubljana, Slovenia, October 2017

"The interpretation of facts in a certain way stimulates other scientists' thoughts. The incorrectness and weakness of a theory cause other minds to formulate the problems more exactly and in this way scientific progress is made." (Robert Bárány)

Acknowledgments

I wish to thank my supervisor Asst. Prof. Dr. Gašper Tavčar for a rich and intense educational process that helped me become a better chemist.

I would also like to thank everyone else that participated in this process in any way, from small contributions that made me laugh to helping me with data interpretation. Thank you all for enabling me to be where I am today.

Abstract

This thesis describes the chemistry of persistent *N*-heterocyclic carbene (NHC), namely, 1,3-bis(2,6-diisopropylphenyl)-1,3-dihydro-2*H*-imidazol-2-ylidene (L^{Dipp}) and its fluoride salt 1,3-bis(2,6-diisopropylphenyl)imidazolium fluoride, [(L^{Dipp})H][F], with different metalloid fluoride substrates. It consists of three parts summarizing the results published in three scientific papers. The focus of the research was the reactivity of group 14 and 15 metalloid fluorides, namely, SiF_4, GeF_4 and SbF_3, with [(L^{Dipp})H][F] and (L^{Dipp}).

In the first part we take a look at how NHCs react with antimony(III) fluoride, the problems that arose from this system and how we solved and explained all the unexpected phenomena of the reaction system. We managed to explain the reaction mechanism and behaviour of this system in the solution and in the solid state together with the characterization of the synthesized products with spectroscopic and chemical analyses.

During the research work, we found a need for a suitable fluoride donor that would be based on a persistent L^{Dipp} NHC. By reacting L^{Dipp} NHC with various HF sources, we managed to obtain pure, anhydrous imidazolium fluoride [(L^{Dipp})H][F] that served us as a good reagent. The path that led us to the isolation of the imidazolium fluoride also produced analogous imidazolium poly(hydrogen fluoride) salts that were all characterized with spectroscopic and chemical analyses.

In the last part we explored the reactivity of imidazolium fluoride with SiF_4 and GeF_4 compounds and managed to obtain discrete trigonal bipyramidal SiF_5^- and GeF_5^- anions, respectively. Trigonal bipyramidal geometry is relatively rare compared to the octahedral geometry of anions. Additionally, we report the first ^{19}F NMR spectra of GeF_5^- and GeF_6^{2-} anions in organic solvents, namely acetonitrile. We conclude the thesis with a rich discussion on stability of trigonal bipyramidal *vs.* octahedral species along with explained disorder in the crystals structure that arises from either anion rotation or Berry pseudorotation mechanisms of the prepared anions.

Povzetek

Doktorska disertacija opisuje kemijo obstojnih *N*-heterocikličnih karbenov, in sicer 1,3-bis(2,6-diizopropilfenil)-1,3-dihidro-2*H*-imidazol-2-ilidena (L^{Dipp}) in njegove fluoridne soli, 1,3-bis(2,6-diizopropilfenil)imidazolijevega fluorida, $[(L^{Dipp})H][F]$, z različnimi fluoridnimi viri. Razdeljena je na tri dele, ki povzemajo delo, objavljeno v treh znanstvenih člankih. Poudarek teh raziskav je na reaktivnosti pol-kovinskih fluoridov, in sicer SiF_4, GeF_4 in SbF_3 z $[(L^{Dipp})H][F]$ in (L^{Dipp}).

Prvi del opisuje, kako NHC-ji reagirajo z antimonovim(III) fluoridom, težave, ki se pojavijo v reakcijskem sistemu, in kako smo rešili ter razložili vsa nepričakovana opažanja v tem sistemu. Uspešno smo razložili reakcijski mehanizem in reaktivnost v sistemu tako v raztopini kot v trdnem stanju. Dobljene produkte smo okarakterizirali s spektroskopskimi in kemijskimi analizami.

Med raziskovalnim delom se je izkazala potreba po dobrem donorju fluoridnega iona. Z reakcijo L^{Dipp} in različnimi viri HF smo sintetizirali čist, brezvoden imidazolijev fluorid $[(L^{Dipp})H][F]$, ki nam je služil kot dober reagent. Pot, ki nas je vodila do izolacije imidazolijevega fluorida, je v ustreznih molskih razmerjih (L^{Dipp}):HF vodila do priprave imidazolijevih polihidrogenfluoridnih anionov, ki so bili prav tako okarakterizirani s spektroskopskimi in kemijskimi analizami.

V zadnjem delu smo raziskali reaktivnost imidazolijevega fluorida $[(L^{Dipp})H][F]$ s spojinami SiF_4 in GeF_4 in izolirali diskretne trigonalno bipiramidalne SiF_5^- in GeF_5^- anione. Takšna geometrija anionov je relativno redka v primerjavi z oktaedrično geometrijo anionov. Objavili smo tudi prva ^{19}F NMR spektra GeF_5^- in GeF_6^{2-} anionov v organskih topilih, in sicer v acetonitrilu. Delo smo zaključili s primerjavo stabilnosti trigonalno bipiramidalnih proti oktaedričnim zvrstem skupaj z razlago nereda v kristalni strukturi kot posledico toge rotacije ali Barryjeve psevdorotacije pripravljenih anionov.

Contents

Acknowledgments **v**

Abstract **vii**

Povzetek **ix**

Contents **xi**

List of Figures **xiii**

Abbreviations **xv**

1 Introduction **1**
1.1 Carbenes – What are They and How They Came to Be? ... 2
1.1.1 What are carbenes? ... 2
1.1.2 Historic overview ... 3
1.2 Chemical Background of NHCs ... 4
1.2.1 Electron configuration on carbene carbon atom ... 4
1.2.2 *N*-heterocyclic carbenes (NHCs) ... 5
1.2.2.1 Persistent *vs.* non-persistent NHCs and Wanzlick equilibrium . 5
1.2.2.2 Synthesis and variability of persistent NHCs ... 6
1.2.2.3 Stabilization factors of NHCs ... 7
1.2.2.4 Synthesis of NHC→M (M = d- or p-block element) coordination compounds ... 7
1.2.2.5 Properties of NHC metal coordination compounds ... 10
1.2.3 Modes of NHC coordination – *n*NHC *vs. a*NHC ... 10
1.2.3.1 Characteristics of aNHCs ... 11
1.2.3.2 Effects on nNHC or "C2" *vs.* aNHC or "C4" coordination ... 11
1.2.4 General utility of NHCs ... 13
1.2.4.1 NHCs in d-block chemistry ... 13
1.2.4.2 NHCs in p-block chemistry ... 14
1.3 Importance of Fluoride Donors ... 15
1.3.1 Overview of selected tools for fluoride anion generation ... 15
1.3.1.1 HF as a fluoride source ... 15
1.3.1.2 Metal fluorides as fluoride sources ... 15
1.3.1.3 Fluoride sources based on sulphur-fluoride bond ... 16
1.3.1.4 Quarternary ammonium/phosphorous salts and fluoride sources based on fluoridosilicates and fluoridostanates ... 16
1.3.1.5 Novel imidazole and imidazoline based reagents ... 17

2 Aims and Hypothesis **19**
2.1 Aim ... 19

2.2 Hypothesis....20

3 Methodology and Tools 21
3.1 Handling of Air-Sensitive Chemistry....21
3.1.1 Schlenk line....21
3.1.2 Nickel vacuum line....22

4 Results and Discussion - Overview 25

5 Small Molecule Activation: SbF_3 Auto-Ionization Supported by Transfer and Mesoionic NHC Rearrangement 27

6 Reaction of *N*-Heterocyclic Carbene (NHC) with Different HF Sources and Ratios – a Free Fluoride Reagent Based on Imidazolium Fluoride 59

7 Discrete GeF_5^- Anion Structurally Characterized with a Readily Synthesized Imidazolium Based Naked Fluoride Reagent 77

8 Summary and Conclusions 99
8.1 Summary....99
8.2 Outlook....101
8.3 Final Remark....101

Bibliography 103
Journal Articles....103
Conference Paper....103

Biography 105

References 107

List of Figures

Figure 1.1: Types of carbenes. 2
Figure 1.2: First known NHC complexes. *[5] **[6] 3
Figure 1.3: Two distinct sets of carbenes based on the electronic situation on the carbon atom. 4
Figure 1.4: Difference in reactivity of triplet *vs.* singlet carbenes. 4
Figure 1.5: (a) a general representation of NHC formula; (b) first isolated persistent NHC. 5
Figure 1.6: Wanzlick equilibrium. 5
Figure 1.7: One of the synthesis procedures of persistent NHCs. 6
Figure 1.8: Examples of NHC structural diversity. 6
Figure 1.9: Electron situation on N-C-N moiety of NHCs. 7
Figure 1.10: Reaction of a free carbene with a metal substrate. 8
Figure 1.11: Reaction of imidazolium salt with a transition metal possessing a basic anion or a ligand. 8
Figure 1.12: Synthesis of NHC metal coordination compounds via carbene transfer reagent. 9
Figure 1.13: Synthesis of NHC metal coordination compounds with a transition metal substrate in the presence of a weak base. 9
Figure 1.14: Electron configuration of different carbenes in metal coordination compounds. Left Schrock (nucleophilic) carbene, centre NHC and right Fischer (electrophilic) carbene. 10
Figure 1.15: First example of »C4« or aNHC/MIC coordination on metal centre. 10
Figure 1.16: "Normal" carbene *vs.* "abnormal" carbene representation. 11
Figure 1.17: Mechanisms that lead to either normal "C2" or mesoionic "C4" coordination complex. 12
Figure 1.18: Synthesis of 2nd generation Grubbs catalyst. 13
Figure 1.19: Illustration of Frustrated Lewis Pair formation and small molecule activation. 14
Figure 1.20: HF based reagents. 15
Figure 1.21: Common metal fluorides used as fluoride sources. 15
Figure 1.22: Fluoride sources based on sulphur-fluoride bond. 16
Figure 1.23: Naked fluoride reagents and fluoride donors masked by a week Lewis acid. 17
Figure 1.24: Imidazole and imidazoline based reagents. 17
Figure 3.1: Standard Schlenk line assembly. 21
Figure 3.2: FEP reactor vessel assembly (picture by Dr. Z. Mazej). 22
Figure 3.3: Nickel-PTFE Vacuum line (picture by Dr. Z. Mazej). 23

Abbreviations

NHC	... *N*-heterocyclic carbene
caac	... cyclic alkyl amino carbene
BICAAC	... bicyclic alkyl amino carbene
acac	... acetylacetone
MIC	... mesoionic carbene
aNHC	... abnormal *N*-heterocyclic carbene
rNHC	... remote *N*-heterocyclic carbene
nNHC	... normal *N*-heterocyclic carbene
tmen	... *N,N,N′,N′*-tetramethylethane-1,2-diamine
Mes	... mesityl group
py	... pyridine
Dipp	... diisopropylphenyl group
aHF	... anhydrous hydrogen fluoride
TMAF	... tetramethyl ammonium fluoride
TBAF	... tetrabutyl ammonium fluoride
PTFE	... polytetrafluoridoethylene
FEP	... tetrafluoridopropylene-hexafluoridopropylene block copolymer
(L^{Dipp})	... 1,3-bis(2,6-diisopropylphenyl)imidazole-2-ylidene
[(L^{Dipp})H][F]	... 1,3-bis(2,6-diisopropylphenyl)imidazolium fluoride
NMR	... nuclear magnetic resonance
VSEPR	... valence shell electron pair repulsion
ax	... axial
eq	... equatorial

Chapter 1

Introduction

I would like to begin this thesis with a short paragraph of its structure and parts. The work begins with a description of the group of ligands called *N*-heterocyclic carbenes (NHCs). In the first pages, I cover several questions to understand the motives and justification for the research performed during my PhD studies. For example, I will try to explain: How carbenes came to be? How diverse is their family? What is their nature and chemical background? What kind of reactions are they participating in? Are they useful and how? The answer to the last question falls partly within our research since we found an elegant way to transform an NHC into a good naked fluoride reagent. Consequently, the end of the introduction chapter investigates the selected tools for fluoride anion generation. After covering the Aims, Hypothesis and Methodology sections, the core of this thesis is presented by the three scientific papers that represent the work performed in three and a half years on my road of becoming the author of this thesis. At the end I summarize the key findings and take a look onwards.

1.1 Carbenes – What are They and How They Came to Be?

1.1.1 What are carbenes?

Carbene molecules possess a neutral carbon moiety with a valence of two and two unshared electrons. The simplest of all carbene molecules would be the methylene molecule with a chemical formula H_2C:, but a whole range of substituted R_2C: molecules exist. Types of carbenes (Figure 1.1), based on the electron situation that the carbene carbon atom possesses, are:

- Simple carbenes (methylene (H_2C:), dichloromethylene (Cl_2C:))
- Electrophilic carbenes (Fischer carbenes)
- Nucleophilic carbenes (Schrock carbenes)
- *N*-heterocyclic carbenes (NHC or Arduengo carbenes)
- Remote and mesoionic *N*-Heterocyclic carbenes (MIC, 1,2,3-triazolylidenes, pyrazolinylidenes, others based on tetrazole, thiazole and isoxazole)
- Cyclic alkyl amino carbenes (caac or Bertrand carbenes)
- Anionic *N*-heterocyclic dicarbenes
- Bicyclic alkyl amino carbenes (BICAAC)

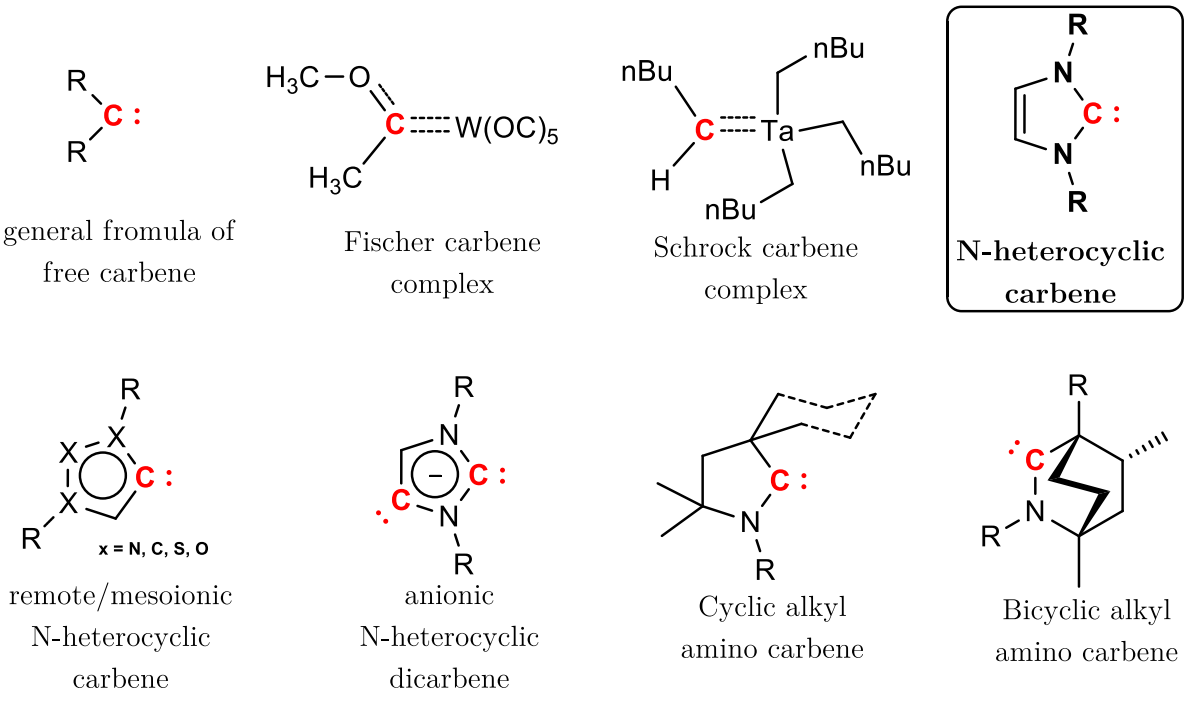


Figure 1.1: Types of carbenes.

1.1.2 Historic overview

Simple carbene chemistry dates back to the beginning of 1900 when methylene (H_2C:) was postulated as an intermediate species of a reaction mechanism [1, 2]. However, real carbene potential and its application value was first exemplified in 1954 when William von Eggers Doering published *in situ* formation of dichloromethylidene (Cl_2C:) generated from chloroform and its further addition to olefins [3].

In 1964, Fischer and Maasbol introduced the first electrophilic carbenes (Fischer carbenes) [4]. Four years after the Fischer's initial report of $[(CO)_5WC(OCH_3)(CH_3)]$ (Figure 1.1), in 1968, the onset of N-heterocyclic carbene chemistry comes to light. Ofele and Wanzlick & Schonherr published the synthesis of the first transition metal NHC complexes (Figure 1.2), but still were not able to synthesize a free stable NHC [5, 6]. The NHC species back then could only be formed *in-situ* from imidazolium salts and were considered as highly reactive intermediates, not stable in isolated form.

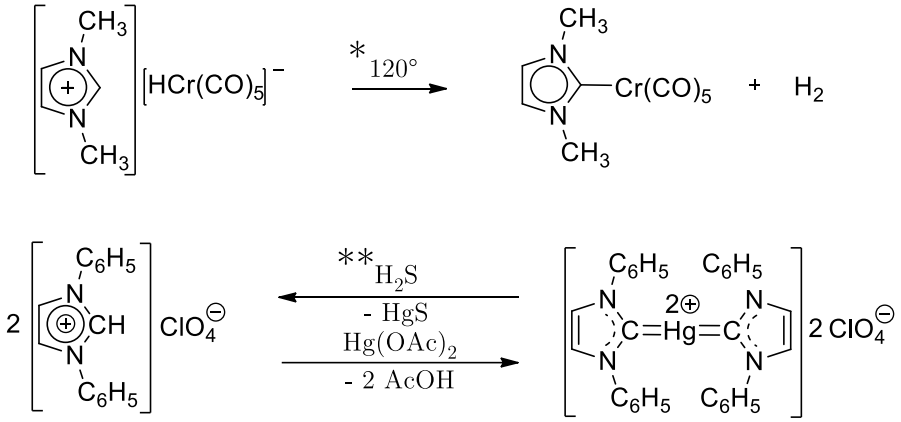


Figure 1.2: First known NHC complexes. *[5] **[6]

In 1974, a new type of organometallic complexes featuring C–M bond were introduced to the world of chemistry, called Schrock carbenes (Figure 1.1). This type of carbene, with nucleophilic reactivity, was named after Richard Royce Schrock who synthesized $[(Me_3CCH_2)_3Ta(CHMe_3)]$ [7].

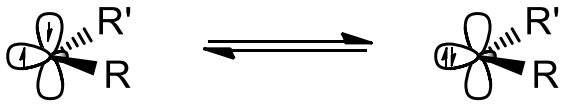
At the time, Schrock carbene complexes displayed reactivity not observed before and opened a new field in preparative organic chemistry. All types of carbenes at that time still shared a common disadvantage, as they were only metastable and could not be isolated in their free form. This final stability barrier was overcome in 1991, when the chemistry of NHCs and their transition metal complexes started to flourish with the introduction of the first solid, isolable, stable and "bottleable" NHC, synthesized by Arduengo *et al.* in laboratories at DuPont [8].

After their isolation, researchers began to study their electronic and steric properties. These properties, along with their reactivity, gave them applicative momentum as ligands for d-block and p-block complexes amongst others. Today they are an invaluable tool as *ligands for catalysts*, for small molecule activation, metal-free catalysts, precursors for fluorination reagents and much more (see Section 1.2.4 General utility of NHCs).

1.2 Chemical Background of NHCs

1.2.1 Electron configuration on carbene carbon atom

Two electrons on carbene carbon atom (Figure 1.3) that are not involved in bonding can be unpaired (triplet state) or spin-paired (singlet state) [9].



triplet singlet

Figure 1.3: Two distinct sets of carbenes based on the electronic situation on the carbon atom.

Two different electron configurations at carbene carbon atom exhibit different reactivity; while triplet carbenes usually react as biradicals in a two-step reaction mechanism [10, 11], the singlet carbenes participate in cheletropic reactions [3, 12]. Products obtained from such olefin insertion reactions are stereospecific in case of singlet carbene and steroselective in the case of triplet carbene insertion (Figure 1.4).

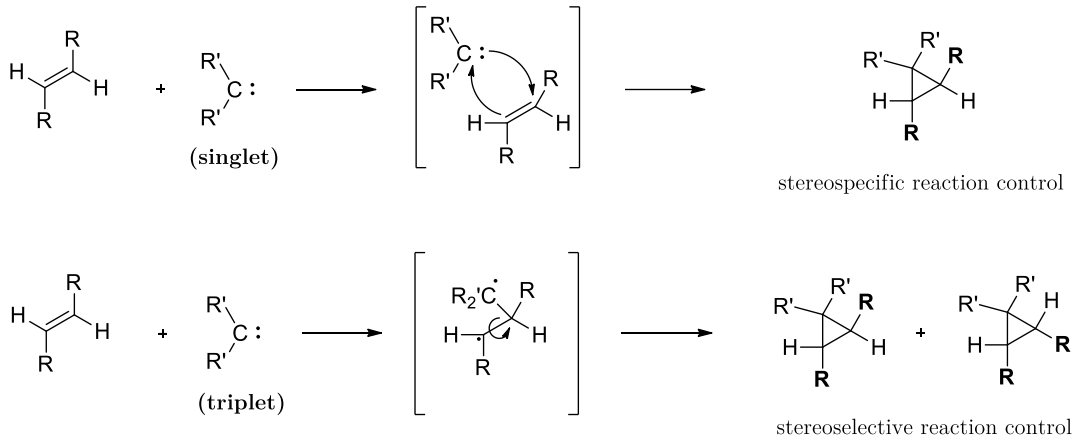


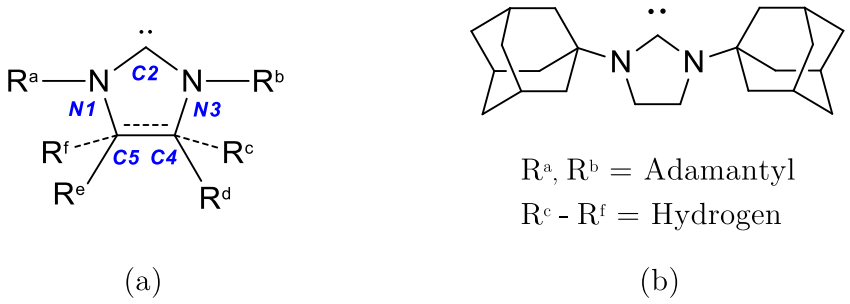
Figure 1.4: Difference in reactivity of triplet *vs.* singlet carbenes.

Based on the type of substituents around the carbon atom and stabilization factors present in either configuration, carbenes are highly reactive species prone to different side reactions such as dimerization that renders them unreactive [13].

Although stabilization of triplet carbenes remains a challenge to this day and no viable stabilization method has been discovered [9, 14], chemists made significant progress in stabilization of singlet carbenes [8]. While simple, Fischer and Schrock carbenes can only be formed *in-situ*, the same is not true for the other three groups of carbenes. With isolation of "bottleable" NHCs, scientists were also able to obtain persistent (stable) mesoionic carbenes [15] and cyclic alkyl amino carbenes [16].

1.2.2 *N*-heterocyclic carbenes (NHCs)

In this work, the *N*-heterocyclic carbenes (NHCs) are defined as heterocyclic species containing two nitrogen atoms within the cycle. Such broad definition allows for many diverse structures with different cycle sizes to a great number of possible substituents. A general representation of NHC is shown in Figure 1.5a with the first persistent carbene synthesized in 1991 in Figure 1.5b [8].



(a) (b)

Figure 1.5: (a) a general representation of NHC formula; (b) first isolated persistent NHC.

1.2.2.1 Persistent *vs.* non-persistent NHCs and Wanzlick equilibrium

Structural diversity of such compounds is enormous, allowing a variety of applications. The substituents on nitrogen atoms are the most important from the stability point of view. Persistent NHCs are stabilized kinetically by the large *N*-substituents which prevents the formation of its thermodynamically more favourable olefin dimerization product (Figure 1.6) [17].

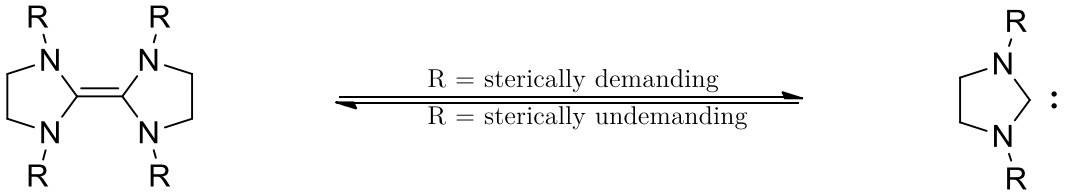


Figure 1.6: Wanzlick equilibrium.

A general rule of thumb is that if R substituents are small (e.g. H, Me, Et) the equilibrium is shifted strongly towards the formation of the thermodynamically stabilized dimer (left). NHCs with such *N*-substituents can only be formed *in-situ* because their half-life is generally short [18]. On the contrary, if larger groups are used (*e.g.* *t*-Bu, Ph, Mes, Ad, Dipp, etc.) the formation of the dimer is disfavoured to the kinetic stabilization of corresponding carbene moiety (right). These carbenes are called *persistent* NHCs. The equilibrium between the stable NHC moiety and its corresponding dimer was first proposed by H. W. Wanzlick in 1960 (called Wanzlick equilibrium) and has only been proven in 2000, exactly 40 years after its proposition [13, 19-22].

The imidazolium backbone carbon atoms (positions C4 and C5) can also be greatly manipulated. They can be either saturated or unsaturated [23]. Here we note that if the carbene backbone is unsaturated, then the carbene moiety is stabilized regardless of the *N*-substituent size [22, 24]. Furthermore, one can affect the carbenes properties to achieve the desired effect by changing the substituents on C4 and C5 positions of the imidazole cycle,

leading to the first air-stable carbene [25] or functionalized ligands for asymmetric synthesis [26-28].

1.2.2.2 Synthesis and variability of persistent NHCs

There are many possible routes for the synthesis of persistent NHCs [8, 23, 29, 30]. One of the simplest methods is the preparation of imidazolium chloride salts via 1,4-diazadienes, with subsequent deprotonation to form NHC (Figure 1.7).

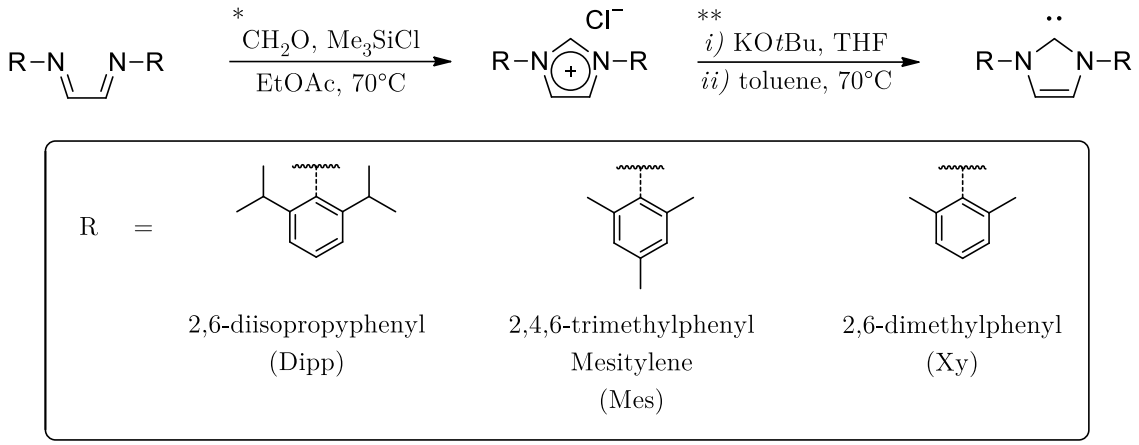


Figure 1.7: One of the synthesis procedures of persistent NHCs.

The R groups in Figure 1.7 are most widely used, as they are readily accessible, and the synthesis of their carbene precursors has been optimized [29]. However, synthesis procedures allow for a wide range of different alkyl or aryl substituents to be incorporated on the nitrogen atoms of the imidazolium ring that affect the carbene reactivity. In this sense we talk about functionalized NHCs with different properties for various applications depending on the chemists needs (Figure 1.8) [31].

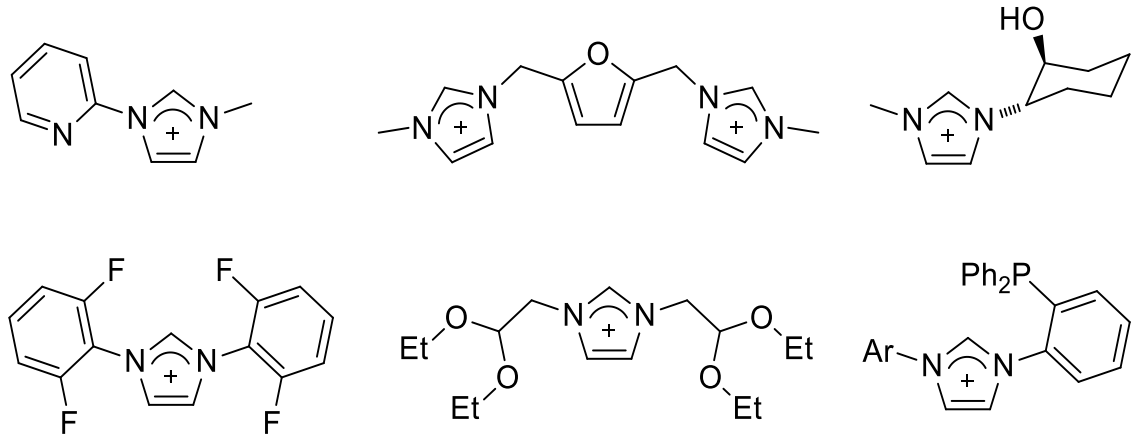


Figure 1.8: Examples of NHC structural diversity.

1.2.2.3 Stabilization factors of NHCs

As was previously mentioned, NHCs can be stable in their free form. Stability of a free NHC can be contributed to various factors. Steric hindrance of bulky groups on nitrogen atom certainly contributes to the stability, but the electronic situation in the N–C–N moiety appears to be essential (Figure 1.9) [32].

For simple R–C–R carbenes, with R being alkyl group, triplet state structures have energies lower than singlet carbenes, thus, in general, the triple state is the ground state. The energy differences between triplet ground and excited singlet state are generally low, ranging from 0, where both states exist in equilibrium, to about 15 kcal/mol [9]. Stabilization of a triplet ground state is not trivial and straightforward, but substituents that can donate electron density into empty p–orbital of carbene carbon atom by delocalization can stabilize the singlet state. The largest stabilizing effect for NHCs is attributed to carbene push-pull N–C–N electronic properties. Large electron withdrawing effect of electronegative nitrogen atoms on the σ–electrons of C–N single bond stabilizes the free σ–electron pair, whilst N–C back donating effect partially fills the empty p–orbital on the carbon atom (Figure 1.9) [32, 33].

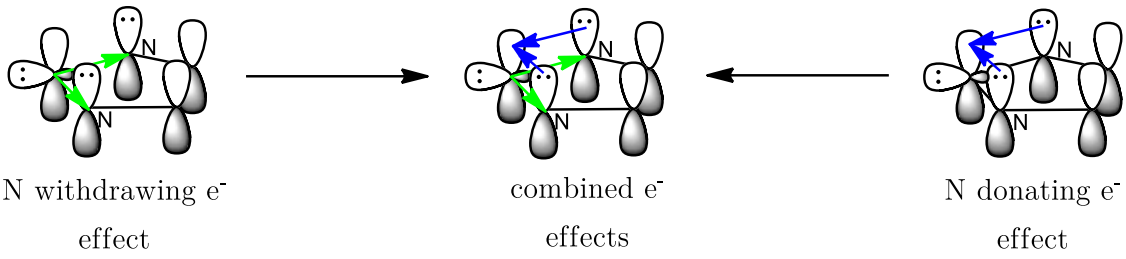


Figure 1.9: Electron situation on N-C-N moiety of NHCs.

Net result of those two combining electron effects is that NHCs have a singlet state stabilized to the extent that it becomes the ground state. Additionally, it gives NHC a very large singlet-triplet gap, which is usually larger than 65 kcal/mol, making their nature nucleophilic rather than radical [34].

1.2.2.4 Synthesis of NHC→M (M = d- or p-block element) coordination compounds

Synthesis of NHC-metal complexes can be achieved by several different methods. The universal and generally applied are four of them:

- Reaction of free carbene with a metal substrate.
- Reaction of imidazolium salt with a transition metal possessing a basic anion or a ligand [35-39].
- Via carbene transfer reagent [40].
- Reaction of imidazolium salt with a transition metal salt in the presence of a weak base [41-49].

1.2.2.4.1 Reaction of free carbene with a metal substrate

This is a simple reaction where NHC as a strong nucleophile coordinates to the metal compound or displaces some other weakly coordinated ligand (Figure 1.10).

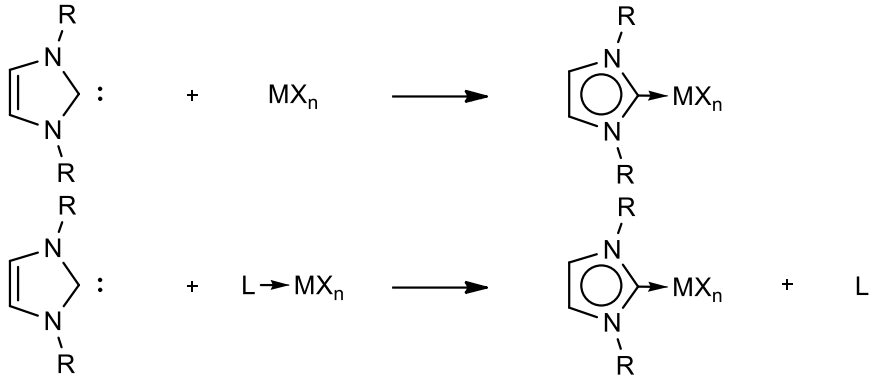


Figure 1.10: Reaction of a free carbene with a metal substrate.

The possibilities for this synthetic route are broad and the choice of coordination compounds as a starting material for this method is far greater than for any other. The problem is narrowed down to solubility of either NHC or metal precursor and the tolerance of functional groups towards the reagents used.

1.2.2.4.2 Reaction of imidazolium salt with a transition metal possessing a basic anion or a ligand

Drawback of the free carbene ligand is its sensitivity to oxygen and water, so it must be handled under inert conditions. This limitation is somewhat reduced if precursor imidazolium salts are used to form carbene *in situ* in the reaction with transition metal complexes with basic anion or ligand, including acac, chlorate (VII), acetoxy or alkoxy groups. Such reactions are usually not sensitive to water and oxygen and are carried out under heating or reflux (Figure 1.11).

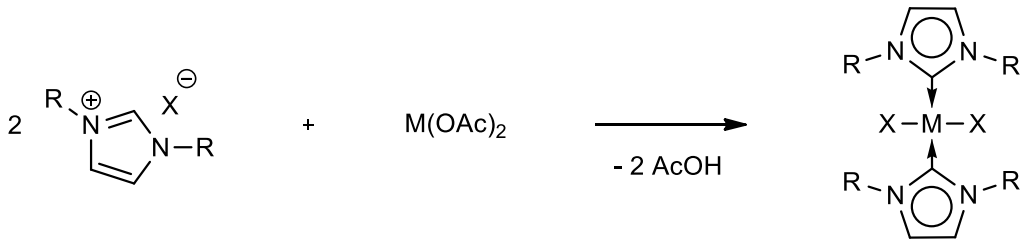


Figure 1.11: Reaction of imidazolium salt with a transition metal possessing a basic anion or a ligand.

1.2.2.4.3 Via carbene transfer reagent

The first well characterized Ag(I)–NHC complexes were synthesized by Arduengo et al. in reaction between free carbene and silver(I) salts, but the method got its reputation only after I. J. B. Lin *et al.* reported the formation of Ag(I)–NHC complexes by employing Ag_2O in the reaction with benzimidazolium salt in CH_2Cl_2 under ambient conditions. Ag(I)–NHC complexes have become the most studied carbene transfer reagents due to their simple preparation as well as being sources of other M–NHC complexes through transmetalation as a consequence of weakly coordinated Ag(I) atom which can be easily replaced by another metal of choice (Figure 1.12).

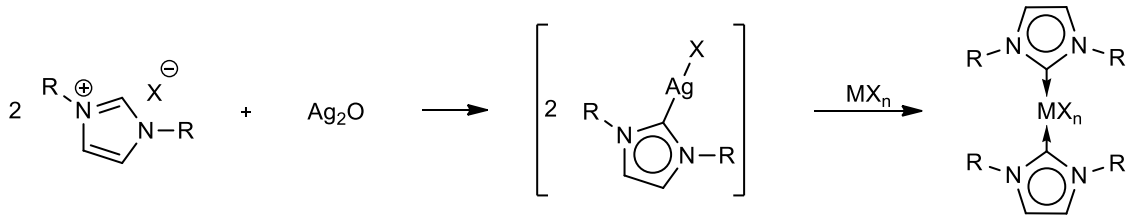


Figure 1.12: Synthesis of NHC metal coordination compounds via carbene transfer reagent.

1.2.2.4.4 Reaction of imidazolium salt with a transition metal salt in the presence of a weak base

In cases when transition metal complexes do not contain basic ligands, an additional base can be applied (Figure 1.13). That can be beneficial, for example in certain coupling reactions when an additional weak base is required to promote the reaction. The idea is that the NHC–M catalyst (see 1.2.4 General utility of NHCs) and coupling product are formed with the same base *in situ* and hence greatly simplifying the process by generating an active catalyst and coupling product from start to finish in one step.

The equilibrium between imidazolium salt and its deprotonated base (carbene) is formed in the reaction mixture. This equilibrium is strongly shifted towards imidazolium salt, because NHCs are known as one of the strongest Lewis bases known, but in the presence of a metal centre the thermodynamic force of NHC coordination to metal centre and NHC–M complex formation is greater still. The most common bases used are Na_2CO_3, K_2CO_3, NEt, pyridine and NaOAc.

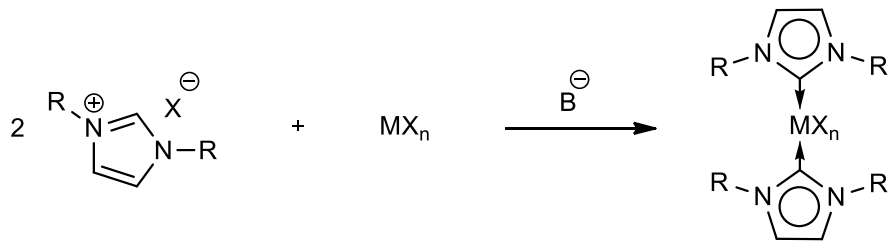
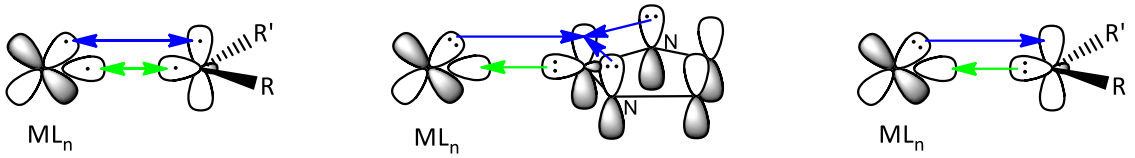


Figure 1.13: Synthesis of NHC metal coordination compounds with a transition metal substrate in the presence of a weak base.

1.2.2.5 Properties of NHC metal coordination compounds

NHC reactivity differs from Fischer or Schrock carbenes. NHC transition metal complexes exhibit exceptional stability due to N–C–N π–π bonding interactions (Figure 1.14). p–orbital of the carbene carbon atom is partially filled by a donor effect of neighbouring nitrogen atoms and π–back bonding from coordinated metal, so it is no longer available for nucleophilic attack. Carbon atom does not have a lone π electron pair and consequently cannot engage in nucleophilic attack on its own, therefore it remains unreactive and takes the middle ground between opposing electrophilic Fischer and more nucleophilic Schrock carbene type [39]. Such stabilization and electron factors make them a perfect candidate as a ligand for substrates for most elements in the periodic table [17].



Schrock carbene | Wanzlick - Arduengo carbene | Fischer carbene

Figure 1.14: Electron configuration of different carbenes in metal coordination compounds. Left Schrock (nucleophilic) carbene, centre NHC and right Fischer (electrophilic) carbene.

1.2.3 Modes of NHC coordination – *n*NHC *vs. a*NHC

NHCs most reactive site on NHC is C2 atom in N1—C2—N3 moiety (Figure 1.5a and 1.16). Deprotonation of imidazolium salt occurs on the most acidic proton located on the C2 position. Subsequent coordination of NHC to a metal centre consequently takes place on the C2 atom. However, in 2002 *Crabtree et al.* observed the first example of "abnormally" coordinated NHC when performing *in situ* deprotonation reaction of an imidazolium salt in the presence of $IrH_5(PPh_3)_2$ (Figure 1.15). Instead of normal NHC coordination (nNHC) this product featured "abnormal" (aNHC), mesoionic or C4 coordination on Iridium metal centre [50-52]. This mode of coordination opened the doors for stabilization of different mesoionic carbenes (MIC), dianionic carbenes [53], cyclic alkyl amino carbenes (caac) [54] and even bicyclic alkyl amino carbenes (BICAAC) [55], which gave chemists a new tool that enables them to stabilize highly reactive species, which could not be stabilized before.

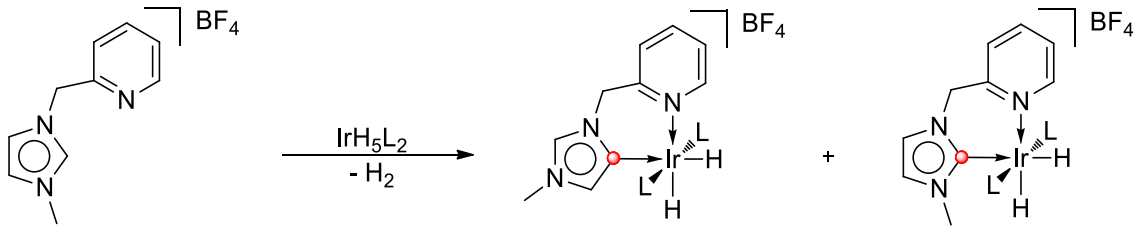


Figure 1.15: First example of »C4« or aNHC/MIC coordination on metal centre.

1.2.3.1 Characteristics of aNHCs

The term abnormal NHC (aNHC) applies to all cases where the free ligand cannot be written in a neutral form and one is obliged to use the positive and negative formal charges. In other words, no resonance with an all-neutral form can be written [56]. Following this logic **A** is normal and **B** is abnormal (remote) or mesoionic carbene (Figure 1.16).

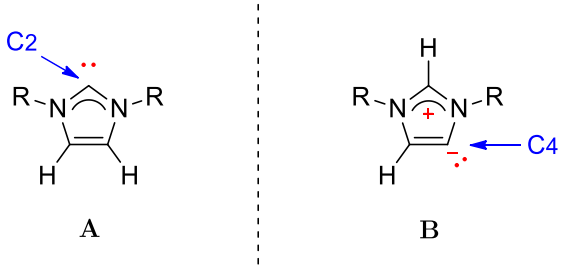


Figure 1.16: "Normal" carbene *vs.* "abnormal" carbene representation.

Numerous normal NHCs (nNHCs) were known decades before the abnormal ones (aNHC). Although nNHCs are already very strong donors amongst neutral ligands, the aNHCs exhibit yet a larger σ–electron donating effect. This is important because such mode of coordination broadens the electronic and steric properties of NHCs and in some rare cases, when "C2" or nNHC metal complex is inert for catalysis, its aNHC analogue displays catalytic activity for specific Suzuki-Miyaura and Heck reactions [57].

There are several important differences between nNHCs and aNHCs/MICs such as the absence of dimerization product and lack of viable description of carbene carbon atom with six valance electrons in aNHC/MIC free form. As later described by *R. H. Crabtree*, most of those discrepancies disappear once they form coordination compounds with substrates and are thus, rightfully so, treated as the same group of molecules [56].

1.2.3.2 Effects on nNHC or "C2" *vs.* aNHC or "C4" coordination

The fact that we sometimes observe metalation on C4 position of imidazole ring, instead of C2, is remarkable, especially from the standpoint of proton abstraction. As mentioned before, the most acidic proton on the imidazolium ring is C2−H proton. Acidity of C2−H has been determined experimentally as well as computationally with pKa = 24±1 [58, 59] versus C4−H proton with pKa = 33 determined computationally [60]. The nine units lower pKa value of C4−H proton suggests that aspects other than the acidity of the protons control the regioselectivity of coordination [61].

Experimental and calculation methods of the coordination, by *in-situ* generation of NHC from imidazolium salts, showed that the type of anion can influence the mode of NHC coordination. Researchers proposed that large *N*-substituents on the carbene ligand in combination with larger anions, such as BF_4, can promote C4−H activation and subsequent carbene coordination (abnormal reaction pathway, Figure 1.17). In contrast, C2−H heterotic cleavage and subsequent C2 coordination is favoured with small halide counter-ions because of stronger ion paring capabilities by C−H···X (X = small anion) hydrogen bonding (normal reaction pathway, Figure 1.17) [52]. Counter ion effect is thus *on par* with the size of NHC nitrogen substituents "wingtips". If smaller (*e.g.* R = Me, Et) *N*-substituents are used, the NHCs favour C2 coordination, whilst NHCs with bigger substituents (R= Mes, py, Dipp, etc.) make C4 coordination possible. Explanation to why this is the case can be rendered down to invoked steric hindrance of bulky "wingtip" substituents on nitrogen atoms and weaker ion paring of C−H···X (X = large anion) [52, 62]. However, the authors of the original research also note that anion-dependent selectivity

change is a result of several criteria and further examples would help or deny the general principles proposed for this reaction system [52].

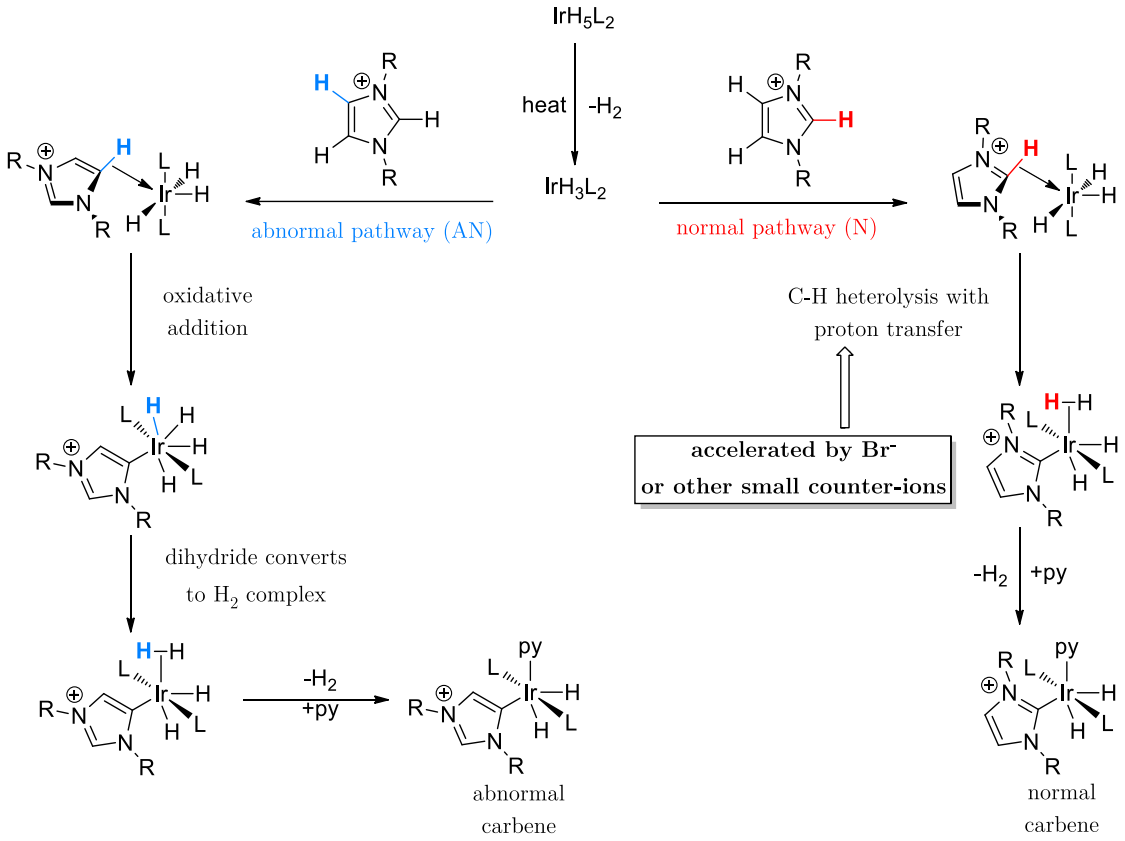


Figure 1.17: Mechanisms that lead to either normal "C2" or mesoionic "C4" coordination complex.

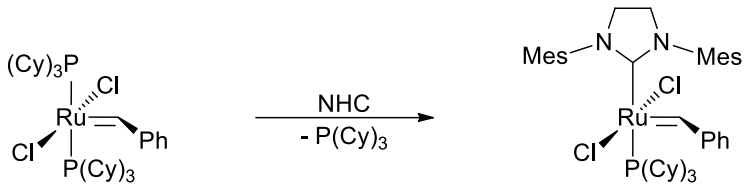
Another aspect of NHC coordination regioselectivity are additives. Research on Palladium substrate showed that the presence of a Cs_2CO_3 in the reaction mixture promotes C2−H activation and metalation, while without the additive NHC coordinates through "C4" position. Explanation to why this happens lies in the presence of basic anions. CO_3^{2-} is supposed to deprotonate C2−H position and favour C2 metalation whilst without the presence of the base, the oxidative addition to Pd centre is favoured and thus C4 metalation is promoted [57].

1.2.4 General utility of NHCs

1.2.4.1 NHCs in d-block chemistry

First notable application of NHCs as ligands in d-block metal complexes revealed itself in 1995 when Wolfgang A. Herrmann *et al.* reported NHC-palladium catalyst that showed activity for C−C Heck coupling reaction [38]. Reported catalyst showed high thermal durability, long shelf life, stability towards oxidation and easy accessibility.

In 1999, Christopher W. Bielawski and Robert H. Grubbs prepared a 2nd generation of Grubbs Catalysts by substitution of one $P(Cy)_3$ ligand with NHC ligand on Ruthenium metal centre (Figure 1.18) [63]. The 2nd generation Grubbs Catalysts showed dramatic increase in catalyst activity, functional groups tolerance and decreased sensitivity for the presence of moisture and oxygen in different olefin metathesis system. This meant that organic chemists had an easily obtainable catalyst at their disposal and could now perform many new reactions, unachievable before, by doing simple "table" chemistry without inert reaction conditions. Consequently, for all this advances in olefin metathesis, the Royal Swedish Academy of Sciences awarded Robert H. Grubbs a shared Nobel Prize for chemistry in 2005 along with Yves Chauvin and Richard R. Schrock [64-66].



first generation Grubbs catalyst

second generation Grubbs catalyst

Figure 1.18: Synthesis of 2nd generation Grubbs catalyst.

Of course, many other catalytic application systems were researched, such as hydrogenation, hydrosilylation and hydrogen transfer [67] and π-bond activation [68], but the most prominent areas, where applications of NHCs as ligands in d-block metal coordination compounds come to light, remain cross-coupling and olefin metathesis reactions.

1.2.4.2 NHCs in p-block chemistry

Many coordination compounds of NHCs with p-block substrates were reported. The driving force of these complexation reactions is donation of the carbene lone electron pair into vacant σ–accepting orbital of p-block substrates [17]. NHC coordinated p-block substrates exhibit a wide range of properties and structural motives never before achieved with any other ligands. Such properties include:

- Stabilization of radicals [69, 70].
- Stabilization of non-metals in low/zero-oxidation state [71, 72].
- Formation of frustrated Lewis pairs (FLPs) (Figure 1.19) [73, 74].
- Small molecule activation (Figure 1.19) [72, 73].

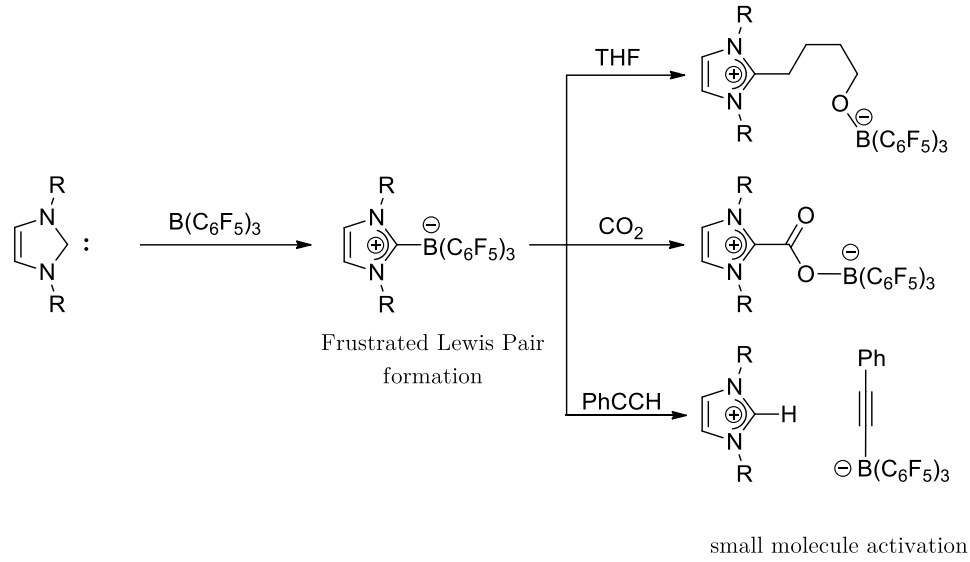


Figure 1.19: Illustration of Frustrated Lewis Pair formation and small molecule activation.

1.3 Importance of Fluoride Donors

Synthesis and preparation of new fluoride sources is in demand due to specific characteristics of molecules bearing fluoride anion. Introduction of fluoride into molecules can drastically change their physical and chemical properties [75] and is thus an essential element in many basic or applicative fields of chemistry. Especially organofluorine chemistry where C–F bond is found in numerous agrochemicals, fluoridopolymers, refrigerants, surfactants, oil or water repellents to name just a few [76, 77]. In inorganic chemistry, fluorides are used as a tool to study high coordination number chemistry [78, 79]. It is an invaluable element in materials (Teflon®, Gore-Tex®, Nafion, Viton, etc.), medicinal application (Lipitor, Prevacide, Seretide, Prozac, Celebrex, etc.) and many more, without which we cannot imagine our lives.

1.3.1 Overview of selected tools for fluoride anion generation

Among three general types of reagents for incorporation of F atom into molecules, namely oxidative, electrophilic and nucleophilic reagents, the latter are preferential from the economical point of view and ease of handling in the laboratory [80, 81]. Although numerous fluoride sources are known, the fluorination of organic or inorganic species to this day remains a challenge [82-84].

1.3.1.1 HF as a fluoride source

For example, the simplest and most widely used reagent for the introduction of fluoride anion to different species would be anhydrous HF (aHF). However, due to its low boiling point, high corrosiveness and toxicity, it has to be handled in specialized labware.

Milder HF reagents can be prepared by reacting HF with different amines, producing HF complexes such as the Olah's reagent or $Et_3N{\times}3HF$ [85]. These HF complexes can be handled by classical chemical methods (even in glassware for short time intervals), but so far, they have not achieved wider acceptance (Figure 1.20).

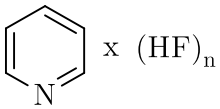
aHF	$(Et)_3N$ x 3HF		KHF_2
anhydrous hydrofluoric acid	Triethylamine trihydrogenfluoride	Olah's reagent	Potassium bifluoride

Figure 1.20: HF based reagents.

1.3.1.2 Metal fluorides as fluoride sources

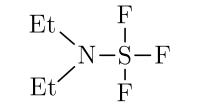
Metal fluorides (MF; M = K, Na, Cs, Ag …) are the next in line as fluoride sources from the standpoint of simplicity and economic perspective. Although easy to handle, not corrosive or too dangerous, their limited solubility in organic solvents prevents their widespread use. Poor solubility of alkali earth metal fluorides can be somewhat overcome by the introduction of different crown ethers, but that increases their price and the removal of these ancillary ligands can be problematic (Figure 1.21) [86].

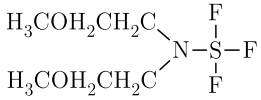
NaF	KF	CsF	AgF
Sodium fluoride	Potassium fluoride	Cesium fluoride	Silver(I) fluoride

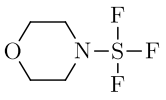
Figure 1.21: Common metal fluorides used as fluoride sources.

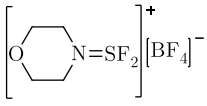
1.3.1.3 Fluoride sources based on sulphur-fluoride bond

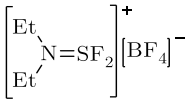
The group of fluoride sources derived from SF_4 are either thermally unstable or their synthesis and isolation is in some way problematic. Although they are too reactive to be used selectively for specific tasks (Figure 1.22), they proved to be excellent deoxyfluorination reagents [87-91].


DAST


Deoxo-Fluor


Morpholino-DAST


XtalFluor-M


XtalFluor-E

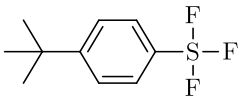

4-tert-Butyl-2,6-dimethylphenylsulfur trifluoride

Figure 1.22: Fluoride sources based on sulphur-fluoride bond.

1.3.1.4 Quarternary ammonium/phosphorous salts and fluoride sources based on fluoridosilicates and fluoridostanates

A few organic "naked" fluoride reagents are known. Tetramethyl ammonium fluoride (TMAF) and especially tetrabutyl ammonium fluoride (TBAF) are widely used. Despite reagent's profound solubility in acetonitrile (compared to MF compounds), they slowly decompose and react with organic solvents (including acetonitrile). Consequently, they undergo a different side reaction, such as Hofmann elimination, resulting in the formation of amine and alkene side products [92, 93]. Additionally, the synthesis or preparation of most of the organic naked fluoride sources requires substitution of another anion, *i.e.* halide, with MF reagents. Such synthetic approach depends on the introduction of water to the reaction system because of the poor solubility of MF compounds in organic solvents, resulting in vigorous drying conditions of the synthesized naked fluoride reagents that often lead to their increased decomposition [93-97]. Water is problematic, since the research shows that water solvation deactivates the nucleophilic and basicity properties of "naked" F^- anion due to strong H···F bonding of the solvent and F^- anion [86]. Here we emphasize that problems with a double nature of fluoride anion (as a nucleophile and base)[82, 86] were solved to some degree by masking the fluoride ion as an adduct with the weak Lewis acids [80, 98-100], by anhydrous synthesis of TBAF [101] or its solvation with tert-butanol (Figure 1.23) [102]. However, there is still a need for new fluoride sources that would not display the aforementioned problems.

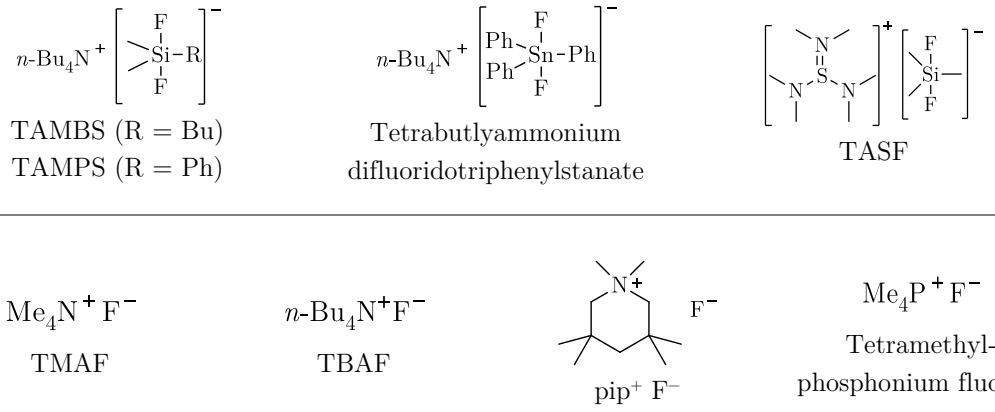


Figure 1.23: Naked fluoride reagents and fluoride donors masked by a week Lewis acid.

1.3.1.5 Novel imidazole and imidazoline based reagents

As mentioned before, the reagents for the introduction of fluoride anion have problems with solubility or stability in organic solvents, others with tolerance of functional groups, side reactions or thermal stability. In 2011, Ritter *et al.* reported novel 1,3-bis(2,6-diisopropylphenyl)-2,2-difluoro-imidazole (PhenoFluor™) [103], and in 2016 another reagent 1,3-bis(2,6-diisopropylphenyl)-2-fluoro-imidazolium tetrafluoridoborate (AlkyFluor), derived from NHC [104]. Both reagents exhibit exceptional resistance towards moisture and high thermal stability. Their analogues such as 2,2-difluoro-1,3-dimethylimidazolidine (DFI) prepared by a different synthetic route have been used in inorganic frameworks [105, 106]. Currently, PhenoFluor™ and AlkylFluor seem to be the reagents of choice for aromatic and alky deoxyfluorination processes of organic molecules (Figure 1.24).

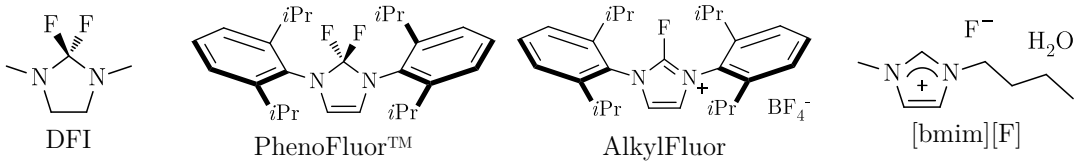


Figure 1.24: Imidazole and imidazoline based reagents.

Chapter 2

Aims and Hypothesis

Metal and metalloid fluorides are used in many different applications and are utilized in a wide variety of research fields. However, they are scarcely soluble in organic solvents due to high lattice energies and are thus deactivated as a homogenous catalyst, thin-layer building blocks and as fluorinating reagents. To achieve numerous significant advances in the research field of metal fluorides in many applications, their solubility problem should be addressed. Solubility shortcomings can be resolved by introducing large, sterically hindering *N*-heterocyclic carbene ligands. Their coordination could prevent the formation of long polymer chains of bridging fluoride atoms with high lattice energies and afford NHC stabilized monomeric or dimeric units that would have increased solubility in non-polar organic solvents. The research will focus on the preparation and reactivity of an NHC with selected MF_n compounds and other fluoride sources.

2.1 Aim

The aim of this thesis is to examine and explain the behaviour, mechanistic insights and other phenomena of combining the NHC chemistry with fluorine chemistry to better understand and achieve the aforementioned goals and increase the utility of metal/metalloid fluorides. Obtained products will be characterized by:

1. Single crystal X-ray diffraction
2. Multinuclear NMR analysis (^{1}H, ^{19}F and ^{13}C)
3. Raman vibrational spectroscopy
4. CHN elemental analysis
5. Chemical computational methods

2.2 Hypothesis

Different metal fluorides, in the form of either weak or strong Lewis acids, should react with NHC, which was established to be a strong Lewis base. The thermodynamic driving force in these systems should lead to the coordination of NHC to a metal centre and isolation of a neutral NHC coordination product. However, in the case of metal fluorides, abstraction of the proton from the solvent molecule followed by the formation of a new imidazolium salt is possible. The reactions should produce either:

a) an imidazolium salt with metal fluoride anion
b) a formation of neutral NHC-MF_n coordination compound
c) a formation of NHC-HF salt

Reaction of a persistent *N*-heterocyclic carbene with the addition of HF source should produce easy obtainable *N,N*-disubstituted imidazolium fluoride product which could serve as a new fluoride source, hopefully stable and soluble in organic solvents. Additionally, such approach should render the formed product anhydrous and free of any other impurities resulting from substitution reactions. The use of sterically hindering *N*-substituents on imidazolium cation could have beneficial stabilization properties, making it an excellent candidate to achieve novel structurally characterized species that could not be prepared before. Hypothesized reactivity of the formed product could lead to the preparation of new organic or inorganic fluoride bearing compounds.

Chapter 3

Methodology and Tools

Most of the compounds we are dealing with are air sensitive and can easily react with water and oxygen, so they have to be handled under inert conditions. Non-volatiles were handled in the M. Braun glove box (LABSTAR & MB200MOD) under an Argon atmosphere, where quantity of water or oxygen did not exceed 0.1 ppm. Reactions were carried out on a Schlenk line, whereas corrosive volatiles such as aHF, F_2 and other fluoride gasses were handled on a Nickel/PTFE high-vacuum line.

3.1 Handling of Air-Sensitive Chemistry

3.1.1 Schlenk line

One of the pioneers in air sensitive chemistry was German chemist Wilhelm Schlenk (1879 - 1943). In his early years, he was dealing with highly unstable radicals and reported the preparation of first organolithium compounds in 1917 that were also unstable in air; thus, he had to develop new methods, glassware and apparatus for handling such delicate compounds. The commonly known apparatus he developed, named after him, is the Schlenk line (Figure 3.1) and general methods applied on it are known as the Schlenk techniques [107].

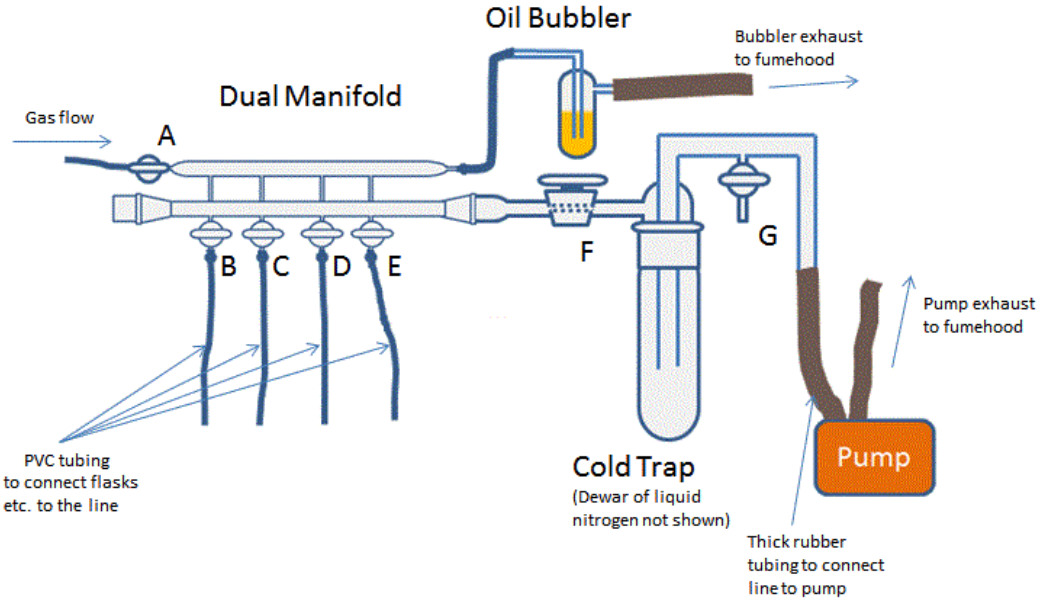


Figure 3.1: Standard Schlenk line assembly [108].

The Schlenk line (also vacuum gas manifold) consists of a dual manifold to which several connectors for reaction vessels are attached (B, C, D and E). One manifold is attached to the inlet of an inert gas (A), usually nitrogen or argon. The manifold is connected to exhaust through a bubbler that prevents back-flow of air and blocks the build-up of pressure in the manifold. The second manifold is linked to a rotary vane pump via cold trap to accomplish vacuum in the manifold. Then, by turning the valves on reaction vessel ports and on Schlenk flasks, one can easily control the atmosphere in the reaction vessel and enable a variety of manipulations under inert conditions, such include:

- solvent addition via cannula transfer
- counter flow addition of air-stable solid reagents against a flow of inert gas
- use of syringes and septa for liquid reagents addition
- filtration
- chromatography techniques
- volatile compounds removal under vacuum

3.1.2 Nickel vacuum line

Due to reactivity with glass, aHF and other corrosive reagents have to be manipulated on a high-vacuum line constructed of Nickel and polytetrafluoridoethylene (PTFE, Teflon®) joints. Vacuum in the Nickel manifold is generated by Edwards RV3 rotary vane pump and achieves pressures to about 0.1 Pa. High vacuum is applied by Oil diffusion pump where pressures to about 0.0001 Pa can be maintained.

Specialized reaction and crystallization vessels are manufactured from tetrafluoridopropylene-hexafluorido propylene block copolymer (FEP; Poltytetry, GmbH, Germany) tubes. Tube with inner diameter 16 mm and outer diameter 19 mm is cut at the desired length. One end of the tube is heat-sealed and the other end equipped with PTFE inlay where the PTFE T-shaped connector or PTFE valve is attached. Vessel for single crystal growth was designed from the combination of tubes with inner diameter 16 mm and outer diameter 19 mm and the second tube with 4 mm inner diameter and 6 mm outer diameter, connected via PTFE T-shaped connector at 90°. PTFE valve is attached directly to the inlay of the reaction vessel or to the T-shaped connector at 180° (in case the crystallization vessel is built). To ensure the strength and prevent their deformation, all PTFE parts are shielded with brass alloy parts (Figure 3.2).

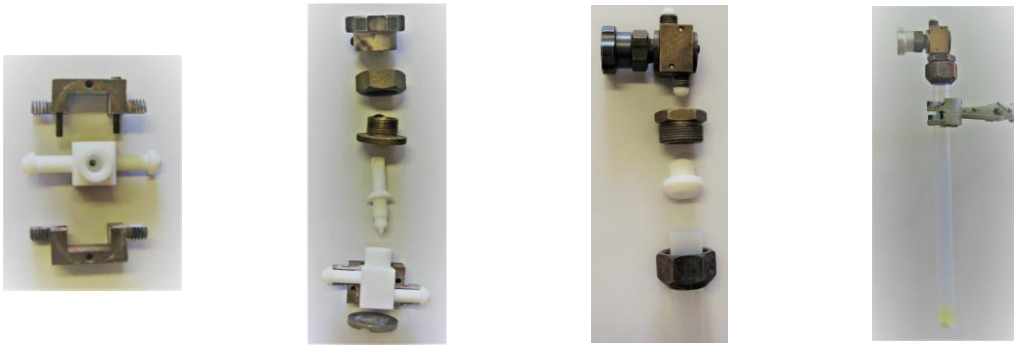


Figure 3.2: FEP reactor vessel assembly (picture by Dr. Z. Mazej).



Figure 3.3: Nickel-PTFE Vacuum line (picture by Dr. Z. Mazej).

Chapter 4

Results and Discussion - Overview

Results and discussion sections of this work are divided into three parts covered by three publications in scientific journals. The first part, describes the reaction system between *N*-heterocyclic carbenes and SbF_3 compound. It explains how these two systems inter-cross and discuss problems encountered in the research field. It addresses the reaction system from the mechanistic point of view and thoroughly analyses the products obtained from this system. The results were published in article: "B. Ališ, A. Štefančič, and G. Tavčar, "Small molecule activation: SbF_3 auto-ionization supported by transfer and mesoionic NHC rearrangement," *Dalton Transactions,* vol. 46, pp. 3338-3346, 2017".

The second part addresses the synthesis of three new imidazolium fluoride salts. Two of them can be classified as imidazolium poly(hydrogen fluoride) salts and 1,3-bis(2,6-diisopropylphenyl)imidazolium fluoride ([(L^{Dipp})H]F) obtained from the reaction of (L^{Dipp}):HF in 1:1 stoichiometry demonstrates the characteristics of a naked fluoride reagent. All three have potential as new nucleophilic fluoride reagents. The research takes an extensive look at the synthesis which is important in terms of possible mass production and broad use of the compounds. It investigates their physical and chemical properties in the solution and in solid. The results were published in article: "B. Ališ and G. Tavčar, "Reaction of *N*-heterocyclic carbene (NHC) with different HF sources and ratios – A free fluoride reagent based on imidazolium fluoride," *Journal of Fluorine Chemistry,* vol. 192, pp. 141-146, 2016".

The third part demonstrates the first reactivity examples of 1,3-bis(2,6-diisopropylphenyl)imidazolium fluoride ([(L^{Dipp})H]F). It explains the reactivity and synthesis of the products obtained with this novel reagent. Reactions with MF_4 (M= Si, Ge) Lewis acids lead to their discrete, pentacoordinated trigonal bipyramidal MF_5^- anions. Crystal structure containing discrete GeF_5^- anions was obtained for the first time. Additionally, we show that sterically hindering cations stabilize trigonal bipyramidal pentafluorido anions of silicon and germanium relative to octahedral coordinated ones. The results were published in article: "B. Ališ, M. Tramšek, A. Kokalj, and G. Tavčar, "Discrete GeF_5^- Anion Structurally Characterized with a Readily Synthesized Imidazolium Based Naked Fluoride Reagent," *Inorganic Chemistry,* vol. 56, pp. 10070-10077, 2017."

The idea behind this thesis is to intertwine the chemistry of persistent 1,3-bis(2,6-diisopropylphenyl)-1,3-dihydro-2*H*-imidazol-2-ylidene *N*-heterocyclic carbene and its fluoride salts with different fluoride substrates and draw conclusions from these reaction systems. The second goal is to explain how this, however small, portion of chemistry deeply embeds in the bigger aspect of fluoride and NHC chemistry. Let us see what we found out.

Chapter 5

Small Molecule Activation: SbF_3 Auto-Ionization Supported by Transfer and Mesoionic NHC Rearrangement

In this chapter, article entitled: »Small molecule activation: SbF_3 auto-ionization supported by transfer and mesoionic NHC rearrangement«, by **Blaž Alič**, Aleš Štefančič, and Gašper Tavčar is presented. For this article, the candidate performed all synthesis procedures with techniques for handling air-sensitive chemicals, obtained single crystals, performed X-ray single crystal diffraction analysis and prepared final .cif files of the obtained products. Furthermore, the candidate performed the multinuclear NMR spectroscopy and Raman spectroscopy, prepared the samples for CHN elemental analysis and actively participated in data interpretation. The candidate wrote the first manuscript draft and was the leading author during its refinement and publication process.

Aleš Štefančič did some preliminary experiments. Gašper Tavčar proposed the idea, coordinated the work and actively participated in experimental data interpretation.

In this article we showed that the reaction of SbF_3 with (L^{Dipp}) in thf or MeCN forms the product $[(L^{Dipp})H]^+[SbF_4]^-$ (**1**). Reactions performed in CH_3CN *vs.* CD_3CN show a proton abstraction from the solvent molecules and H/D exchange for all three imidazolium protons with solvent molecules.

SbF_3 reacts with tmen affording $[SbF_3(tmen)]$ complex (**2**) which can be used as SbF_3 synthon in non-polar solvents (*e.g.* toluene). Subsequent reaction of (**2**) with (L^{Dipp}) in toluene or benzene yields auto-ionization product (**4**) with $[(L^{Dipp})_2SbF_2]^+$ cation stabilized by two NHC ligands of which one underwent rearrangement to mesoionic carbene (mNHC). Product (**4**) is formed through neutral unstable intermediate product $[(L^{Dipp})SbF_3]$ (**3**), and its existence was confirmed only with ^1H and ^{19}F NMR spectroscopy in the solution. It is surprising that no evidence of product (**4**) formation can be observed with the solution NMR analysis. That suggests that the conversion of (**3**) to (**4**) is fast and, when formed, it immediately precipitates out of the solution due to negligible solubility in non-polar solvents. Both products (**3**) and (**4**) were obtained by the presence of either tmen or dme in the system. Reaction mechanism was proven to be independent of tmen, which was suggested to be involved in similar rearrangement in previous research [109], and just like dme, it serves only as auxiliary ligand to help with SbF_3 solubility in non-polar solvents.

Structural analysis of (**4**) is in full accordance with the VSEPR model where the more electronegative F^- ligands are both in axial positions, whereas in other three reported

$[(L)_2SbF_2]^+$ cations that is not the case [110-112]. Product (**4**) also represents the first example of a reaction where, to the best of our knowledge, *N*-heterocyclic carbene ligand facilitates the auto-ionization product in any system reported up to date.

Dalton Transactions

PAPER

View Article Online
View Journal



Cite this: DOI: 10.1039/c6dt04909e

Small molecule activation: SbF_3 auto-ionization supported by transfer and mesoionic NHC rearrangement†

Blaž Alič,[a,b] Aleš Štefančič[a,b] and Gašper Tavčar*[a,b]

Received 30th December 2016,
Accepted 9th February 2017

DOI: 10.1039/c6dt04909e

rsc.li/dalton

The reactivity of antimony trifluoride, SbF_3, in non-polar aprotic solvents has been unexplored due to its negligible solubility. The reaction of the [SbF_3(tmen)] complex (**2**) with the N-heterocyclic carbene, 1,3-bis(2,6-diisopropylphenyl)imidazole-2-ylidene, (L^{Dipp}), probably leads to the formation of a neutral [(L^{Dipp})SbF_3] intermediate (**3**) in non-polar solvents. Mild heat treatment of the reaction mixture unexpectedly activates the SbF_3 molecules to undergo the auto-ionization reaction. In this process, one of the (L^{Dipp}) ligands undergoes rearrangement into the mesoionic carbene (MIC) and further coordinates to the cation to form $[(L^{Dipp})_2SbF_2]^+[SbF_4]^-$, product (**4**). Studies have confirmed that *N*,*N*,*N*′,*N*′-tetramethylethane-1,2-diamine (tmen) present in the solution is not involved in the conversion mechanism and serves solely as an auxiliary ligand to increase the solubility of SbF_3. The compound (**4**) shows a rare pnictogen(III) halide auto-ionization process with the first mesoionic NHC rearrangement on any metal/metalloid fluoride compound and the first reported reaction system where a N-heterocyclic carbene ligand facilitates the auto-ionization process on a fluorido substrate.

Introduction

N-Heterocyclic carbenes (NHCs) are attractive species that rival phosphine ligands across organometallic chemistry. In terms of p-block adducts and the extensive "tuning" abilities of their steric and electronic properties, they are invaluable tools in various applications such as conversions of small molecules or stabilization of rare chemical species.[1]

NHC chemistry with fluoride substrates (MF) has not received much attention and their reaction systems have not been investigated in appreciable amounts. We portray this fact in the following table, showing the number of NHC coordination compounds that feature either normal "C2" or mesoionic "C4" coordination, based on a CCDC search from the beginning of 2016 (Table 1).

As a result, the reaction pathways of NHC–MF systems and their applicability remain more or less uncharted territories.

To date, most of the studies conducted on pnictogen fluorides (PnF_y; Pn = P, As, Sb, Bi; y = 3 or 5) and NHCs have been on pnictogen(v) fluorides, carried out by Arduengo *et al.*, who prepared the NHC complexes with P(v), As(v) and Sb(v) fluorides in 2000.[2] In 2011, an alternative route to phosphorous(v) fluorides coordinated with NHC ligands was reported by G. V. Röschenthaler *et al.*;[3,4] however, practically no work has been done on pnictogen(III) fluorides. During recent years, antimony(III) chloride has been studied with different carbene ligands. Crystallographically characterized species include NHC($SbCl_3$),[5] CAAC($SbCl_3$), CAAC(SbCl) and $CAAC_2(Sb_2)$;[6] the closely related NHC($SbCl_2$)$^+$ species were prepared by chloride abstraction from $SbCl_3$ with [NHC($SiMe_3$)$^+$][OTf]$^-$ reagent.[7]

Organic ligands can induce the auto-ionization process of different halides. Such behaviour can be found for main group elements and is most common for the group 13 halides. In the case of gallium, auto-ionization was observed in the reaction of $GaCl_3$ with different NHCs.[8] It is much less commonly seen for group 14 elements and rarely seen for halides of group 15 elements. The only exception is bismuth, where the formation of ion pairs was observed in coordination compounds with different ligands.[9–12] Structurally characterized products of the auto-ionization of antimony(III) chloride are scarce; among

Table 1 CSD search for known NHC complexes (ESI S30)

Substrate	C2 or C2–C2	C4 or C2–C4	C4–C4
Any	9069	318	38
MF	95	0	0

[a]Jožef Stefan Institute, Jamova cesta 39, 1000 Ljubljana, Slovenia.
E-mail: gasper.tavcar@ijs.si
[b]Jožef Stefan International Postgraduate School, Jamova cesta 39, 1000 Ljubljana, Slovenia

†Electronic supplementary information (ESI) available: NMR and Raman spectra. CCDC 1454012, 1454013, 1523950 and 1523951. For ESI and crystallographic data in CIF or other electronic format see DOI: 10.1039/c6dt04909e

these are the products of $[Cl_2Sb\{Fe(CO)_2(\eta^5\text{-}C_5H_5)\}_2][Sb_2Cl_7]$[13] and $[SbCl_2([18]aneO_4Se_2)]_2[Sb_3Cl_{11}]$.[14] Such behaviour is expected to be more common for fluorides, due to the small size and higher electronegativity of F^-, and was observed for Ta(v) and Nb(v) fluorides.[15–17] In contrast, all the reported pnictogene trihalides (PnX_3) (X = F, Cl, Br, I) form neutral Lewis pair adducts with different group 15[18–21] and group 16 ligands.[19,22–26] Furthermore, several MF_5 auto-ionization products in melts have been reported with the emphasis on d-block elements such as Ta(v) and Nb(v),[27,28] V(v)[29] and Mo(v)[30] halides, but for the p-block halides, including pnictogene pentafluorides (PnF_5) or trifluorides (PnF_3), such results are scarce or non-existent. However, the electrical conductivity of molten SbF_3 has been explained by the auto-ionization process, yielding $[SbF_2]^+$ and $[SbF_4]^-$ ions.[31] Additionally, based on conductivity, density and viscosity measurements, it was concluded that metal fluorides have a far greater tendency to follow the auto-ionization process, given by equation $2MX_n \rightarrow [MX_{(n-1)}]^+[MX_{(n+1)}]^-$, compared to their heavier halide analogues.[28]

Herein, we report the NHC assisted activation of SbF_3, which undergoes the auto-ionization reaction. The aforementioned process takes place *via* NHC transfer, with rearrangement to mesoionic carbene (MIC), making product $[(L^{Dipp})_2SbF_2]^+[SbF_4]^-$ (**4**) an anomaly that requires further investigation.

Results and discussion

Synthesis of $[(L^{Dipp})H]^+[SbF_4]^-$ (1)

We initiated our investigation of the SbF_3 reactivity in aprotic solvents with N-heterocyclic carbenes, by reacting SbF_3 with 1,3-bis(2,6-diisopropylphenyl)imidazole-2-ylidene (L^{Dipp}) in tetrahydrofuran (THF). The reaction proceeded at room temperature, affording the $[(L^{Dipp})H]^+[SbF_4]^-$ salt (**1**) in good yield (71%) (Scheme 1 and Fig. 1). The ^1H and ^{19}F NMR spectra (ESI S4 and S5†) agree with the crystal structure of the formed complex and do not indicate any traces of other soluble products. Based on literature reports,[2,32] the proton source was not thoroughly examined previously; therefore, we performed the reactions of SbF_3 with (L^{Dipp}) in CH_3CN and CD_3CN solvents to investigate the proton source in the obtained product. ^1H NMR spectra of both reaction mixtures show the same signals, except the signals assigned to protons in the imidazolium ring at 9.22 and 7.90 ppm, which were present in the reaction carried out in CH_3CN, but were absent in the product obtained in deuterated solvent (ESI S8†). This denotes that the C(2)–H proton originated from a solvent molecule, and both imidazolium protons undergo H/D exchange. The observed reactivity is in accordance with previous reports,[33] and all the reactions in THF or acetonitrile yielded only product (**1**). Consequently, we changed the solvent to toluene, despite the expected negligible solubility of SbF_3 in non-polar solvents. The reaction in toluene did not occur even when carried out at elevated temperatures; thus, we concluded that improving the solubility of SbF_3 in non-polar organic solvents is essential in order to carry out the reaction in toluene (Scheme 1).

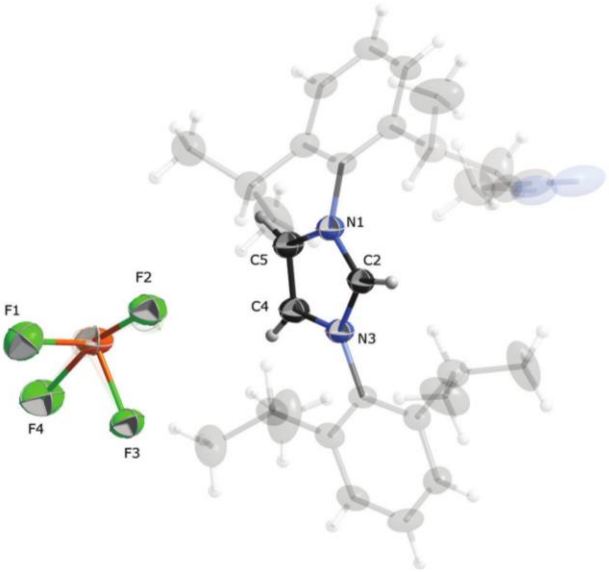
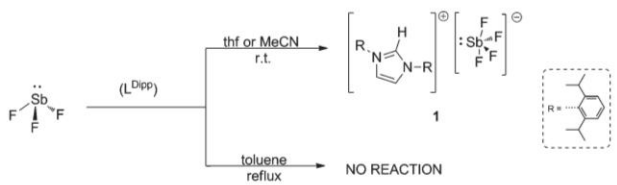


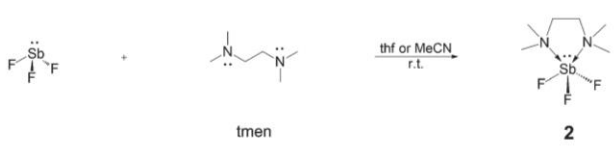
Fig. 1 Crystal structure of $[(L^{Dipp})H]^+[SbF_4]^-$ (**1**). Thermal ellipsoids are shown at the 50% probability level. 2,6-diisopropylphenyl groups, solvent and anion disorder are shaded for clarity. Selected bond lengths [Å] and angles [°]: Sb1–F1 1.62(1), Sb1–F2 2.008(5), Sb1–F3 1.914(5), Sb1–F4 2.016(5); F1–Sb1–F3 104.6(4), F4–Sb1–F2 162.0(3).



Scheme 1 Reactivity of SbF_3 with (L^{Dipp}) in THF *vs.* toluene.

Synthesis of $[SbF_3(tmen)]$ (2)

Based on our initial findings, we used an alternative approach, by preparing a SbF_3 complex soluble in non-polar solvents. *N*,*N*,*N*′,*N*′-Tetramethylethane-1,2-diamine (tmen), which coordinates to SbF_3 as a bidentate ligand and forms a pentacoordinated antimony(III) complex (**2**), was found to be a convenient coordinating reagent (Scheme 2 and Fig. 2).



Scheme 2 Synthesis of $[SbF_3(tmen)]$ complex (**2**) in THF or acetonitrile (CH_3CN).

This journal is © The Royal Society of Chemistry 2017

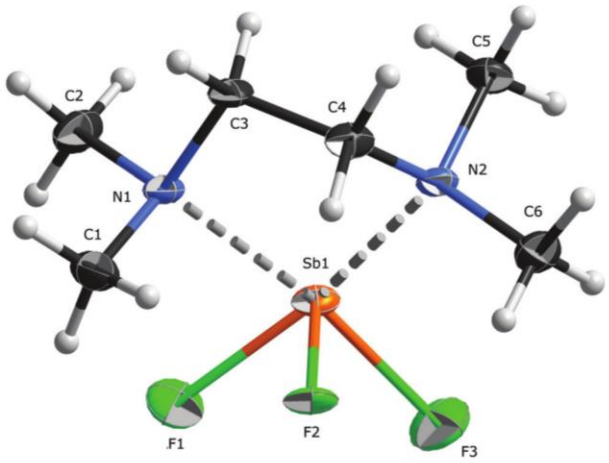


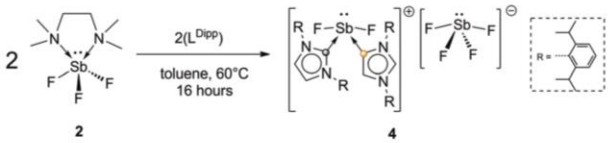
Fig. 2 Crystal structure of [SbF_3(tmen)] (**2**). Thermal ellipsoids are shown at 50% probability level. Selected bond lengths [Å] and angles [°]: Sb1–F1 1.971(2), Sb1–F2 1.922(2), Sb1–F3 1.974(2), Sb1–N1 2.484(3), Sb1–N2 2.465(3); N1–Sb1–N2 74.3(1), F1–Sb1–F2 82.1(1), F1–Sb1–F3 94.1(1), F2–Sb1–F3 83.7(1).

The isolated complex (**2**) is unstable and has to be kept at a low temperature under inert conditions. The complex (**2**) is soluble in non-polar solvents and as such, is suitable as a SbF_3 synthon (ESI S12 and S13†). After the reaction, unbound tmen can be easily removed under dynamic vacuum due to its substantial vapour pressure at room temperature.

Synthesis of $[(L^{Dipp})_2SbF_2]^+[SbF_4]^-$ (4)

Reaction of [SbF_3(tmen)] (**2**) with (L^{Dipp}) in toluene at elevated temperatures yields a transparent crystalline product (**4**) that slowly forms in the reaction vessel. The crystal structure analysis of (**4**) revealed the auto-ionization product of SbF_3 and stabilization of a rare $[(L^{Dipp})_2SbF_2]^+$ cation that was isolated in only two other systems.[34–36] Previous reports on this observation exemplify the amphoteric nature of SbF_3, where one of the SbF_3 molecules behaves as a donor and another as an acceptor of a F^- anion (Scheme 3).[36]

Two (L^{Dipp}) ligands coordinate to the antimony metal centre, forming the $[(L^{Dipp})_2SbF_2]^+$ cation, which represents the first example of a carbon based ligand coordinated to the SbF_2 moiety. Additionally, one (L^{Dipp}) ligand undergoes rearrangement into a mesoionic carbene, MIC, in the product (**4**) (Scheme 3 and Fig. 4), representing a unique complex of MIC coordinated to any metal/metalloid fluorido substrate. Similar rearrangement was described by Weigand *et al.* for the $[(L^{Dipp})PCl_2]^+[OTf]^-$ system, where the addition of (L^{Dipp}) ligand led to the rearrangement of one ligand, and the double coordinated product.[37] Once (**4**) crystallizes from the reaction mixture, it becomes insoluble in non-polar solvents. Dissolution of (**4**) in polar aprotic solvents, such as THF, dichloromethane and acetonitrile, leads to its decomposition and the formation of product (**1**), which makes the solution NMR analysis of (**4**) impossible. All attempts at the crystallization of the reaction mixture yielded solely product (**4**). Although product (**4**) cannot be analysed with solution NMR methods due to its decomposition, we repeated the reaction in deuterated solvent to follow the formation of (**4**) with NMR spectroscopy. We have not found any evidence of an auto-ionization product in the solution; instead, we have most probably observed a neutral $[(L^{Dipp})SbF_3]$ complex (**3**),‡ along with free tmen ligand present in the reaction mixture (Chart 1 and Scheme 4). The most significant difference that indicates coordination of (L^{Dipp}) to SbF_3 and the formation of product (**3**), is the larger magnetic inequality between isopropyl CH_3 protons of 2,6-diisopropylphenyl substituents (R), characteristic of this complex (Chart 1).

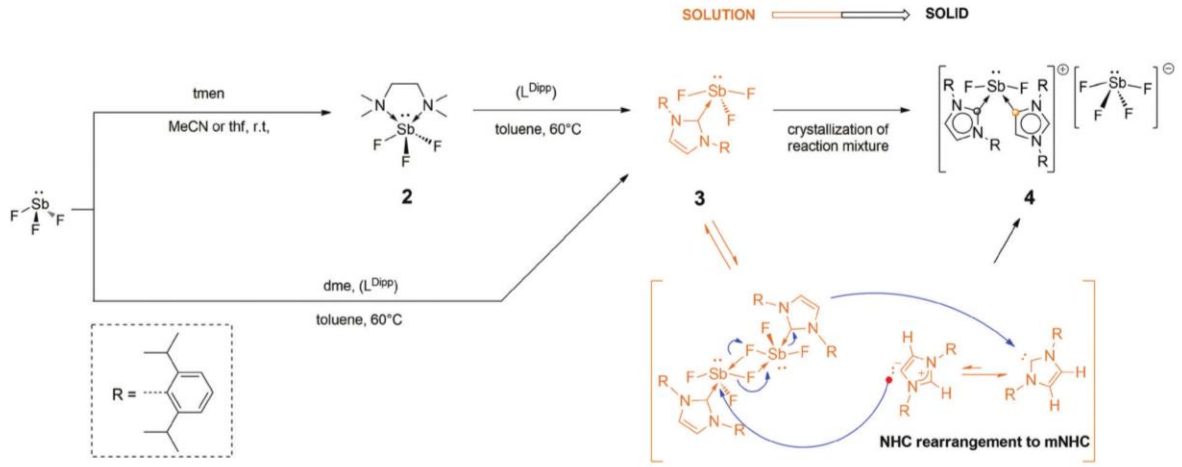


Scheme 3 Preparation of the auto-ionization product (**4**) from [SbF_3(tmen)] (**2**) in non-polar solvent. The cation of (**4**) is stabilized by two (L^{Dipp}) ligands. This is the first known example of mesoionic NHC coordinated on any metal/metalloid fluoride.

Studies of $[(L^{Dipp})_2SbF_2]^+[SbF_4]^-$ (4) formation

The involvement of tmen as a base in the mechanism of carbene rearrangement into the mesoionic form, followed by its further coordination to a metal centre, was previously reported in the literature.[38] In order to test this hypothesis, we carried out the reaction between (L^{Dipp}) and SbF_3 in C_6D_6 with the addition of 1,2-dimethoxyethane (dme) instead of the basic tmen ligand. According to ^{1}H NMR analysis, the results with dme show the same pattern as with tmen (ESI S16 and S21†) and the CH_3 protons of the isopropyl substituents on (R) show even larger inequality by ^{1}H NMR analysis when dme is present in the reaction mixture, compared to tmen (Chart 1). This indicates stronger interaction between the "(L^{Dipp})C2" carbon atom and the antimony(III) centre, when dme is present in the reaction mixture instead of tmen (Chart 1). Formation of the neutral $[(L^{Dipp})SbF_3]$ complex (**3**) in solution is followed by the auto-ionization reaction, yielding product (**4**) (Scheme 4), whether the reactions are performed with tmen or dme ligands, in toluene or C_6D_6 solvents. Furthermore, the ^{1}H chemical shifts of the reaction mixture in C_6D_6 are in perfect agreement with chemical shifts for pure dme[39] and tmen, and do not indicate significant interactions between auxiliary ligands (dme or tmen) and the formed product (**3**). Additionally, we carried out the reaction between [SbF_3(tmen)] (**2**), (L^{Dipp}) and two additional equivalents of free tmen, to investigate the interactions in solution and determine if tmen, (L^{Dipp}) or both ligands were coordinated to the antimony in

‡Product (**3**) was characterized only in the reaction mixture by multinuclear NMR analysis with either tmen or dme present in deuterated C_6D_6 before conversion to (**4**). We were not able to obtain an isolable product (**3**), which would allow characterization that is more detailed.



Scheme 4 Formation of the auto-ionization product (**4**) with mesoionic (L^{Dipp}) rearrangement *via* the neutral [(L^{Dipp})SbF_3] complex (**3**).

the solution. The ^{1}H NMR spectrum of the solution with excess tmen revealed only peaks of unbound tmen for the [(L^{Dipp})SbF_3] (**3**) complex, confirming that there is no significant interaction between the antimony centre and tmen in solution and any other mixed complex (ESI S19 and S20†). Additionally, according to ^{19}F NMR analysis, two fluorine signals in the reaction mixture of [(L^{Dipp})SbF_3] (**3**) were observed. For the reaction carried out with dme, signals at −83.78 ppm (broad) and −131.12 ppm (weak) were observed. In the case of the reaction performed with tmen ligand, signals at −84.17 ppm (broad) and −130.93 ppm (weak) were observed. The broad signals at *ca.* −84 ppm were assigned to the fluorine atoms of the neutral [(L^{Dipp})SbF_3] (**3**) complex. The signal at *ca.* −131 ppm, with substantially lower intensity, becomes significant only at prolonged reaction times when the concentration of (**3**) in the reaction mixture is reduced due to the precipitation of (**4**) (ESI S17, S20 and S22†). This ^{19}F NMR signal is in the region of numerous fluorido species and we find it difficult to assign it to any, since (**4**) is, to the best of our knowledge, the first NHC metal/metalloid fluorido product of auto-ionization observed.

The aforementioned findings on the same behaviour of reaction mixtures, when either dme or tmen coordinating solvents were used, tell us that both solvents are only assisting with the solubility process of SbF_3 in non-polar solvents and the mechanism of auto-ionization can be described as "ligand assisted and heat induced auto-ionization".

Based on all these facts, we concluded that auto-ionization of [(L^{Dipp})SbF_3] (**3**) probably proceeds through the formation of the [(L^{Dipp})$_2Sb_2F_6$] dimer, similar to the [Sb_2F_6(phen)$_2$] dimer,[20] which further separates into [(L^{Dipp})$_2SbF_2$]$^+$[SbF_4]$^-$ (**4**) as shown on our proposed mechanism (Scheme 4).

In order to synthesise the analogue of compound (**4**) with "C2–C2" coordinated cation, we performed the reaction with the (Cl_2L^{Dipp}) ligand that has "C4" and "C5" sites substituted with chloride substituents. The imidazolium backbone of this ligand is consequently unavailable for coordination and only

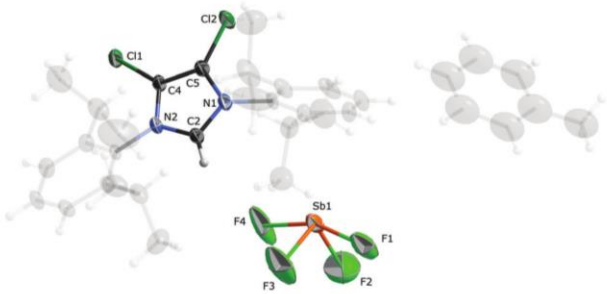
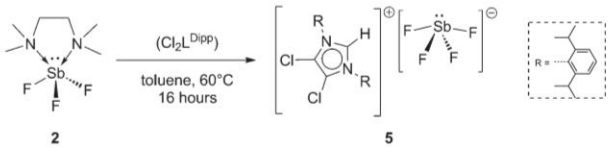


Fig. 3 Crystal structure of [(Cl_2L^{Dipp})H]$^+$[SbF_4]$^-$ (**5**). 2,6-Diisopropylphenyl groups and solvent are shaded for clarity. Thermal ellipsoids are shown at the 50% probability level. Selected bond lengths [Å] and angles [°]: Sb1–F1 2.047(4), Sb1–F2 1.890(6), Sb1–F3 1.911(4), Sb1–F4 1.954(4); F1–Sb1–F4 158.8(2), F2–Sb1–F3 95.3(3).



Scheme 5 Reaction of [SbF_3(tmen)] (**2**) with (Cl_2L^{Dipp}) ligand in toluene.

"C2–C2" coordination should be possible in the expected [(Cl_2L^{Dipp})$_2SbF_2$]$^+$ species. However, the reaction in toluene between (Cl_2L^{Dipp}) and [SbF_3(tmen)] (**2**) yielded only the [(Cl_2L^{Dipp})H]$^+$[SbF_4]$^-$ salt (**5**), which crystallizes directly from the reaction mixture as a solvate with toluene. Compound (**5**) was the only product obtainable from the reaction mixture (Scheme 5 and Fig. 3).§

§ Solution NMR analysis of (**5**) recorded in C_6D_6 afforded empty spectra. – No other soluble compound was obtained from this reaction (ESI S28†).

This journal is © The Royal Society of Chemistry 2017

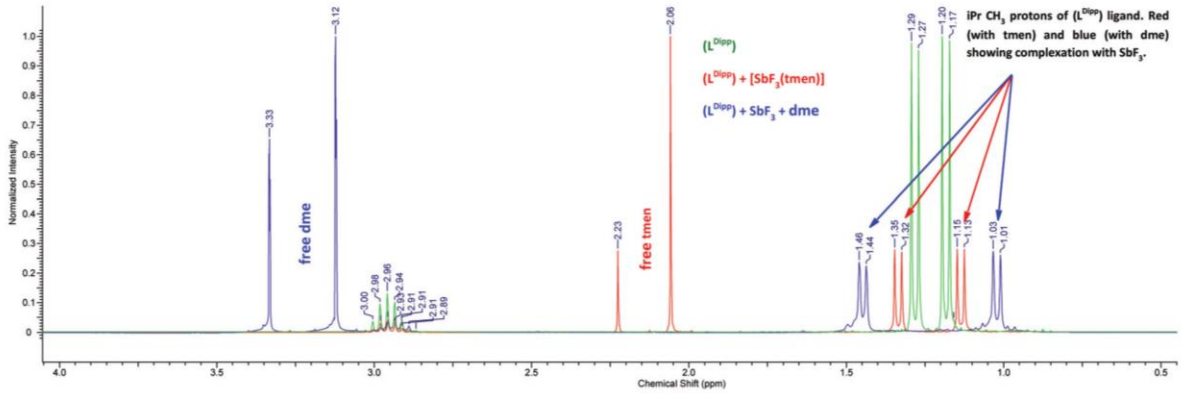


Chart 1 ^{1}H NMR spectra; green signals represent the free (L^{Dipp}) ligand. Red and blue peaks were obtained by reacting (L^{Dipp}) + [SbF_3(tmen)] (1 : 1), and SbF_3 + (L^{Dipp}) + dme (1 : 1 : 2), respectively. Both reactions yielded the same $[(L^{Dipp})_2SbF_2]^+[SbF_4]^-$ product (**4**) upon crystallization. All the NMR spectra were recorded in C_6D_6.

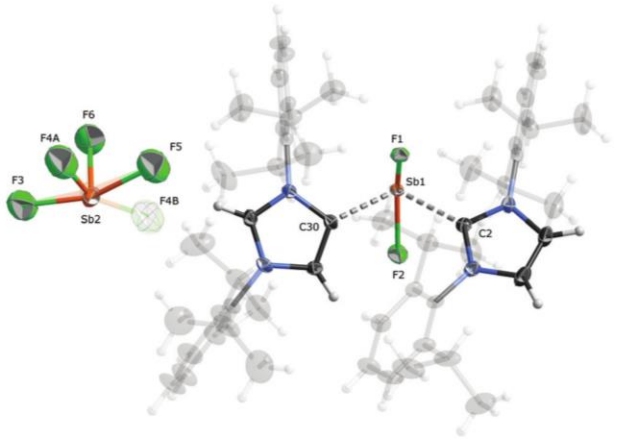


Fig. 4 Crystal structure of $[(L^{Dipp})_2SbF_2]^+[SbF_4]^-$ (**4**). Solvent is omitted and 2,6-diisopropylphenyl groups along with the anion disorder are shaded for clarity. Thermal ellipsoids are shown at the 50% probability level. Selected bond lengths [Å] and angles [°]: Sb1–F1 2.029(2), Sb1–F2 2.020(2), Sb1–C2 2.197(3), Sb1–C30 2.165(3); F1–Sb1–F2 149.16(9), C2–Sb1–C30 111.01(12).

Crystal structure analysis of $[(L^{Dipp})_2SbF_2]^+[SbF_4]^-$ (4)

Product (**4**) crystallizes in the triclinic $P\bar{1}$ space group (Table 2). The central antimony atom in the $[(L^{Dipp})_2SbF_2]^+$ cation is tetra-coordinated with disphenoidal geometry. The coordination of two carbene moieties in the sterically less demanding equatorial site, and two F^- ligands in axial positions, are consistent with the VSEPR model for the AX_4E geometry in terms of size, electronegativity and bonding electron-pair domains of ligands, where smaller and more electronegative F^- anions take up more crowded positions than bulky NHC ligands.[40] However, Arduengo *et al.* states that nucleophilic addition to such a system is expected to proceed along a pathway in which the incoming nucleophile approaches from the axial position to add to the SbF_3 complex.[41] In compound (**4**), the position of both (L^{Dipp}) ligands is equatorial and F^- ligands are in the axial position. Although we were not able to attain the crystal structure of the neutral $[(L^{Dipp})SbF_3]$ complex (**3**), we propose that the exchange of the tmen ligand from the pyramidal AX_5E [SbF_3(tmen)] complex (**2**) to the AX_4E $[(L^{Dipp})SbF_3]$ complex (**3**) proceeds at the equatorial position with (L^{Dipp}). Upon the successive auto-ionization process of $[(L^{Dipp})SbF_3]$ (**3**), the substitution of fluoride by the less electronegative (L^{Dipp}) ligand also takes place at equatorial positions, in accordance with the VSEPR model of molecular geometry, explaining the formation of (**4**).[40] However, we have to note that the ^{19}F NMR spectra of the reaction mixture during the preparation of product (**4**) show only singlet peaks, and not separate ones for axial and equatorial positions of fluorido ligands, suggesting possible intramolecular pseudo-rotation at antimony centres.

The "(L^{Dipp})C2"–Sb1 (2.197(3) Å) and "(L^{Dipp})C30"–Sb1 (2.165(3) Å) distances in (**4**) are much shorter than in the related NHC compound $(L^{Mes})Sb(CF_3)_3$ (2.821(5) Å),[41] showing that the strength of the coordination bond is higher in the case of positively charged species.

Sb–F distances in the crystal structure of trigonal pyramidal AX_3E, SbF_3, are 1.90(2) and 1.94(2) Å respectively.[42]

In the product (**4**), the two Sb–F distances are slightly elongated. Such a difference in distance that arises between previously reported $[(L)_2SbF_2]^+$ compounds and $[(L^{Dipp})_2SbF_2]^+$ (**4**) is most probably the consequence of the axial position of F^- ligands in (**4**). In the case of $[(R_2Ir)_2SbF_2]^+$ and $[(R_2Pt)_2SbF_2]^+$, the metal ligands are in the axial position and both F^- ligands are in the equatorial position, with the $F_{eq.}$–Sb–$F_{eq.}$ angles of 83.7(8)° and 89.8(4)°, respectively.[34,36] Moreover, in $[(bipy)SbF_2]^+$, the positions of the F^- ligands are both in the axial and equatorial positions due to steric limitations of the (bipy) ligand, with F_{eq}–Sb–F_{ax} angle of 83.92(6)°.[35]

Table 2 Crystal data and structure refinement for (1), (2), (4) and (5)

	(1)	(2)	(4)	(5)
CCDC ref. code	1523950	1454012	1454013	1523951
Formula	$C_{27}H_{37}N_2{\cdot}F_4Sb{\cdot}C_2H_3N$	$C_6H_{16}F_3N_2Sb$	$C_{54}H_{72}F_2N_4Sb{\cdot}F_4Sb{\cdot}C_6H_6$	$C_{27}H_{35}Cl_2N_2{\cdot}C_7H_8{\cdot}F_4Sb$
FW [g mol]	628.39	294.96	1212.76	748.35
Crystal system	Orthorhombic	Monoclinic	Triclinic	Monoclinic
Space group	*Pnma*	$P2_1/n$	$P\bar{1}$	$P2_1/c$
a [Å]	21.3988(4)	5.9966(1)	10.5992(1)	11.0739(1)
b [Å]	13.5732(3)	27.9637(3)	15.5739(2)	19.2629(2)
c [Å]	10.4153(2)	6.4187(1)	19.6928(2)	17.4089(2)
α [°]	90	90	112.660(1)	90
β [°]	90	106.031(1)	95.754(1)	106.0196(9)
γ [°]	90	90	90.099(1)	90
V [Å^3]	3025.13(11)	1034.48(3)	2981.78(6)	3569.38(6)
Z	4	4	2	4
Reflections collected	40 036	41 386	71 296	21 917
Independ. reflect., R(int)	2830, 0.088	2071, 0.070	10 675, 0.043	6306, 0.047
T [K]	150	150	150	150
μ [mm^{-1}]	7.622	21.224	7.655	7.890
Final R indices [$I > 2\sigma(I)$]	$R = 0.059$	$R = 0.024$	$R = 0.040$	$R = 0.056$
	w$R = 0.148$	w$R = 0.063$	w$R = 0.108$	w$R = 0.159$
R indices (all data)	$R = 0.060$	$R = 0.025$	$R = 0.042$	$R = 0.059$

In contrast to the previous reports, the fluorides are in axial positions in the $[(L^{Dipp})_2SbF_2]^+$ cation of (**4**), with the F_{ax}–Sb–F_{ax} angle 149.16(9)°. This explains the elongation of both Sb–F distances in $[(L^{Dipp})_2SbF_2]^+$ (**4**) (2.029(2) and 2.020(2) Å), in comparison to 1.95(2) and 1.98(2) Å in $[(R_2Ir)_2SbF_2]^+$, 1.932(2) and 1.934(2) Å in $[(R_2Pt)_2SbF_2]^+$ and 1.933(1) and 1.939(1) Å in $[(bipy)SbF_2]^+$. Observed distances are typical for AX_4E disphenoidal geometry and in accordance with the VSEPR model, where the axial positions are more crowded than the equatorial positions. Thus, to minimize overlap with their neighbours, the axial bond-pair domains are farther from the central core than the equatorial bond domains in the structure.[40]

Raman analysis of products

Raman spectroscopy was used in order to detect the antimony species present in the sample, but due to extensive vibrations of the (L^{Dipp}) ligand it is difficult, if not impossible, to assign those species. Raman active vibrational frequencies observed for pyramidal SbF_3 in the matrix are reported at 654(m), 259(m) and 624(s) cm^{-1}.[43] The only coordination compound with neutral SbF_3 species that we were able to isolate was $[SbF_3(tmen)]$ (**2**), where the bands at 555 and 568 cm^{-1} could be attributed to the vibrations of SbF_3 (ESI S14†). Other synthesized products contain the monomeric $[SbF_4]^-$ anion, which is formed in cases where large $[NEt_4]^+$ or $[NBu_4]^+$ cations were used. The reported Raman active vibrational frequencies for the $[SbF_4]^-$ anion observed for $[Et_4N]^+[SbF_4]^-$ are 586(s), 552(mw), 436(mw), 380(sh), 280(w), 258(w) and 212(w, sh) cm^{-1}.[43] In $[(L^{Dipp})H]^+[SbF_4]^-$ (**1**) the band at 607 cm^{-1} could be probably attributed to the vibrations of $[SbF_4]^-$ (ESI S7†) and similarly, the band at 594 cm^{-1} in the $[(Cl_2L^{Dipp})H]^+[SbF_4]^-$ compound (**5**) (ESI S29†). The most interesting product $[(L^{Dipp})_2SbF_2]^+[SbF_4]^-$ (**4**) is also the most difficult to assign. The only product reporting heavily polarized SbF_3 species that could be reported as the $[SbF_2]^+$ cation with Raman spectroscopy was labeled as the SbF_3SbF_5 adduct, with the Raman band at 605(ms) assigned to the $[SbF_2]^+$ cation.[44] However, later research on the crystal structure of the SbF_3SbF_5 adduct showed that the $[SbF_2]^+$ cation cannot be distinguished from the structure.[45] The band at 611 cm^{-1} could probably be assigned to the vibration of $[SbF_4]^-$ (ESI S24†). Due to the complicated Raman spectrum of the ligand, and the non-existence of reliable $[SbF_2]^+$ Raman spectra, it is currently impossible to assign bands to the cationic antimony species in the $[(L^{Dipp})_2SbF_2]^+[SbF_4]^-$ product (**4**). Thus, Raman spectra of $[SbF_2]^+$ species remains an unsolved problem.

Experimental section

General information

All experiments and manipulations were carried out under a dry argon atmosphere, either in a glove box (<0.1 ppm of H_2O and O_2) or by using a standard Schlenk techniques. Toluene (Fischer Chemical, 99.99%) and tetrahydrofuran (Sigma-Aldrich ≥99.9%) were dried under a mixture of sodium and benzophenone for at least two days, distilled under argon atmosphere and stored over 3 Å molecular sieves. Acetonitrile (Merck, ≥99.9%) and deuterated solvents were dried over 3 Å molecular sieves (at least 20% w/w) and stored in the glove box. Glassware was oven-dried overnight at 150 °C prior to use.

Manipulation and preparation of starting materials. SbF_3 (Alfa Aesar, ≥99.0%) was purified by sublimation prior to use. (L^{Dipp}) and (Cl_2L^{Dipp}) were synthesised after standard literature procedures.[46,47] Tmen (Alfa Aesar, 99.0%) was distilled under argon atmosphere and stored in a Schlenk flask. 1,2-Dimethoxyethane (Fischer Scientific, ≥99.0%) was dried over 3 Å molecular sieves (at least 20% w/w) and stored in the glove box.

NMR spectroscopy. Samples were loaded into NMR tubes in a glove box under argon atmosphere. NMR spectra (^{1}H, ^{19}F

This journal is © The Royal Society of Chemistry 2017

and ^{13}C) were recorded at the Slovenian NMR Centre of the National Institute of Chemistry (Agilent Technologies Unity Inova 300 MHz; ^{1}H at 302 MHz, ^{19}F at 285.1 MHz and ^{13}C at 79.16 MHz). The chemical shifts were referenced as follows: ^{1}H and ^{13}C to residual signals of deuterated solvent peaks and ^{19}F to $CFCl_3$ as an external standard.

Raman spectroscopy. Raman spectra with a resolution of 0.5 cm^{-1} were recorded at room temperature on a Horiba Jobin Yvon Labram-HR spectrometer coupled with an Olympus BXFM-ILHS microscope. Samples were excited by the 633 nm emission line of a 24.3 mW He–Ne laser with a power output of 14 mW on the sample. The samples were loaded inside the glove box into 0.3 mm quartz capillaries, which were previously vacuum-dried. The spectra obtained from the powdered samples corresponded completely to the spectra taken from several randomly oriented single crystals, the identities of which were additionally confirmed by the unit cell measurement on the single-crystal X-ray diffractometer.

Crystal structure determination. Single-crystal data for all compounds were collected on a Gemini A diffractometer equipped with an Atlas CCD detector, using graphite monochromated Cu Kα radiation. The data were treated using the CrysAlisPro software suite program package.[48] Analytical absorption correction was applied to all data sets.[49] Structures were solved with the SHELXT program.[50] Structure refinement was performed with the SHELXL software,[51] implemented in the program package Olex2.[52] Figures were prepared using *Diamond* 4.0 software.[53]

CHN elemental analysis. Since the compounds are moisture sensitive, they were transferred into silver foils in a glove box under argon atmosphere. Carbon, hydrogen and nitrogen contents were determined using a CHNS elemental analyser, vario EL cube (Elementar), operating in the CHN mode.

Synthesis of products

Synthesis of $[(L^{Dipp})H]^+[SbF_4]^-$ (1). MeCN (50 mL) was added to the mixture of SbF_3 (n = 1.0 mmol; m = 178 mg) and (L^{Dipp}) (n = 1.0 mmol; 1 eq.; m = 388 mg) in a Schlenk flask at room temperature. Reactants were stirred for 16 hours. A small amount of observed precipitate was removed by filtration using Celite®. The solvent was concentrated and placed in the refrigerator at 5 °C to obtain crystals suitable for X-ray diffraction analysis. Yield (420 mg, 71%). **^{1}H NMR** (303 MHz, CD_3CN) δ 9.21 (1H, t, J = 1.6 Hz, N–C(H)–N), 7.92 (2H, d, J = 1.6 Hz, CH═CH), 7.70–7.60 (2H, m, *p*-ArH), 7.50–7.45 (4H, m, *m*-ArH), 2.42 (4H, hept, J = 6.8 Hz, CH), 1.27 (12H, d, J = 6.8 Hz, $(CH_3)_2$), 1.20 (12H, d, J = 6.9 Hz, $(CH_3)_2$) ppm. **^{19}F NMR** (285.1 MHz, THF-d^8, 25 °C): δ −57.30 (4F, s, SbF_4^-) ppm. **^{13}C NMR** (76 MHz, CD_3CN) δ 146.43, 139.35, 133.16, 131.00, 127.16, 125.75, 29.96, 24.56, 23.94. **Anal. Calcd for $C_{27}H_{37}F_4N_2Sb \times 0.5CH_3CN$ (606.71):** C, 55.32; H, 6.38; N, 5.76; Found: C, 55.49; H, 6.55; N, 5.64

Alternative synthesis of $[(L^{Dipp})H]^+[SbF_4]^-$ (1):

THF (40 mL) was added to the mixture of $[SbF_3(tmen)]$ (n = 1.0 mmol; m = 294 mg) and (L^{Dipp}) (n = 1.0 mmol; 1 eq.; m = 388 mg) in a Schlenk flask at room temperature. Reactants were stirred for 16 hours. A small amount of observed precipitate was removed by filtration using Celite®. The solvent was removed under vacuum. The white product was dissolved in acetonitrile and placed in the refrigerator at 5 °C to obtain crystals suitable for X-ray diffraction analysis.

Synthesis of $[SbF_3(tmen)]$ (2). SbF_3 (n = 5.735 mmol; m = 1025 mg) was weighed into a 250 mL Schlenk flask and approximately 100 mL of THF was added. Tmen (*N*,*N*,*N*′,*N*′-tetramethylethane-1,2-diamine; n = 17.206 mmol, 3 eq.; m = 2000 mg; ρ = 0.7765 mg μL^{-1}; V = 2575.6 μL) was added with a syringe. Reactants were left stirring at room temperature for 16 hours and a small amount of white precipitate remained. The reaction mixture was filtered, followed by concentration. The flask was placed in the refrigerator at 5 °C, and colourless monocrystals suitable for X-ray diffraction analysis were obtained. Yield (1.54 g, 91%). **^{1}H NMR** (302 MHz, THF-d^8, 25 °C): δ 2.54 (4H, s, CH_2), 2.28 (12H, s, CH_3) ppm. **^{19}F NMR** (285.05 MHz, THF-d^8, 25 °C): δ −85.10 (3F, s, SbF_3) ppm. **^{1}H NMR** (302 MHz, C_6D_6, 25 °C): δ 1.82 (12H, s, CH_3), 1.71 (4H, s, CH_2) ppm. **^{19}F NMR** (285.05 MHz, C_6D_6, 25 °C): δ −84.91 (3F, s, SbF_3) ppm.

Synthesis of $[(L^{Dipp})SbF_3]$ (3). Reaction "$[SbF_3(tmen)]$ + (L^{Dipp}) → $[(L^{Dipp})SbF_3]$":

^{1}H NMR (302 MHz, C_6D_6, 25 °C): δ 7.31–7.23 (2H, m, ArH), 7.19–7.13 (11H, m, ArH + residual C_6D_6), 6.55 (2H, s, CH═CH), 2.96 (4H, hept, J = 6.8 Hz, CH), 1.34 (12H, d, J = 6.8 Hz, $(CH_3)_2$), 1.14 (12H, d, J = 6.9 Hz, $(CH_3)_2$) ppm.**^{19}F NMR** (285.05 MHz, C_6D_6, 25 °C): δ −84.17 (3F, s, SbF_3) ppm. **^{13}C NMR** (76 MHz, C_6D_6, 25 °C): δ 146.32, 137.29, 129.54, 123.79, 122.00, 28.80, 24.24, 24.18.

Reaction "SbF_3 + (L^{Dipp}) + 2dme → $[(L^{Dipp})SbF_3]$":

^{1}H NMR (302 MHz, C_6D_6, 25 °C): δ 7.24–7.05 (7H, m, ArH + residual C_6D_6), 6.47 (2H, s, CH═CH), 2.94 (4H, hept, J = 6.8 Hz, CH), 1.45 (12H, d, J = 6.8 Hz, $(CH_3)_2$), 1.02 (12H, d, J = 6.9 Hz, $(CH_3)_2$) ppm. **^{19}F NMR** (285.05 MHz, C_6D_6, 25 °C): δ −83.78 (3F, s, SbF_3) ppm.

Synthesis of $[(L^{Dipp})_2SbF_2]^+[SbF_4]^-$ (4). Toluene (100 mL) was added to the mixture of $[SbF_3(tmen)]$ (n = 1.0 mmol; m = 294 mg) and (L^{Dipp}) (n = 1.0 mmol; 1 eq.; m = 388 mg) in a Schelnk flask and heated to 60 °C. Reactants were stirred for 16 hours. A small amount of observed precipitate was removed by filtration using Celite®. The slightly concentrated reaction mixture was stored at 5 °C, which afforded monocrystals that were suitable for X-ray diffraction analysis. Yield (434 mg, 77%). **Anal. Calcd for $C_{54}H_{72}F_6N_4Sb_2 \times C_6H_5CH_3$ (1226.82):** C, 59.72; H, 6.57; N, 4.57; Found: C, 59.89; H, 6.51; N, 4.59.

Synthesis of $[(Cl_2L^{Dipp})H]^+[SbF_4]^-$ (5). Toluene (100 mL) was added to the mixture of $[SbF_3(tmen)]$ (n = 0.435 mmol; m = 128 mg) and (Cl_2L^{Dipp}) (n = 0.435 mmol; 1 eq.; m = 200 mg) in a Schelnk flask and heated to 60 °C. The reactants were stirred for 16 hours and a small amount of observed precipitate was removed by filtration using Celite®. The slightly concentrated reaction mixture was stored at 5 °C, from which suitable monocrystals were obtained for X-ray diffraction analysis. Yield (198 mg, 69%). **^{1}H NMR** (303 MHz, THF-d_8) δ 11.62

(1H, s, N–C(H)–N), 7.65–7.55 (2H, m, *p*-ArH), 7.47–7.40 (4H, m, *m*-ArH), 2.45 (4H, hept, J = 6.7 Hz, CH), 1.30–1.25 (24H, m, $(CH_3)_2$) ppm. **^{19}F NMR** (285.1 MHz, THF-d^8, 25 °C): δ −64.87 (4F, s, SbF_4^-) ppm. **Anal. Calcd for $C_{27}H_{35}Cl_2F_4N_2Sb \times 0.25C_6H_5CH_3$ (677.13)**: C, 59.72; H, 6.57; N, 4.57; Found: C, 59.89; H, 6.51; N, 4.59.

Conclusions

The reaction of SbF_3 with (L^{Dipp}) in THF or MeCN produced $[(L^{Dipp})H]^+[SbF_4]^-$ (**1**). Reactions performed in CH_3CN *vs.* CD_3CN showed that protons were abstracted from the solvent molecules. Additionally, the reaction in CD_3CN did not show signals for imidazolium backbone protons, suggesting H/D exchange with solvent molecules. Reaction of SbF_3 with tmen afforded the [SbF_3(tmen)] complex (**2**), which can be used as a SbF_3 synthon in non-polar solvents (*e.g.* toluene). Subsequent reaction of (**2**) with (L^{Dipp}) in toluene or benzene yielded the auto-ionization product (**4**) with the $[(L^{Dipp})_2SbF_2]^+$ cation stabilized by two NHC ligands, one of which underwent rearrangement to MIC. Product (**4**) was formed through the neutral intermediate product $[(L^{Dipp})SbF_3]$ (**3**), stable only in solution, and its existence was confirmed with ^{1}H and ^{19}F NMR solution spectroscopy. It is surprising that no evidence of product (**4**) formation can be observed from the solution NMR analysis, which would suggest that the conversion of (**3**) to (**4**) is fast and when formed, it immediately precipitates out of solution. Both products (**3**) and (**4**) were obtained by the presence of either tmen or dme in the system. The reaction mechanism was proven to be independent of tmen, which was suggested to be involved in a similar rearrangement in previous research,[38] and just like dme, it serves only as an auxiliary ligand to help with SbF_3 solubility in non-polar solvents. To obtain the C2–C2 coordinated cation of product (**4**), we attempted to perform a reaction with the (Cl_2L^{Dipp}) ligand, where the imidazolium backbone is unavailable for coordination. The reaction proceeded to the formation of the $[(Cl_2L^{Dipp})H]^+[SbF_4]^-$ salt (**5**), and all other attempts to obtain the $[(Cl_2L^{Dipp})_2SbF_2]^+$ cation were unsuccessful. Structural analysis of (**4**) is in full accordance with the VSEPR model, where the more electronegative F^- ligands are both in axial positions, which is not the case for the other three reported $[(L)_2SbF_2]^+$ cations.[34–36] Product (**4**) also represents, to the best of our knowledge, the first example of a reaction where the N-heterocyclic carbene ligand facilitates the auto-ionization product on a fluorido substrate.

Acknowledgements

Funding from Slovenian Research Agency is gratefully acknowledged.

Authors would also like to thank Slovenian NMR Centre of National Institute of Chemistry for all their resources.

References

1 M. N. Hopkinson, C. Richter, M. Schedler and F. Glorius, *Nature*, 2014, **510**, 485.
2 A. J. Arduengo III, F. Davidson, R. Krafczyk, W. J. Marshall and R. Schmutzler, *Monatsh. Chem.*, 2000, **131**, 251.
3 T. Böttcher, S. Steinhauer, N. Allefeld, B. Hoge, B. Neumann, H. G. Stammler, B. S. Bassil, M. Winter, N. W. Mitzel and G.-V. Röschenthaler, *Dalton Trans.*, 2014, **43**, 2979.
4 T. Böttcher, O. Shyshkov, M. Bremer, B. S. Bassil and G.-V. Röschenthaler, *Organometallics*, 2011, **31**, 1278.
5 Y. Wang and G. H. Robinson, *Dalton Trans.*, 2012, **41**, 337.
6 R. Kretschmer, D. A. Ruiz, C. E. Moore, A. L. Rheingold and G. Bertrand, *Angew. Chem., Int. Ed.*, 2014, **53**, 8176.
7 F. D. Henne, A. T. Dickschat, F. Hennersdorf, K. O. Feldmann and J. J. Weigand, *Inorg. Chem.*, 2015, **54**, 6849.
8 A. El-Hellani, J. Monot, R. Guillot, C. Bour and V. Gandon, *Inorg. Chem.*, 2013, **52**, 506.
9 M. Imran, B. Neumann, H.-G. Stammler, U. Monkowius, M. Ertl and N. W. Mitzel, *Dalton Trans.*, 2014, **43**, 1267.
10 M. A. Tershansy, A. M. Goforth, M. D. Smith and H.-C. Zur Loye, *J. Chem. Crystallogr.*, 2008, **38**, 453.
11 N. W. Alcock, M. Ravindran and G. R. Willey, *J. Chem. Soc., Chem. Commun.*, 1989, 1063.
12 R. D. Rogers, A. H. Bond, S. Aguinaga and A. Reyes, *J. Am. Chem. Soc.*, 1992, **114**, 2967.
13 F. W. B. Einstein and R. D. G. Jones, *Inorg. Chem.*, 1973, **12**, 1690.
14 P. Farina, W. Levason and G. Reid, *Polyhedron*, 2013, **55**, 102.
15 S. L. Benjamin, A. Hyslop, W. Levason and G. Reid, *J. Fluorine Chem.*, 2012, **137**, 77.
16 R. Bini, C. Chiappe, F. Marchetti, G. Pampaloni and S. Zacchini, *Inorg. Chem.*, 2010, **49**, 339.
17 R. Haiges, P. Deokar and K. O. Christe, *Z. Anorg. Allg. Chem.*, 2014, **640**, 1568.
18 J. Burt, W. Levason and G. Reid, *Coord. Chem. Rev.*, 2014, **260**, 65.
19 S. L. Benjamin, W. Levason and G. Reid, *Chem. Soc. Rev.*, 2013, **42**, 1460.
20 S. L. Benjamin, J. Burt, W. Levason, G. Reid and M. Webster, *J. Fluorine Chem.*, 2012, **135**, 108.
21 W. Levason, M. E. Light, S. Maheshwari, G. Reid and W. Zhang, *Dalton Trans.*, 2011, **40**, 5291.
22 A. J. Barton, N. J. Hill, W. Levason, B. Patel and G. Reid, *Chem. Commun.*, 2001, 95.
23 N. J. Hill, W. Levason and G. Reid, *Inorg. Chem.*, 2002, **41**, 2070.
24 M. S. Fonari, E. V. Ganin, V. O. Gelmboldt, J. Lipkowski, S. A. Kotlyar and G. L. Kamalov, *Acta Crystallogr., Sect. E: Struct. Rep. Online*, 2006, **62**, m1021.
25 N. A. Barnes, S. M. Godfrey, R. G. Pritchard and S. Ratcliffe, *Polyhedron*, 2010, **29**, 1822.

 This journal is © The Royal Society of Chemistry 2017

26 W. Levason, S. Maheshwari, R. Ratnani, G. Reid, M. Webster and W. Zhang, *Inorg. Chem.*, 2010, **49**, 9036.
27 F. Fairbrother, W. C. Frith and A. A. Woolf, *J. Chem. Soc.*, 1954, 1031.
28 F. Fairbrother, K. H. Grundy and A. Thompson, *J. Chem. Soc.*, 1965, 761.
29 H. C. Clark and H. J. Emeleus, *J. Chem. Soc.*, 1957, 2119.
30 A. A. Opalovskii and K. A. Khaldoyanidi, *B. Acad. Sci. USSR CH+*, 1973, **22**, 270.
31 A. F. Holleman, E. Wiberg and N. Wiberg, *Lehrbuch der anorganischen Chemie*, Walter de Gruyter, 2007.
32 C. Bour, J. Monot, S. Tang, R. Guillot, J. Farjon and V. Gandon, *Organometallics*, 2014, **33**, 594.
33 M. K. Denk and J. M. Rodezno, *J. Organomet. Chem.*, 2000, **608**, 122.
34 A. L. Balch, V. J. Catalano, M. A. Chatfield, J. K. Nagle, M. M. Olmstead and P. E. Reedy, *J. Am. Chem. Soc.*, 1991, **113**, 1252.
35 S. S. Chitnis, N. Burford and M. J. Ferguson, *Angew. Chem., Int. Ed.*, 2013, **52**, 2042.
36 H. Braunschweig, R. D. Dewhurst, F. Hupp and J. Wolf, *Chem. – Eur. J.*, 2015, **21**, 1860.
37 K. Schwedtmann, M. H. Holthausen, K.-O. Feldmann and J. J. Weigand, *Angew. Chem., Int. Ed.*, 2013, **52**, 14204.
38 A. A. Danopoulos, N. Tsoureas, J. A. Wright and M. E. Light, *Organometallics*, 2004, **23**, 166.
39 G. R. Fulmer, A. J. M. Miller, N. H. Sherden, H. E. Gottlieb, A. Nudelman, B. M. Stoltz, J. E. Bercaw and K. I. Goldberg, *Organometallics*, 2010, **29**, 2176.
40 R. J. Gillespie and I. Hargittai, *The VSEPR Model of Molecular Geometry*, Dover Publications, Incorporated, 2012.
41 A. J. Arduengo III, R. Krafczyk, R. Schmutzler, W. Mahler and W. J. Marshall, *Z. Anorg. Allg. Chem.*, 1999, **625**, 1813.
42 A. J. Edwards, *J. Chem. Soc. A*, 1970, 2751.
43 C. J. Adams and A. J. Downs, *J. Chem. Soc. A*, 1971, 1534.
44 T. Birchall, P. A. W. Dean, B. D. Valle and R. J. Gillespie, *Can. J. Chem.*, 1973, **51**, 667.
45 R. J. Gillespie, D. R. Slim and J. E. Vekris, *J. Chem. Soc., Dalton Trans.*, 1977, 971.
46 L. Hintermann, *Beilstein J. Org. Chem.*, 2007, **3**, 22.
47 A. J. Arduengo III, R. Krafczyk, R. Schmutzler, H. A. Craig, J. R. Goerlich, W. J. Marshall and M. Unverzagt, *Tetrahedron*, 1999, **55**, 14523.
48 *CrysAlisPro, Agilent Technologies, Version 1.171.37.33 (release 27-03-2014 CrysAlis171.NET) (compiled Mar 27 2014,17:12:48)*.
49 R. C. Clark and J. S. Reid, *Acta Crystallogr., Sect. A: Fundam. Crystallogr.*, 1995, **51**, 887–897.
50 G. M. Sheldrick, *Acta Crystallogr., Sect. A: Fundam. Crystallogr.*, 2015, **71**(1), 3.
51 G. M. Sheldrick, *Acta Crystallogr., Sect. C: Cryst. Struct. Commun.*, 2015, **71**(1), 3.
52 O. V. Dolomanov, L. J. Bourhis, R. J. Gildea, J. A. K. Howard and H. Puschmann, *J. Appl. Crystallogr.*, 2009, **42**(2), 339.
53 Diamond – Crystal and Molecular Structure Visualization, Crystal Impact - Dr H. Putz and Dr. K. Brandenburg GbR, Kreuzherrenstr. 102, 53227 Bonn, Germany http://www.crystalimpact.com/diamond.

Dalton Transactions

Supporting information

Small molecule activation: SbF_3 auto-ionization supported by transfer and mesoionic NHC rearrangement

B. Alič,[a, b] A. Štefančič[a, b] and G. Tavčar[a, b, *]

[a] *Jožef Stefan Institute, Jamova cesta 39, 1000 Ljubljana, Slovenia*

[b] *Jožef Stefan International Postgraduate School, Jamova cesta 39, 1000 Ljubljana, Slovenia*

(S2) Contents

(S3) $[(L^{Dipp})H]^+[SbF_4]^-$ (1) 3

(S4) 1H NMR spectrum of $[(L^{Dipp})H]^+[SbF_4]^-$ in CD_3CN, Frequency (MHz) 302.97: 4

(S5) ^{19}F NMR spectrum of $[(L^{Dipp})H]^+[SbF_4]^-$ in CD_3CN, Frequency (MHz) 285.05: 4

(S6) ^{13}C NMR spectrum of $[(L^{Dipp})H]^+[SbF_4]^-$ in CD_3CN, Frequency (MHz) 76.19: 5

(S7) Raman spetra of $[(L^{Dipp})H]^+[SbF_4]^-$ (1) 5

(S8) Superimposed spectra of reaction (L^{Dipp}) + SbF_3 -> $[(L^{Dipp})H]^+[SbF_4]^-$ (1) performed in CH_3CN *vs.* CD_3CN 6

(S9) $[SbF_3(tmen)]$ (2) 7

(S10) ^1H NMR spectrum of $[SbF_3(tmen)]$ complex in THF-d^8, Frequency (MHz) 302.97: 8

(S11) ^{19}F NMR spectrum of $[SbF_3(tmen)]$ complex in THF-d^8, Frequency (MHz) 285.05: 8

(S12) ^1H NMR spectrum of $[SbF_3(tmen)]$ complex in C_6D_6, Frequency (MHz) 302.97: 9

(S13) ^{19}F NMR spectrum of $[SbF_3(tmen)]$ complex in C_6D_6, Frequency (MHz) 285.05: 9

(S14) Raman spectra of $[SbF_3(tmen)]$ (2) 10

(S15) $[(L^{Dipp})SbF_3]$ (3) 11

(S16) ^1H NMR spectrum for reaction "$[SbF_3(tmen)]$ + (L^{Dipp}) –> $[(L^{Dipp})SbF_3]$" in C_6D_6, Frequency (MHz) 302.97: 12

(S17) ^{19}F NMR spectrum for reaction "$[SbF_3(tmen)]$ + (L^{Dipp}) –> $[(L^{Dipp})SbF_3]$" in C_6D_6, Frequency (MHz) 285.05: 12

(S18) ^{13}C NMR spectrum for reaction "$[SbF_3(tmen)]$+ (L^{Dipp}) –> $[(L^{Dipp})SbF_3]$" in C_6D_6, Frequency (MHz) 76.19: 13

(S19) ^1H NMR spectrum for reaction "$[SbF_3(tmen)]$ + (L^{Dipp}) + 2tmen –> $[(L^{Dipp})SbF_3]$" in C_6D_6, Frequency (MHz) 302.97: 13

(S20) ^{19}F NMR spectrum for reaction "$[SbF_3(tmen)]$ + (L^{Dipp}) + 2tmen –> $[(L^{Dipp})SbF_3]$" in C_6D_6, Frequency (MHz) 285.05: 14

(S21) ^1H NMR spectrum for reaction "SbF_3 + (L^{Dipp}) + 2dme –> $[(L^{Dipp})SbF_3]$" in C_6D_6, Frequency (MHz) 302.97: 14

(S22) ^{19}F NMR spectrum for reaction "SbF_3 + (L^{Dipp}) + 2dme –> $[(L^{Dipp})SbF_3]$" in C_6D_6, Frequency (MHz) 285.05: 15

(S23) $[(L^{Dipp})_2SbF_2]^+[SbF_4]^-$ (4) 16

(S24) Raman spectra of $[(L^{Dipp})_2SbF_2]^+[SbF_4]^-$ (4) 16

(S25) $[(Cl_2L^{Dipp})H]^+[SbF_4]^-$ (5) 17

(S26) ^1H NMR spectrum of $[(Cl_2L^{Dipp})H]^+[SbF_4]^-$ in THF-d^8, Frequency (MHz) 302.97: 18

(S27) ^{19}F NMR spectrum of $[(Cl_2L^{Dipp})H]^+[SbF_4]^-$ in THF-d^8, Frequency (MHz) 285.05: 18

(S28) ^1H NMR spectrum of $[(Cl_2L^{Dipp})H]^+[SbF_4]^-$ in C_6D_6, Frequency (MHz) 302.97: 19

(S29) Raman spectra of $[(Cl_2L^{Dipp})H]^+[SbF_4]^-$ (5) 19

(S30) CSD search details 20

(S3) $[(L^{Dipp})H]^+[SbF_4]^-$ (1)

Reaction "$[SbF_3(tmen)]$ + (L^{Dipp}) –> $[(L^{Dipp})H]^+[SbF_4]^-$":

^{1}H NMR spectrum CD_3CN

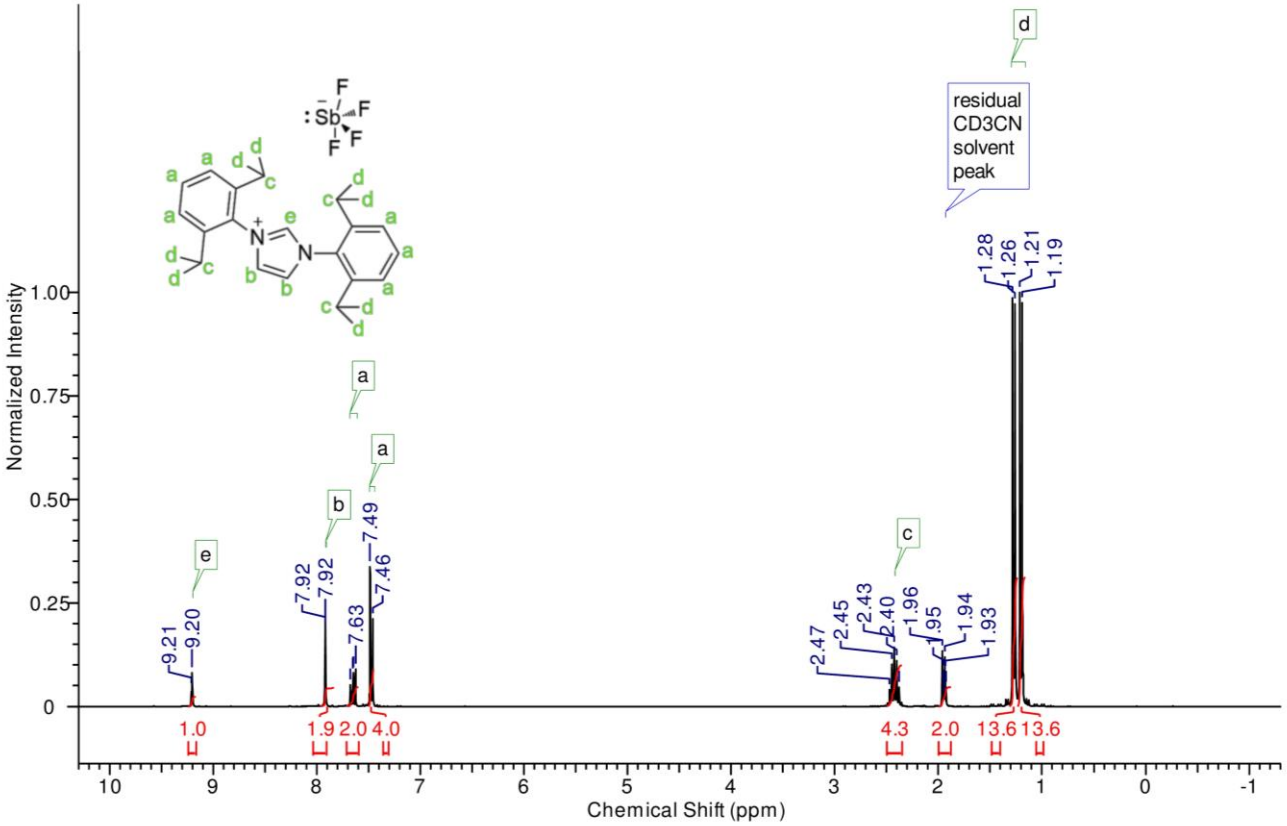
^{19}F spectrum NMR CD_3CN

^{13}C spectrum NMR CD_3CN

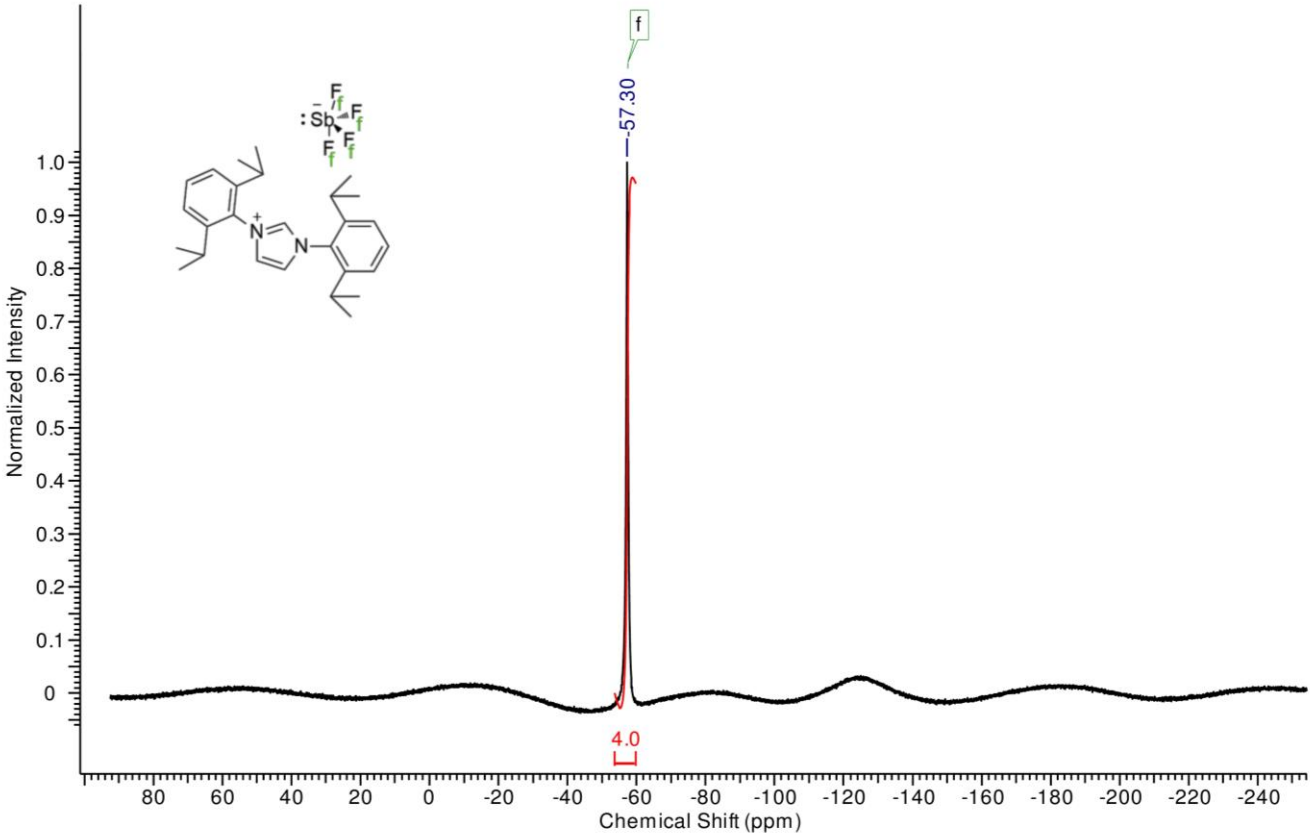
Raman spectrum

Superimposed spectra of reaction (L^{Dipp}) + SbF_3 -> $[(L^{Dipp})H]^+[SbF_4]^-$ (**1**) performed in CH_3CN *vs.* CD_3CN

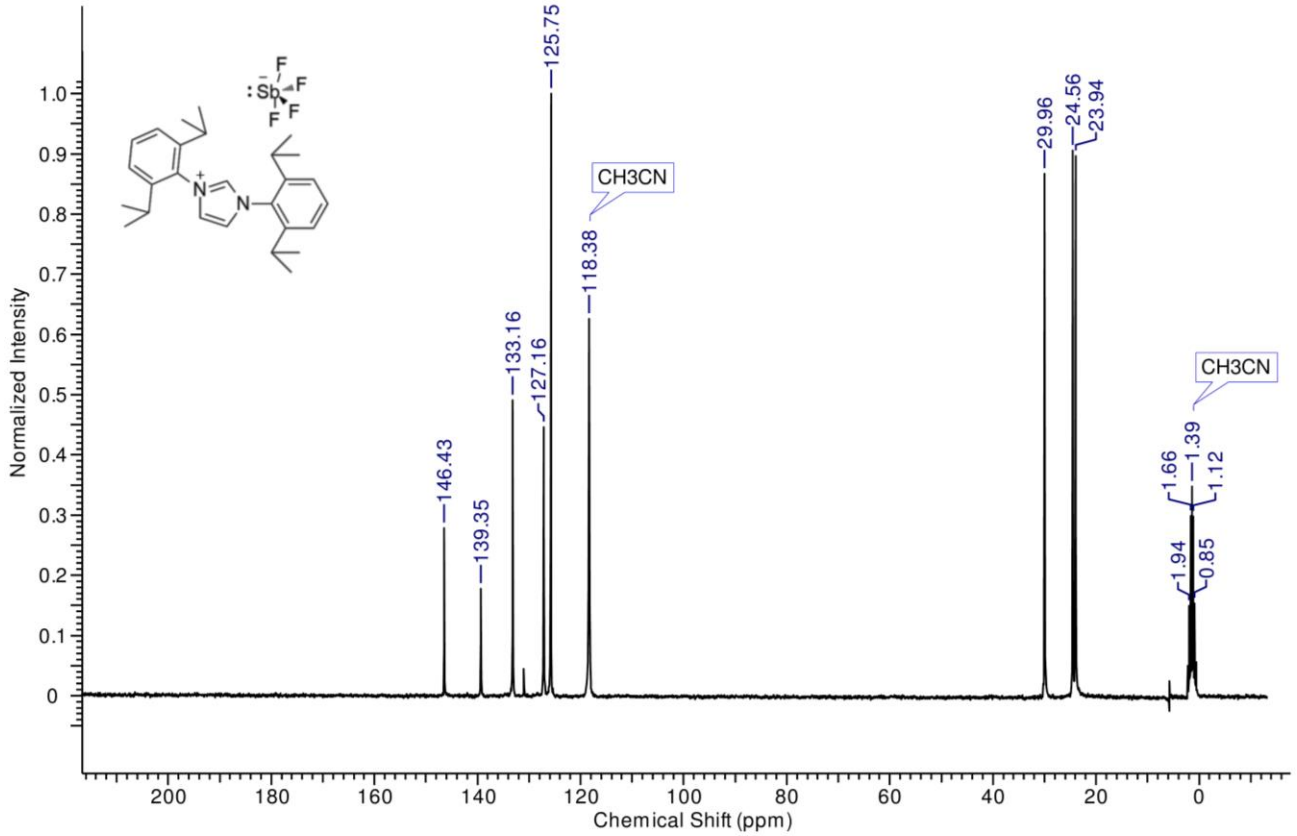
(S4) 1H NMR spectrum of $[(L^{Dipp})H]^+[SbF_4]^-$ in CD_3CN, Frequency (MHz) 302.97:



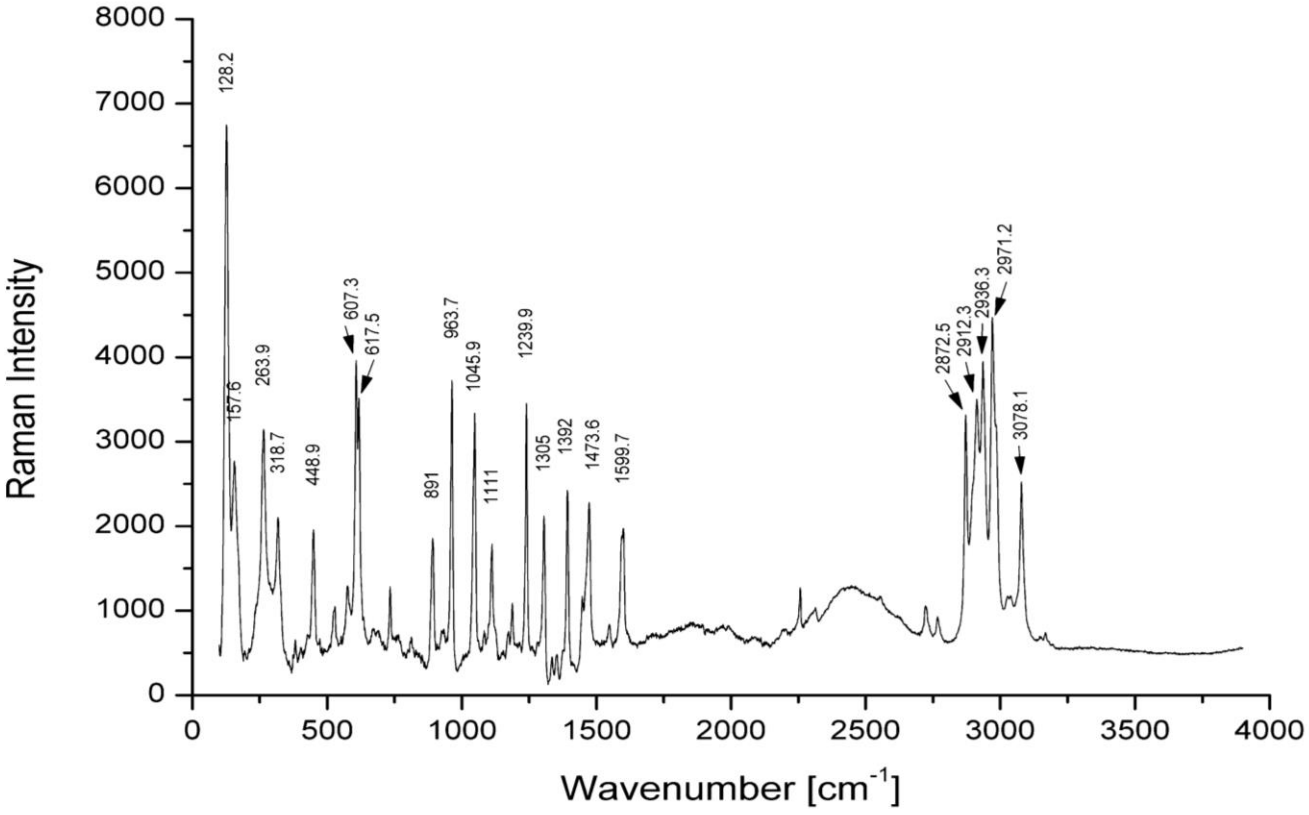
(S5) ^{19}F NMR spectrum of $[(L^{Dipp})H]^+[SbF_4]^-$ in CD_3CN, Frequency (MHz) 285.05:



(S6) ^{13}C NMR spectrum of $[(L^{Dipp})H]^+[SbF_4]^-$ in CD_3CN, Frequency (MHz) 76.19:



(S7) Raman spetra of $[(L^{Dipp})H]^+[SbF_4]^-$ (1)



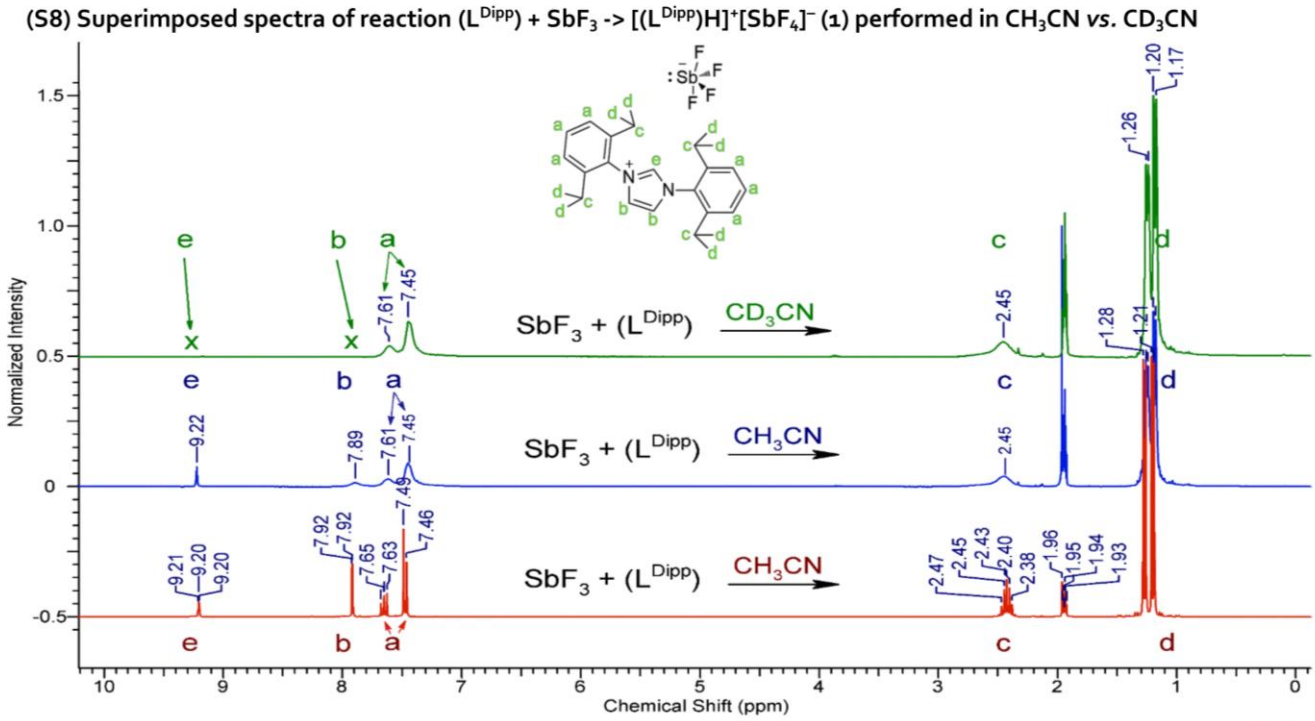


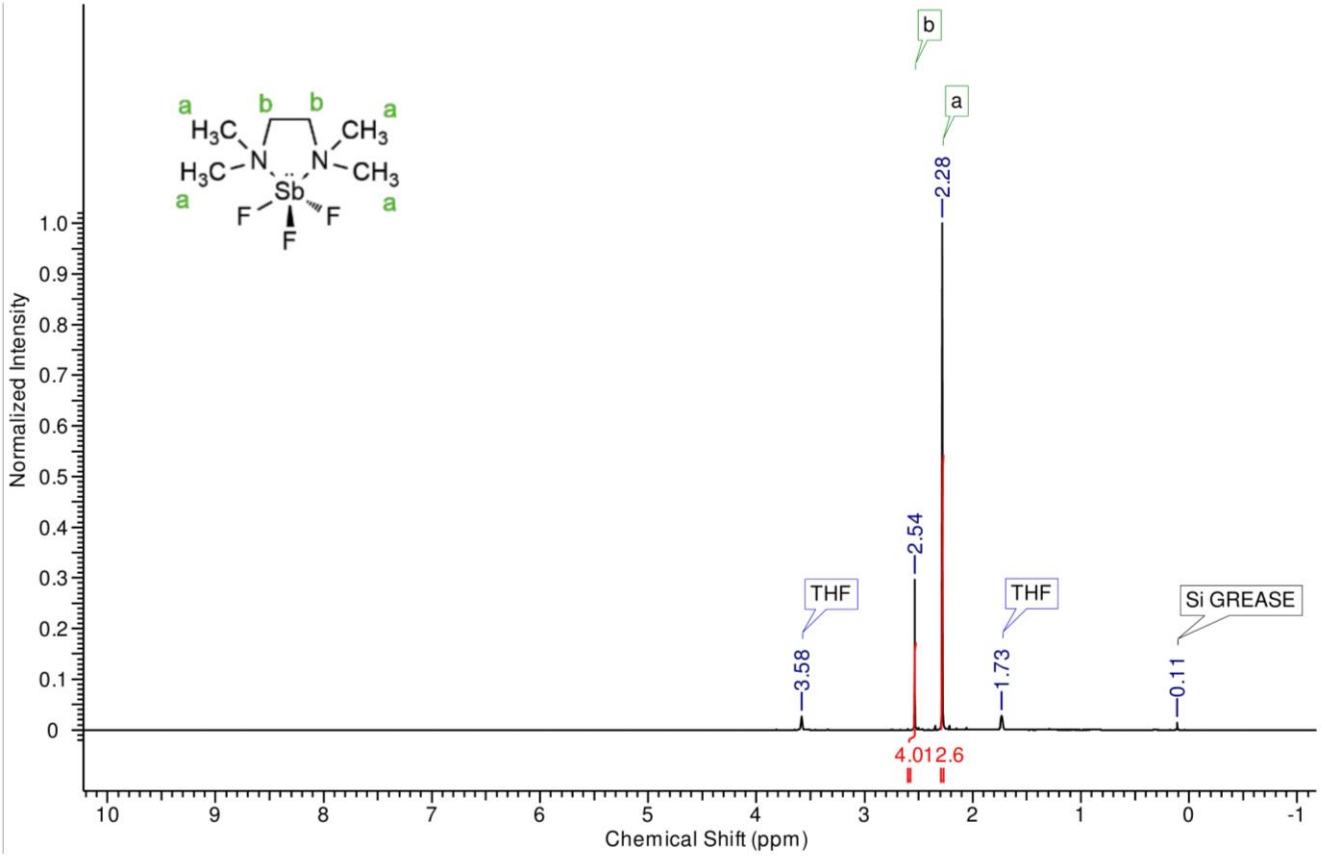
*Figure 1: Superimposed spectra of reaction "SbF_3 + (L^{Dipp})" performed in CH_3CN vs. CD_3CN. Reaction in CH_3CN (**blue**) shows all imidazolium peaks for protons (e) and (b) while reaction in CD_3CN (**green**) shows no imidazolium peaks, showing: **a)** proton (e) arrises from solvent molecule and **b)** all three imidazolium protons (e) and (b) undergo H/D exchange with deuterated solvent. **Red** spectra, for comparison, represents isolated product of [(L^{Dipp})H]$^+$[SbF_4]$^-$ (**1**)*

(S9) [SbF_3(tmen)] (2)

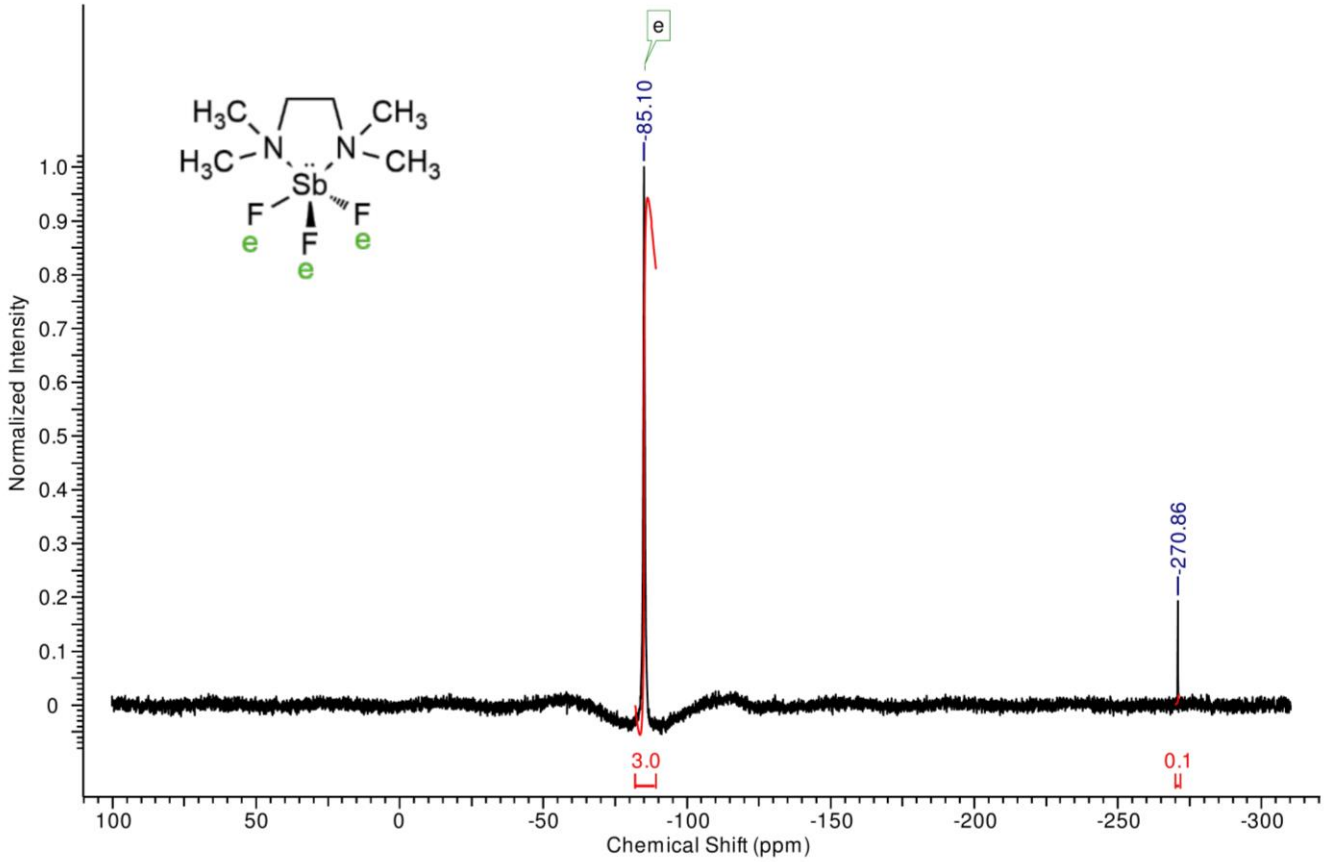
Reaction "SbF_3 + 3tmen + –> [SbF_3(tmen)]":

^{1}H NMR spectrum in THF-d^8
^{19}F NMR spectrum in THF-d^8
^{1}H NMR spectrum in C_6D_6
^{19}F NMR spectrum in C_6D_6
Raman spectrum

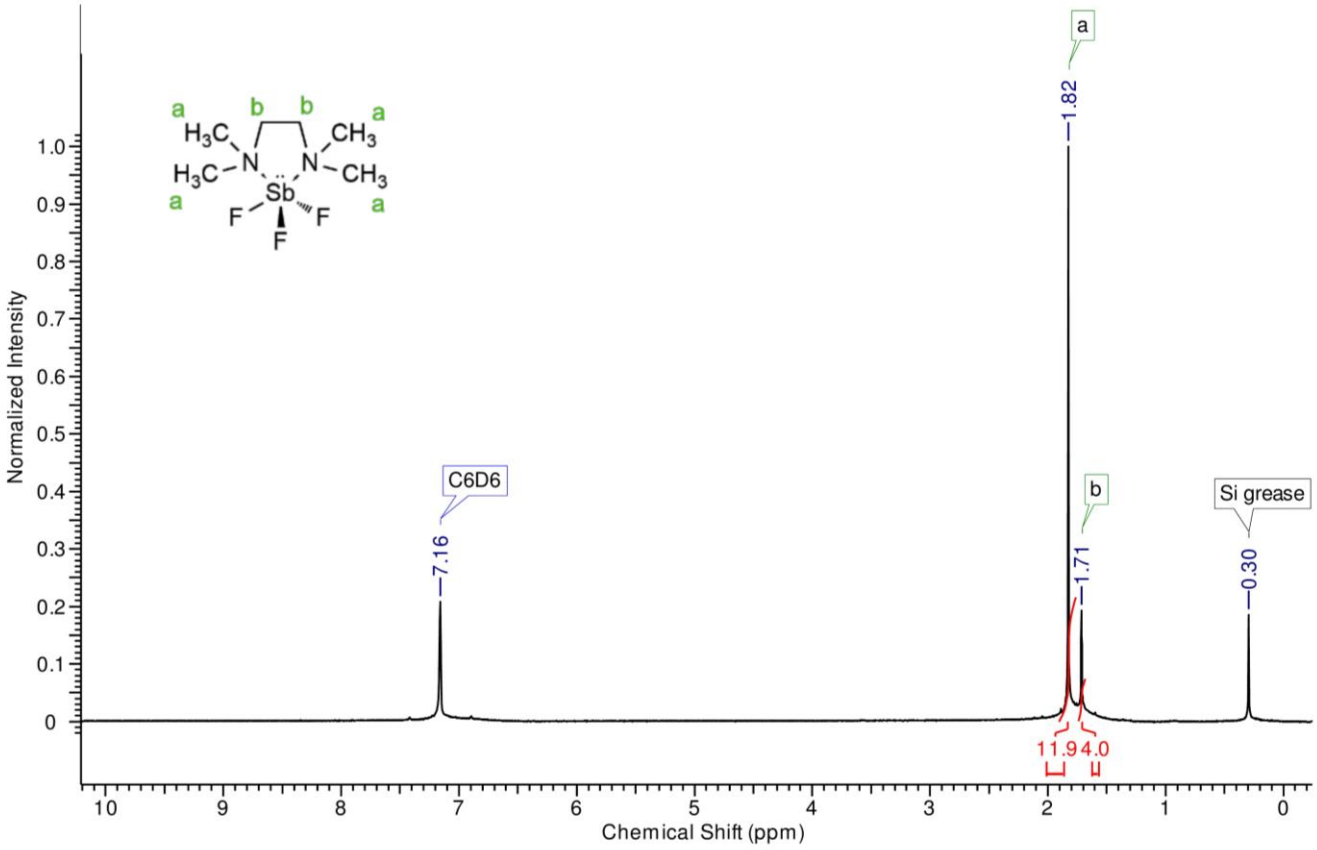
(S10) ^{1}H NMR spectrum of [SbF_3(tmen)] complex in THF-d^8, Frequency (MHz) 302.97:



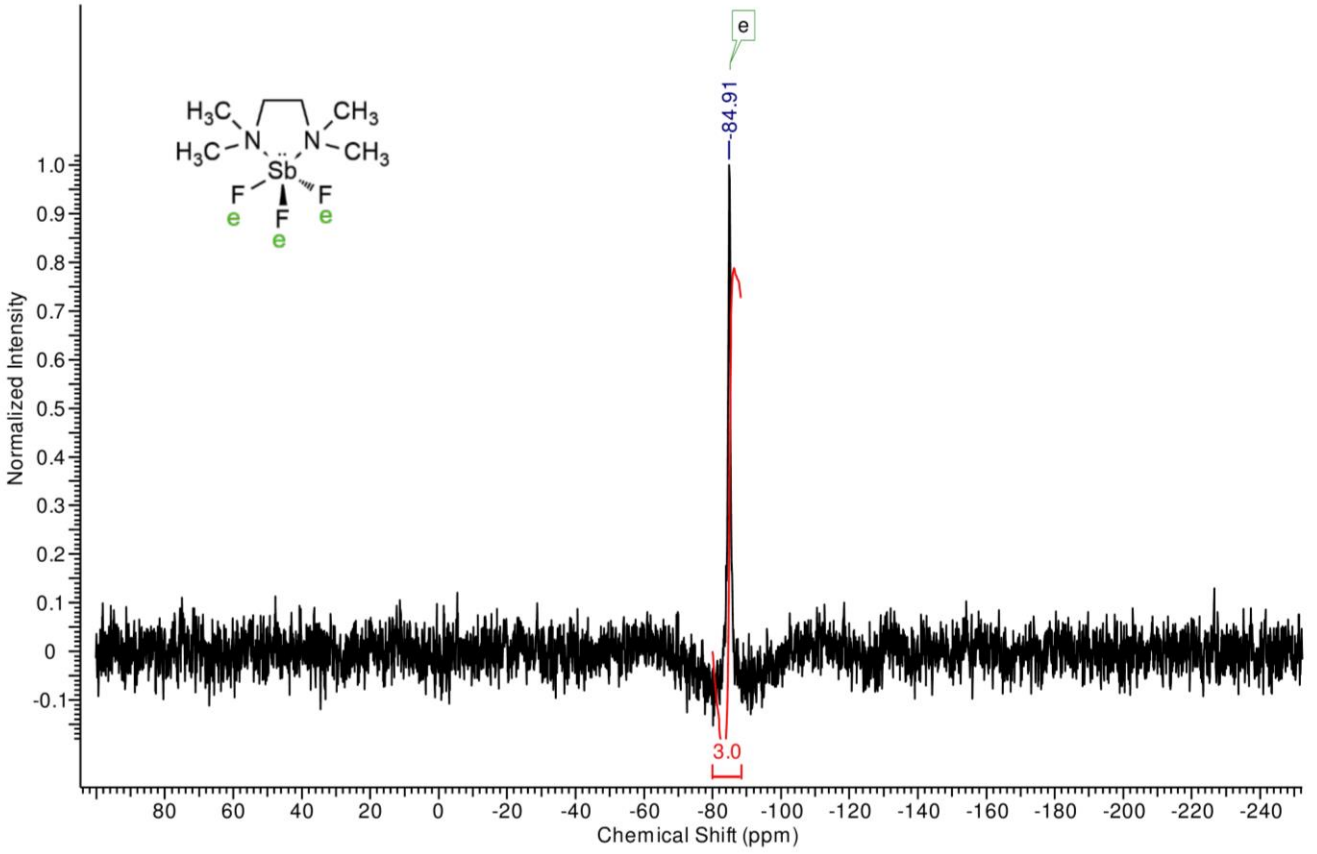
(S11) ^{19}F NMR spectrum of [SbF_3(tmen)] complex in THF-d^8, Frequency (MHz) 285.05:



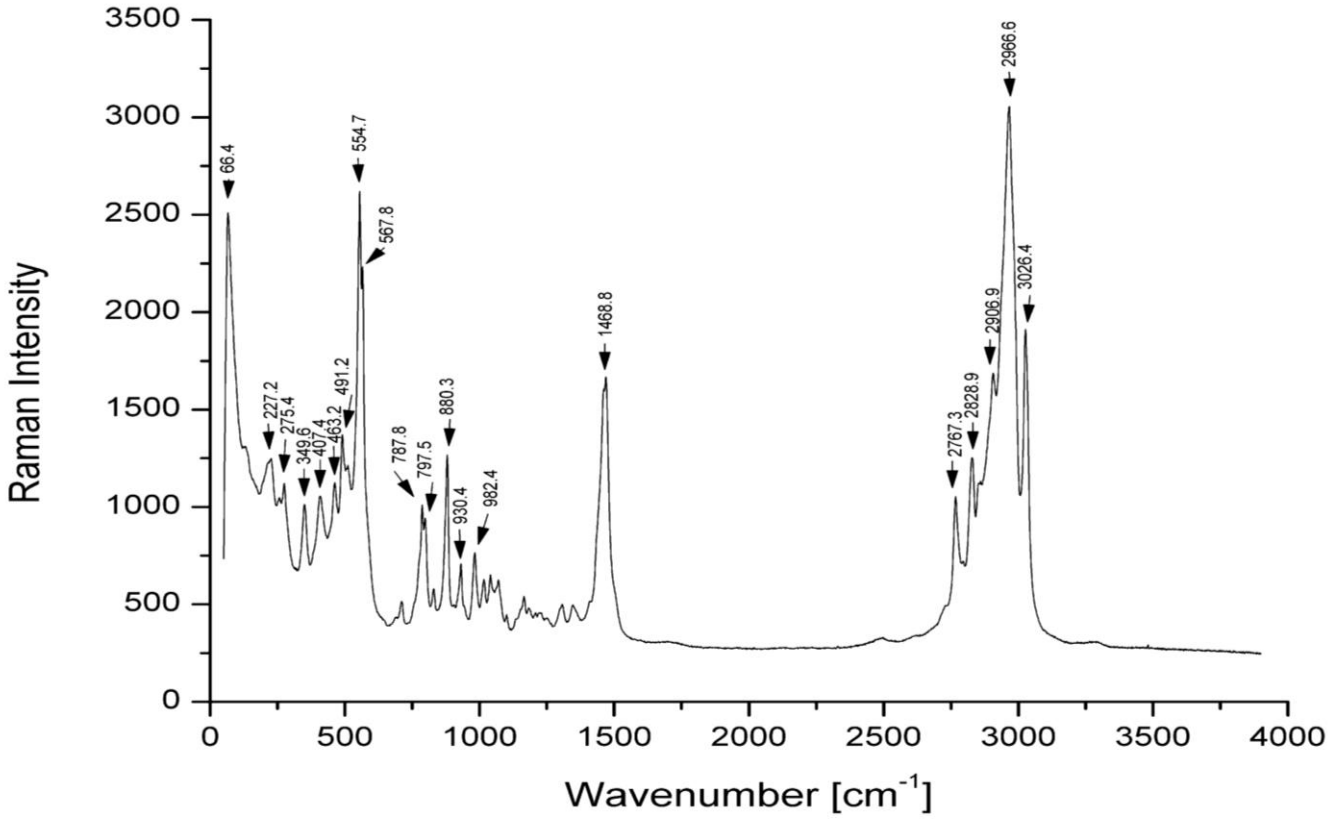
(S12) ^{1}H NMR spectrum of [SbF_3(tmen)] complex in C_6D_6, Frequency (MHz) 302.97:



(S13) ^{19}F NMR spectrum of [SbF_3(tmen)] complex in C_6D_6, Frequency (MHz) 285.05:



(S14) Raman spectra of [SbF_3(tmen)] (2)



(S15) [(L^{Dipp})SbF_3] (3)

Reaction "[SbF_3(tmen)] + (L^{Dipp}) –> [(L^{Dipp})SbF_3]":

^{1}H NMR spectrum in C_6D_6

^{19}F NMR spectrum in C_6D_6

^{13}C NMR spectrum in C_6D_6

Reaction "[SbF_3(tmen)] + (L^{Dipp}) +2tmen –> [(L^{Dipp})SbF_3]":

^{1}H NMR spectrum in C_6D_6

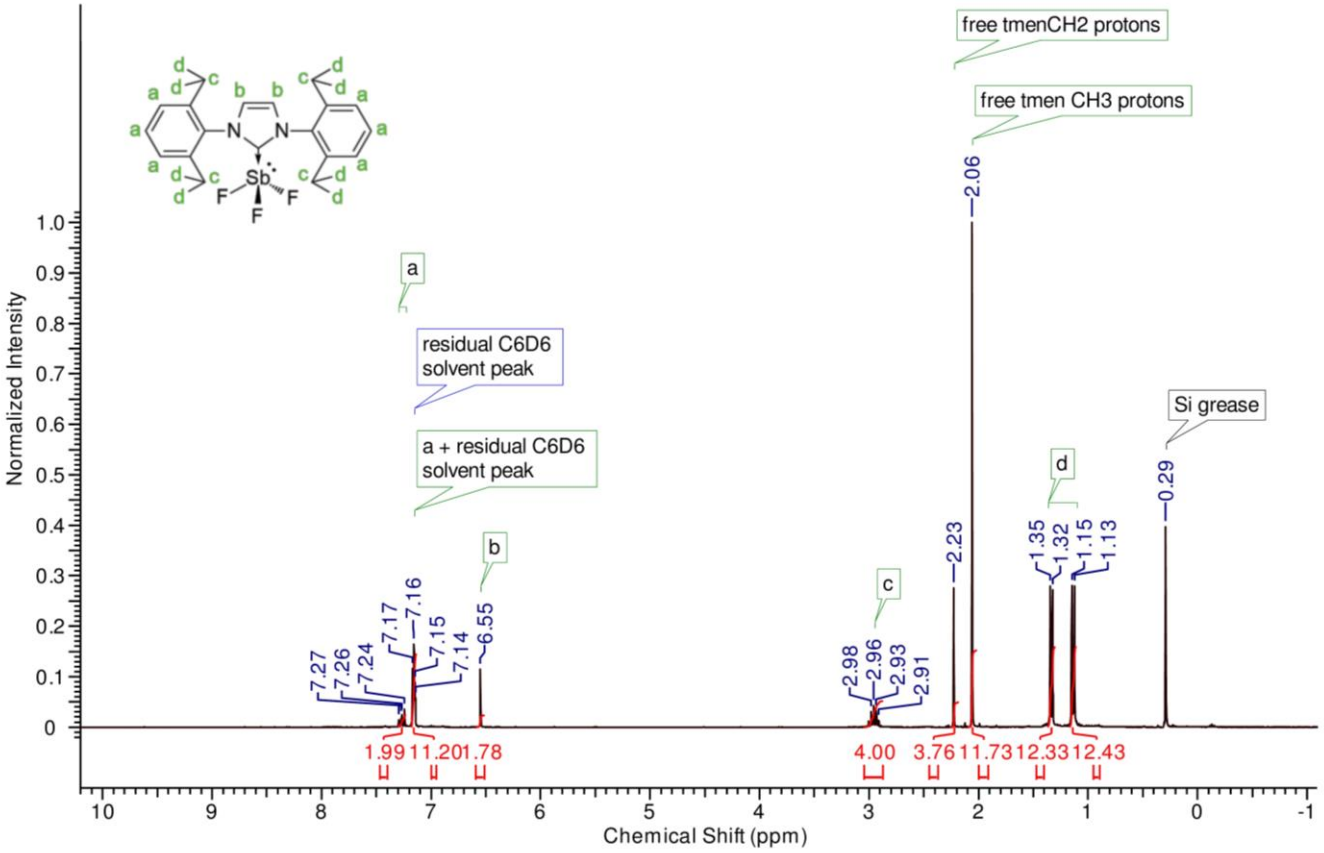
^{19}F NMR spectrum in C_6D_6

Reaction "SbF_3 + (L^{Dipp}) + 2dme –> [(L^{Dipp})SbF_3]":

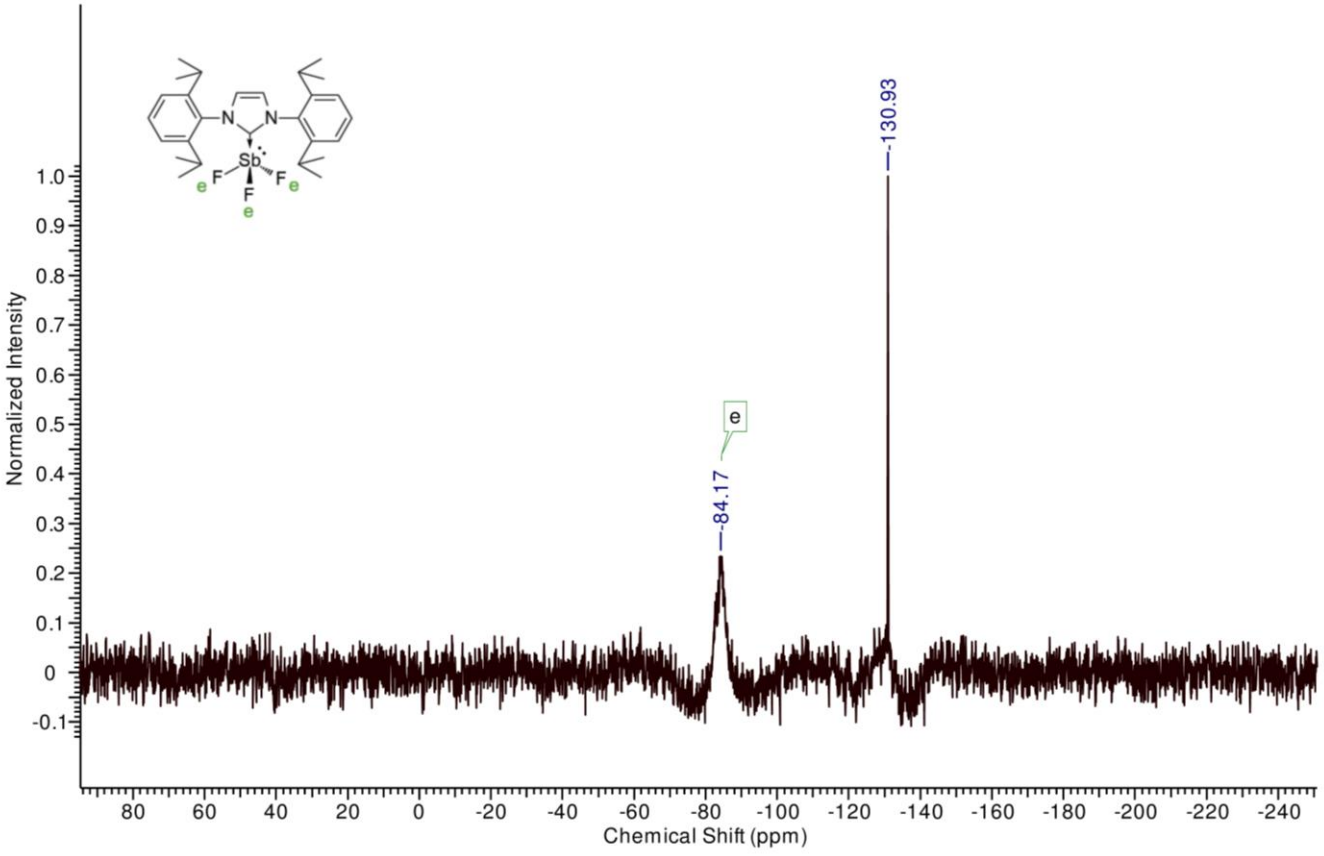
^{1}H NMR spectrum in C_6D_6

^{19}F NMR spectrum in C_6D_6

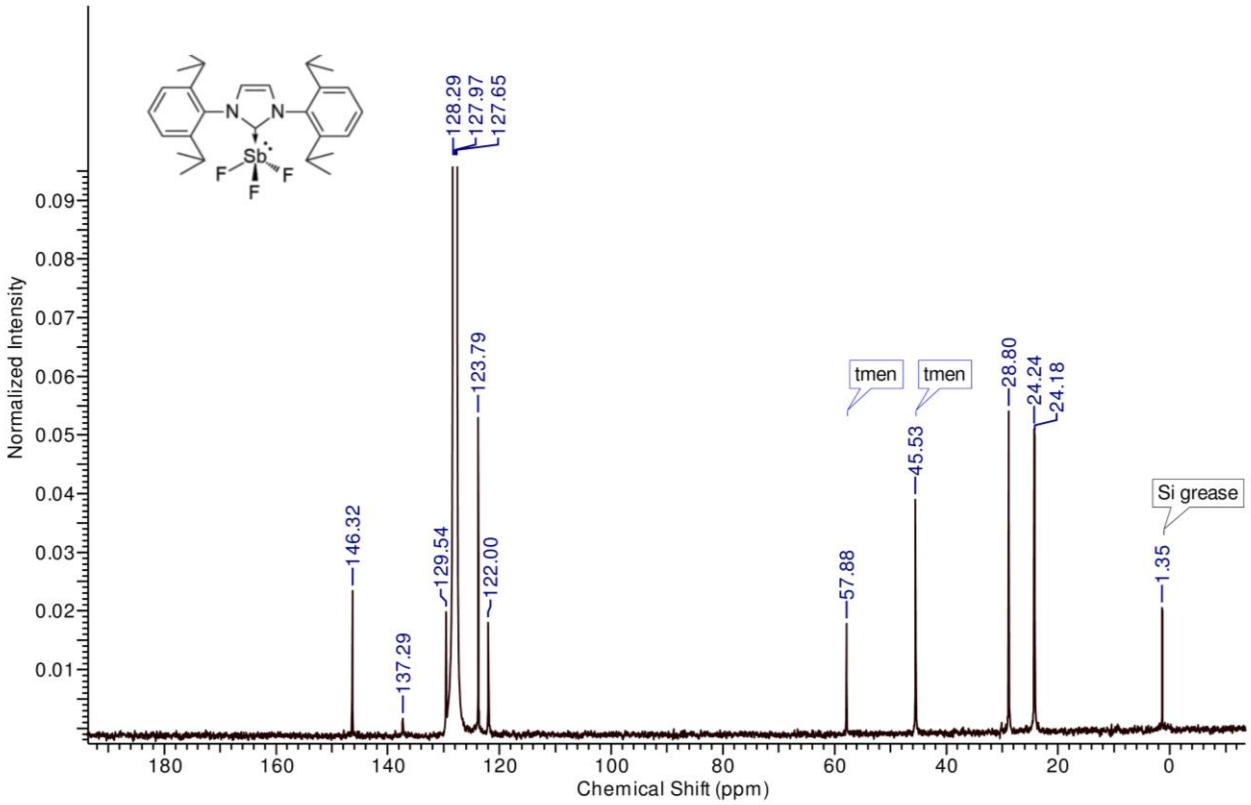
(S16) ^{1}H NMR spectrum for reaction "[SbF_3(tmen)] + (L^{Dipp}) –> [(L^{Dipp})SbF_3]" in C_6D_6, Frequency (MHz) 302.97:



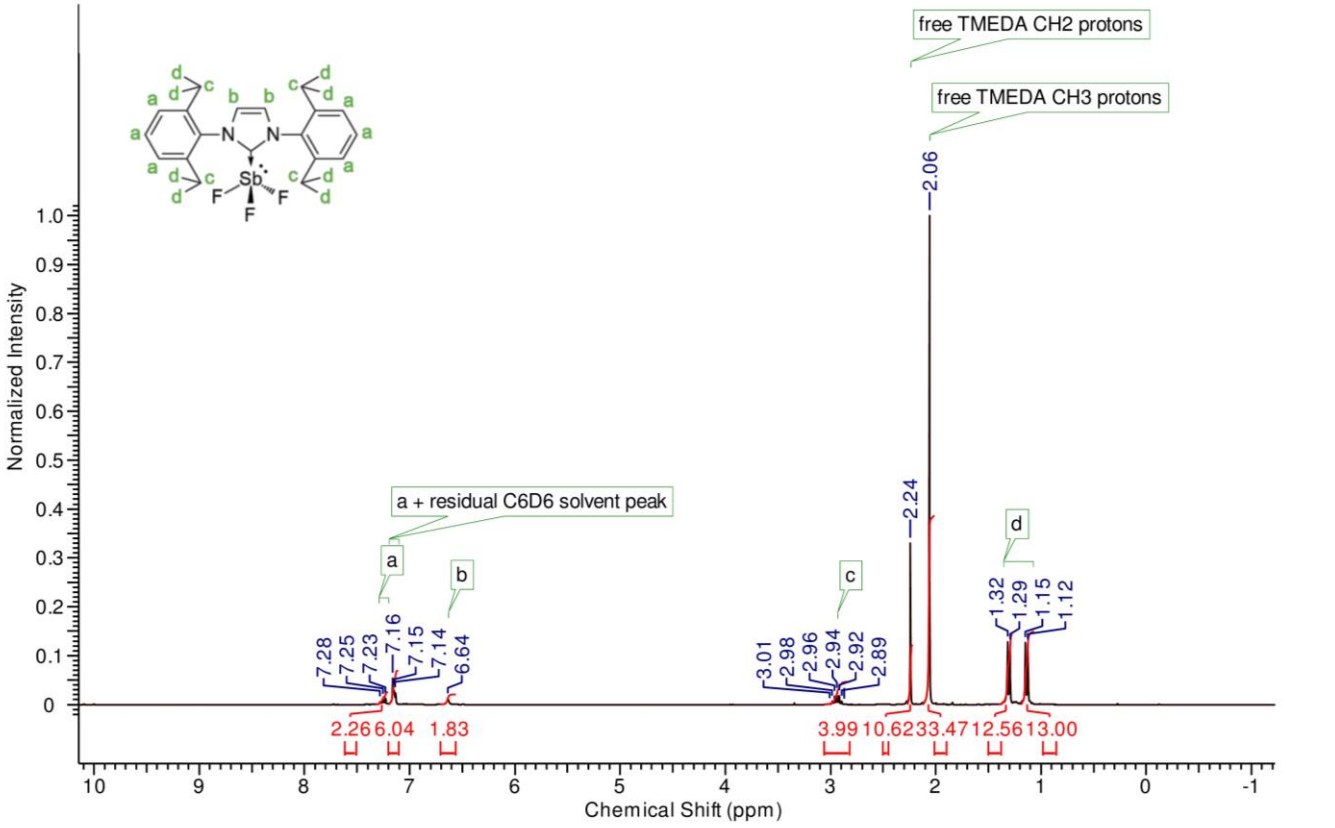
(S17) ^{19}F NMR spectrum for reaction "[SbF_3(tmen)] + (L^{Dipp}) –> [(L^{Dipp})SbF_3]" in C_6D_6, Frequency (MHz) 285.05:



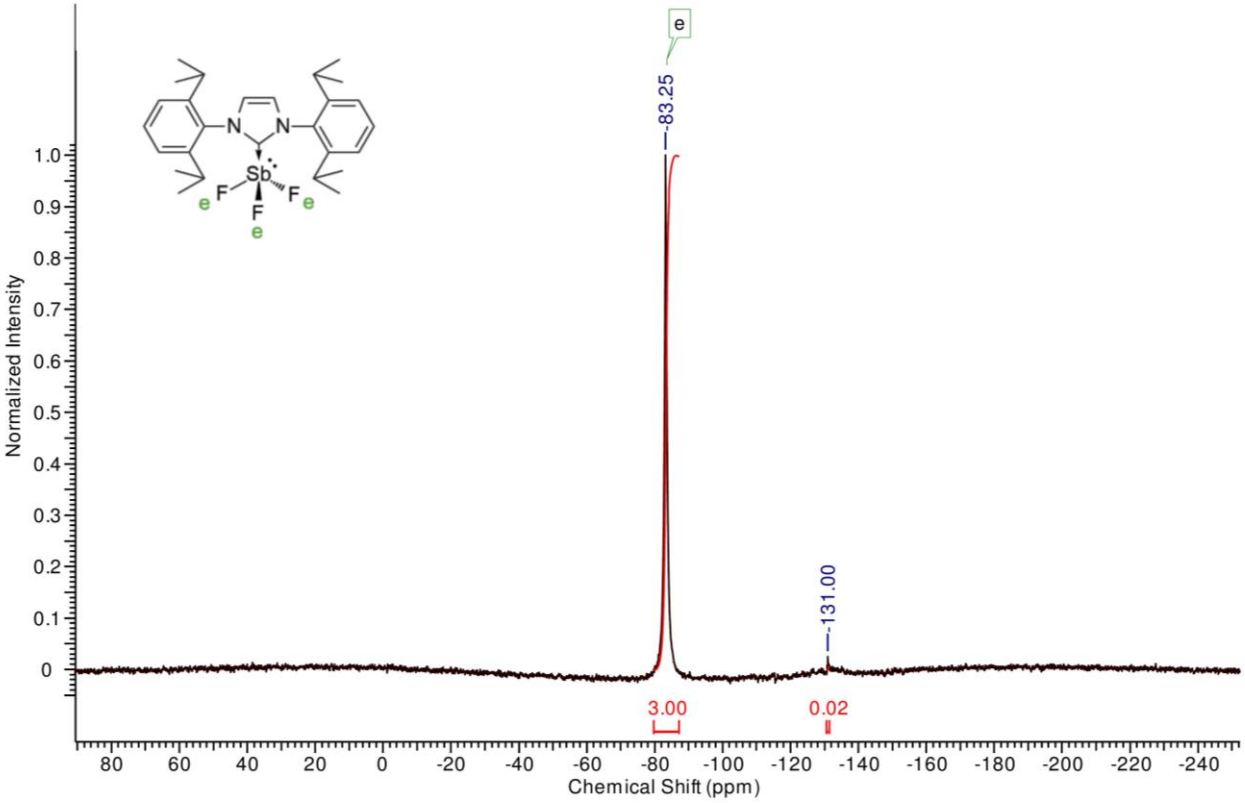
(S18) ^{13}C NMR spectrum for reaction "[SbF_3(tmen)]+ (L^{Dipp}) –> [(L^{Dipp})SbF_3]" in C_6D_6, Frequency (MHz) 76.19:



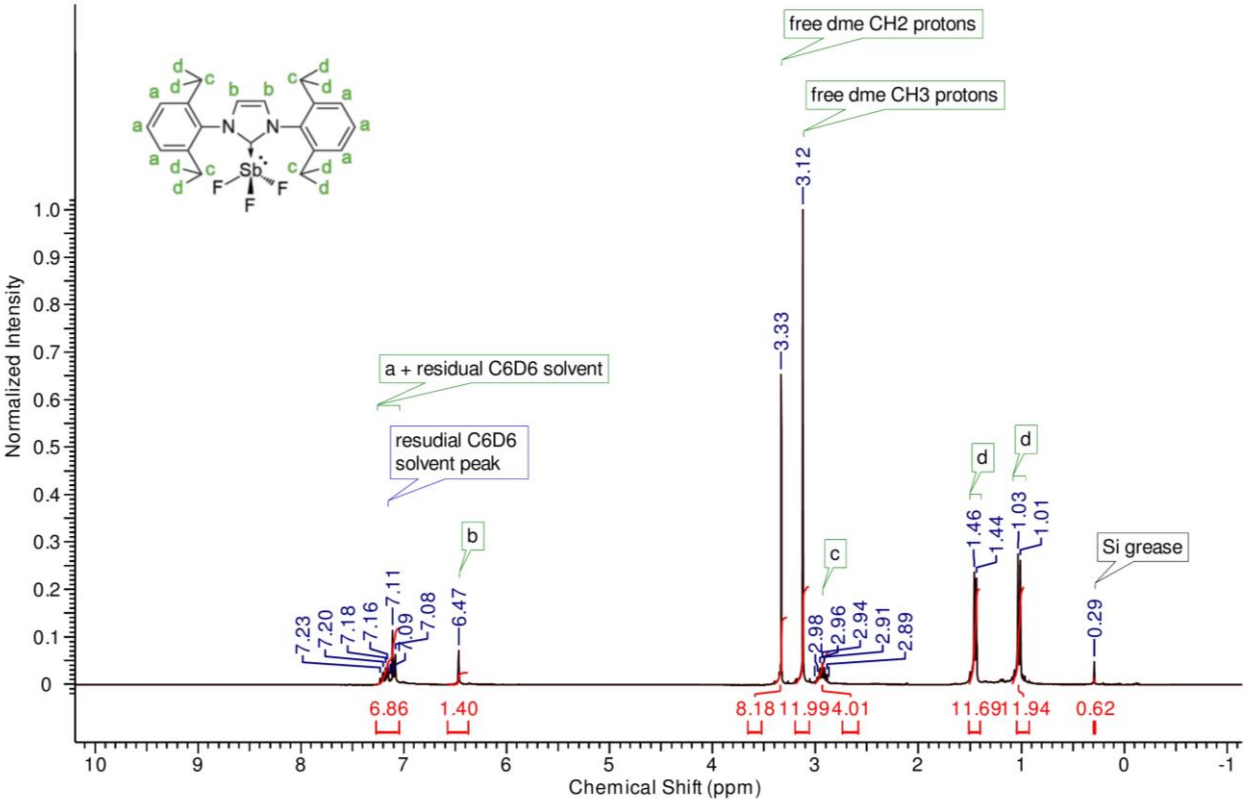
(S19) ^{1}H NMR spectrum for reaction "[SbF_3(tmen)] + (L^{Dipp}) + 2tmen –> [(L^{Dipp})SbF_3]" in C_6D_6, Frequency (MHz) 302.97:



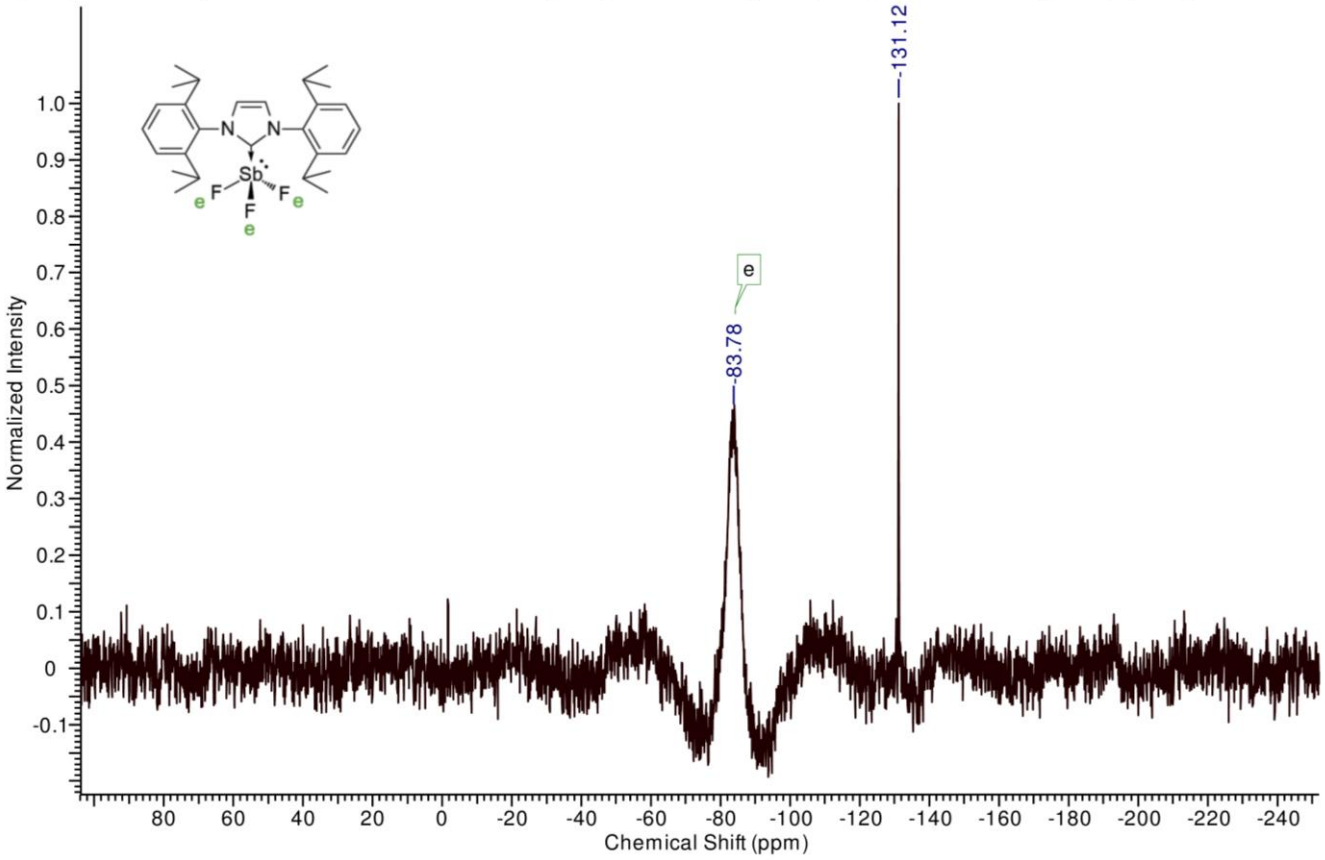
(S20) ^{19}F NMR spectrum for reaction "[SbF_3(tmen)] + (L^{Dipp}) + 2tmen –> [(L^{Dipp})SbF_3]" in C_6D_6, Frequency (MHz) 285.05:



(S21) ^{1}H NMR spectrum for reaction "SbF_3 + (L^{Dipp}) + 2dme –> [(L^{Dipp})SbF_3]" in C_6D_6, Frequency (MHz) 302.97:



(S22) ^{19}F NMR spectrum for reaction "SbF_3 + (L^{Dipp}) + 2dme –> [(L^{Dipp})SbF_3]" in C_6D_6, Frequency (MHz) 285.05:



(S23) $[(L^{Dipp})_2SbF_2]^+[SbF_4]^-$ (4)

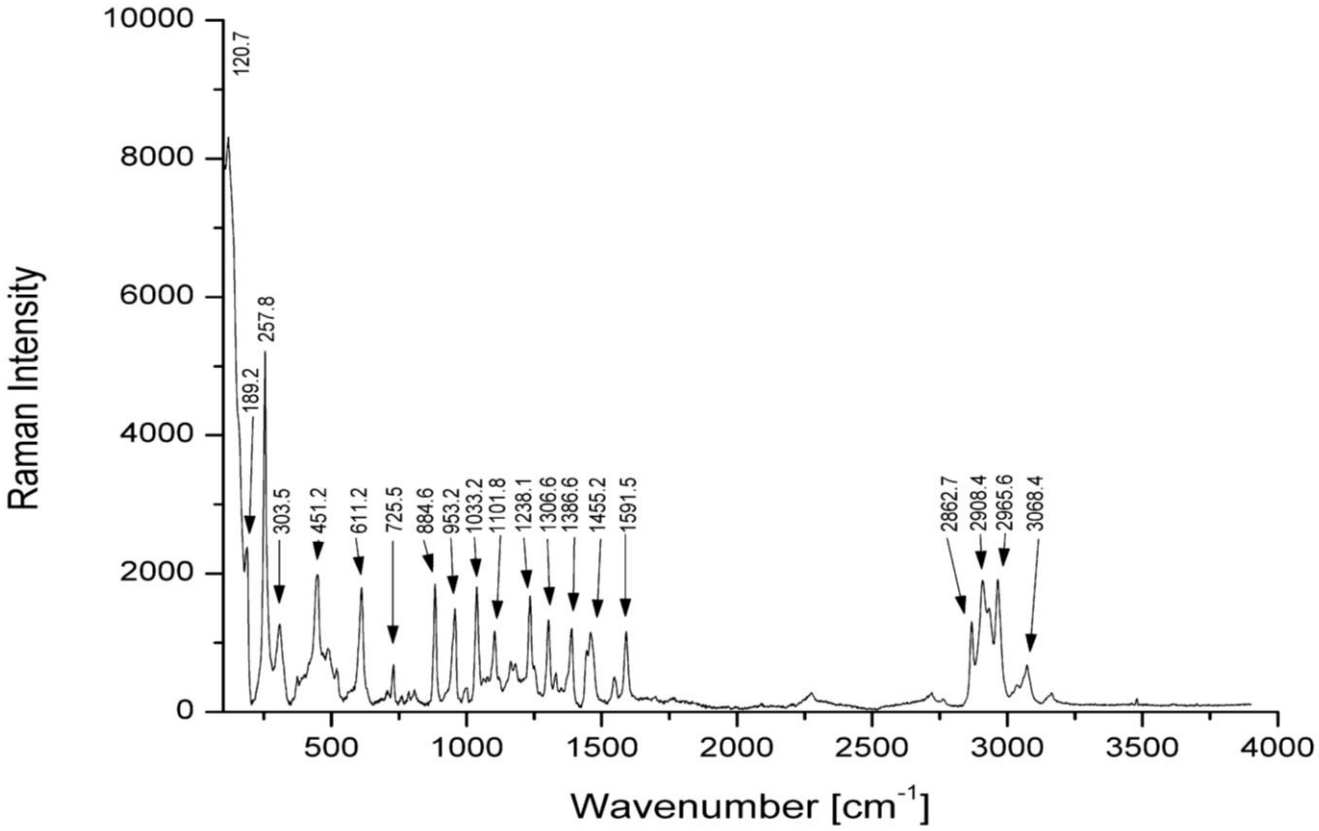
Reaction: "$[SbF_3(tmen)]$ + (L^{Dipp}) –> $[(L^{Dipp})_2SbF_2]^+[SbF_4]^-$"

or

"SbF_3 + 2dme + (L^{Dipp}) –> $[(L^{Dipp})_2SbF_2]^+[SbF_4]^-$"

Raman spectra

(S24) Raman spectra of $[(L^{Dipp})_2SbF_2]^+[SbF_4]^-$ (4)



(S25) $[(Cl_2L^{Dipp})H]^+[SbF_4]^-$ (5)

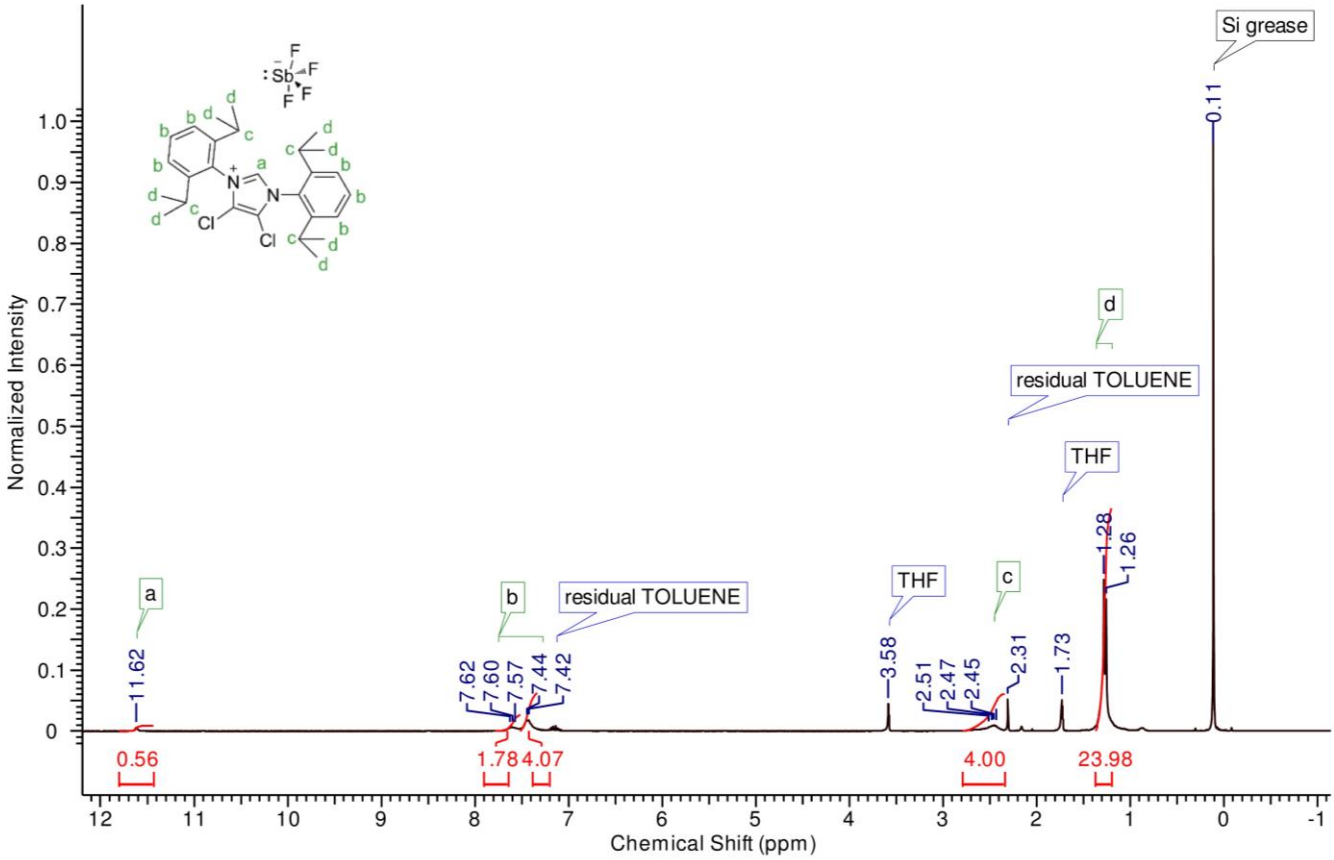
^1H NMR spectrum in THF-d^8

^{19}F NMR spectrum in THF-d^8

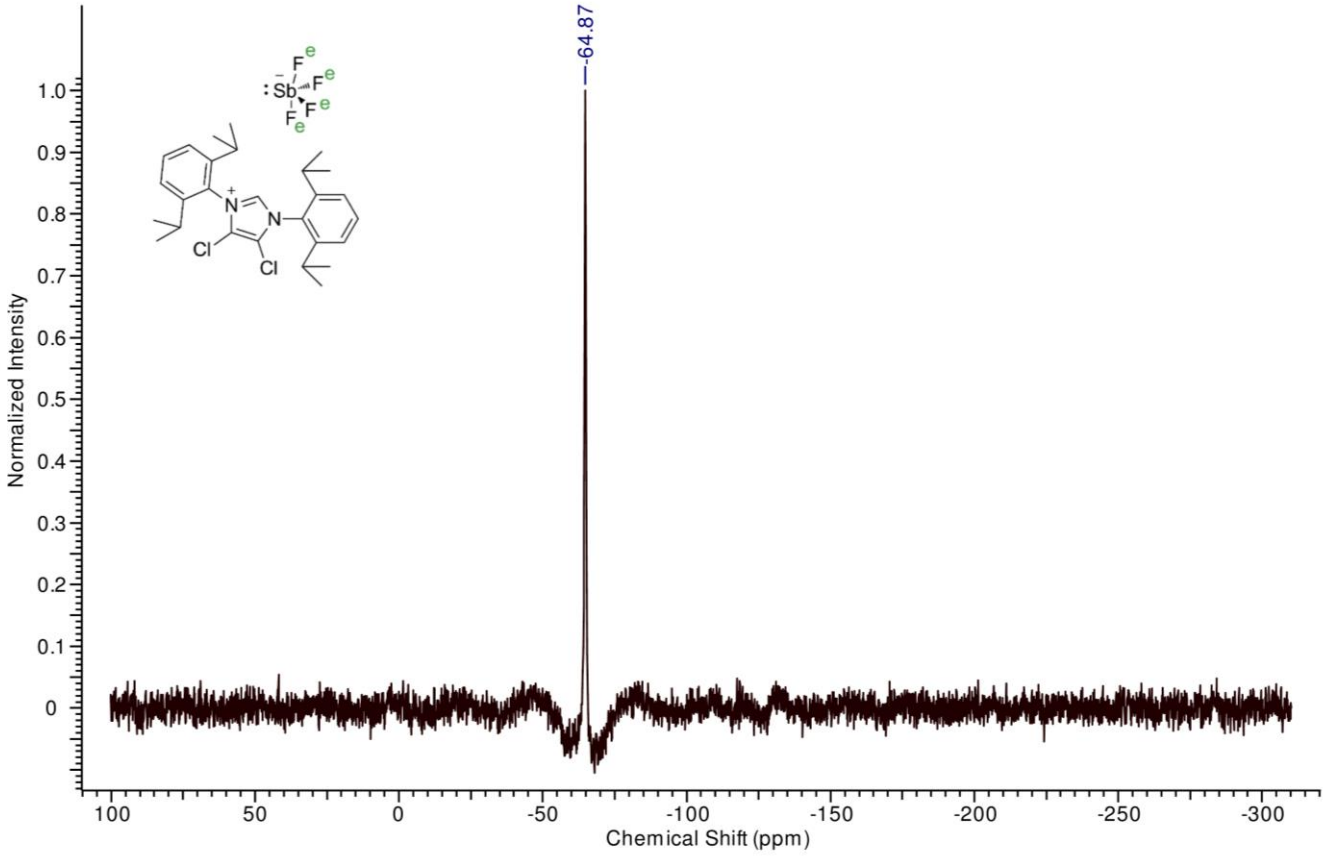
^1H NMR spectrum in C_6D_6 – empty, no other product could be obtained.

Raman spectra

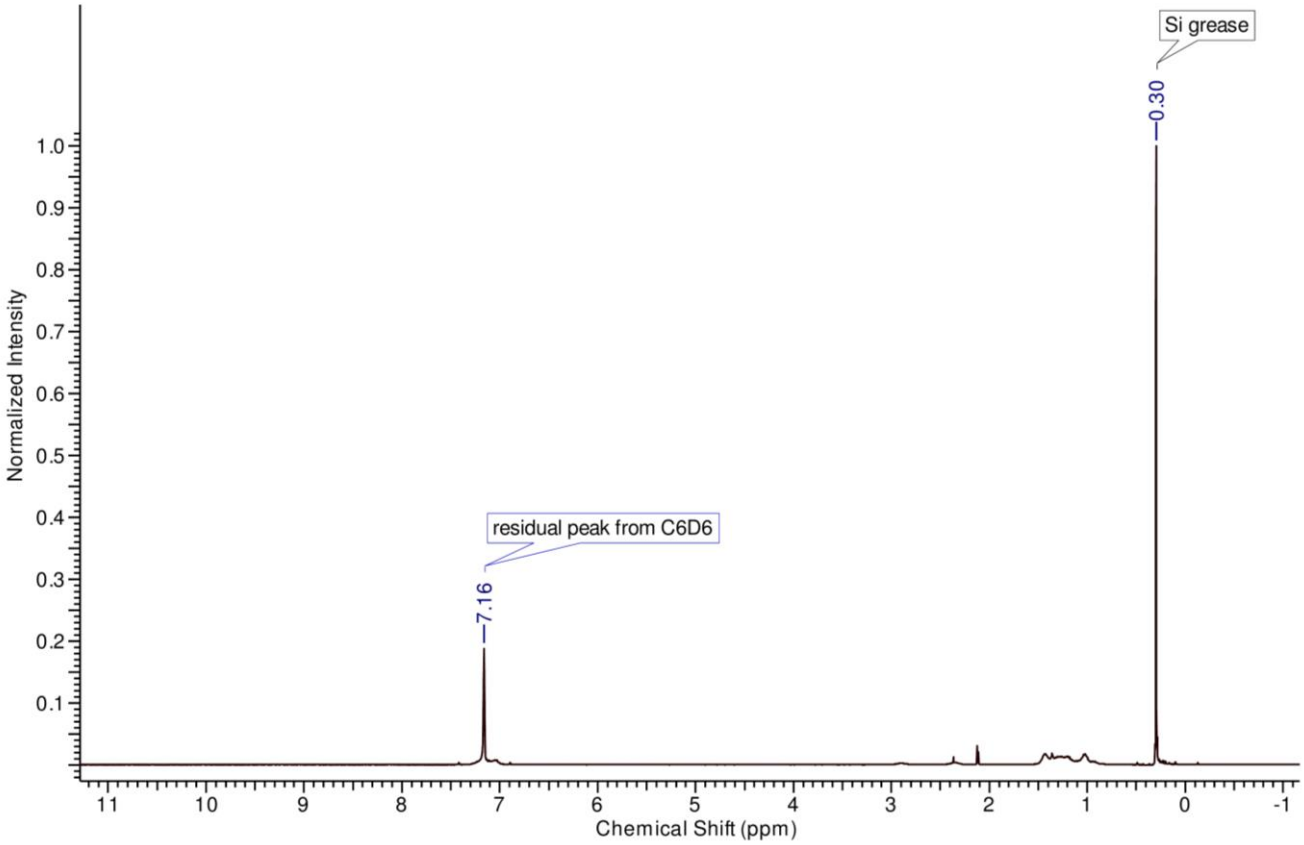
(S26) ^{1}H NMR spectrum of $[(Cl_2L^{Dipp})H]^+[SbF_4]^-$ in THF-d^8, Frequency (MHz) 302.97:



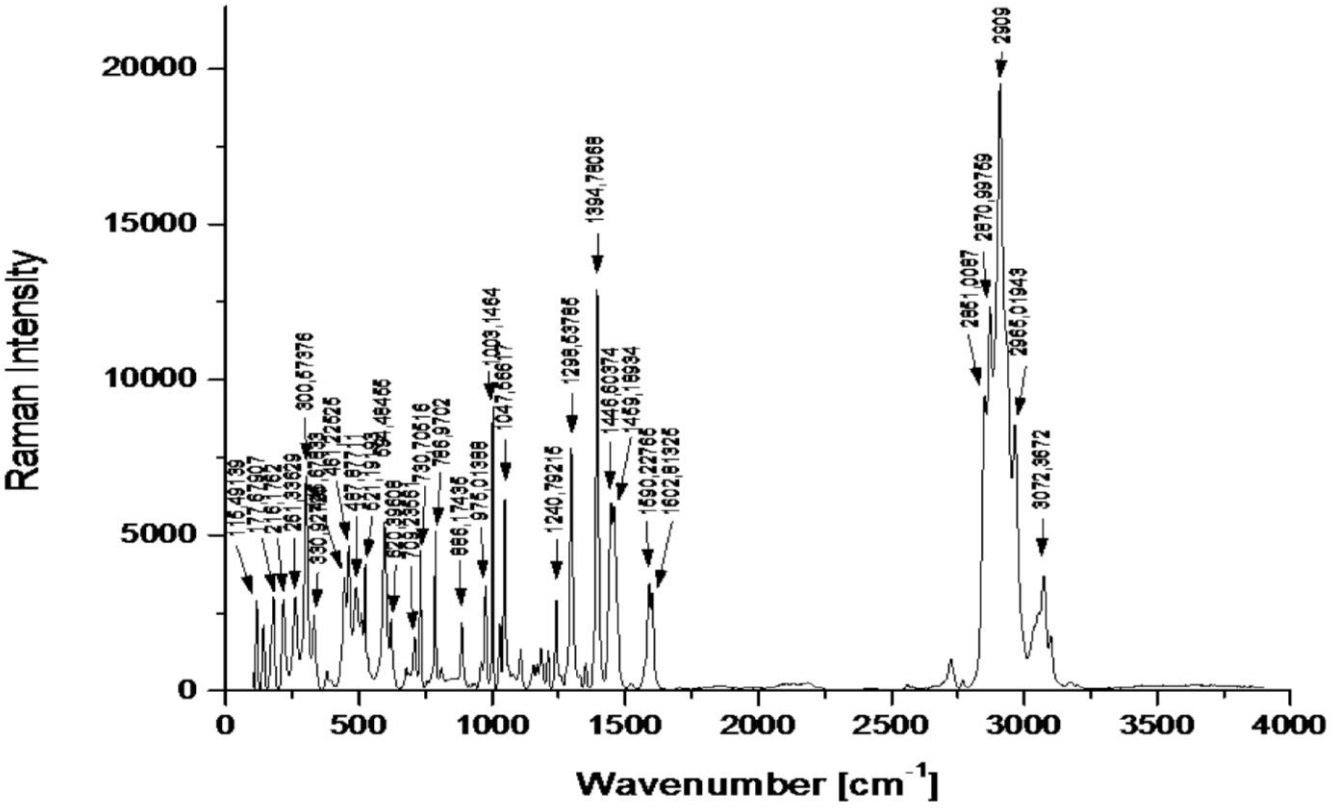
(S27) ^{19}F NMR spectrum of $[(Cl_2L^{Dipp})H]^+[SbF_4]^-$ in THF-d^8, Frequency (MHz) 285.05:



(S28) ^{1}H NMR spectrum of $[(Cl_2L^{Dipp})H]^+[SbF_4]^-$ in C_6D_6, Frequency (MHz) 302.97:

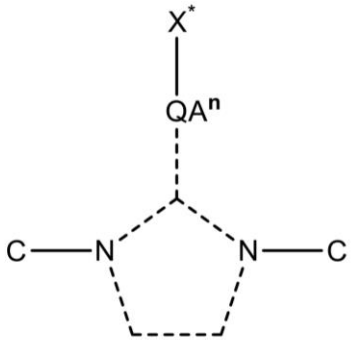


(S29) Raman spectra of $[(Cl_2L^{Dipp})H]^+[SbF_4]^-$ (5)



(S30) CSD search details

Cambridge Structural Database[1] was used for search of existing structures. Search was performed in the following way using CCDC ConQuest Version 1.18 (Built RC1).[2]



------ any bond

——— single bond

QA all elements of periodic table except: C, N, O, S

n number of bonded atoms

X any element of periodic table

* for MF compounds X = F

Table 1: Number of structures with different number of bonded atoms (n) for MF compounds

n	*number of crystal structures found*
2	9
3	1
4	29
5	12
6	44
7	0
SUM	**95**

1. C. R. Groom, I. J. Bruno, M. P. Lightfoot and S. C. Ward, *Acta Crystallog. Sec. B*, 2016, **72**, 171.
2. I. J. Bruno, J. C. Cole, P. R. Edgington, M. Kessler, C. F. Macrae, P. McCabe, J. Pearson and R. Taylor, *Acta Crystallogr. Sec. B*, 2002, **58**, 389.

Chapter 6

Reaction of *N*-Heterocyclic Carbene (NHC) with Different HF Sources and Ratios – a Free Fluoride Reagent Based on Imidazolium Fluoride

In this chapter, article entitled: »Reaction of *N*-heterocyclic carbene (NHC) with different HF sources and ratios – a free fluoride reagent based on imidazolium fluoride«, by **Blaž Ališ** and Gašper Tavčar is presented. For this article, the candidate performed all synthesis procedures with techniques for handling air-sensitive chemicals, obtained monocrystals, performed X-ray single crystal diffraction analysis and prepared the final .cif files of the obtained products. Furthermore, the candidate performed the multinuclear NMR spectroscopy and Raman spectroscopy, interpreted the NMR spectra, prepared the samples for CHN elemental analysis and actively participated in data interpretation. The candidate wrote the first manuscript draft and was the leading author during its refinement and publication process. He was highly involved from the conceptual stage of the research until the publication. The candidate was assigned as a corresponding author of the paper.

Gašper Tavčar did the preliminary experiments, proposed the reactions, coordinated the work and actively participated in data interpretation.

In this work we showed that reactions of *N*-heterocyclic carbene reactions with $Et_3N{\cdot}3HF$ readily afford $[(L^{Dipp})H]^+[F]^-$ (**1**), $[(L^{Dipp})H]^+[(HF)F]^-$ (**2**) and $[(L^{Dipp})H]^+[(HF)_2F]^-$ (**3**) salts, in 1:1, 1:2, 1:3 molar ratios between NHC and HF. Product (**1**) shows characteristics of a naked (free) fluoride reagent and can be selectively synthesized from reactions of (L^{Dipp}) with $Et_3N{\cdot}3HF$ or KHF_2 without any halide or water impurities on a gram scale.

Such reagent is of high value since the preparation of naked fluoride reagents soluble in organic solvents is usually difficult. Problems encountered with different fluoride sources are insolubility, decomposition in organic solvents and lack of metal-free or anhydrous synthesis.

Journal of Fluorine Chemistry 192 (2016) 141–146

Contents lists available at ScienceDirect

Journal of Fluorine Chemistry

journal homepage: www.elsevier.com/locate/fluor

Full Length Article

Reaction of N-heterocyclic carbene (NHC) with different HF sources and ratios – A free fluoride reagent based on imidazolium fluoride

Blaž Ališ[a,b,*], Gašper Tavčar[a,b,*]

[a] Jožef Stefan Institute, Department of Inorganic Chemistry and Technology, Jamova cesta 39, 1000 Ljubljana, Slovenia
[b] Jožef Stefan International Postgraduate School, Jamova cesta 39, 1000 Ljubljana, Slovenia

ARTICLE INFO

Article history:
Received 24 October 2016
Accepted 5 November 2016
Available online 9 November 2016

Keywords:
N-heterocyclic carbene
HF
Imidazolium salts
Crystal structure
Fluoride

ABSTRACT

Treatment of N-heterocyclic carbene (1,3-Bis(2,6-diisopropylphenyl)-1,3-dihydro-2H-imidazol-2-ylidene; (L^{Dipp})) with different sources of hydrofluoric acid ($Et_3N{\cdot}3HF$, anhydrous hydrofluoric acid and KHF_2) in 1:1, 1:2, 1:3 ratios affords $[(L^{Dipp})H]^+[F]^-$ (**1**), $[(L^{Dipp})H]^+[(HF)F]^-$ (**2**) and $[(L^{Dipp})H]^+[(HF)_2F]^-$ (**3**) salts respectively. Different fluoride sources all yield the same products, but ease of manipulation and isolation can influence the choice in the future use.

Compound (**1**), which shows characteristics of a free fluoride reagent, can be obtained with good yield and without the contaminants usually present in such compounds. All products were characterized by X-Ray crystallography, NMR spectroscopy and free fluoride (F_f^-) chemical analysis.

© 2016 Elsevier B.V. All rights reserved.

1. Introduction

Imidazolium salts represent a large family of ionic compounds with a discrete cation and anion pair and high tuning abilities. Different substituents on both nitrogen atoms, ranging from symmetric to asymmetric and from aromatic to aliphatic, can be incorporated in order to tune their properties according to the need. Additionally, substituents on C2, C4 and C5 positions of imidazole ring, together with anion type, can also be manipulated with different synthetic approaches [1–3]. Because of these properties their use expands over many fields of chemistry. Most notably, imidazolium salts are applied in the field of ionic liquids (ILs) as potential replacement for volatile organic solvents [4,5] and as precursors for N-heterocyclic carbene ligands (NHCs) which are increasingly substituting bulky phosphine ligands across organic chemistry [6]. In biological systems, these compounds exhibits anti-tumour and anti-bacterial properties, that are also being studied in detail [7].

Most of the work on imidazolium fluorides was implemented in the area of ILs. The first ILs with fluoride ions were imidazolium tetrafluoridoborate [8] and hexafluoridophosphate [9] which showed stability towards oxygen and moisture. However, as found later [10], during the synthesis of imidazolium hexafluoridophosphate, imidazolium fluoride is formed to some extent as a side product. Further, ionic liquid of [bmim][F] synthesised in 2014 shows extremely good results for nucleophilic substitution of different leaving groups with various substrates [11].

Methods for the incorporation of F^- to imidazolium salts differ from other halides. While synthesis of imidazolium halides can be performed with quarterisation of imidazole nitrogen atoms, the same methods cannot be applied with F^- because of the strength of C—F bonds [12]. As reported so far, the imidazolium fluorides can be obtained:

a) during synthesis of imidazolium hexafluoridophosphate, as a side product [10].
b) from imidazolium halide (halide = Cl, Br, I) and subsequent anion exchange with HF or MF salts [11–13].
c) with Anion Exchange Resins (AER method) [14,15].

Herein we report new imidazolium fluoride $[(L^{Dipp})H]^+[F]^-$ (**1**) and two imidazolium poly(hydrogen fluorides) $[(L^{Dipp})H]^+[(HF)_nF]^-$ (n = 1, 2) derived from persistent N-heterocyclic carbene with introduction of HF in stoichiometric 1:1, 1:2 and 1:3 ratios respectively.

2. Results and discussion

When 1,3-Bis(2,6-diisopropylphenyl)-1,3-dihydro-2H-imidazol-2-ylidene (L^{Dipp}) is treated with stoichiometric quantities of HF source, in the form of $Et_3N{\cdot}3HF$, in ratios (L^{Dipp}:HF) 1:1, 1:2 and 1:3, it affords $[(L^{Dipp})H]^+[F]^-$ (**1**), $[(L^{Dipp})H]^+[(HF)F]^-$ (**2**) and $[(L^{Dipp})$

* Corresponding authors at: Jožef Stefan Institute, Department of Inorganic Chemistry and Technology, Jamova cesta 39, 1000 Ljubljana, Slovenia.
E-mail addresses: blaz.alic@gmail.com (B. Ališ), gasper.tavcar@ijs.si (G. Tavčar).

http://dx.doi.org/10.1016/j.jfluchem.2016.11.004
0022-1139/© 2016 Elsevier B.V. All rights reserved.

$H]^+[(HF)_2F]^-$ (**3**) respectively. Reaction in excess of HF source afforded only crystals of $[(L^{Dipp})H]^+[(HF)_2F]^-$ (**3**) and no higher poly (hydrogen fluoride) anion was observed, even when anhydrous HF (aHF) was used as a reagent and solvent, at room temperature (Scheme 1).

In order to ease the synthetic procedure, we have searched for an alternative reagent to aHF and the choice fell onto triethylamine trihydrofluoride ($Et_3N{\cdot}3HF$), which allowed us to perform the reactions with ease, in laboratory glassware, without any signs of glass etching by the reagent. Moreover, addition of equimolar quantities of HF with $Et_3N{\cdot}3HF$ is far simpler than use of anhydrous HF. Purification and isolation of the products is effortless since remaining Et_3N has a substantial vapour pressure at room temperature and can be removed under reduced pressure.

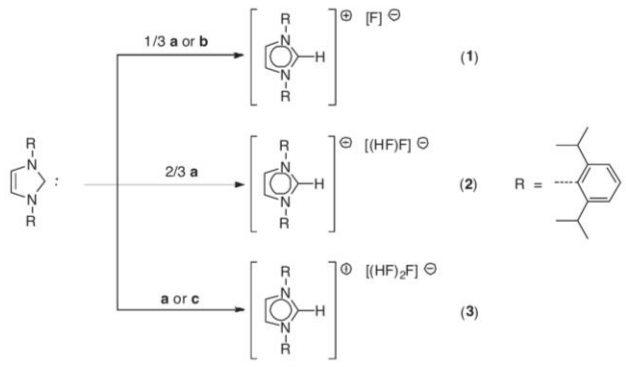
When reacting one equivalent of HF with (L^{Dipp}) at room temperature, kinetically favoured $[(L^{Dipp})H]^+[(HF)F]^-$ (**2**) can be isolated first. Prolonged reaction at room temperature in CH_3CN leads to formation of $[(L^{Dipp})H]^+[F]^-$ (**1**) in quantitative yields. Additionally, reaction of $[(L^{Dipp})H]^+[(HF)F]^-$ (**2**) or KHF_2 with equivalent of (L^{Dipp}) in acetonitrile also affords $[(L^{Dipp})H]^+[F]^-$ (**1**).

2.1. Crystal structure determination of $[(L^{Dipp})H]^+[F]^-$ (1), $[(L^{Dipp})H]^+[(HF)F]^-$ (2) and $[(L^{Dipp})H]^+[(HF)_2F]^-$ (3)

A series of structures with dialkyl imidazolium poly(hydrogen fluoride) were published by Hagiwara et al. [13,16–20], but our goal was obtaining similar product with sterically hindered and widely used (L^{Dipp}), which forms diaryl N-substituted imidazolium fluoride and poly(hydrogen fluoride) salts. Crystal data for $[(L^{Dipp})H]^+[F]^-$ (**1**), $[(L^{Dipp})H]^+[(HF)F]^-$ (**2**) and $[(L^{Dipp})H]^+[(HF)_2F]^-$ (**3**) are listed in Table 1.

All three products crystalize in monoclinic lattice; (**1**) in $P2_1/c$, (**2**) in $P2_1/n$ and (**3**) in $C2/c$ space group. N—C—N angle of imidazolium ring is increasing with higher poly(hydrogen fluoride) anions from 106.9° in (**1**) to 108.2° in (**3**) which is expected in terms of the electronegativity of F^- anion, pulling on the C(2)—H(2) proton. Same trend is observed in imidazolium poly(hydrogen fluoride) structures published by Hagiwara et al., although we have to note that in the highest poly(hydrogen fluoride) anion, $[(FH)_3F]^-$, published in that research, the angle decreases from 109.6(3)° in $DMIm(FH)_2F$ to 108.7° in $DMIm(FH)_3F$ [16].

F^- anion in compound (**1**) is stabilized by four hydrogen bonds in the crystal structure. The strongest arises from C(2)—H(2)···F(1) being 1.72 Å. Second hydrogen bond is formed with C(5)—H(5)···F(1) proton from imidazolium backbone of symmetrically generated unit with 1.97 Å, third from acetonitrile methyl proton C(30)—H(30B)···F(1) with 2.07 Å and the weakest from para proton on diisopropybenzene "wingtip" C(21)—H(21)···F(1) with 2.23 Å, from another symmetrically generated (L^{Dipp}) (Fig. 1).



Scheme 1. Synthesis of $[L(^{Dipp})H]^+[(HF)_nF]^-$ (n = 0–2) (1–3 salts); a: Et3N·3HF in MeCN or THF; b: KHF2 in MeCN, c: aHF(reagent and solvent).

When crystallization of (**1**) was attempted from chloroform, an ion exchange was observed and single crystals of $[(L^{Dipp})H]^+[Cl]^-$ were isolated. Such reactivity is consistent with reactivity of a free fluoride reagent, as observed for different free fluoride reagents in the literature [21–23].

$[(HF)F]^-$ anion of compound (**2**) is stabilized by four hydrogen bonds. Three come from chloroform molecules and one from protonated imidazolium ring C(2)—H(2)···F(1), which has the strongest interaction with the distance of 1.99 Å. From three chloroform molecules, one is directed towards proton in $[(HF)F]^-$ anion. Observed electron density peak that could be assigned to hydrogen atom in F(1)—H(1)—F(2) anion showed a slightly bent structure of anion with 164° angle (Fig. 2, Table 2). The C(31)—H(31) proton from the chloroform molecule forms bifurcated, three-centred interaction with F(1) and F(2) atoms and has geometry consistent for other reported bifurcated bonds [24]. Result of such interaction is a short H(1)···H(31) nonbonded contact interaction of 2.07 Å (Fig. 2). Although this H···H nonbonded distance is at the beginning of distribution curve of reported H···H nonbonded contact interactions [25], it is still far from the shortest reported in the literature [26,27].

Structure (**3**) is the most symmetrical of the three, with asymmetric unit containing only half of imidazolium cation and anion. $[(HF)_2F]^-$ anion of product (**3**) is packed between four imidazolium cations. Terminal F(2) and symmetrically generated F(2)' atoms are each stabilized by C(4)—H(4)···F(2) hydrogen bond and with hydrogen bond arising from meta proton on diisopropybenzene "wingtip" of imidazolium cation C(7)—H(7)···F(2) (Fig. 3). We would like to stress that these two interactions should be viewed with some scepticism as they are on the upper limit, as far as angles and distances are concerned, for such interaction and can be probably attributed to packing in crystal structure (Table 2). The disordered central F^-, that was modelled in three positions with approximately 1/3 occupancy each, is loosely stabilized by C(2)—H(2)···F(1) hydrogen bond. The $[(HF)_2F]^-$ anion should be completely planar but due to the disorder of central F^- in the crystal structure it is impossible to describe such shape in product (**3**) (Fig. 3).

2.2. NMR analysis

NMR analysis was performed at room temperature for all three products and is in agreement with their X-ray crystal structures. We weren't able to observe separate peak for C(2)—H(2) proton in ^1H NMR of $[(L^{Dipp})H]^+[F]^-$ (**1**). When we dissolved monocrystals of (**1**) in deuterated acetonitrile, ^{19}F NMR analysis showed a characteristic doublet peak for $[(L^{Dipp})H]^+[(HF)F]^-$ (**2**) at −147.15 and −147.59 ppm ($^1J_{HF}$ = 124.03 Hz) respectively. After 24 h at room temperature the doublet disappeared and a singlet for $[(L^{Dipp})H]^+[F]^-$ (**1**) at −147.94 ppm could be observed. This indicates that with introduction of acetonitrile to the crystals of (**1**), the two imidazolium fluorides form $[(L^{Dipp})H]^+[(HF)F]^-$ (**2**) and a free carbene moiety as kinetically controlled products, and with time, thermodynamically more stable product, $[(L^{Dipp})H]^+[F]^-$ (**1**), can be quantitatively isolated and crystalized from solution (Scheme 2).

^1H NMR of (**2**) shows C(2)—H(2) proton peak at 10.01 ppm. The proton-fluoride coupling for $[(HF)F]^-$, with characteristic triplet at 16.06 ppm in ^1H NMR, and doublet at −147.50 ppm in ^{19}F NMR spectra, can also be seen. The coupling constant, $^1J_{HF}$, for such system should be around 121–125 Hz according to the literature [28,29] and when (**2**) is formed in reaction mixture from (**1**) upon addition of acetonitrile. However, we have observed slightly lower coupling constant value, $^1J_{HF}$ = 115.14 Hz, for the pure isolated $[(L^{Dipp})H]^+[(HF)F]^-$ (**2**) in ^1H NMR spectra. This can be attributed to

Table 1
X-ray data for compounds (**1**), (**2**) and (**3**).

CCDC ref. code	(1) 1488081	(2) 1488080	(3) 1488079
Formula	$C_{27}H_{37}N_2F{\cdot}C_2H_3N$	$C_{27}H_{37}N_2F_2H{\cdot}3(CHCl_3)$	$C_{27}H_{37}N_2{\cdot}F_3H_2$
FW [g/mol]	449.64	786.70	448.60
Crystal System	monoclinic	monoclinic	monoclinic
Space Group	$P2_1/c$	$P2_1/n$	$C2/c$
a [Å]	13.2812 (1)	9.6958 (2)	16.6130(2)
b [Å]	16.2775 (1)	36.5259(8)	9.0171(1)
c [Å]	13.6886 (1)	11.1478(3)	17.2328(2)
α [°]	90	90	90
β [°]	114.174 (1)	104.114(2)	90.866(1)
γ [°]	90	90	90
V [Å^3]	2699.76 (4)	3828.8(2)	2581.20(5)
Z	4	4	4
Crystal size [mm^3]	0.43 × 0.31 × 0.24	0.64 × 0.11 × 0.10	0.50 × 0.39 × 0.12
Temperature [K]	150	100	150
θ range [°]	67.1–3.7	73.0–4.3	67.1–5.1
Reflections collected	24568	25470	13440
Independ. Reflect., R(int)	4821, 0.018	7495, 0.037	2308, 0.018
Completeness	1.000	0.996	0.999
Data/restraints/parameters	4821, 0, 307	7495, 0, 400	2308, 0, 158
Goodness-of-fit on F^2	1.03	1.02	1.06
Final R indices [I > 2σ(I)]	R = 0.043	R = 0.050	R = 0.043
	wR = 0.113	wR = 0.136	wR = 0.112
R indices (all data)	R = 0.045	R = 0.064	R = 0.044

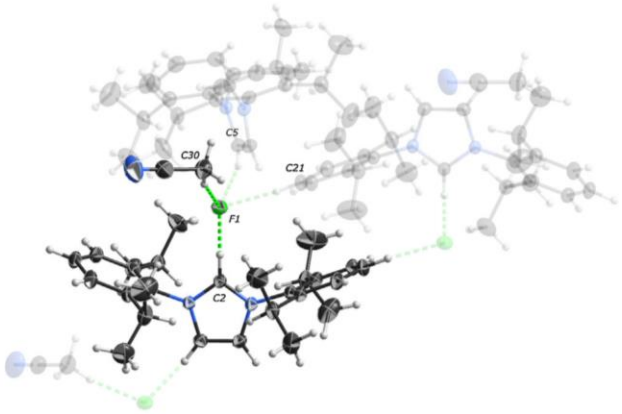


Fig. 1. Asymmetric unit (bold) and packing (blurred) of structure $[(L^{Dipp})H]^+[F]^-$ (**1**). Ellipsoids are drawn with 50% probability.

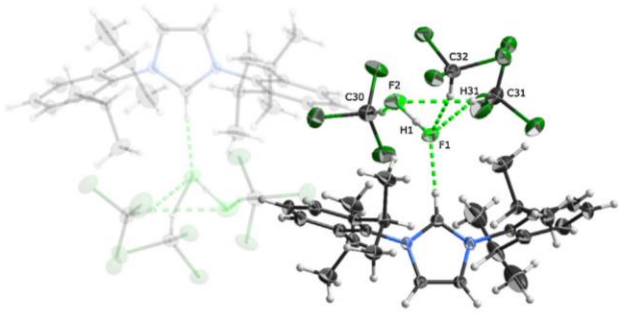


Fig. 2. Asymmetric unit (bold) and packing (blurred) of structure $[(L^{Dipp})H]^+[(HF)F]^-$ (**2**). Ellipsoids are drawn with 50% probability.

broadened signals of $[(HF)F]^-$ in ^1H and ^{19}F spectra, where the exact point of peak can be somewhat arbitrarily chosen to the extent of ± 0.02 ppm. The heteronuclear coupling constant, $^1J_{HF}$, in ^1H NMR of $[(HF)F]^-$ is in agreement with ^{19}F NMR coupling constant where its value is $^1J_{HF}$ = 114.24 Hz. Again, discrepancies of $\Delta^1J_{HF} \approx 1$ Hz between ^1H and ^{19}F spectra can arise due to broadened peaks. Repeated synthesis of (**2**) and NMR analysis gave the same results.

NMR analysis of (**3**) agrees with crystal structure obtained on single crystals. C(2)—H(2) proton shows a signal at 9.10 ppm, characteristic for imidazolium salts. It is even split in to a triplet with a small coupling constant of 1.5 Hz with C(4)—H(4) and C(4′)—H(4) protons. Further downfield at 13.36 ppm in ^1H NMR spectra is a broad peak that integrates for two and is characteristic for $[(HF)_2F]^-$ anion [28]. Proton-fluoride heterocoupling can't be observed at room temperature. The same is true for ^{19}F spectra of $[(HF)_2F]^-$ anion, where only a singlet peak at −167.28 ppm can be observed at room temperature and no proton-fluoride heterocoupling or fluoride-fluoride coupling can be seen.

3. Conclusions

Reactions of N-heterocyclic carbene with $Et_3N{\cdot}3HF$ reagent readily affords $[(L^{Dipp})H]^+[(HF)_nF]^-$ (n = 0–2) salts with 1:1, 1:2, 1:3 ratios of HF. Product (**1**) shows a free fluoride reagent characteristics and can be selectively synthesised from reactions of (L^{Dipp}) with stoichiometric quantities of $Et_3N{\cdot}3HF$ or KHF_2 without any halide or water impurities on a gram scale. All products were characterized with NMR, X-Ray, Raman and free fluoride (F_f^-) chemical analysis. Reactions of $Et_3N{\cdot}3HF$ or KHF_2 with (L^{Dipp}) were performed in glassware with no sign of glass etching by the reagents.

4. Experimental

4.1. General experimental procedure and reagents

All experiments and manipulations were carried out under an inert atmosphere of dried argon, either in glovebox (M. Braun) or using standard Schlenk techniques. THF was dried in a mixture of sodium and benzophenone for at least two days, distilled under argon atmosphere and stored over 3 Å molecular sieves. Acetonitrile was stored over 3 Å molecular sieves and left for at least 48 h prior to use. Deuterated solvents were dried over 3 Å molecular

Table 2
Specified hydrogen bonds for (**1**), (**2**) and (**3**).

	D—H	H···A	D···A	<(DHA)
	$[(L^{Dipp})H]^+[F]^-$ (**1**)			
C2—H2···F1	0.93	1.72	2.644(1)	176.9
C5—H5···F1	0.93	1.97	2.867(1)	160.5
C21—H21···F1	0.93	2.22	3.147(1)	170.9
C30—H30B···F1	0.96	2.07	3.002(2)	164.4
	$[(L^{Dipp})H]^+[(HF)F]^-$ (**2**)			
C2—H2···F1	0.93	1.99	2.920(3)	176.0
C31—H31···F1	0.98	2.30	3.234(4)	159.0
C31—H31···F2	0.98	2.58	3.377(3)	138.9
C32—H32···F1	0.98	2.08	3.011(3)	157.2
C30—H30···F2	0.98	2.06	3.004(3)	160.8
F1—H1—F2	1.08	1.22	2.277(2)	164
	$[(L^{Dipp})H]^+[(HF)_2F]^-$ (**3**)			
C2—H2···F1A	0.93	1.98	2.91(2)	180.0
C2—H2···F1B	0.93	2.00	2.92(1)	168.0
C4—H4···F2	0.93	2.45	3.213(2)	138.9
C7—H7···F2	0.93	2.52	3.421(2)	162.9
F2—H1···F1A	1.08	1.31	2.334(9)	154.5

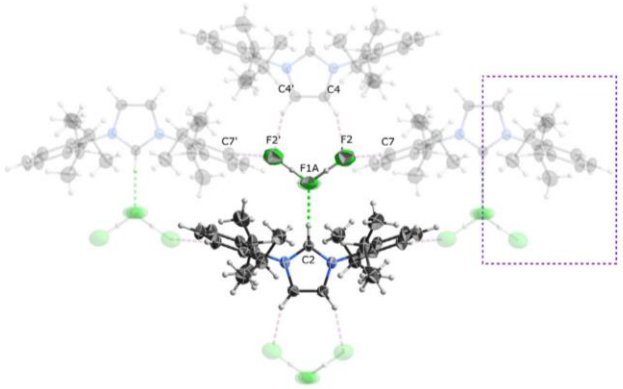
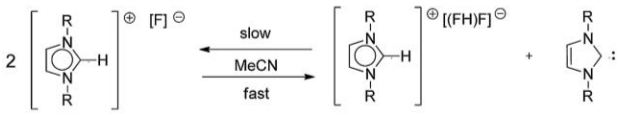


Fig. 3. Asymmetric unit (squared) and packing of structure $[(L^{Dipp})H]^+[(HF)_2F]^-$ (**3**). Ellipsoids are drawn with 50% probability.



Scheme 2. Equilibrium in the acetonitrile solution of $[(L^{Dipp})H]^+[F]^-$ (**1**).

sieves (at least 20% w/w). Glassware was oven-dried overnight at 150 °C.

Anhydrous HF was handled in an all PTFE (polytetrafluoroethylene) vacuum line equipped with PTFE valves. The reaction was carried out in FEP (tetrafluoroethylene-hexafluoropropylene; Polytetra GmbH, Germany) reaction vessels (height 250–300 mm with inner diameter 15.5 mm and outer diameter 18.75 mm) equipped with PTFE valves and PTFE coated stirring bars. T-shaped reaction vessels from PTFE were used for the crystallization process. Caution: aHF must be handled in a well-ventilated fume hood, and protective clothing must be worn at all times.

4.1.1. Manipulation and preparation of starting materials

$Et_3N{\cdot}3HF$ 98% (Sigma-Aldrich) was used without further treatment.

$KHF_2 \geq 99.0\%$ (Sigma-Aldrich) was used without further treatment.

(L^{Dipp}) was synthesised after standard literature procedures [30].

Anhydrous HF (Linde, 99.995%) was treated with K_2NiF_6 (Advance Research Chemicals, Inc.) for several hours prior to use.

4.1.2. NMR spectroscopy

NMR spectra (^1H and ^{19}F) were recorded on Agilent Technologies Unity Inova 300 MHz; (^1H at 303 MHz and ^{19}F at 285.1 MHz). The chemical shifts are referenced: ^1H to residual signals of deuterated solvent peaks and ^{19}F to $CFCl_3$ as an external standard.

4.1.3. Raman spectroscopy

Raman spectra were recorded at room temperature on a Horiba Jobin Yvon Labram-HR spectrometer coupled with an Olympus BXFM-ILHS microscope. Samples were excited by the 633-nm emission line of a 24.3-mW He-Ne laser with a power output of 14 mW on the sample. The samples were loaded into vacuum dried 0.5-mm quartz capillaries inside the glove box. The spectra obtained from the powdered samples corresponded completely with the spectra taken from several, randomly oriented, single crystals, of which the identity was additionally confirmed by the unit-cell measurement on the diffractometer.

4.1.4. Free fluoride analysis

All reagents were of analytical grade and all solutions were prepared using deionized and additionally double-distilled water. The amount of free fluoride (F_f^-) was determined in aqueous solution of the sample using fluoride ion selective electrode [31].

4.1.5. Crystal structure determination

Single-crystal data for all compounds were collected on a Gemini A diffractometer equipped with an Atlas CCD detector, using graphite monochromated Cu Kα radiation. The data were treated using the *CrysAlisPro* software suite program package [32]. Analytical absorption correction has been applied to all data sets [33]. Structures were solved with direct methods using the *ShelXT* program [34]. Structure refinement has been performed with the *ShelXL* software [35] implemented in the program package *Olex2* [36]. Figures were prepared using *Diamond 4.0* software [37].

4.2. Synthesis of products

4.2.1. Synthesis of $[(L^{Dipp})H]^+[F]^-$ (1)

(L^{Dipp}) (n = 1.03 mmol; m = 400 mg) was weighed into 100 mL Schlenk flask and dissolved in 40 mL of THF or 20 mL MeCN. Solution was then cooled to 193 K, to which $Et_3N{\cdot}3HF$ (n = 0.34 mmol (1 eq. of HF); m = 55.31 mg; ρ = 0.989 mg μL^{-1}; V = 55.9 μL) was added dropwise via syringe and left to warm up to R.T. and stirred for 16 h. Solvent was then slowly removed under vacuum. Solid residue was washed with toluene to afford single crystals of $[(L^{Dipp})H]^+[F]^-$ (**1**) in quantitative yields.

Yield 370 mg (88%).

Melting point [°C] = 130 (decomposition)

^1H NMR (303 MHz, CD_3CN, 25 °C): δ 7.53–7.37 (m, 7H, ArH), 2.59 (singlet (broad), 4H, CH), 1.22 (d, J = 6.8 Hz, 12H, $(CH_3)_2$), 1.16 (d, J = 6.9 Hz, 12H, $(CH_3)_2$) ppm.

^{19}F NMR (285.05 MHz, CD3CN, 25 °C): δ−147.94 (s, 1F, F^-) ppm.

Free fluoride determination: 4.4% (experimental), 4.6% (theoretical)

Alternative synthesis of (**1**):

(L^{Dipp}) (n = 2.57 mmol; m = 1000 mg) was weighed into 100 mL Schlenk flask and dissolved in 35 mL of MeCN. KHF_2 (n = 2.56 mmol; m = 200 mg) was added and stirred for 16 h. Reaction mixture was then filtered through 0.45 μm syringe PTFE fliter, and

the filtrate was left to slowly evaporate at room temperature, to afford single crystals of $[(L^{Dipp})H]^+[F]^-$ (**1**).

4.2.2. Synthesis of $[(L^{Dipp})H]^+[(HF)F]^-$ (2)

(L^{Dipp}) (n = 0.51 mmol; m = 200 mg) was weighed into 100 mL Schlenk flask and dissolved in 20 mL of THF. Solution was then cooled to 193 K, to which a THF solution of $Et_3N{\cdot}3HF$ (n = 0.34 mmol (2 eq. of HF); m = 55.31 mg; ρ = 0.989 mg μL^{-1}; V = 55.9 μL) was added dropwise via syringe and left to warm up to room temperature and stirred for an additional hour. Solvent was then removed under vacuum. Compound (**2**) was then crystalized with slow evaporation of chloroform.

Yield 201 mg (91%)

Melting point [°C] = 223.4–227.1 (decomposition)

^{1}H NMR (303 MHz, CD3CN, 25 °C): δ 16.44–15.68 (t, 1H, $^1J_{HF}$ = 115 Hz, $[(HF)F]^-$), 10.01 (s, 1H, C(2)H), 7.83 (s, 2H, CH=CH), 7.66–7.60 (m, 2H, ArH), 7.47–7.44 (m, 4H, ArH), 2.43 (hept, *J* = 6.5 Hz, 4H, CH), 1.26 (d, *J* = 6.9 Hz, 12H, $(CH_3)_2$), 1.19 (d, *J* = 6.9 Hz, 12H, $(CH_3)_2$) ppm.

^{19}F NMR (285.05 MHz, CD_3CN, 25 °C): δ–147.50 (d, 2F, $^1J_{HF}$ = 114 Hz, $[(HF)F]^-$) ppm.

Free fluoride determination: 8.6% (experimental), 8.8% (theoretical)

4.2.3. Synthesis of $[(L^{Dipp})H]^+[(HF)_2F]^-$ (3)

(L^{Dipp}) (n = 6.43 mmol; m = 2500 mg) was weighed to FEP vessel and frozen in liquid nitrogen. Approximately 10 mL of aHF was condensed over the frozen (L^{Dipp}) and left to warm to room temperature. Clear red-brown solution was evaporated on the vacuum line after 30 min. Single crystals of (**3**) were obtained from crystallization in FEP crystallization vessel where a small temperature gradient (10 K) was used for evaporation of aHF from the crystallization part.

Yield 2300 mg (80%)

Melting point [°C] = 232.1–235.1 (decomposition)

^{1}H NMR (303 MHz, CD3CN, 25 °C): δ 13.36 (s (broad), 2H, $[(HF)_2F]^-$), 9.10 (t, *J* = 1.5 Hz, 1H, C(2)H), 7.90 (d, *J* = 1.5 Hz, 2H, CH=CH), 7.69–7.64 (m, 2H, ArH), 7.50–7.47 (m, 4H, ArH), 2.43 (hept, *J* = 6.7 Hz, 4H, CH), 1.28 (d, *J* = 6.7 Hz, 12H, $(CH_3)_2$), 1.20 (d, *J* = 6.9 Hz, 12H, $(CH_3)_2$) ppm.

^{19}F NMR (285.05 MHz, CD3CN, 25 °C): δ–167.28 (s, 2F, $[(HF)_2F]^-$) ppm.

Free fluoride determination: 13.3% (experimental), 12.7% (theoretical)

Alternative synthesis of (**3**):

(L^{Dipp}) (n = 0.51 mmol; m = 200 mg) was weighed into 100 mL Schlenk flask and dissolved in 20 mL of THF. Solution was then cooled to 193 K, to which a THF solution of $Et_3N{\cdot}3HF$ (n = 1.02 mmol (6 eq. of HF); m = 164.4 mg; ρ = 0.989 mg μL^{-1}; V = 167 μL) was added dropwise via syringe and left to warm to room temperature and stirred for an additional hour. Solvent and excess reagent was then removed under vacuum which afforded spectroscopically pure product (**3**).

Acknowledgements

The authors gratefully acknowledge the Slovenian Research Agency (ARRS) for financial support of the Research Program P1-0045 (Inorganic Chemistry and Technology) and Slovenian NMR Centre of National Institute of Chemistry for the use of their NMR spectrometers.

Appendix A. Supplementary data

Supplementary data associated with this article can be found, in the online version, at http://dx.doi.org/10.1016/j.jfluchem.2016.11.004.

References

[1] A. Kruger, L.J.L. Haller, H. Muller-Bunz, O. Serada, A. Neels, S.A. Macgregor, M. Albrecht, Smooth C(alkyl)-H bond activation in rhodium complexes comprising abnormal carbene ligands, Dalton Trans. 40 (2011) 9911–9920.
[2] K. Hirano, S. Urban, C. Wang, F. Glorius, A modular synthesis of highly substituted imidazolium salts, Org. Lett. 11 (2009) 1019–1022.
[3] C. Kison, T. Opatz, Synthesis of highly substituted unsymmetrical 1,2-diamines, 1,2-diimines, imidazolium salts and imidazolylidenes by aldimine cross-coupling, Synthesis 2006 (2006) 3727–3738.
[4] J.P. Hallett, T. Welton, Room-temperature ionic liquids: solvents for synthesis and catalysis. 2, Chem. Rev. 111 (2011) 3508–3576.
[5] T. Welton, Room-temperature ionic liquids. solvents for synthesis and catalysis, Chem. Rev. 99 (1999) 2071–2084.
[6] M.N. Hopkinson, C. Richter, M. Schedler, F. Glorius, An overview of N-heterocyclic carbenes, Nature 510 (2014) 485–496.
[7] S.N. Riduan, Y. Zhang, Imidazolium salts and their polymeric materials for biological applications, Chem. Soc. Rev. 42 (2013) 9055–9070.
[8] J.S. Wilkes, M.J. Zaworotko, Air and water stable 1-ethyl-3-methylimidazolium based ionic liquids, J. Chem. Soc. Chem. Commun. (1992) 965–967.
[9] J. Fuller, R.T. Carlin, H.C. De Long, D. Haworth, Structure of 1-ethyl-3-methylimidazolium hexafluorophosphate: model for room temperature molten salts, J. Chem. Soc. Chem. Commun. (1994) 299–300.
[10] R.P. Swatloski, J.D. Holbrey, R.D. Rogers, Ionic liquids are not always green: hydrolysis of 1-butyl-3-methylimidazolium hexafluorophosphate, Green Chem. 5 (2003) 361–363.
[11] S. Bouvet, B. Pégot, J. Marrot, E. Magnier, Solvent free nucleophilic introduction of fluorine with [bmim][F], Tetrahedron Lett. 55 (2014) 826–829.
[12] Z.-Q. Zhu, M.-Y. Jiang, C.-G. Zheng, J.-C. Xiao, Efficient synthesis of 1-alkyl-3-methylimidazolium fluorides and possibility of the existence of hydrogen bonding between fluoride anion and C(sp3)–H, J. Fluorine Chem. 133 (2012) 160–162.
[13] R. Hagiwara, Y. Ito, Room temperature ionic liquids of alkylimidazolium cations and fluoroanions, J. Fluorine Chem. 105 (2000) 221–227.
[14] E. Alcalde, I. Dinarès, A. Ibáñez, N. Mesquida, A simple halide-to-anion exchange method for heteroaromatic salts and ionic liquids, Molecules 17 (2012) 4007.
[15] I. Dinares, C. Garcia de Miguel, A. Ibanez, N. Mesquida, E. Alcalde, Imidazolium ionic liquids: a simple anion exchange protocol, Green Chem. 11 (2009) 1507–1510.
[16] T. Enomoto, Y. Nakamori, K. Matsumoto, R. Hagiwara, Ion–Ion interactions and conduction mechanism of highly conductive fluorohydrogenate ionic liquids, J. Phys. Chem. C 115 (2011) 4324–4332.
[17] K. Matsumoto, R. Hagiwara, R. Yoshida, Y. Ito, Z. Mazej, P. Benkic, B. Zemva, O. Tamada, H. Yoshino, S. Matsubara, Syntheses, structures and properties of 1-ethyl-3-methylimidazolium salts of fluorocomplex anions, Dalton Trans. (2004) 144–149.
[18] K. Matsumoto, T. Tsuda, R. Hagiwara, Y. Ito, O. Tamada, Structural characteristics of 1-ethyl-3-methylimidazolium bifluoride: HF-deficient form of a highly conductive room temperature molten salt, Solid State Sci. 4 (2002) 23–26.
[19] R. Hagiwara, T. Hirashige, T. Tsuda, Y. Ito, A highly conductive room temperature molten fluoride: EMIF·2.3 HF, J. Electrochem. Soc. 149 (2002) D1–D6.
[20] R. Hagiwara, T. Hirashige, T. Tsuda, Y. Ito, Acidic 1-ethyl-3-methylimidazolium fluoride: a new room temperature ionic liquid, J. Fluorine Chem. 99 (1999) 1–3.
[21] V.V. Grushin, Generation of naked fluoride ions in unprecedentedly high concentrations from a fluoropalladium complex, Angew. Chem. Int. Ed. 37 (1998) 994–996.
[22] A.R. Mahjoub, X. Zhang, K. Seppelt, Reactions of the naked fluoride ion: syntheses and structures of SeF 62– and BrF 6–, Chem. Eur. J. 1 (1995) 261–265.
[23] K.O. Christe, W.W. Wilson, Reaction of the fluoride anion with acetonitrile. Chloroform and methylene chloride, J. Fluorine Chem. 47 (1990) 117–120.
[24] I. Rozas, I. Alkorta, J. Elguero, Bifurcated hydrogen bonds: three-Centered interactions, J. Phys. Chem. A 102 (1998) 9925–9932.
[25] R.S. Rowland, R. Taylor, Intermolecular nonbonded contact distances in organic crystal structures: comparison with distances expected from van der waals radii, J. Phys. Chem. 100 (1996) 7384–7391.
[26] O. Ermer, S.A. Mason, F.A.L. Anet, S.S. Miura, Ultrashort nonbonded hydrogen . . . hydrogen distance in a half-cage pentacyclododecane, J. Am. Chem. Soc. 107 (1985) 2330–2334.
[27] J. Zong, J.T. Mague, R.A. Pascal, Exceptional steric congestion in an in,in-Bis (hydrosilane), J.Am. Chem. Soc. 135 (2013) 13235–13237.
[28] I.G. Shenderovich, S.N. Smirnov, G.S. Denisov, V.A. Gindin, N.S. Golubev, A. Dunger, R. Reibke, S. Kirpekar, O.L. Malkina, H.-H. Limbach, Nuclear magnetic resonance of hydrogen bonded clusters between F- and (HF)n: experiment and theory, Ber. Bunsenge. Phys. Chem. 102 (1998) 422–428.

[29] K.O. Christe, W.W. Wilson, Nuclear magnetic resonance spectrum of the fluoride anion, J. Fluorine Chem. 46 (1990) 339–342.
[30] L. Hintermann, Expedient syntheses of the N-heterocyclic carbene precursor imidazolium salts IPr·HCl IMes·HCl and IXy·HCl, Beilstein J. Org. Chem. 3 (2007) 22.
[31] M. Ponikvar, B. Sedej, B. Pihlar, B. Žemva, Determination of fluoride in M(SbF6) x compounds, Anal. Chim. Acta 418 (2000) 113–118.
[32] CrysAlisPro, Agilent Technologies, (2016) Version 1.171.37.33 (release 27-03-2014 CrysAlis171 .NET) (compiled Mar 27 2014, 17:12:48).
[33] R.C. Clark, J.S. Reid, The analytical calculation of abosorbtion in multifaceted crystals, Acta Cryst. A 51 (1995) 887–897.
[34] G. Sheldrick, SHELXT – integrated space-group and crystal-structure determination, Acta Crystallogr. A 71 (2015) 3–8.
[35] G. Sheldrick, Crystal structure refinement with SHELXL, Acta Crystallogr. C 71 (2015) 3–8.
[36] O.V. Dolomanov, L.J. Bourhis, R.J. Gildea, J.A.K. Howard, H. Puschmann, OLEX2: a complete structure solution, refinement and analysis program, J. Appl. Crystallogr. 42 (2009) 339–341.
[37] H. Putz, K. Brandenburg GbR, Diamond – Crystal and Molecular Structure Visualization Crystal Impact, (2016) Kreuzherrenstr. 102, 53227 Bonn, Germany. http://www.crystalimpact.com/diamond/references.htm.

Supporting Information

Reaction of N-heterocyclic carbene (NHC) with different HF sources and ratios – a free fluoride reagent based on imidazolium fluoride

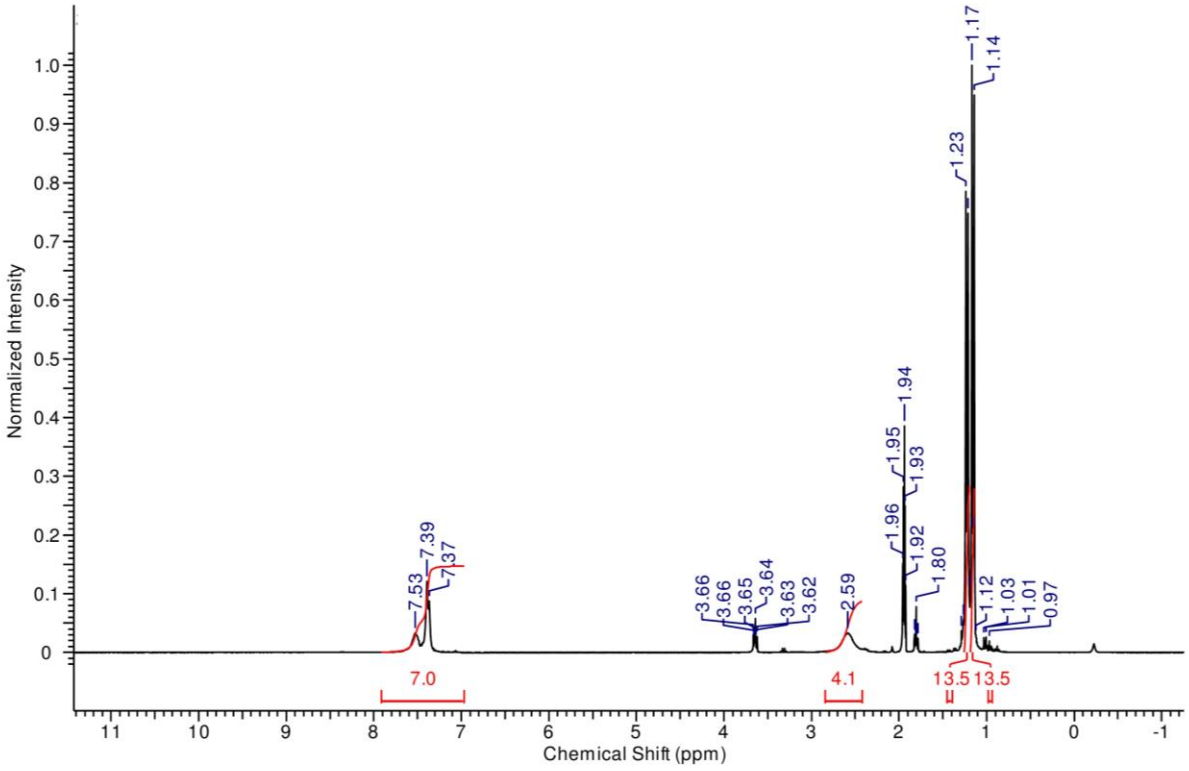
Blaž Alič* [1,2], Gašper Tavčar* [1,2]

[1] Jožef Stefan Institute, Department of Inorganic Chemistry and Technology, Jamova cesta 39, 1000 Ljubljana, Slovenia

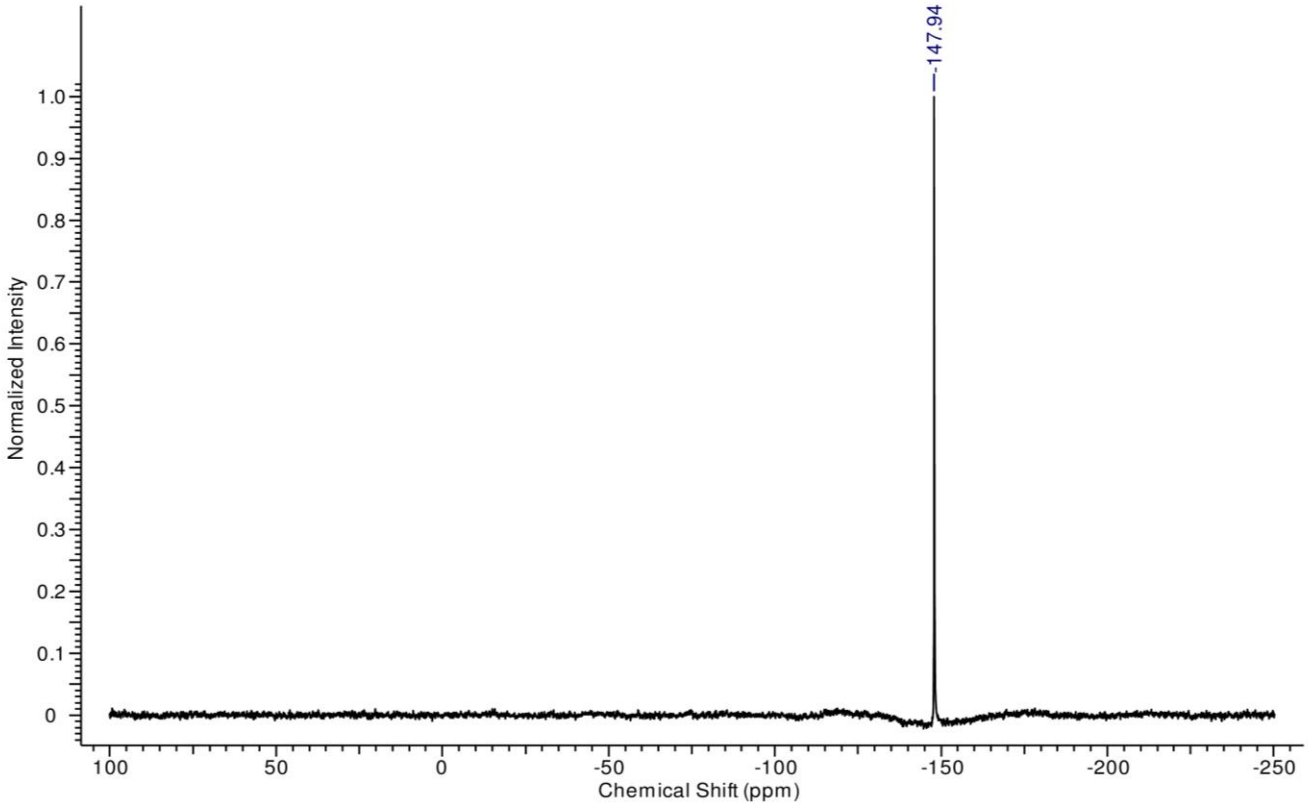
[2] Jožef Stefan International Postgraduate School, Jamova cesta 39, 1000 Ljubljana, Slovenia

*Corresponding author E-mail: gasper.tavcar@ijs.si, blaz.alic@gmail.com

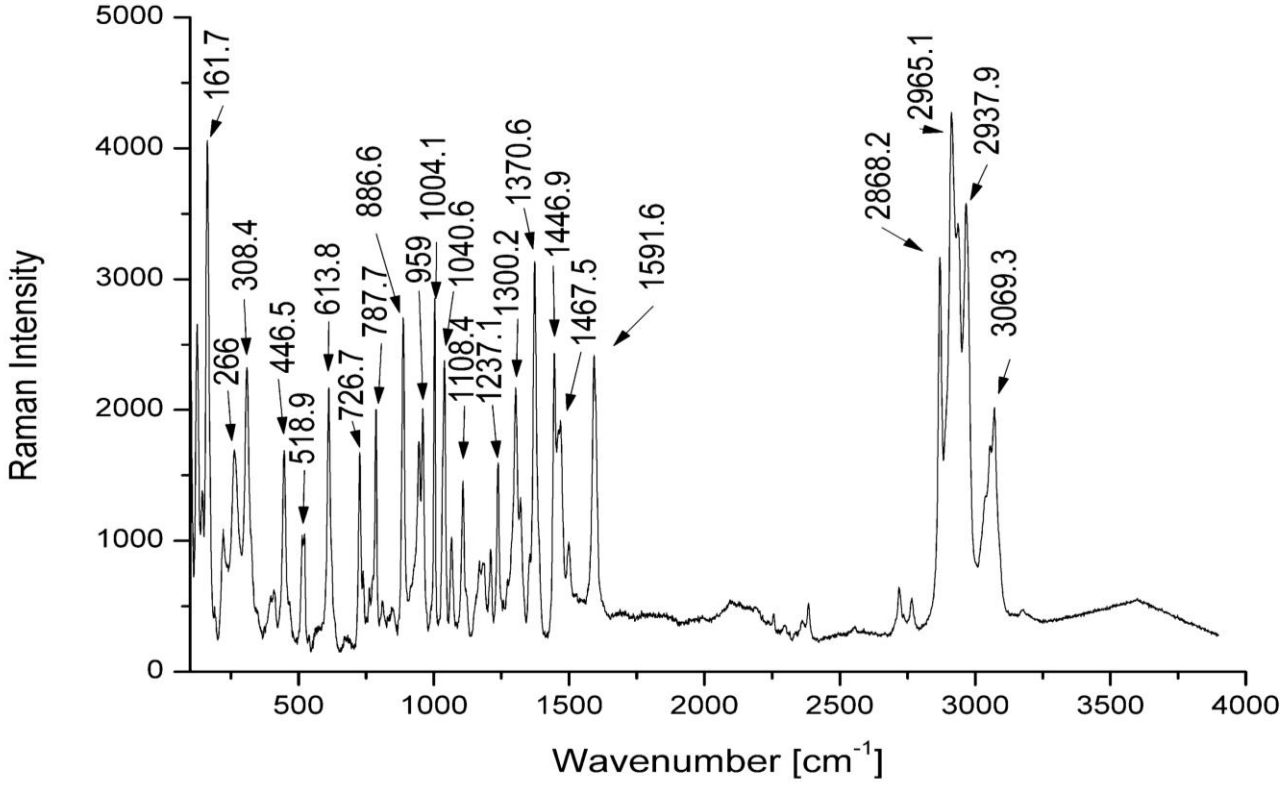
^{1}H NMR of [(L^{Dipp})H]$^{+}$[F]$^{-}$ (1)



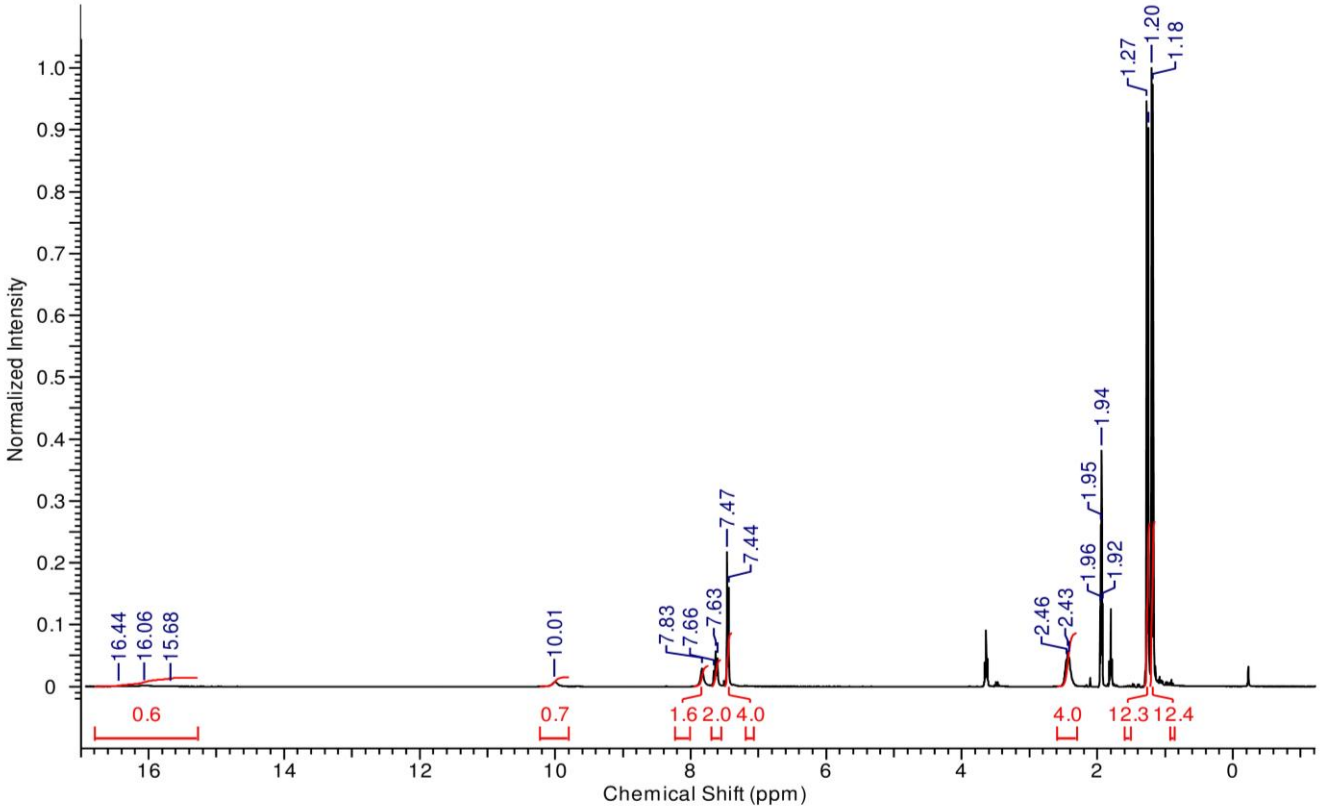
^{19}F NMR of [(L^{Dipp})H]$^{+}$[F]$^{-}$ (1)



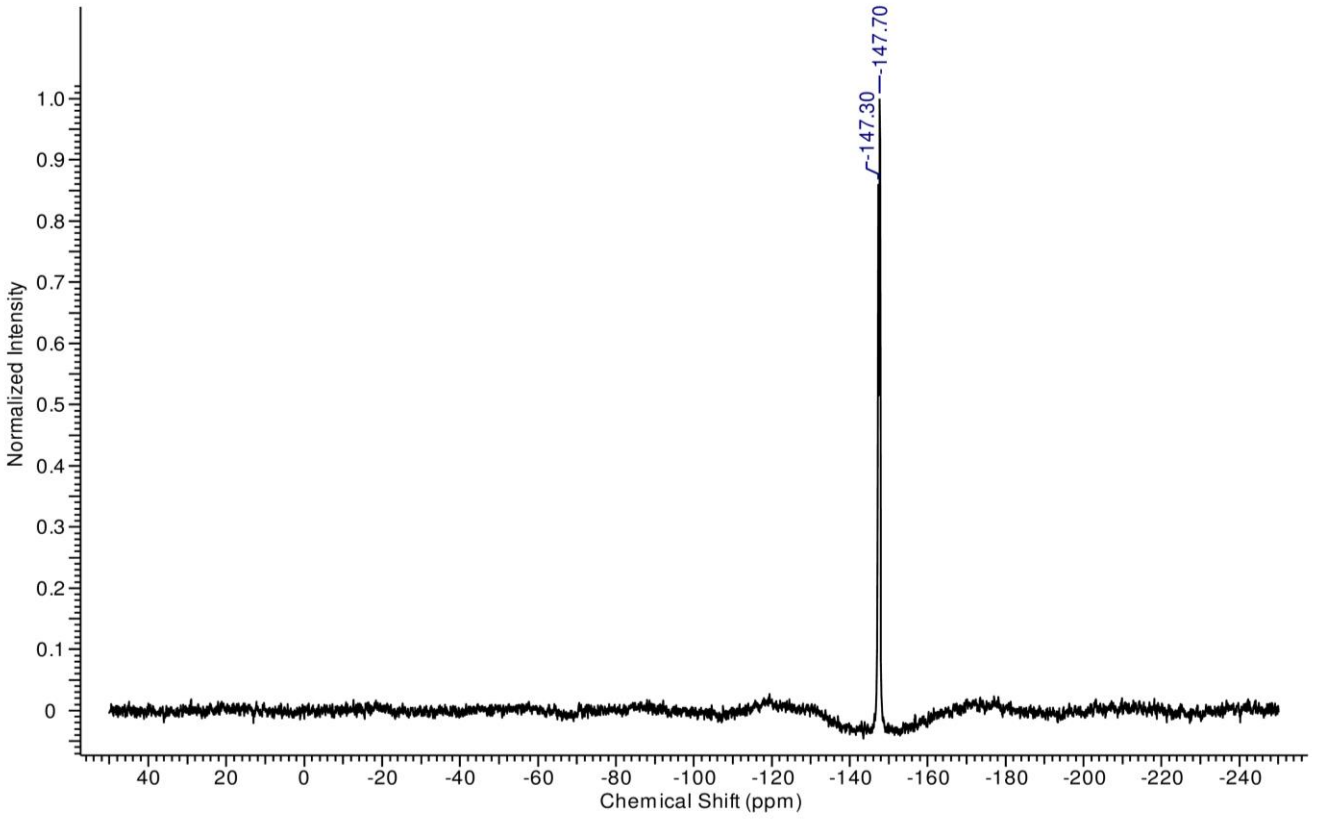
Raman and NMR spectres of $[(L^{Dipp})H]^+[F]^-$ (1)



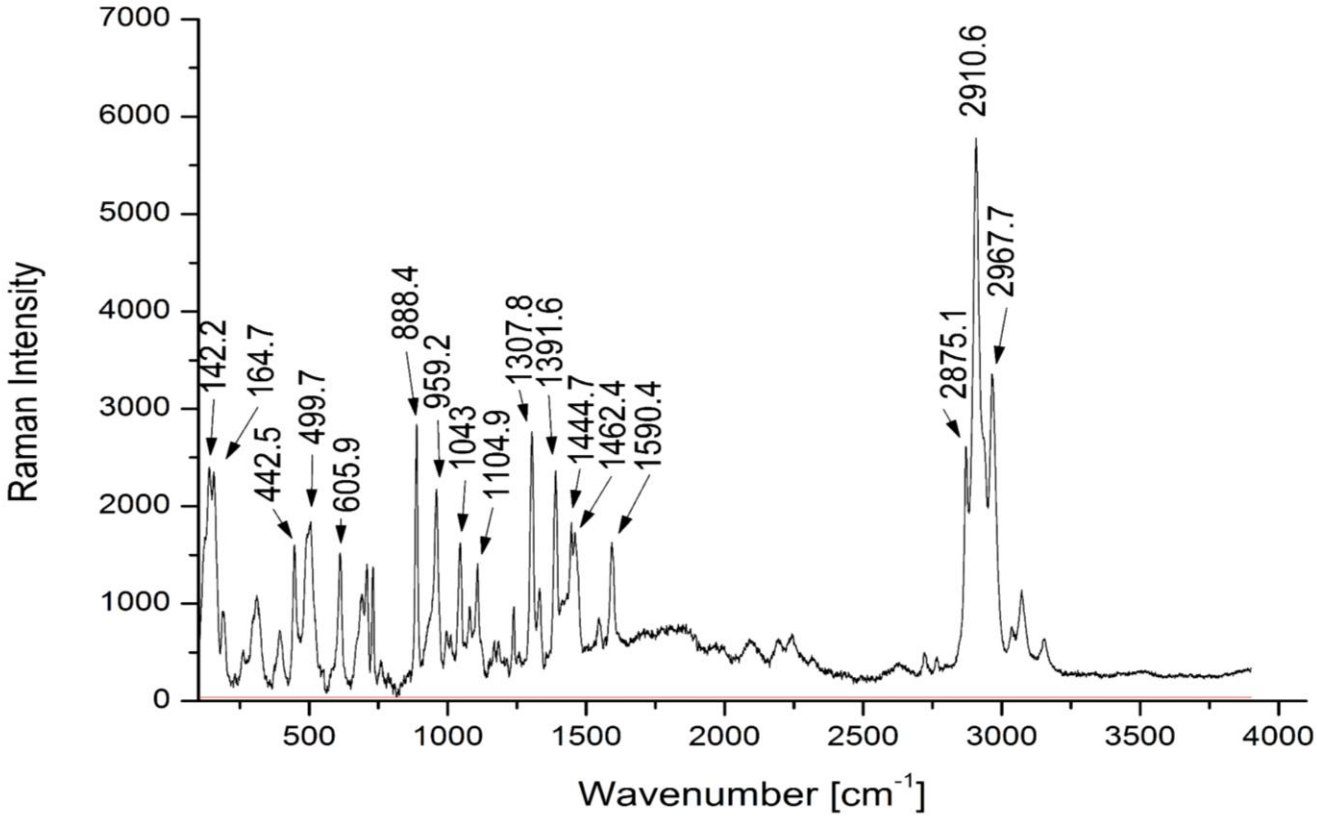
^{1}H NMR of $[(L^{Dipp})H]^{+}[(HF)F]^{-}$ (2)



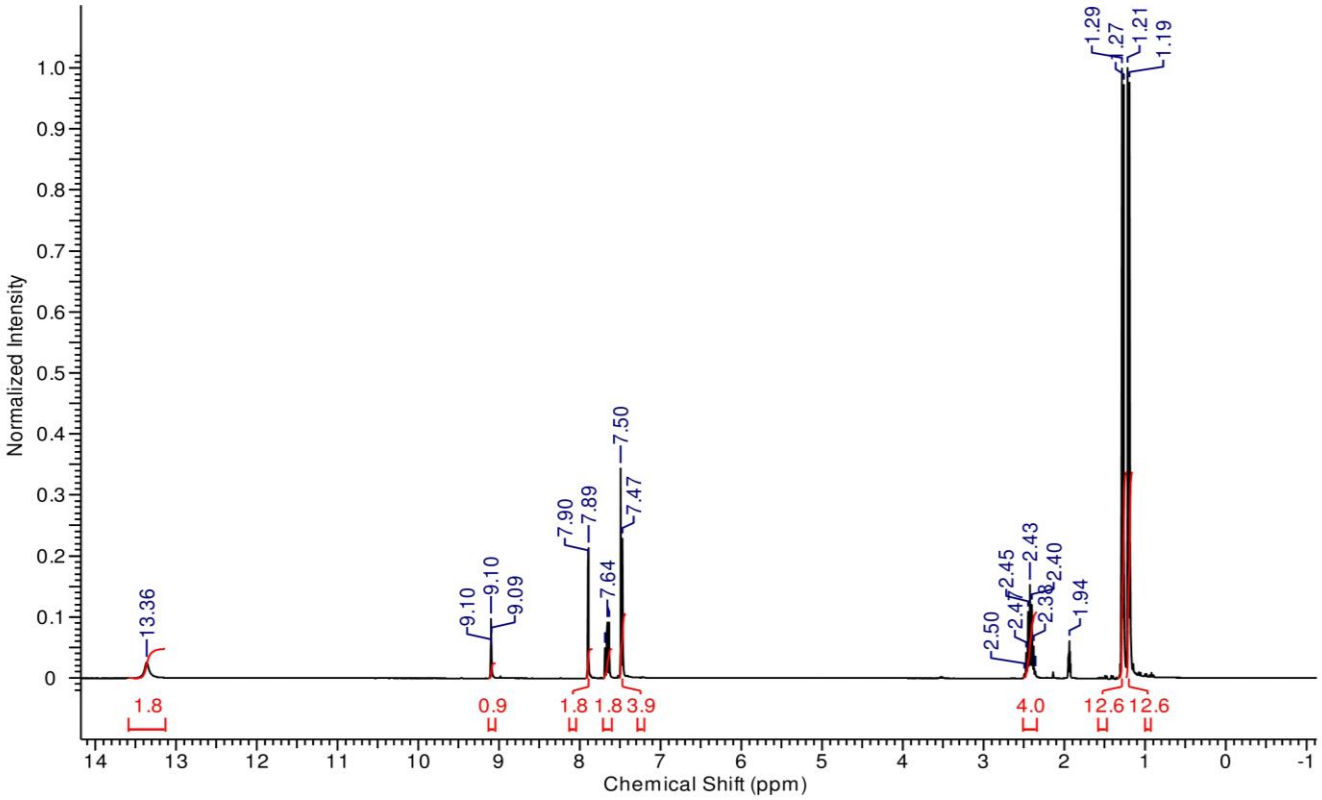
^{19}F NMR of $[(L^{Dipp})H]^{+}[(HF)F]^{-}$ (2)



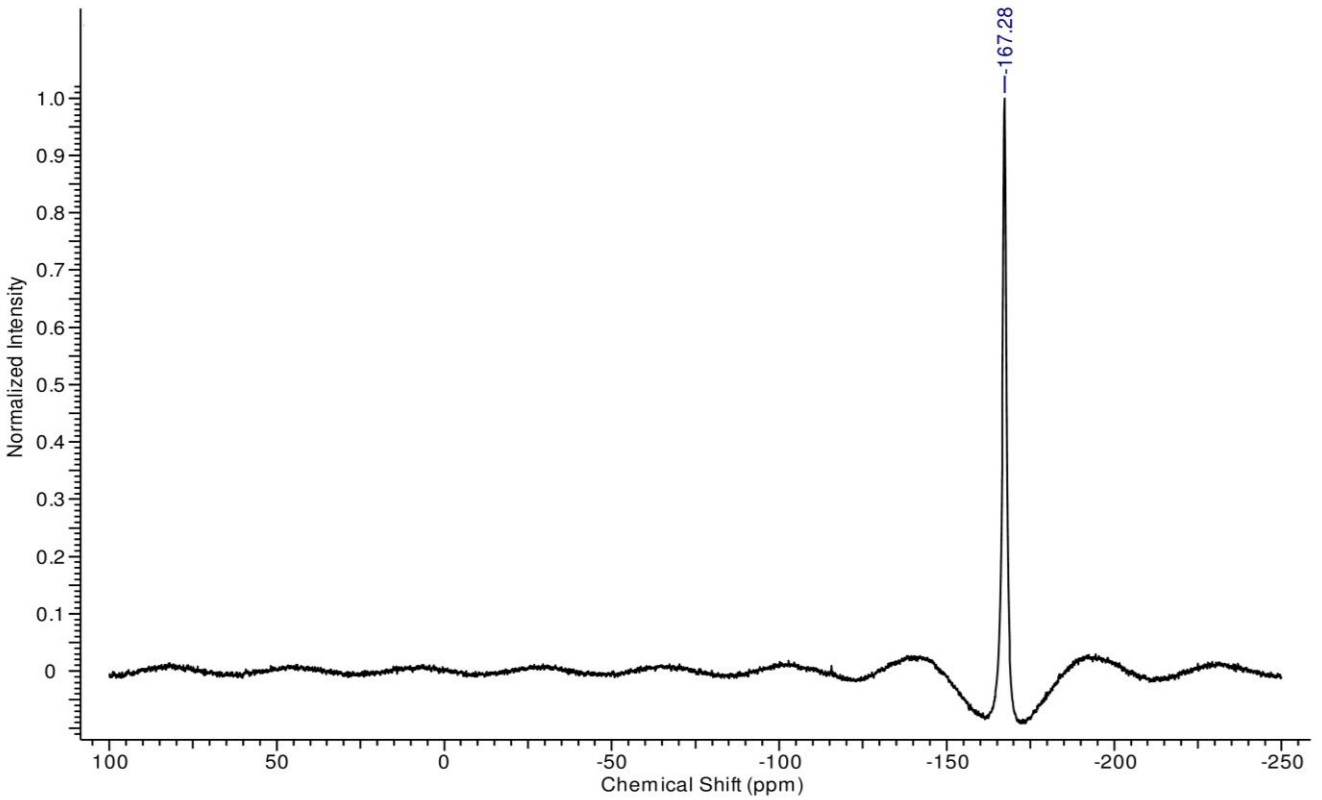
Raman and NMR spectres of $[(L^{Dipp})H]^+[(HF)F]^-$ (2)



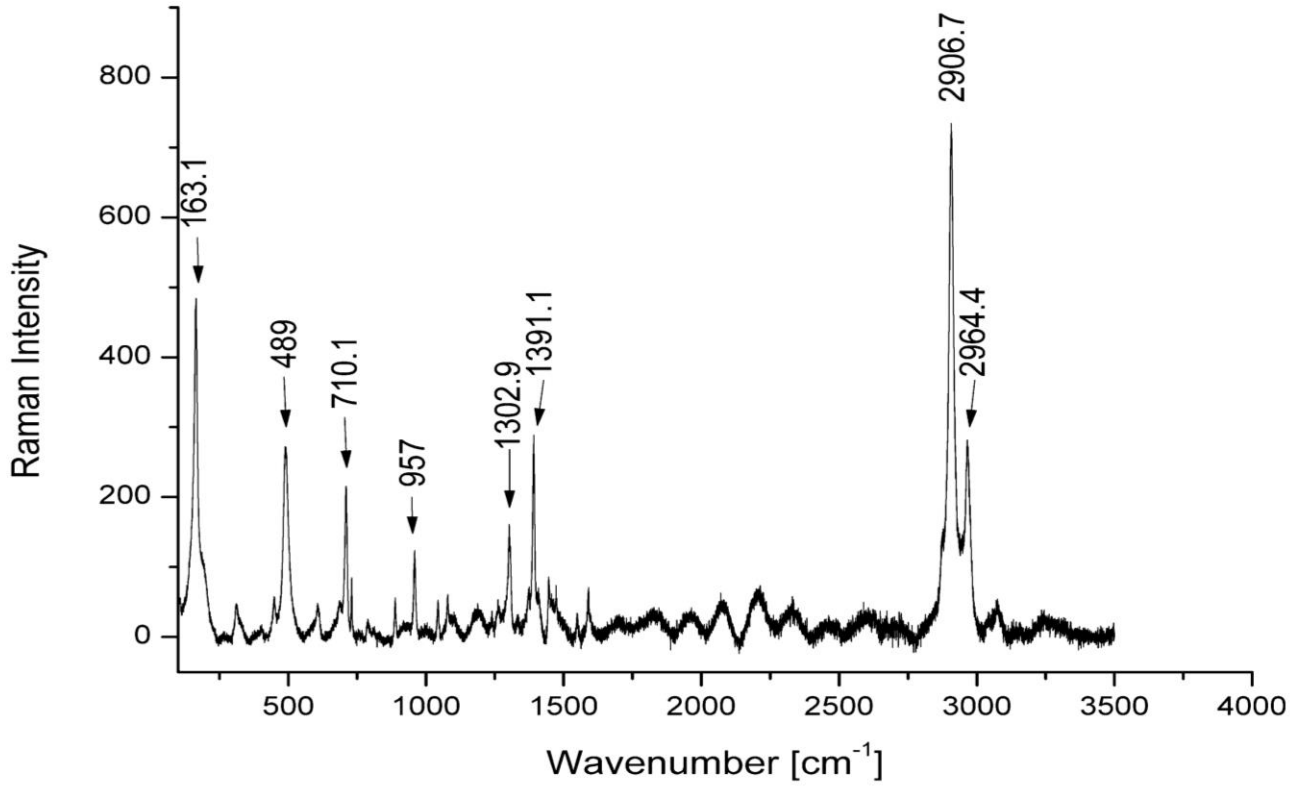
^{1}H NMR of $[(L^{Dipp})H]^{+}[(HF)_2F]^{-}$ (3)



^{19}F NMR of $[(L^{Dipp})H]^{+}[(HF)_2F]^{-}$ (3)



Raman and NMR spectres of $[(L^{Dipp})H]^+[(HF)_2F]^-$ (3)



Chapter 7

Discrete GeF_5^- Anion Structurally Characterized with a Readily Synthesized Imidazolium Based Naked Fluoride Reagent

In this chapter, article entitled: »Discrete GeF_5^- Anion Structurally Characterized with a Readily Synthesized Imidazolium Based Naked Fluoride Reagent«, by **Blaž Alič**, Melita Tramšek, Anton Kokalj and Gašper Tavčar is presented. For this article, the candidate performed all synthesis procedures with techniques for handling air-sensitive chemicals, obtained single crystals, performed X-ray single crystal diffraction analysis and prepared the final .cif files of the obtained products. Furthermore, the candidate performed the multinuclear NMR spectroscopy and Raman spectroscopy, prepared the samples for CHN elemental analysis and actively participated in data interpretation. The candidate wrote the first manuscript draft and was the leading author during its refinement and publication process. He was highly involved in all stages of the work from the conceptual stage of the research until the publication.

Anton Kokalj and Melita Tramšek made all the theoretical calculations and interpreted the Raman spectra. Additionally, Anton Kokalj wrote and designed the substantial Supporting Information document. Gašper Tavčar proposed the experiments, and coordinated the work. All authors actively participated in data interpretation.

In this work we showed that reactions of a new naked (free) fluoride reagent $[(L^{Dipp})H][F]$ treated with a surplus of gaseous MF_4 (M = Si, Ge) result in isolation of $[(L^{Dipp})H][MF_5]$ products. Isolation of a discrete, trigonal bipyramidal MF_5^- anions of silicon and germanium is enabled because of specific steric characteristics of the bulky $[(L^{Dipp})H]^+$ cation.

Research was focused on the preparation, isolation and characterization of discrete MF_5^- anions, with an emphasis on GeF_5^-. Observation of a general tendency that various metal halides preferentially form hexacoordinated structural motives instead of pentacoordinated moieties leads us to the explanation that the increasing size of a cation stabilizes pentacoordinated structural motives of germanium and silicon relative to the octahedral ones. We confirmed that the size of the cation stabilization of MF_5^- anions is due to steric effects as well as electrostatic Coulomb interactions between the anion and the cation. We reported the first crystal structure of the trigonal-bipyramidal GeF_5^- and the first ^{19}F NMR entries for GeF_5^- and GeF_6^{2-} anions in the organic solvent.

Inorganic Chemistry

Article

pubs.acs.org/IC

Discrete GeF_5^- Anion Structurally Characterized with a Readily Synthesized Imidazolium Based Naked Fluoride Reagent

Blaž Alič,[†,‡] Melita Tramšek,[†] Anton Kokalj,[‡,§] and Gašper Tavčar*[,†,‡]

[†]Department of Inorganic Chemistry and Technology, Jožef Stefan Institute, Jamova 39, 1000 Ljubljana, Slovenia

[§]Department of Physical and Organic Chemistry, Jožef Stefan Institute, Jamova 39, 1000 Ljubljana, Slovenia

[‡]Jožef Stefan International Postgraduate School, Jamova 39, 1000 Ljubljana, Slovenia

Supporting Information

ABSTRACT: The recently prepared novel naked fluoride reagent 1,3-bis(2,6-diisopropylphenyl)imidazolium fluoride ($[(L^{Dipp})H][F]$), treated with an excess of MF_4 (M = Si, Ge), results in isolation of $[(L^{Dipp})H][MF_5]$ products with the elusive trigonal bipyramidal MF_5^- anions. Specific steric characteristics of the $[(L^{Dipp})H]^+$ cation readily support isolation of monomeric and discrete trigonal bipyramidal fluorido anions of silicon and germanium. Based on combination of experimental results and DFT calculations, we demonstrate that the role of bulky cation is not solely due to steric hindering but also due to electrostatic effects, which are important in the design of such uncommon species. The discrete GeF_5^- anion was characterized by X-ray single-crystal diffraction for the first time. We report the missing ^{19}F NMR entries for the discrete GeF_5^- and GeF_6^{2-} anions in acetonitrile. All the products were also characterized by Raman spectroscopy and elemental analysis and supported by quantum-mechanical calculations.



INTRODUCTION

Silicon and germanium chemistry is poised for growth. Both elements are very important for the applications in electronics and optics.[1,2] Although the use of Si is already established, one of the very potent fields of application for Ge is in semiconductor technology. Thus, it is not surprising that the first functional 7 nm transistor architecture technology based on Si−Ge alloy was presented in late 2016 for the next generation electronics.[3] While Si chemistry is already thoroughly explored, the chemistry of Ge has not been as extensively studied. Progress in the research of germanium fluoride compounds could have important contributions in a variety of fields. In fact, one of the well-established procedures for the preparation of Si−Ge thin films includes disilane and germanium tetrafluoride,[4,5] thus the basic reactivity of GeF_4 and its properties are worthy of research.

The only structurally characterized examples of pentacoordinated germanium fluorido anions are $[(C_2F_5)_3GeF_2]^-$ and $[(CF_3)_3GeF_2]^-$,[6,7] but pentafluoridogermanate anion (GeF_5^-) was still missing. Hence, its structural characterization is an important contribution. The most reasonable approach for the synthesis of the pentacoordinated GeF_5^- anion is a reaction between the gaseous GeF_4 and a fluoride source. XeF_6, O_2/F_2, $(C_4H_9)_4NF$ (TBAF), $CH_3F/(CH_3)_3N$, NF_4BF_4, SF_3BF_4, NO_2F, and ClO_2F reagents addressed this challenge to a limited extent in the past.[8−11] While these reagents enable the synthesis of compounds with anions in Ge:F = 1:5 stoichiometry, they were apparently unable to stabilize 5-fold coordinated pentafluoridogermanate anion due to its tendency to polymerize. This notion reveals itself in the structures of XeF_5GeF_5 and ClO_2GeF_5, which consist of infinite chains of GeF_6 octahedra.[10]

According to evidence provided by vibrational spectroscopy, polymeric GeF_5^- anion composed of fluoride-bridged GeF_6 octahedra appears also in salts with $[(C_6H_5)_4As]^+$, $[(C_3H_7)_4N]^+$, $[(CH_3)_4N]^+$, NF_4^+, NO_2^+, SF_3^+, and O_2^+ cations. However, these reports lack the crystal structure characterization.[8−12] Even the study that reported the reaction with the well-established tetra-*n*-butylammonium fluoride (TBAF) reagent, which according to vibrational spectroscopy yields trigonal bipyramidal GeF_5^- anion, did not provide its crystal structure.[10,12] Despite these difficulties we believed that fluoride donors featuring bulky cations with specific geometric properties are a logical tool to obtain discrete GeF_5^- units and avoid the formation of higher intracoordinated anion clusters. Additionally, a large cation of a naked fluoride reagent increases its solubility and activity in organic solvents, thus overcoming the solubility limitations of alkali-metal fluorides.[13−15] Commercially available TBAF and tetramethylammonium fluoride reagents generally solve this problem to some degree, but unfortunately they slowly decompose in acetonitrile.[13,16,17] Furthermore, water must be introduced to the system in the key step of their synthesis due to the salt metathesis reaction with either AgF, KF, or HF, resulting in vigorous drying conditions that often lead to the decomposition of the reagents.[13,14,18−20] Although problems with TBAF reactivity were partially solved by its anhydrous synthesis[17] or by the

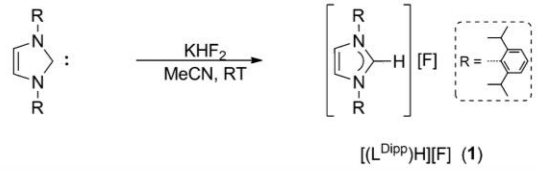
Received: June 27, 2017
Published: August 9, 2017

ACS Publications © 2017 American Chemical Society

DOI: 10.1021/acs.inorgchem.7b01606
Inorg. Chem. 2017, 56, 10070−10077

solvation with *tert*-butanol,[21] there is still demand for new alternative naked fluoride reagents stable in organic solvents. Due to specific steric characteristics and its anhydrous synthesis derived from N-heterocyclic carbene precursor, reagent $[(L^{Dipp})H][F]$ (**1**) does not display the aforementioned problems. It is soluble and stable in acetonitrile with no signs of decomposition after several days in the solution! It was synthesized in our laboratory (Scheme 1), and we reported its structural details and basic properties in late 2016.[22] Herein we report the first examples of its reactivity.

Scheme 1. Preparation of Imidazolium Fluoride $[(L^{Dipp})H][F]$ Reagent (1) in Quantitative Yields

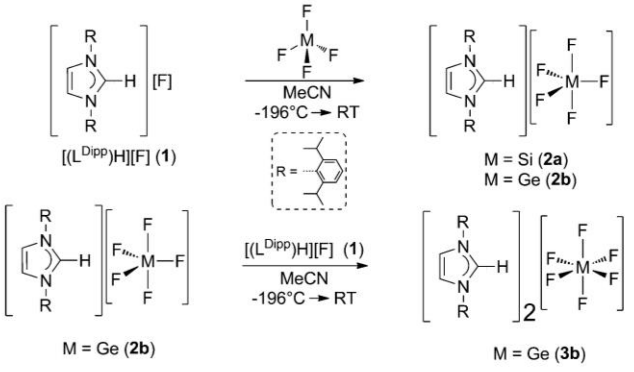


RESULTS AND DISCUSSION

Role of a Cation on Stabilization of Discrete Pentacoordinated MF_5^- Anions. GeF_4 and SiF_4 as Lewis acids react with **1** to yield $[(L^{Dipp})H][MF_5]$ (M = Si (**2a**), Ge (**2b**)) compounds consisting of pentacoordinated MF_5^- anions. The use of large N,N-disubstituted imidazolium cation "wingtips" seems to be important for the formation of the discrete MF_5^- fluorido anions. A similar method has been attempted in a system with the 1-ethyl-3-methylimidazolium chloride ([EMIM]Cl) reagent and $GeCl_4$; however the geometry of the ethyl and methyl N,N-substituted imidazolium cation appears to be unsuitable for the isolation of a discrete $GeCl_5^-$, since the authors only reported the formation of a discrete $GeCl_6^{2-}$ anion regardless of the reagent ratios.[23]

With the standard synthetic procedure, in which we used an excess of gaseous MF_4 in acetonitrile, we successfully prepared two isostructural compounds, **2a** and **2b**, in quantitative yields (Scheme 2). An excess of the MF_4 proved to be important in order to enable the synthesis of phase-pure MF_5^- salts, instead of MF_6^{2-} or their mixture. We observed GeF_6^{2-} anion when compound **2b** reacted with an additional equivalent of **1**, resulting in $[(L^{Dipp})H]_2[GeF_6]$ product **3b** (Scheme 2). Such a change from trigonal bipyramidal arrangement to octahedral structural motif around a Ge(IV) center is similar to carbene baring complexes of Ge(IV) fluorides.[24]

Scheme 2. Controlled Synthesis of Discrete Trigonal Bipyramidal MF_5^- Anions in Compounds 2a and 2b as Well as the Discrete Octahedral GeF_6^{2-} Anion in Compound 3b



A general tendency of various metal halides to form hexacoordinated octahedral structural motifs leads to numerous MX_6^{2-} compounds, whereas the pentacoordinated MX_5^- (X = halide) anions are less common. This generally accepted observation is in agreement with our DFT calculations, according to which octahedral GeF_6^{2-} anions are more likely to form thermodynamically when stabilized by small surrounding cations. On the contrary, the increasing size of the cation relatively stabilizes trigonal bipyramidal GeF_5^- anion, not only due to obvious steric reasons but also due to electrostatic Coulomb interactions. Figure 1, which plots the relative stability of GeF_6^{2-} vs GeF_5^- as a function of the distance between the centers of charge of anion and cation ($R_\pm$), clearly shows that the preference of octahedral GeF_6^{2-} against trigonal bipyramidal GeF_5^- diminishes with increasing size of cation (here the distance between the cation's center-of-charge and the point on its "exterior" in the direction toward the closest anion approach is meant as a criterion for the size of cation). These results will ease the design and isolation of such uncommon moieties in the future. For details of how the relative stability is evaluated, see section S2.5 in the Supporting Information.

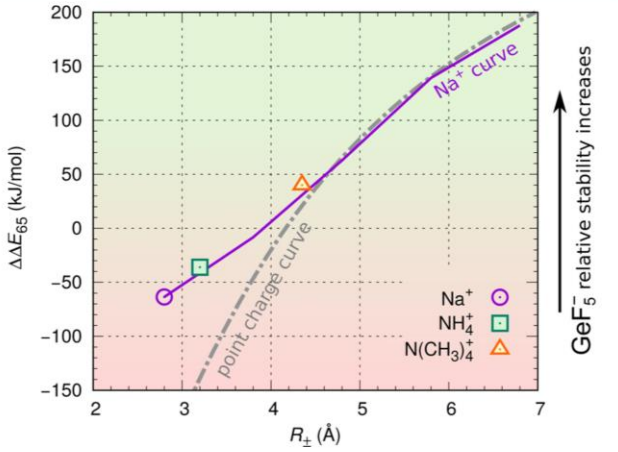


Figure 1. Relative stability of GeF_6^{2-} vs GeF_5^- ($\Delta\Delta E_{65}$) as a function of the distance between the centers of charge of anion and cation ($R_\pm$): the larger the $\Delta\Delta E_{65}$ value, the more the octahedral GeF_6^{2-} is destabilized against GeF_5^-. Points represent the values obtained from optimized structures, whereas curves were obtained by stepwise increasing the $R_\pm$ distance. In contrast to Na^+, NH_4^+, and $N(CH_3)_4^+$, which are all spherical cations and their center of charge can be well-defined, the $[(L^{Dipp})H]^+$ cation is not considered since its center of charge cannot be unambiguously determined. For further details, see the Supporting Information.

Crystal Structure Analysis. Crystal structures of products $[(L^{Dipp})H][SiF_5]$ (**2a**) and $[(L^{Dipp})H][GeF_5]$ (**2b**) were determined by single-crystal X-ray analysis. Data were collected at 100 K and were initially refined in the *C*2*c* space group. In this space group the structure showed disordered MF_5^- anions in two positions from which we could not distinctly define the structure of the anions. Therefore, we lowered the symmetry and refined the structures for **2a** and **2b** in $P2_1/n$ and $P2_1/c$ space groups, respectively. Lowering of the symmetry revealed trigonal bipyramidal anions in two distinct positions (domain A and domain B) populated 50:50 for **2a** and 80:20 for **2b** at 100

DOI: 10.1021/acs.inorgchem.7b01606
Inorg. Chem. 2017, 56, 10070−10077

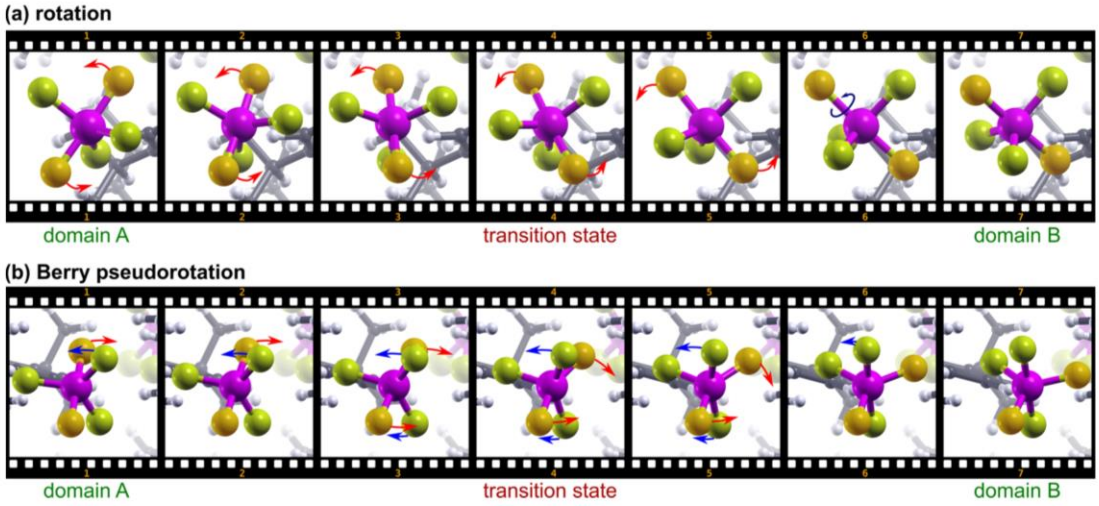


Figure 2. Snapshots of the PBE calculated transition of GeF_5^- anion from domain A to domain B via (a) rotation and (b) Berry pseudorotation mechanism. The PBE calculated activation energy for transition from domain A to domain B is $E^*_{A\rightarrow B}$ = 12 kJ/mol for both mechanisms (i.e., going from left to the right in the movie sequence), whereas the barrier for the reverse transition is $E^*_{B\rightarrow A}$ = 10 kJ/mol.

K, hence one domain is slightly more stable in **2b**. The experimentally observed stability of the two positional domains of the trigonal bipyramidal MF_5^- anions in **2a** and **2b** is well reproduced by periodic DFT calculations (section S2.1). MF_5^- anion can readily flip from one position to the other, either by rotation (R) or by the Berry pseudorotation mechanism (BM) (Figure 2). Symmetry of the anion in both **2a** and **2b** structures is very close to the ideal trigonal bipyramid. Slight distortion is found due to the interactions with the surrounding cations. Figure 3 shows the asymmetric unit of **2b**, i.e., $[(L^{Dipp})H][GeF_5]$ ion pair with GeF_5^- in domain A. With the aid of DFT calculations we could clearly identify two H-bonds per MF_5^- anion that are formed with imidazolium fragment (for both compounds), i.e., one bifurcated C2−H···$F1A_{ax}$($F4A_{eq}$) bond and one singular C4−H···$F2A_{ax}$ bond (domain A, Figure 4) and C2−H···$F2B_{ax}$($F4B_{eq}$) and C5−H···$F1B_{ax}$ (domain B).

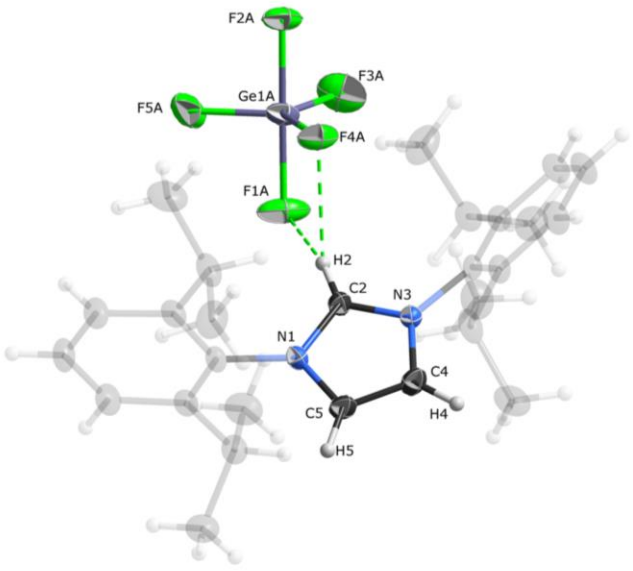


Figure 3. Asymmetric unit of the $[(L^{Dipp})H][GeF_5]$ (**2b**). Ellipsoids are drawn at 50% probability. Disordered (domain B) anion component is omitted, and $[(L^{Dipp})H]^+$ cation "wingtips" are shaded for clarity. Selected bond lengths [Å] and angles [deg]: Ge1A−$F1A_{ax}$ 1.759(3), Ge1A−$F2A_{ax}$ 1.759(2), Ge1A−$F3A_{eq}$ 1.716(2), Ge1A−$F4A_{eq}$ 1.726(3), Ge1A−$F5A_{eq}$ 1.702(2); $F1A_{ax}$−Ge1A−$F2A_{ax}$ 178.5(2), $F3A_{ax}$−Ge1A−$F4A_{ax}$ 121.2(2), $F3A_{ax}$−Ge1A−$F5A_{ax}$ 117.7(1), $F4A_{ax}$−Ge1A−$F5A_{ax}$ 121.1(2). Detailed description of the anion geometry can be found in sections S2.1 and S2.2 of the Supporting Information.

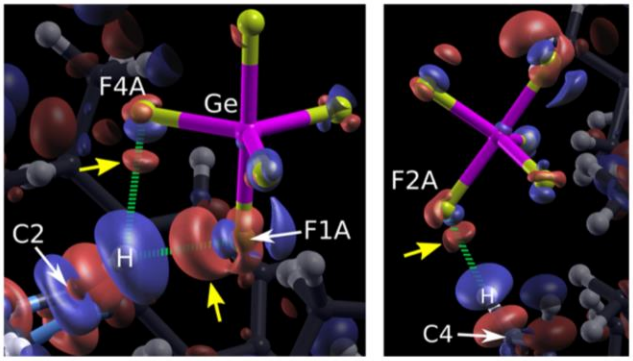


Figure 4. H-bonding between GeF_5^- anion and $[(L^{Dipp})H]^+$ cations (for the domain A) as revealed by DFT calculated charge density difference according to eq 1 (see Computational Section). Electron excess regions are colored red, while electron deficit regions are blue (isosurfaces are drawn at ±0.001 e/bohr^3). The criterion for the identification of H-bond is the existence of an electron charge accumulation lobe between the H···F atoms: such lobes are marked by yellow arrows.

DFT calculated activation energies for R and BM mechanisms in compound **2b** are almost equal and very small, 12 kJ/mol (section S2.4), which implies that both mechanisms are similarly probable. While BM is consistent with the ^{19}F NMR spectroscopy, as we only observed a single signal instead of two for axial and equatorial fluorides, the R mechanism cannot be excluded (see NMR Spectroscopy).

As for the M−F bond lengths and F−M−F bond angles (caption of Figure 3, Tables S5 and S6), the periodic DFT calculations reproduce experimentally observed distortion from the ideal bipyramidal structure of MF_5^- anions, i.e., the axial

DOI: 10.1021/acs.inorgchem.7b01606
Inorg. Chem. 2017, 56, 10070−10077

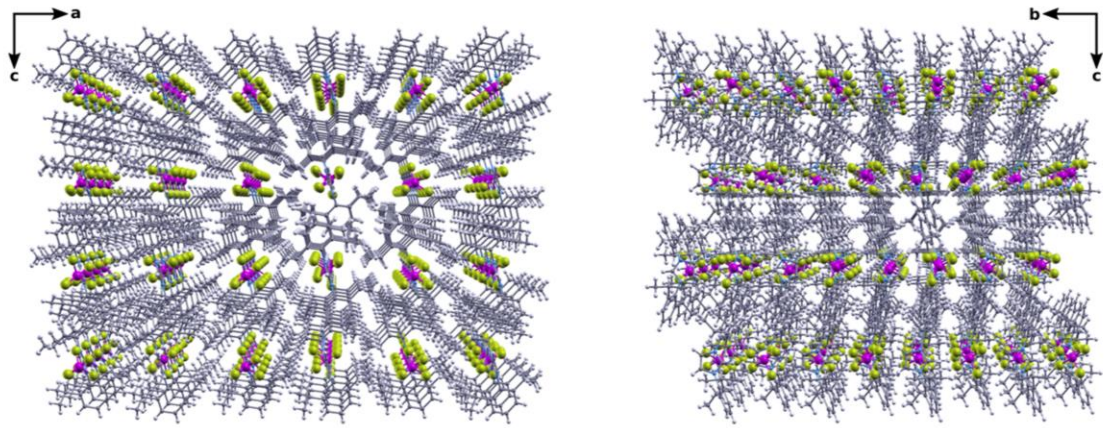


Figure 5. Perspective view of the $[(L^{Dipp})H][GeF5]$ (**2b**) crystal structure with GeF_5^- anions in domain A: (010) and (100) planes are shown on the left and right, respectively. GeF_5^- anions are visually emphasized (Ge = purple, F = greenish).

F_{ax}–M–F_{ax} angle is smaller than 180° and equatorial F_{eq}–M–F_{eq} angles are distorted from 120°. While calculations predict similar distortions for the two domains, the experimentally determined distortion of domain B is slightly larger than that of domain A. According to both experiments and calculations, the axial M–F_{ax} bonds are longer than the equatorial M–F_{eq} bonds, which is in accordance with the valence shell electron pair repulsion (VSEPR) model of molecular geometry.[25] For further details about the local structure of MF_5^- anions, see section S2.2.

In the crystal structure 6 MF_5^- anions are packed around each $[(L^{Dipp})H]^+$ cation and vice versa (6 cations around each anion), forming the distorted NaCl type structure (Figure S4). Bader population analysis confirms that compounds **2a** and **2b** can indeed be described according to chemist's expectation as consisting of MF_5^- anions and $[(L^{Dipp})H]^+$ cations. Namely, calculated Bader charge is −0.96 for both anions, SiF_5^- and GeF_5^-. Analysis of charge density difference calculated via eq 1 reaffirms the absence of any significant charge transfer between MF_5^- anions and $[(L^{Dipp})H]^+$ cations. The corresponding crystal data are summarized in Table S2, the asymmetric unit for GeF_5^- is shown in Figure 3, that of SiF_5^- is in Figure S3 (left), and a perspective view of the crystal structure **2b** is presented in Figure 5.

Raman Spectroscopy. Raman spectra of **2a** and **2b** differ for SiF_5^- and GeF_5^- anions, respectively. Only one peak in the Raman spectra can be definitely assigned to the M–F vibration of the trigonal bipyramidal MF_5^- anions due to intense vibrations of the cation in the same region that are masking the rest of the anion peaks. The position of the most intense Si–F ν_1 vibration for symmetrical stretch mode can be found at 709 cm^{-1} (MP2 calcd 693 cm^{-1}), and that of the Ge–F vibration can be observed at 664 cm^{-1} (MP2 calcd 663 cm^{-1}) (Figure 6). The position of the Ge–F vibration corresponds well with the published data for $(C_4H_9)_4NGeF_5$ (665 cm^{-1}):[10] note that ref 10 lacks the crystal structure characterization.

With the use of Raman spectroscopy we also checked the stability of the $[(L^{Dipp})H][MF_5]$ compounds **2a** and **2b** exposed to air. Raman spectra were taken in a sealed capillary and on the sample that was exposed to the air for 24 h (Figure S9). According to the Raman spectroscopy, there is no difference in the position of the ν_1 vibrations of the MF_5^- anions and cations. The compounds **2a** and **2b** are therefore stable in air at room temperature (section S2.6).

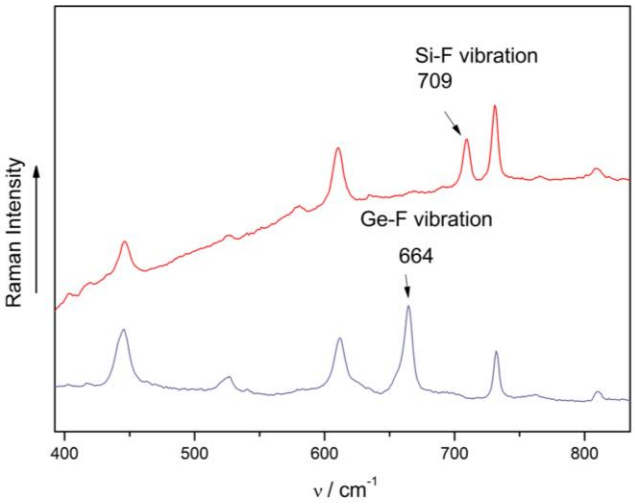


Figure 6. Raman spectra of $[(L^{Dipp})H][SiF_5]$ (**2a**) and $[(L^{Dipp})H][GeF_5]$ (**2b**). Full vibration characterization can be found in section S2.6 of the Supporting Information.

NMR Spectroscopy. Yet another point should be emphasized. While all fluoridosilicate ^{19}F NMR entries along with GeF_4 are known,[26,27] there were no available NMR data for the discrete GeF_5^- and GeF_6^{2-} anions in any organic solvent. The only reported ^{19}F NMR values were found for water and BrF_5 solutions.[8,28] Herein we report ^{19}F NMR spectra of obtained products **2b** and **3b** in acetonitrile and compare them to related fluoridosilicate species (Table 1). Note that ^{19}F NMR shows a single peak at 136.60 ppm for GeF_5^- in deuterated acetonitrile, hence the sequence of NMR peaks of GeF_4, GeF_5^-, and GeF_6^{2-} follows the SiF_4, SiF_5^-, and SiF_6^{2-} series in acetonitrile, i.e., $[\delta(GeF_4) - \delta(GeF_5^-)]$:

Table 1. ^{19}F NMR Chemical Shifts vs $CFCl_3$ at 25 °C for Completed Series of Fluoridosilicate and Fluoridogermanate Species: MF_4, MF_5^-, and MF_6^{2-} (M = Si, Ge) in Acetonitrile

	MF_4	MF_5^-	MF_6^{2-}
Si [ppm]	−163[a]	−137.08[c]	−125[b]
Ge [ppm]	−176[a]	−136.60[c]	−119.03[c]

[a]Reference 26. [b]Reference 27. [c]This work.

DOI: 10.1021/acs.inorgchem.7b01606
Inorg. Chem. 2017, 56, 10070−10077

$[\delta(GeF_5^-) - \delta(GeF_6^{2-})] \approx [\delta(SiF_4) - \delta(SiF_5^-)]:[\delta(SiF_5^-) - \delta(SiF_6^{2-})] \approx 11:5$.

The spectra taken near the temperature of the melting point of acetonitrile (−44 °C) did not reveal splitting of the signal. This observation is consistent with our DFT calculations according to which the transition of the anion between the two domains is still a lot faster than the NMR time scale even at much lower temperatures (section S2.4).

■ CONCLUSIONS

In this work, we showed that isolation and the structural characterization of previously unknown salt with monomeric bipyramidal GeF_5^- anion could easily be achieved with the use of our novel sterically hindering imidazolium fluoride (**1**). Despite various known nucleophilic fluorinating reagents,[29] the characteristics of **1**—high stability and solubility as well as its ease of synthesis in acetonitrile—are at least on par with those of other naked fluoride reagents. Its advantages could lead to the widespread use in various biological, organic, inorganic, and materials systems showing the full scope of its applicability. With this in mind, we would like to encourage colleagues within the chemical community to explore the reactivity and properties of this reagent on different systems and use it in imaginative ways to explore the new frontiers of fluorination chemistry such as structural characterization of discrete trigonal bipyramidal GeF_5^- anion observed for the first time.

■ EXPERIMENTAL SECTION

General Experimental Procedures and Reagents. All experiments and manipulations were carried out under an inert atmosphere of dried argon, either in a glovebox (M. Braun) or by using standard Schlenk techniques. Acetonitrile was stored over 3 Å molecular sieves and left for at least 48 h prior to use. Deuterated solvents were dried over 3 Å molecular sieves (at least 20% w/w). Glassware was oven-dried overnight at 150 °C.

GeF_4 (CERAC, Inc., 99.99%) was used as supplied. SiF_4 was synthesized by modified literature procedures.[30] L^{Dipp} was synthesized according to standard literature procedures.[31] $[(L^{Dipp})H][F]$ was prepared according to modified literature procedures.[22]

CAUTION! *GeF_4 and SiF_4 must be handled in a well-ventilated hood and protective clothing must be worn at all times! The experimentalist must become familiar with these reagents and the hazards associated with them.*

NMR Spectroscopy. Samples were loaded into NMR tubes in the glovebox under an argon atmosphere. NMR spectra (^1H, ^{13}C, and ^{19}F) were recorded at the Slovenian NMR Centre of the National Institute of Chemistry on Agilent Technologies Unity Inova 300 MHz (^1H at 303 and 298 MHz, ^{13}C at 76 MHz, and ^{19}F at 285 MHz). The chemical shifts are referenced as ^1H and ^{13}C to residual signals of deuterated solvent peaks and ^{19}F to $CFCl_3$ as an internal standard.

X-ray Structural Analysis. Single-crystal data for all compounds were collected on a Gemini A diffractometer equipped with an Atlas CCD detector, using graphite monochromated Cu Kα radiation. The data were treated using the CrysAlisPro software suite program package.[32] Analytical absorption correction was applied to all data sets.[33] Structures were solved using the ShelXT program.[34] Structure refinement was performed with the ShelXL-2015 software[35] implemented in the program package Olex2.[36] Figures of experimental structures (except for Figures 4 and 5) were prepared using Diamond 4.0 software.[37]

Raman Spectroscopy. Raman spectra with a resolution of 1 cm^{-1} were recorded at room temperature on a Horiba Jobin Yvon Labram-HR spectrometer coupled with an Olympus BXFM-ILHS microscope. Samples were excited by the 633 nm emission line of a 24.3 mW He−Ne laser with a power output of 14 mW on the sample. The samples were loaded inside the glovebox into 0.3 mm quartz capillaries which were previously vacuum-dried. The spectra obtained from the powdered samples correspond completely to the spectra taken from several, randomly oriented, single crystals of which the identity was additionally confirmed by the unit cell measurement on the single-crystal X-ray diffractometer.

CHN Elemental Analysis. Compounds were transferred into silver foils in the glovebox under an argon atmosphere. Carbon, hydrogen, and nitrogen contents were determined using a CHNS elemental analyzer vario EL cube (Elementar) operating in the CHN mode.

Synthesis of $[(L^{Dipp})H][SiF_5]$ (2a). A solution of $[(L^{Dipp})H][F]$ (M = 408.3 g mol^{-1}; n = 0.245 mmol; m = 100 mg) in MeCN (5 mL) was transferred to a FEP reaction vessel equipped with a magnetic stirring bar. The solution was frozen in liquid nitrogen, and SiF_4 (M = 104.08 g mol^{-1}; n = 0.367 mmol (1.5 equiv); m = 38.2 mg) was condensed over the frozen solution. The solution was left to warm up slowly to room temperature and left to stir overnight. The reaction vessel was then briefly evacuated to remove excess SiF_4 gas, and remaining solution was transferred to a glass crystallization vessel without further treatment. Slow evaporation of solvent under the static vacuum and 20 °C temperature gradient afforded clear colorless single crystals suitable for X-ray diffraction analysis. Yield: 120 mg (95.2%).

The ^1H NMR (302 MHz, CD_3CN, 25 °C) spectrum is shown in Figure S2 (top-left panel): δ 8.95 (t, J = 1.5 Hz, 1H, C(2)H), 7.87 (d, J = 1.5 Hz, 2H, CH=CH), 7.70−7.63 (m, 2H, p-ArH), 7.51−7.46 (m, 4H, m-ArH), 2.42 (hept, J = 6.9 Hz, 4H, iPrCH), 1.28 (d, J = 6.7 Hz, 12H, iPr$(CH_3)_2$), 1.20 (d, J = 6.9 Hz, 12H, iPr$(CH_3)_2$) ppm.

The ^{19}F NMR (285.05 MHz, CD_3CN, 25 °C) spectrum is shown in Figure S2 (middle-left panel): δ −137.08 (s, 5F, SiF_5^-) ppm.

The ^{13}C NMR (76 MHz, CD_3CN, 25 °C) spectrum is shown in Figure S2 (bottom-left panel): δ 146.40, 138.82, 133.27, 130.86 127.16, 125.81, 29.97, 24.56, 23.90.

Elemental analysis for $C_{27}H_{37}N_2SiF_5$ (512.67) (%), stoichiometric, C, 63.25; H, 7.27; N, 5.46; found, C, 63.40; H, 7.32; N, 5.64.

Synthesis of $[(L^{Dipp})H][GeF_5]$ (2b). A solution of $[(L^{Dipp})H][F]$ (M = 408.3 g mol^{-1}; n = 0.73 mmol; m = 298 mg) was transferred to a FEP reaction vessel equipped with a magnetic stirring bar. GeF_4 (M = 148.6 g mol^{-1}; n = 0.79 mmol (1.09 equiv); m = 118.2 mg) was condensed over the frozen solution and was slowly warmed to room temperature and left to stir overnight. The reaction vessel was then briefly evacuated to remove excess GeF_4 gas, and remaining solution was transferred to a glass crystallization vessel without further treatment. Slow evaporation of solvent under the static vacuum and 20 °C temperature gradient afforded clear colorless single crystals suitable for X-ray diffraction analysis. Yield: 389 mg (95.6%).

The ^1H NMR (302 MHz, CD_3CN, 25 °C) spectrum is shown in Figure S2 (top-right panel): δ 8.98 (t, J = 1.6 Hz, 1H, C(2)H), 7.94 (d, J = 1.6 Hz, 2H, CH=CH), 7.69−7.62 (m, 2H, p-ArH), 7.50−7.45 (m, 4H, m-ArH), 2.43 (hept, J = 6.8 Hz, 4H, iPrCH), 1.27 (d, J = 6.7 Hz, 12H, iPr$(CH_3)_2$), 1.20 (d, J = 6.9 Hz, 12H, iPr$(CH_3)_2$) ppm.

The ^{19}F NMR (285.05 MHz, CD_3CN, 25 °C) spectrum is shown in Figure S2 (middle-right panel): δ −136.60 (s, 5F, GeF_5^-) ppm.

The ^{13}C NMR (76 MHz, CD_3CN, 25 °C) spectrum is shown in Figure S2 (bottom-right panel): δ 146.40, 138.84, 133.25, 130.87, 127.17, 125.80, 29.97, 24.56, 23.92.

Elemental analysis for $C_{27}H_{37}N_2GeF_5$ (557.23) (%): stoichiometric, C, 58.20; H, 6,69; N, 5.03; found, C, 58.16; H, 6.70; N, 5.14.

Synthesis of $[(L^{Dipp})H]_2[GeF_6]$ (3b). A solution of $[(L^{Dipp})H][F]$ (M = 408.3 g mol^{-1}; n = 0.12 mmol; m = 49 mg) in MeCN (5 mL) was mixed with $[(L^{Dipp})H][GeF_5]$ (M = 557.23 g mol^{-1}; n = 0.12 mmol; m = 67 mg) in MeCN (5 mL) at room temperature under inert conditions. The solution was left to stir overnight. The reaction vessel was evacuated to remove all volatiles. Dissolution of **3b** in dichloromethane and slow diffusion of diethyl ether afforded colorless monocrystals suitable for X-ray analysis. Yield: 111.3 mg (96.0%).

The ^1H NMR (297.80 MHz, CD_3CN, 25 °C) spectrum is shown in Figure S1 (top panel): δ 9.03 (t, J = 1.6 Hz, 1H, C(2)H), 8.01 (d, J = 1.6 Hz, 2H, CH=CH), 7.68−7.61 (m, 2H, p-ArH), 7.49−7.44 (m, 4H, m-ArH), 2.43 (hept, J = 6.8 Hz, 4H, iPrCH), 1.27 (d, J = 6.8 Hz, 12H, iPr$(CH_3)_2$), 1.20 (d, J = 6.8 Hz, 12H, iPr$(CH_3)_2$) ppm.

The ^{19}F NMR (285.05 MHz, CD_3CN, 25 °C) spectrum is shown in Figure S1 (middle panel): δ −119.02 (s, 6F, GeF_6^{2-}) ppm.

DOI: 10.1021/acs.inorgchem.7b01606
Inorg. Chem. 2017, 56, 10070−10077

The ^{13}C NMR (76 MHz, CD_3CN, 25 °C) spectrum is shown in Figure S1 (bottom panel): δ 146.73, 139.08, 133.39, 131.34, 127.91, 126.01, 30.25, 24.87, 24.23.

Elemental analysis for $C_{54}H_{74}N_4GeF_6{\cdot}CH_3CN$ (1006.87) (%): stoichiometric, C, 66.80; H, 7.71; N, 6.96; found, C, 66.96; H, 7.51; N, 6.87.

■ COMPUTATIONAL SECTION

DFT Calculations of Crystal Structures. Calculations of crystal structures were performed in the framework of density-functional (DFT) theory, using the generalized gradient approximation of Perdew−Burke−Ernzerhof (PBE)[38] and the PWscf code from the QUANTUM ESPRESSO distribution.[39] Because plain GGA functionals, PBE included, cannot describe dispersion interactions, which are expected to be important to properly describe the interactions between bulky $[(L^{Dipp})H]^+$ cations, we also utilized the consistently applied empirical dispersion correction of Grimme,[40,41] known as D2, that consists of a damped C_6R^{-6} like energy term on top of the PBE. The results obtained by this scheme are referred to by the PBE-D2 denotation. We used the pseudopotential method with ultrasoft pseudopotentials.[42] Kohn−Sham orbitals were expanded in a plane-wave basis set up to a kinetic energy cutoff of 50 Ry (400 Ry for the charge-density cutoff); these cutoffs yield well converged results. Ultrasoft pseudopotentials for H, C, N, Si, and Ge were taken from the Quantum Espresso PseudoPotential Download Page: http://www.quantum-espresso.org/pseudopotentials (files: H.pbe-rrkjus.UPF, C.pbe-rrkjus.UPF, N.pbe-rrkjus.UPF, F.pbe-n-van.UPF, Si.pbe-n-rrkjus_psl.0.1.UPF, and Ge.pbe-dn-rrkjus_psl.0.2.2.UPF). All degrees of freedom including the unit-cell size and shape were relaxed using a variable-cell Broyden−Fletcher−Goldfarb−Shanno optimization. After optimization all structures were recalculated as to account for the change in the basis set due to a change in the unit-cell geometry during the optimization. Brillouin-zone (BZ) integrations were performed using only the gamma k-point. Vibrational frequencies associated with SiF_5^- and GeF_5^- anions in the crystal structures were calculated using density-functional perturbation theory[43] and the PHONON packages from the QUANTUM ESPRESSO distribution.

Rotations and Berry pseudorotations of GeF_5^- anion between the two possible orientations within the crystal structure were modeled as the minimum-energy paths (MEPs) connecting the two orientations using the climbing image nudged elastic band (CI-NEB) method.[44,45] Only one GeF_5^- anion per unit cell was reoriented. The configuration with the maximum energy along the MEP is identified as the transition state (TS). The respective activation energies (E^*) are calculated as $E^*_{A\rightarrow B} = E_{TS} - E_A$ and $E^*_{B\rightarrow A} = E_{TS} - E_B$, where E_A and E_B are total energies of the crystal unit cell with pertinent GeF_5^- anion oriented in the A and B domain, respectively, and E_{TS} is the total energy of the transition state; $E^*_{A\rightarrow B}$ and $E^*_{B\rightarrow A}$ are therefore the activation energies for A → B and B → A transitions, respectively.

The charge transfer (or the lack of it) between constituent fragments, i.e., $[(L^{Dipp})H]^+$ cations and MF_5^- anions (M = Si and Ge), and the chemical bonding between them (e.g., H-bonding interactions) were characterized in terms of charge density difference, $\Delta\rho(\mathbf{r})$, calculated as

$$\Delta\rho(\mathbf{r}) = \rho_{tot}(\mathbf{r}) - \sum_{i=1}^{N^+} \rho_i^+(\mathbf{r}) - \sum_{j=1}^{N^-} \rho_j^-(\mathbf{r}) \quad (1)$$

where $\rho_{tot}(\mathbf{r})$ is the charge density of the whole crystal structure, N^+ and N^- are the number of $[(L^{Dipp})H]^+$ cations and MF_5^- anions in the unit cell, respectively ($N^+ = N^- = 4$), $\rho_i^+(\mathbf{r})$ is the charge density of the ith cation, and $\rho_j^-(\mathbf{r})$ is the charge density of the jth anion. Note that the geometry of the individual anions and cations is kept the same as in the whole crystal structure.

Bader charge analysis was performed using the Bader code[46,47] by generating charge densities with the PAW (projector-augmented-wave) potentials[48] and 1000 Ry kinetic energy cutoff for charge density. Charge density difference plots and molecular graphics were produced by the XCRYSDEN graphical package.[49]

Molecular DFT and MP2 Calculations of Isolated Anions and Molecules. Molecular calculations (e.g., vibrational frequency calculations for isolated SiF_5^- and GeF_5^- anions) were performed with the Gaussian09 program[50] using three different methods. In particular, we used (1) pure GGA functional, i.e., PBE (for consistency reasons with the crystal-structure DFT calculations described above); (2) hybrid B3LYP functional;[51] and (3) post Hartree−Fock Møller−Plesset second order perturbation theory (MP2).[52] Electrons were described with all electron basis sets. Convergence tests revealed that triple-ζ basis sets augmented with polarization (and diffuse) functions yield converged results (i.e., def2-TZVP[53] and aug-cc-pVTZ[54−57] yield very similar vibrational frequencies and almost identical bond distances, which are also quite close to those given by the quadruple-ζ aug-cc-pQVZ basis set, see Table S1). Def2-TZVP basis sets were obtained from the Basis Set Exchange (BSE) portal (https://bse.pnl.gov/bse/portal) and the EMSL Basis Set Library.[58,59]

■ ASSOCIATED CONTENT

Supporting Information

The Supporting Information is available free of charge on the ACS Publications website at DOI: 10.1021/acs.inorgchem.7b01606.

Additional results and discussion on crystal structure determination, local structure of MF_5^- anions, transition of MF_5^- anions between domains A and B, their relative stabilities, and vibrational characterization (PDF)

Accession Codes

CCDC 1545731−1545733 contain the supplementary crystallographic data for this paper. These data can be obtained free of charge via www.ccdc.cam.ac.uk/data_request/cif, or by emailing data_request@ccdc.cam.ac.uk, or by contacting The Cambridge Crystallographic Data Centre, 12 Union Road, Cambridge CB2 1EZ, UK; fax: +44 1223 336033.

■ AUTHOR INFORMATION

Corresponding Author

*E-mail: gasper.tavcar@ijs.si.

ORCID

Blaž Alič: 0000-0002-8845-4335

Notes

The authors declare no competing financial interest.

■ ACKNOWLEDGMENTS

The authors gratefully acknowledge the Slovenian Research Agency (ARRS) for the financial support of the Research Programs P1-0045 (Inorganic Chemistry and Technology), P2-

0393 (Advanced Materials for Low Carbon and Sustainable Society), and PR-05552 (Young Researcher Program). Authors would also like to thank Slovenian NMR Centre of National Institute of Chemistry for all their resources and support.

REFERENCES

(1) Wu, S.; Han, C.; Iocozzia, J.; Lu, M.; Ge, R.; Xu, R.; Lin, Z. Germanium-Based Nanomaterials for Rechargeable Batteries. *Angew. Chem., Int. Ed.* **2016**, *55* (28), 7898−7922.

(2) Amato, M.; Palummo, M.; Rurali, R.; Ossicini, S. Silicon−Germanium Nanowires: Chemistry and Physics in Play, from Basic Principles to Advanced Applications. *Chem. Rev.* **2014**, *114* (2), 1371−1412.

(3) Xie, R.; Montanini, P.; Akarvardar, K.; Tripathi, N.; Haran, B.; Johnson, S.; Hook, T.; Hamieh, B.; Corliss, D.; Wang, J.; Miao, X.; Sporre, J.; Fronheiser, J.; Loubet, N.; Sung, M.; Sieg, S.; Mochizuki, S.; Prindle, C.; Seo, S.; Greene, A.; Shearer, J.; Labonte, A.; Fan, S.; Liebmann, L.; Chao, R.; Arceo, A.; Chung, K.; Cheon, K.; Adusumilli, P.; Amanapu, H. P.; Bi, Z.; Cha, J.; Chen, H. C.; Conti, R.; Galatage, R.; Gluschenkov, O.; Kamineni, V.; Kim, K.; Lee, C.; Lie, F.; Liu, Z.; Mehta, S.; Miller, E.; Niimi, H.; Niu, C.; Park, C.; Park, D.; Raymond, M.; Sahu, B.; Sankarapandian, M.; Siddiqui, S.; Southwick, R.; Sun, L.; Surisetty, C.; Tsai, S.; Whang, S.; Xu, P.; Xu, Y.; Yeh, C.; Zeitzoff, P.; Zhang, J.; Li, J.; Demarest, J.; Arnold, J.; Canaperi, D.; Dunn, D.; Felix, N.; Gupta, D.; Jagannathan, H.; Kanakasabapathy, S.; Kleemeier, W.; Labelle, C.; Mottura, M.; Oldiges, P.; Skordas, S.; Standaert, T.; Yamashita, T.; Colburn, M.; Na, M.; Paruchuri, V.; Lian, S.; Divakaruni, R.; Gow, T.; Lee, S.; Knorr, A.; Bu, H.; Khare, M. A 7nm FinFET technology featuring EUV patterning and dual strained high mobility channels. In *2016 IEEE International Electron Devices Meeting (IEDM)*, San Francisco, 2016; pp 2.7.1−2.7.4.

(4) Zhang, J. J.; Shimizu, K.; Zhao, Y.; Xue, J. M.; Geng, X. H.; Xiong, S. Z.; Wu, C. Y.; Hanna, J. Influences of GeF_4 on poly-SiGe films prepared by reactive thermal CVD. *J. Non-Cryst. Solids* **2006**, *352* (9−20), 1275−1278.

(5) Hanna, J. I.; Lim, C. H.; Hoshino, T. Direct fabrication of poly-SiGe thin films on amorphous substrates and its application to bottom-gate TFTs. In *2010 10th IEEE International Conference on Solid-State and Integrated Circuit Technology (ICSICT)*, Shanghai, China, 2010; pp 840−843.

(6) Pelzer, S.; Neumann, B.; Stammler, H.-G.; Ignat'ev, N.; Hoge, B. Hypervalent Pentafluoroethylgermanium Compounds, $[(C_2F_5)_nGeX_{5-n}]^-$ and $[(C_2F_5)_3GeF_3]^{2-}$ (X = F, Cl; n = 2−5). *Chem. - Eur. J.* **2016**, *22* (46), 16460−16466.

(7) Brauer, D. J.; Wilke, J.; Eujen, R. Tris- and tetrakis-(trifluoromethyl)fluorogermanates; the structure of an anion with pentacoordinated germanium. *J. Organomet. Chem.* **1986**, *316* (3), 261−269.

(8) Christe, K. O.; Schack, C. J.; Wilson, R. D. Low-temperature ultraviolet photolysis and its application to the synthesis of novel and known tetrafluoronitrogen(1+) salts. *Inorg. Chem.* **1976**, *15* (6), 1275−1282.

(9) Christe, K. O.; Wilson, R. D.; Goldberg, I. B. Dioxygenyl pentafluorogermanate(IV), 02+GeF5. *Inorg. Chem.* **1976**, *15* (6), 1271−1274.

(10) Mallouk, T. E.; Desbat, B.; Bartlett, N. Structural studies of salts of cis and trans.mu.-fluoro-bridged polymers of pentafluorogermanate-(1-) and of the pentafluorogermanate(1-) monomer. *Inorg. Chem.* **1984**, *23* (20), 3160−3166.

(11) Gnann, R. Z.; Wagner, R. I.; Christe, K. O. Direct syntheses of tetramethylammonium salts of complex fluoroanions. *J. Fluorine Chem.* **1997**, *83* (2), 191−194.

(12) Wharf, I.; Onyszchuk, M. Preparation and acceptor power of the pentafluorogermanate ion. *Can. J. Chem.* **1970**, *48* (14), 2250−2256.

(13) Christe, K. O.; Wilson, W. W.; Wilson, R. D.; Bau, R.; Feng, J. A. Syntheses, properties, and structures of anhydrous tetramethylammonium fluoride and its 1:1 adduct with trans-3-amino-2-butenenitrile. *J. Am. Chem. Soc.* **1990**, *112* (21), 7619−7625.

(14) Mahjoub, A. R.; Zhang, X.; Seppelt, K. Reactions of the "Naked" Fluoride Ion: Syntheses and Structures of SeF_6^{2-} and BrF_6^-. *Chem. - Eur. J.* **1995**, *1* (4), 261−265.

(15) Christe, K. O.; Jenkins, H. D. B. Quantitative Measure for the "Nakedness" of Fluoride Ion Sources. *J. Am. Chem. Soc.* **2003**, *125* (31), 9457−9461.

(16) Sharma, R. K.; Fry, J. L. Instability of anhydrous tetra-n-alkylammonium fluorides. *J. Org. Chem.* **1983**, *48* (12), 2112−2114.

(17) Sun, H.; DiMagno, S. G. Anhydrous Tetrabutylammonium Fluoride. *J. Am. Chem. Soc.* **2005**, *127* (7), 2050−2051.

(18) Schwesinger, R.; Link, R.; Thiele, G.; Rotter, H.; Honert, D.; Limbach, H.-H.; Männle, F. Stable Phosphazenium Ions in Synthesis—an Easily Accessible, Extremely Reactive "Naked" Fluoride Salt. *Angew. Chem., Int. Ed. Engl.* **1991**, *30* (10), 1372−1375.

(19) Gnann, R. Z.; Wagner, R. I.; Christe, K. O.; Bau, R.; Olah, G. A.; Wilson, W. W. Naked Fluoride Ion Sources: Synthesis, Characterization, and Coupling Reaction of 1-Methylhexamethylenetetramine Fluoride. *J. Am. Chem. Soc.* **1997**, *119* (1), 112−115.

(20) Bouvet, S.; Pégot, B.; Marrot, J.; Magnier, E. Solvent free nucleophilic introduction of fluorine with [bmim][F]. *Tetrahedron Lett.* **2014**, *55* (4), 826−829.

(21) Kim, D. W.; Jeong, H.-J.; Lim, S. T.; Sohn, M.-H. Tetrabutylammonium Tetra(tert-Butyl Alcohol)-Coordinated Fluoride as a Facile Fluoride Source. *Angew. Chem., Int. Ed.* **2008**, *47* (44), 8404−8406.

(22) Ališ, B.; Tavčar, G. Reaction of N-heterocyclic carbene (NHC) with different HF sources and ratios − A free fluoride reagent based on imidazolium fluoride. *J. Fluorine Chem.* **2016**, *192* (Part A), 141−146.

(23) Bartlett, P. N.; Cummings, C. Y.; Levason, W.; Pugh, D.; Reid, G. Halometallate Complexes of Germanium(II) and (IV): Probing the Role of Cation, Oxidation State and Halide on the Structural and Electrochemical Properties. *Chem. - Eur. J.* **2014**, *20* (17), 5019−5027.

(24) Böttcher, T.; Bassil, B. S.; Röschenthaler, G.-V. Complexes of Ge(IV)- and Sn(IV)-Fluorides with Cyclic and Acyclic Carbenes: Bis(dialkylamino)-difluoromethylenes as Carbene Sources. *Inorg. Chem.* **2012**, *51* (2), 763−765.

(25) Gillespie, R. J.; Popelier, P. L. A. *Chemical Bonding and Molecular Geometry: From Lewis to Electron Densities*; Oxford University Press: 2001.

(26) Atwood, D. A. In *Encyclopedia of Inorganic and Bioinorganic Chemistry*; John Wiley & Sons, Ltd: 2011.

(27) Senaweera, S. M.; Singh, A.; Weaver, J. D. Photocatalytic Hydrodefluorination: Facile Access to Partially Fluorinated Aromatics. *J. Am. Chem. Soc.* **2014**, *136* (8), 3002−3005.

(28) Dean, P. A. W.; Evans, D. F. Spectroscopic studies of inorganic fluoro-complexes. Part I. The 19F nuclear magnetic resonance and vibrational spectra of hexafluorometallates of Groups IVA and IVB. *J. Chem. Soc. A* **1967**, *0*, 698−701.

(29) Liang, T.; Neumann, C. N.; Ritter, T. Introduction of Fluorine and Fluorine-Containing Functional Groups. *Angew. Chem., Int. Ed.* **2013**, *52* (32), 8214−8264.

(30) *In Handbuch Der Präparativen Anorganischen Chemie*, 3rd ed.; Brauer, G., Ed.; Ferdinand Enke Verlag: Stuttgart, 1975; Chapter 3, Fluor, Vol. *1*, p 227.

(31) Hintermann, L. Expedient syntheses of the N-heterocyclic carbene precursor imidazolium salts IPr·HCl, IMes·HCl and IXy·HCl. *Beilstein J. Org. Chem.* **2007**, *3*, 22.

(32) *CrysAlisPro, Agilent Technologies*, 1.171.37.33 (release 27-03-2014 CrysAlis171.NET) (compiled Mar 27, 2014,17:12:48).

(33) Clark, R. C.; Reid, J. S. The analytical calculation of absorption in multifaceted crystals. *Acta Crystallogr., Sect. A: Found. Crystallogr.* **1995**, *51* (6), 887−897.

(34) Sheldrick, G. M. SHELXT - Integrated space-group and crystal-structure determination. *Acta Crystallogr., Sect. A: Found. Adv.* **2015**, *71* (1), 3−8.

(35) Sheldrick, G. M. Crystal structure refinement with SHELXL. *Acta Crystallogr., Sect. C: Struct. Chem.* **2015**, *71* (1), 3−8.

DOI: 10.1021/acs.inorgchem.7b01606
Inorg. Chem. 2017, 56, 10070−10077

(36) Dolomanov, O. V.; Bourhis, L. J.; Gildea, R. J.; Howard, J. A. K.; Puschmann, H. OLEX2: a complete structure solution, refinement and analysis program. *J. Appl. Crystallogr.* **2009**, *42* (2), 339−341.
(37) Brandenburg, K.; Putz, H. *Diamond—Crystal and Molecular Structure Visualization Crystal Impact*; GbR: Kreuzherrenstr. 102, 53227 Bonn, Germany.
(38) Perdew, J. P.; Burke, K.; Ernzerhof, M. Generalized Gradient Approximation Made Simple. *Phys. Rev. Lett.* **1996**, *77* (18), 3865−3868.
(39) Giannozzi, P.; Baroni, S.; Bonini, N.; Calandra, M.; Car, R.; Cavazzoni, C.; Ceresoli, D.; Chiarotti, G. L.; Cococcioni, M.; Dabo, I.; Dal Corso, A.; Gironcoli, S. d.; Fabris, S.; Fratesi, G.; Gebauer, R.; Gerstmann, U.; Gougoussis, C.; Kokalj, A.; Lazzeri, M.; Martin-Samos, L.; Marzari, N.; Mauri, F.; Mazzarello, R.; Paolini, S.; Pasquarello, A.; Paulatto, L.; Sbraccia, C.; Scandolo, S.; Sclauzero, G.; Seitsonen, A. P.; Smogunov, A.; Umari, P.; Wentzcovitch, R. M. QUANTUM ESPRESSO: a modular and open-source software project for quantum simulations of materials. *J. Phys.: Condens. Matter* **2009**, *21* (39), 395502. Code available from http://www.quantum-espresso.org/.
(40) Grimme, S. Semiempirical GGA-Type Density Functional Constructed with a Long-Range Dispersion Correction. *J. Comput. Chem.* **2006**, *27*, 1787−1799.
(41) Barone, V.; Casarin, M.; Forrer, D.; Pavone, M.; Sambi, M.; Vittadini, A. Role and Effective Treatment of Dispersive Forces in Materials: Polyethylene and Graphite Crystals as Test Cases. *J. Comput. Chem.* **2009**, *30*, 934−939.
(42) Vanderbilt, D. Soft self-consistent pseudopotentials in a generalized eigenvalue formalism. *Phys. Rev. B: Condens. Matter Mater. Phys.* **1990**, *41*, 7892−7895.
(43) Baroni, S.; de Gironcoli, S.; Dal Corso, A.; Giannozzi, P. Phonons and related crystal properties from density-functional perturbation theory. *Rev. Mod. Phys.* **2001**, *73*, 515−562.
(44) Henkelman, G.; Jonsson, H. Improved tangent estimate in the nudged elastic band method for finding minimum energy paths and saddle points. *J. Chem. Phys.* **2000**, *113*, 9978−9985.
(45) Henkelman, G.; Uberuaga, B. P.; Jonsson, H. A climbing image nudged elastic band method for finding saddle points and minimum energy paths. *J. Chem. Phys.* **2000**, *113*, 9901−9904.
(46) Tang, W.; Sanville, E.; Henkelman, G. A grid-based Bader analysis algorithm without lattice bias. *J. Phys.: Condens. Matter* **2009**, *21* (8), 084204.
(47) Arnaldsson, A.; Tang, W.; Henkelman, G.; et al. *Computer program for Bader charge analysis*; http://theory.cm.utexas.edu/henkelman/code/bader/, 2017.
(48) Blöchl, P. E. Projector augmented-wave method. *Phys. Rev. B: Condens. Matter Mater. Phys.* **1994**, *50* (24), 17953−17979.
(49) Kokalj, A. XCrySDen − a new program for displaying crystalline structures and electron densities. *J. Mol. Graphics Modell.* **1999**, *17*, 176−179. Code available from http://www.xcrysden.org/.
(50) Frisch, M. J.; Trucks, G. W.; Schlegel, H. B.; Scuseria, G. E.; Robb, M. A.; Cheeseman, J. R.; Scalmani, G.; Barone, V.; Mennucci, B.; Petersson, G. A.; Nakatsuji, H.; Caricato, M.; Li, X.; Hratchian, H. P.; Izmaylov, A. F.; Bloino, J.; Zheng, G.; Sonnenberg, J. L.; Hada, M.; Ehara, M.; Toyota, K.; Fukuda, R.; Hasegawa, J.; Ishida, M.; Nakajima, T.; Honda, Y.; Kitao, O.; Nakai, H.; Vreven, T.; Montgomery, J. A., Jr.; Peralta, J. E.; Ogliaro, F.; Bearpark, M.; Heyd, J. J.; Brothers, E.; Kudin, K. N.; Staroverov, V. N.; Kobayashi, R.; Normand, J.; Raghavachari, K.; Rendell, A.; Burant, J. C.; Iyengar, S. S.; Tomasi, J.; Cossi, M.; Rega, N.; Millam, J. M.; Klene, M.; Knox, J. E.; Cross, J. B.; Bakken, V.; Adamo, C.; Jaramillo, J.; Gomperts, R.; Stratmann, R. E.; Yazyev, O.; Austin, A. J.; Cammi, R.; Pomelli, C.; Ochterski, J. W.; Martin, R. L.; Morokuma, K.; Zakrzewski, V. G.; Voth, G. A.; Salvador, P.; Dannenberg, J. J.; Dapprich, S.; Daniels, A. D.; Farkas, Ö.; Foresman, J. B.; Ortiz, J. V.; Cioslowski, J.; Fox, D. J. *Gaussian 09*, Revision A.1; Gaussian, Inc.: Wallingford, CT, 2009.
(51) Becke, A. D. Density-functional thermochemistry. III. The role of exact exchange. *J. Chem. Phys.* **1993**, *98*, 5648−5652.
(52) Møller, C.; Plesset, M. S. *Phys. Rev.* **1934**, *46*, 618−622.
(53) Weigend, F.; Ahlrichs, R. Balanced basis sets of split valence, triple zeta valence and quadruple zeta valence quality for H to Rn: Design and assessment of accuracy. *Phys. Chem. Chem. Phys.* **2005**, *7* (18), 3297−3305.
(54) Dunning, T. H., Jr. Gaussian basis sets for use in correlated molecular calculations. I. The atoms boron through neon and hydrogen. *J. Chem. Phys.* **1989**, *90* (2), 1007−1023.
(55) Kendall, R. A.; Dunning, T. H., Jr.; Harrison, R. J. Electron affinities of the first row atoms revisited. Systematic basis sets and wave functions. *J. Chem. Phys.* **1992**, *96* (9), 6796−6806.
(56) Woon, D. E.; Dunning, T. H., Jr. Gaussian basis sets for use in correlated molecular calculations. III. The atoms aluminum through argon. *J. Chem. Phys.* **1993**, *98* (2), 1358−1371.
(57) Wilson, A. K.; Woon, D. E.; Peterson, K. A.; Dunning, T. H., Jr. Gaussian basis sets for use in correlated molecular calculations. IX. The atoms gallium through krypton. *J. Chem. Phys.* **1999**, *110* (16), 7667−7676.
(58) Feller, D. The role of databases in support of computational chemistry calculations. *J. Comput. Chem.* **1996**, *17* (13), 1571−1586.
(59) Schuchardt, K. L.; Didier, B. T.; Elsethagen, T.; Sun, L.; Gurumoorthi, V.; Chase, J.; Li, J.; Windus, T. L. Basis Set Exchange: A Community Database for Computational Sciences. *J. Chem. Inf. Model.* **2007**, *47* (3), 1045−1052.

DOI: 10.1021/acs.inorgchem.7b01606
Inorg. Chem. 2017, 56, 10070−10077

Supporting Information

Discrete GeF_5^- Anion Structurally Characterized with the Readily Synthesized Imidazolium Based Naked Fluoride Reagent

Blaž Alič,[a,c] Melita Tramšek,[a] Anton Kokalj,†[b,c] Gašper Tavčar*[a,c]

[a] Department of Inorganic Chemistry and Technology, Jožef Stefan Institute, Jamova 39, SI-1000 Ljubljana (Slovenia)
[b] Department of Physical and Organic Chemistry, Jožef Stefan Institute, Jamova 39, SI-1000 Ljubljana (Slovenia)
[c] Jožef Stefan International Postgraduate School, Jamova 39, SI-1000 Ljubljana (Slovenia)

July 19, 2017

Table of Contents

S1 Preliminaries **S2**

S1.1 NMR spectra S2

S1.2 Convergence of Gaussian basis sets for Molecular DFT and MP2 Calculations S2

S2 Results and Discussion **S2**

S2.1 Crystal Structure Determination S2

S2.2 Local Structure of MF_5^- Anions S5

S2.3 H-Bonding Between MF_5^- Anion and Surrounding $[(L^{Dipp})H]^+$ Cations S8

S2.4 Transition of MF_5^- Anions Between Domain A and B S10

S2.5 Relative Stabilities of Anions: Bipyramidal GeF_5^- vs Octahedral GeF_6^{2-} S10

S2.6 Vibrational Characterization of SiF_5^- and GeF_5^- as well as SiF_6^{2-} and GeF_6^{2-} Anions S12

S2.6.1 Raman Spectra S12

S2.6.2 Vibrational Calculations S12

S1 Preliminaries

S1.1 NMR spectra

^1H, ^{19}F, and ^{13}C NMR spectra of compound $[(L^{Dipp})H]_2[GeF_6]$ (**3b**) are shown in the top, middle, and bottom panels of Figure S1, respectively, whereas for the compounds $[(L^{Dipp})H][SiF_5]$ (**2a**) and $[(L^{Dipp})H][GeF_5]$ (**2b**) they are shown in Figure S2.

S1.2 Convergence of Gaussian basis sets for Molecular DFT and MP2 Calculations

Molecular calculations (e.g., vibrational frequency calculations for isolated SiF_5^- and GeF_5^- anions) were performed with all electron Gaussian basis sets. Convergence tests reveal that triple-zeta basis sets augmented with polarization (and diffuse) functions yield converged results, i.e., def2-TZVP [1] and aug-cc-pVTZ [2–5] yield very similar vibrational frequencies and almost identical bond-distances, which are also quite close to those given by the quadruple-zeta aug-cc-pQVZ basis set, see Table S1.

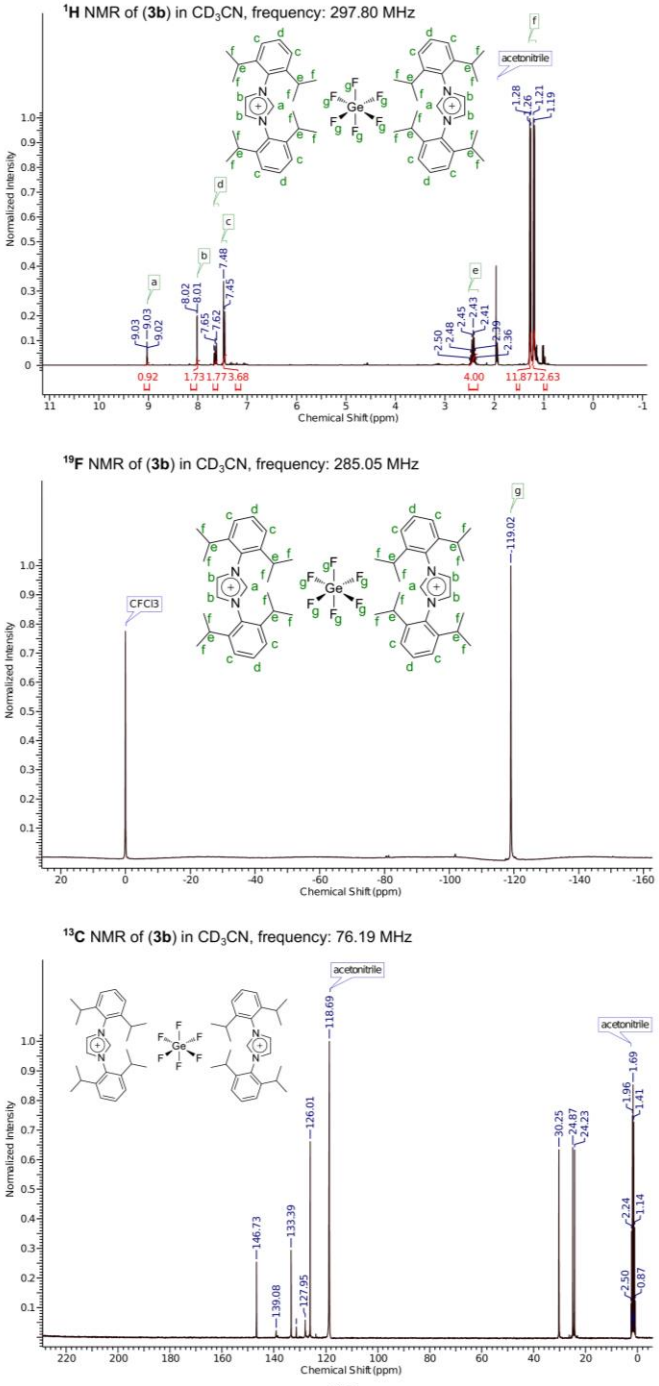


Figure S1. NMR spectra of $[(L^{Dipp})H]_2[GeF_6]$ compound (**3b**) in deuterated acetonitrile. From top to bottom: ^1H, ^{19}F, and ^{13}C NMR spectra. Letters (a–f) denote the observed protons and (g) the single peak observed in ^{19}F spectra for GeF_6^{2-} anion. Spectra were recorded on bulk of the sample, without further treatment and before crystallization process.

S2 Results and Discussion

S2.1 Crystal Structure Determination

Crystal structures of $[(L^{Dipp})H][SiF_5]$ and $[(L^{Dipp})H][GeF_5]$ compounds (**2a**) and (**2b**) were determined by single crystal X-ray analysis. Data were collected at 100 K and were initially refined in $C2/c$ space group. In this space group the structure showed dissordered MF_5^- anions in two positions from which we couldn't distinctly define t he s tructure o f the anions. Therefore, we lowered the symetry and refined the structures for (**2a**) and (**2b**) in $P2_1/n$ and $P2_1/c$ space groups respectively. Lowering of the symmetry revealed trigonal-bypiramidal anions in two distinct positions (domain A and

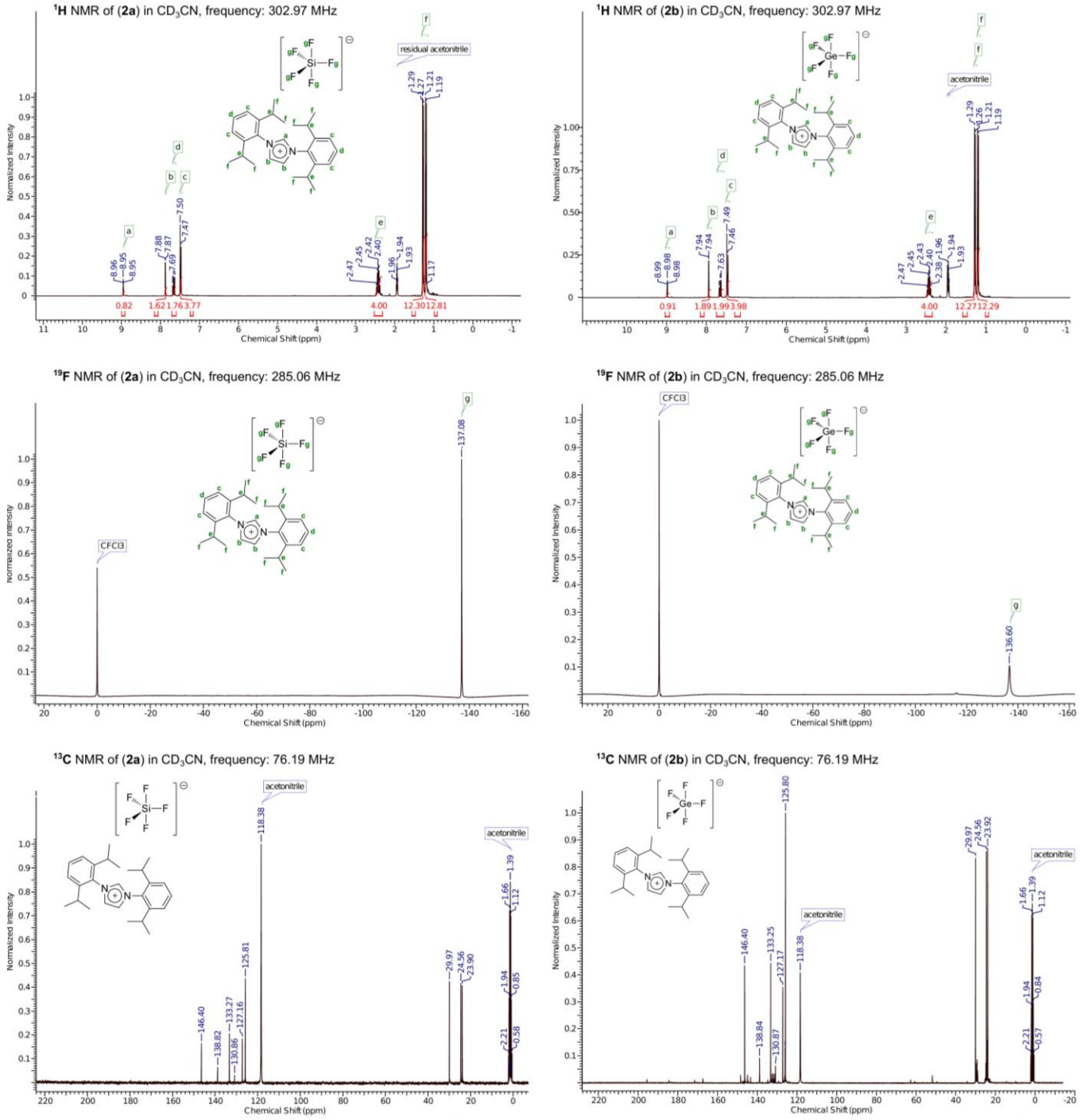


Figure S2. NMR spectra of $[(L^{Dipp})H][\mathbf{Si}F_5]$ (left) and $[(L^{Dipp})H][\mathbf{Ge}F_5]$ (right) in deuterated acetonitrile. From top to bottom: ^{1}H, ^{19}F, and ^{13}C NMR spectra. Letters (a–f) denote the observed protons and (g) the single peak observed in ^{19}F spectra for SiF_5^- and GeF_5^- anions. Spectra were recorded on bulk of the sample, without further treatment and before crystallization process.

domain B) populated 50:50 for (**2a**) and 80:20 for (**2b**) at 100 K. The corresponding crystal data are summarized in Table S2, asymmetric units are shown in Figure S3, and perspective view of the crystal structure (**2b**) is presented in Figure 5 in the main paper.

In the crystal structure 6 MF_5^- anions are packed around each $[(L^{Dipp})H]^+$ cation and *vice-versa* (6 cations around each anion), forming the distorted NaCl type structure, see Figure S4. Note that the plots in this figure show only 4 counter-ions around each ion, because structural elements that lie in front and behind the paper plane are omitted for clarity, i.e., there is one counter-ion in front and one counter-ion behind each ion, resulting in overall packing of 6 cations around each anion and *vice versa*.

Crystal structure of $[(L^{Dipp})H]_2[GeF_6]$ compound (**3b**) was determined by single crystal X-ray analysis analogously to those of (**2a**) and (**2b**). The corresponding crystal data are summarized in the last-column of Table S2, whereas its

Table S1. Gaussian basis set convergence, i.e., comparison of B3LYP and MP2 results for isolated MF_5^- anions (M = Si, Ge) in bipyramidal D_{3h} symmetry obtained with various Gaussian basis sets. F_{ax} and F_{eq} stands for axial and equatorial F atoms, respectively.

	B3LYP def2-SVPD	B3LYP aug-cc-pVDZ	B3LYP def2-TZVP	B3LYP def2-TZVPD	B3LYP aug-cc-pVTZ	B3LYP aug-cc-pVQZ	MP2 aug-cc-pVTZ	MP2 aug-cc-pVQZ
bond distances [Å]								
Si–F_{ax}	1.695	1.704	1.676	1.677	1.682	1.678	1.679	1.673
Si–F_{eq}	1.661	1.669	1.634	1.634	1.641	1.635	1.638	1.631
Ge–F_{ax}	1.798	1.804	1.787	1.785	1.789	1.787	1.773	1.765
Ge–F_{eq}	1.773	1.779	1.763	1.752	1.761	1.758	1.743	1.736
frequencies [cm^{-1}]								
ν_1 (SiF_5^-)	669	652	689	687	682	685	693	698
ν_1 (GeF_5^-)	614	611	632	613	630	632	663	670

Table S2. Summary of crystal data and structure refinements for $[(L^{Dipp})H][SiF_5]$ (**2a**), $[(L^{Dipp})H][GeF_5]$ (**2b**), and $[(L^{Dipp})H]_2[GeF_6]$ (**3b**).

Compound	$[(L^{Dipp})H][SiF_5]$ (**2a**)	$[(L^{Dipp})H][GeF_5]$ (**2b**)	$[(L^{Dipp})H]_2[GeF_6]$ (**3b**)
CCDC No.	1545731	1545732	1545733
Formula	$C_{27}H_{37}N_2 \cdot F_5Si$	$C_{27}H_{37}N_2 \cdot F_5Ge$	$2(C_{27}H_{37}N_2) \cdot F_6Ge \cdot 0.842(C_4H_9O) \cdot 0.646(CH_2Cl_2)$
F_w	512.67	557.17	1082.18
T (K)	100	100	100
Crystal system	Monoclinic	Monoclinic	Monoclinic
Space group	$P2_1/n$	$P2_1/c$	$P2_1/c$
a (Å)	16.0805 (4)	16.0694 (2)	12.2381 (2)
b (Å)	9.8425 (2)	9.9063 (1)	15.4667 (2)
c (Å)	17.6856 (3)	17.7594 (2)	31.8258 (5)
β (°)	90.502 (2)	90.691 (1)	94.370 (1)
V (Å^3)	2799.02 (9)	2826.88 (6)	6006.57 (16)
Z	4	4	4
Mass density (g/cm^3)	1.217	1.309	1.197
Crystal size (mm)	0.36 × 0.30 × 0.14	0.69 × 0.42 × 0.28	0.24 × 0.20 × 0.17
Radiation type	Cu $K\alpha$	Cu $K\alpha$	Cu $K\alpha$
λ (Å)	1.54184	1.54184	1.54184
μ (mm^{-1})	1.18	1.91	1.70
F (000)	1088	1160	2294.6
Θ_{max} (°)	73.2	67.1	67.1
Index ranges	−19 ≤ h ≤ 17 −12≤ k ≤ 12 −21 ≤ l ≤ 21	−19 ≤ h ≤ 18 −11≤ k ≤ 11 −21 ≤ l ≤ 21	−14 ≤ h ≤ 14 −18≤ k ≤ 15 −33 ≤ l ≤ 38
Reflections collected	44580	63471	43421
Independent reflections	5522	5033	10742
Reflections with [$I > 2\sigma(I)$]	3337	4771	9825
R_{int}	0.025	0.042	0.034
R_{sigma}	0.0105	0.0136	0.0266
Data/restraints/parameters	5522 / 0 / 379	5033 / 15 / 379	10742 / 0 / 786
S[a]	1.06	1.13	1.24
R_1[b], wR_2[c] [$I > 2\sigma(I)$]	0.050, 0.145	0.037, 0.105	0.083, 0.191
R_1[b], wR_2[c] [all data]	0.065, 0.159	0.039, 0.106	0.088, 0.193
$\Delta\rho_{min}$, $\Delta\rho_{max}$ (eÅ^{-3})	−0.237, 0.294	−0.252, 0.423	−0.658, 1.137

[a] $S = [\Sigma(w(F_o^2 - F_c^2)^2)/(N_o - N_p)]^{½}$.
[b] $R_1 = \Sigma||F_o| - |F_c||/\Sigma|F_o|$.
[c] $wR_2 = [\Sigma(w(F_o^2 - F_c^2)^2)/\Sigma(w(F_o^2)^2)]^{½}$.

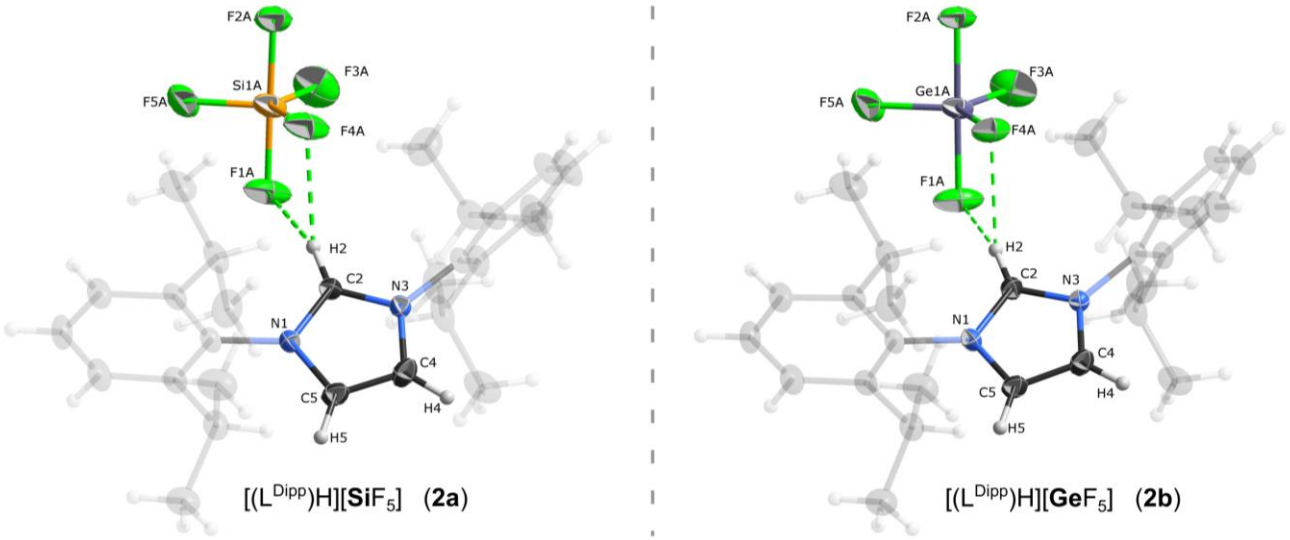


Figure S3. Asymetric units of $[(L^{Dipp})H][SiF_5]$ (**2a**) and $[(L^{Dipp})H][GeF_5]$ (**2b**) with MF_5^- anions (M = Si, Ge) in position A.

asymmetric unit is shown in Figure S5.

Crystal structures of compounds (**2a**) and (**2b**) were also calculated at the PBE/pw and PBE-D2/pw level of theory, where the label "pw" stands for the plane-wave basis set (these calculations utilized periodic-boundary-conditions). For these calculations the experimentally determined structures were used as starting input structures. Note that fractional occupations that stem from two possible positions of MF_5^- anions (M = Si and Ge)—labeled as domain A and domain B in the following—were treated such that either all MF_5^- anions were exclusively located either in domain A or in domain B. The corresponding PBE/pw and PBE-D2/pw results—lattice parameters, unit-cell volume, and relative stabilities and populations of the two domains—are compared to experimental results in Tables S3 and S4, whereas the experimental vs computational comparison of M–F bond lengths and F–M–F bond angles is provided in Tables S5 and S6 for the Si and Ge compounds (**2a**) and (**2b**), respectively.

It can be seen from Tables S3 and S4 that PBE overestimates and PBE-D2 underestimates the *a*, *b*, *c* lattice parameters and correspondingly the unit-cell volume. In particular, PBE overestimates the lattice parameters by about 4% and 5% and volume by 13% and 16% for Ge and Si compounds, respectively, whereas PBE-D2 underestimates the lattice parameters by 2.5% and volume by about 7% for both compounds. The reason that PBE overestimates the lattice parameters and volume is due to neglected dispersion interactions, which are important for the proper description of interactions between neighboring bulky $[(L^{Dipp})H]^+$ cations. In contrast, PBE-D2 apparently overestimates these dispersion interactions and consequently underestimates lattice parameters and unit-cell volume. This reasoning is corroborated by the fact that both functionals predict very similar relative stabilities of the two positional domains of MF_5^- anions, which implies that the difference between the two functionals is not due to description of anion–cation interactions, but rather due to treatment of interactions between neighboring bulky $[(L^{Dipp})H]^+$ cations (note that anions are well separated from each other in the crystal structure, see Figure 5 in the main paper) The predicted populations of the two domains as derived from their relative stabilities agree remarkably well with the experimental values for both Ge and Si compounds (Tables S3 and S4). These populations were calculated by assuming that position/orientation of a given anion is independent from the position of the neighboring anions, which leads to a two-level model. The populations p_A and p_B were therefore estimated as:

$$p_A = q^{-1}, \qquad p_B = q^{-1} \exp(-\frac{\Delta E}{k_B T}), \tag{S1}$$

where

$$q = 1 + \exp(-\frac{\Delta E}{k_B T}) \qquad \text{and} \qquad \Delta E = (E_B - E_A). \tag{S2}$$

The E_A and E_B are the energies of domain A and B, respectively.

S2.2 Local Structure of MF_5^- Anions

As for the M–F bond lengths and F–M–F bond angles (Tables S5 and S6), calculations reproduce the experimentally observed distortion from the ideal bipyramidal structure of MF_5^- anions, i.e., the axial F_{ax}–M–F_{ax} angle is smaller than 180° and equatorial F_{eq}–M–F_{eq} angles are distorted from 120°. While calculations predict similar distortions for the two domains, the experimentally determined distortion of domain B is slightly larger than that of domain A. According to both experiments and calculations the axial M–F_{ax} bonds are longer than the equatorial M–F_{eq} bonds, which is in accordance with valence-shell-electron-pair-repulsion (VSEPR) model of molecular geometry. Namely, the trigonal bipyramid has two sets of vertices that are not equivalent: equatorial and axial. The axial vertices have three close neighbors (equatorial vertices), whereas the equatorial vertices have two close neighbors (the axial vertices)

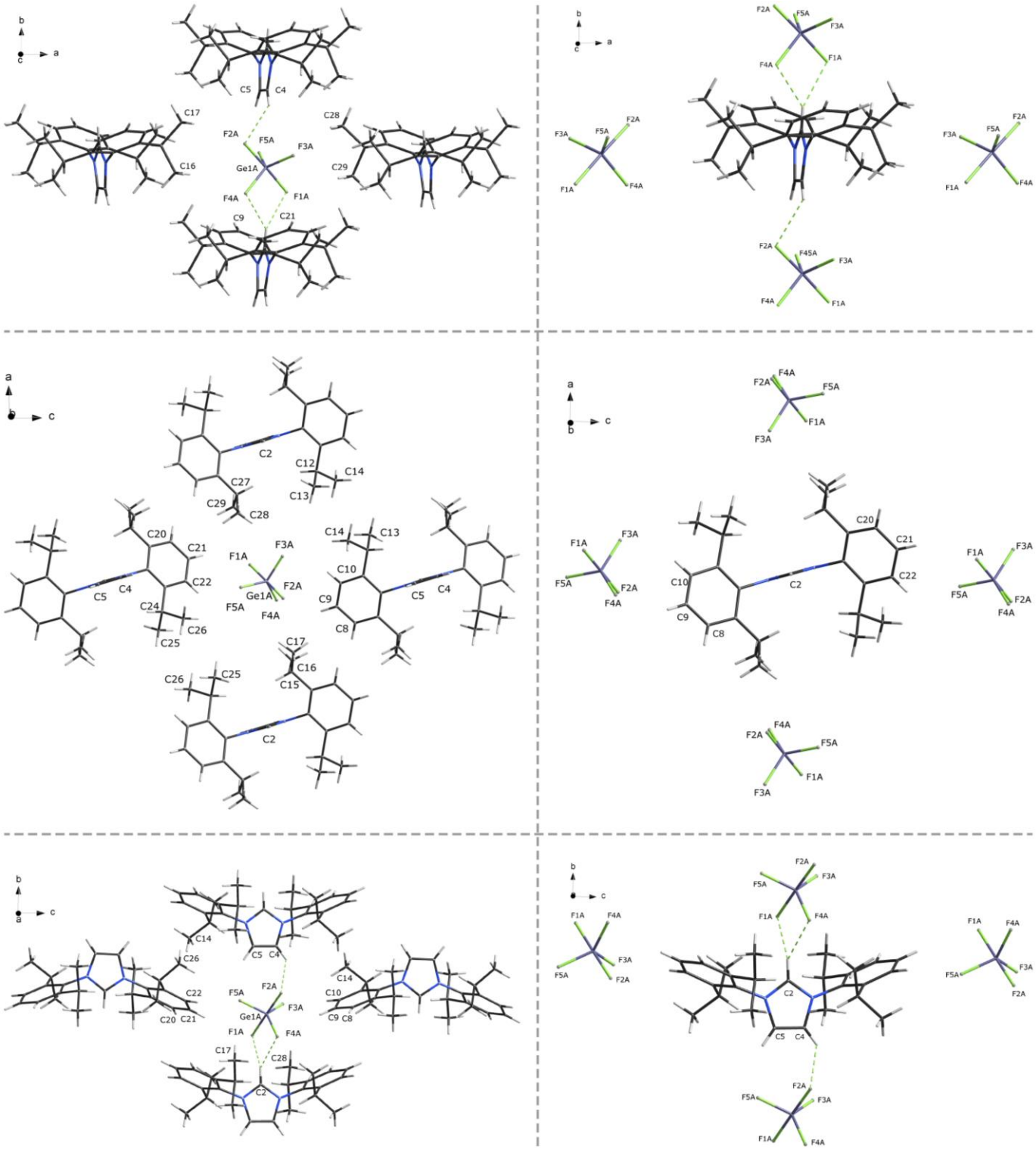


Figure S4. Packing of $[(L^{Dipp})H]^+$ cations around GeF_5^- anion (left) and of GeF_5^- anions around $[(L^{Dipp})H]^+$ cation (right) in the crystal structure of $[(L^{Dipp})H][GeF_5]$ (**2b**). Only domain A is considered. From top to bottom: packing in the *ab*, *ac*, and *bc* planes.

and two more that are farther away (the other two equatorial vertices).[6] Because of this nonequivalence of the vertices of the trigonal bipyramid the axial bond lengths in the trigonal bipyramidal species are longer that the equatorial bond lengths.[6]

Unconstrained refinement of (**2b**) resulted in uncharacteristic bond lengths for trigonal-bipyramidal geometry in the domain B with one elongated equatorial bond and one shortened axial bond, whereas domain A of (**2b**) completely reproduced expected trigonal-bipyramidal geometry. These discrepancies were attributed to uncertainty of X-ray measurements due to low electron density of domain B with only 20% occupancy in (**2b**). Therefore the SAME restraint was

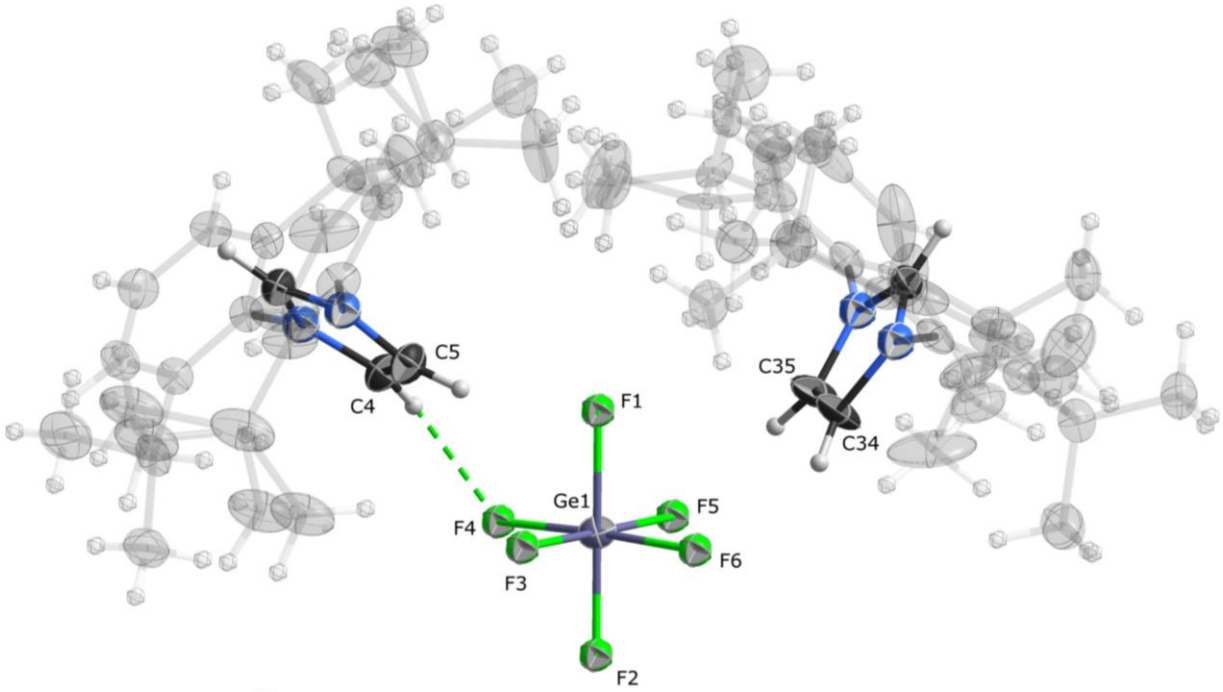


Figure S5. Asymetric unit of $[(L^{Dipp})H]_2[GeF_6]$ compound (**3b**). Solvent molecules (dichloromethane and diethyl ether) are removed and $[(L^{Dipp})H]^+$ "wingtips" shaded for clarity. Experimentally determined bond lengths (Å) and angles (°) in the GeF_6^{2-} anion: Ge1–F1 1.787(3), Ge1–F2 1.800(3), Ge1–F3 1.797(3), Ge1–F4 1.797(3), Ge1–F5 1.803(3), Ge1–F6 1.798(3); F1–Ge1–F2 179.9(2), F3–Ge1–F4 90.4(1), F4–Ge1–F5 90.1(1), F5–Ge1–F6 90.1(1), F6–Ge1–F3 89.5(1).

Table S3. PBE and PBE-D2 calculated and experimentally determined crystal structure data of $[(L^{Dipp})H][SiF_5]$ compound (**2a**). Calculations are performed with all anions oriented exclusively either into domain A or into domain B. Labels have the following meaning: a, b, c, $\beta \equiv$ unit-cell lattice parameters, $E \equiv$ total energy. E_A stands for the total energy of the "domain A" oriented structure ($E - E_A$ therefore measures the energy with respect to the energy of the domain A).

$[(L^{Dipp})H][\mathbf{Si}F_5]$	PBE		PBE-D2		Expt.
	domain A	domain B	domain A	domain B	disordered
a [Å]	17.04	17.04	15.48	15.48	16.08
b [Å]	10.34	10.34	9.64	9.64	9.84
c [Å]	18.44	18.43	17.38	17.38	17.69
β [°]	90.0	89.9	92.0	92.0	90.5
V [Å^3]	3248	3249	2592	2592	2799
$E - E_A$ [kJ mol^{-1}/ anion]	0.0	–0.05[a]	0.0	+0.005[a]	0.0 (A), +0.0 (B)[c]
Domain population[b] [%]					
at T = 100 K	49%	51%	50%	50%	50% (A), 50% (B)
at T = 300 K	50%	50%	50%	50%	

[a] Value smaller than the computational accuracy.
[b] Populations p_A and p_B are calculated as $p_A = q^{-1}$ and $p_B = q^{-1}\exp(-\Delta E / k_B T)$, where $q = 1 + \exp(-\Delta E / k_B T)$ and $\Delta E = (E_B - E_A)$.
[c] Obtained from p_A as $E_B - E_A = -k_B T \ln(p_A^{-1} - 1)$, where k_B is Boltzmann constant.

used for the refinement of the domain B and the resulting Ge–F bond distances agree much better with the PBE calculated ones and conform with the expected trend of two longer axial and three shorter equatorial bonds. The agreement between experiments and calculations is fair, e.g., for the domain A the PBE/pw and PBE-D2/pw calculated M–F bond lengths are by about 0.07 Å longer than the experimental ones.

An interesting aspect is the above mentioned distortion of MF_5^- anions from the ideal bipyramidal D_{3h} structure, which is obviously due to interaction with surrounding cations, because molecular calculations of isolated MF_5^- anions predict the ideal D_{3h} symmetric structure. Comparison between crystal PBE/pw calculations and the PBE/pw calculations of isolated MF_5^- anion[†] reveals that apart from the distortion of the D_{3h} structure, the effect of the crystal field on the (average) M–F bond lengths is rather minute—below 0.01 Å for equatorial bonds and even smaller for axial bonds (compare the "PBE/pw (domain A)" and "PBE/pw (isolated)" columns

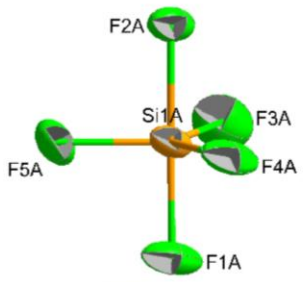
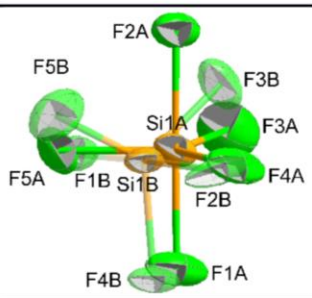
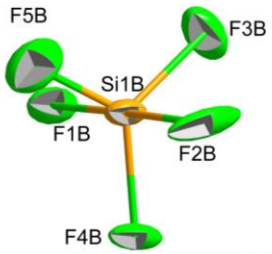
[†]Isolated MF_5^- is modeled as an anion enclosed in a big box with the compensating counter-charge background.

Table S4. As in Table S3 but for the Ge compound (**2b**). Labels have the same meaning as in Table S3.

$[(L^{Dipp})H][GeF_5]$	PBE		PBE-D2		Expt.
	domain A	domain B	domain A	domain B	disordered
a [Å]	16.68	16.63	15.53	15.47	16.07
b [Å]	10.37	10.40	9.60	9.77	9.91
c [Å]	18.43	18.43	17.45	17.48	17.76
β [°]	90.1	90.0	92.2	91.8	90.7
V [Å^3]	3188	3188	2599	2641	2827
$E - E_A$ [kJ mol^{-1}/anion]	0.0	+2.4	0.0	+2.9	0.0 (A), +1.2 (B)[b]
Domain population[a] [%]					
at T = 100 K	95%	5%	97%	3%	80% (A), 20% (B)
at T = 300 K	72%	28%	76%	24%	

[a] Populations p_A and p_B are calculated as $p_A = q^{-1}$ and $p_B = q^{-1}\exp(-\Delta E / k_B T)$, where $q = 1 + \exp(-\Delta E / k_B T)$ and $\Delta E = (E_B - E_A)$.
[b] Obtained from p_A as $E_B - E_A = -k_B T \ln(p_A^{-1} - 1)$, where k_B is Boltzmann constant.

Table S5. Experimental and calculated bond lengths and angles for both domains of SiF_5^- anion of $[(L^{Dipp})H][SiF_5]$ compound (**2a**). PBE and PBE-D2 calculated values are reported as "PBE [PBE-D2]", i.e., PBE-D2 values are stated in square brackets.

Domain A		**Anion as observed**		**Domain B**	
					
Bond length [Å] (calcd)	**Bond**	Bond length [Å] (expt)		**Bond**	Bond length [Å] (calcd)
		Domain A	Domain B		
1.703 [1.701]	**Si1A—F1A**	1.623 (11)	1.657 (4)	**Si1B—F1B**	1.691 [1.680]
1.691 [1.680]	**Si1A—F2A**	1.643 (4)	1.649 (13)	**Si1B—F2B**	1.703 [1.700]
1.640 [1.643]	**Si1A—F3A**	1.585 (3)	1.591 (3)	**Si1B—F3B**	1.646 [1.643]
1.648 [1.644]	**Si1A—F4A**	1.592 (13)	1.630 (10)	**Si1B—F4B**	1.647 [1.644]
1.645 [1.643]	**Si1A—F5A**	1.594 (4)	1.591 (4)	**Si1B—F5B**	1.640 [1.643]
Angle [°] (calcd)	**Angle**	Angle [°] (expt)		**Angle**	Angle [°] (calcd)
		Domain A	Domain B		
179.2 [179.1]	**$F1A_{ax}$—Si1A—$F2A_{ax}$**	178.4 (4)	176.1 (6)	**$F1B_{ax}$— Si1B—$F2B_{ax}$**	179.0 [179.0]
120.5 [120.0]	**$F3A_{eq}$— Si1A—$F4A_{eq}$**	122.4 (6)	122.5 (3)	**$F3B_{eq}$— Si1B—$F4B_{eq}$**	120.1 [120.0]
119.8 [120.0]	**$F3A_{eq}$— Si1A—$F5A_{eq}$**	118.3 (3)	117.1 (3)	**$F3B_{eq}$— Si1B—$F5B_{eq}$**	119.5 [120.0]
119.7 [120.0]	**$F4A_{eq}$— Si1A—$F5A_{eq}$**	119.3 (6)	120.4 (3)	**$F4B_{eq}$— Si1B—$F5B_{eq}$**	120.4 [120.0]

in Table S7). Molecular B3LYP/aug-cc-pVTZ and MP2/aug-cc-pVTZ calculations predict slightly shorter M–F bond distances compared to the PBE distances, but they are still longer than the experimental bond lengths (Table S7).

S2.3 H-Bonding Between MF_5^- Anion and Surrounding $[(L^{Dipp})H]^+$ Cations

With the analysis of charge density difference, eq (1) in the main paper, we could clearly identify two H-bonds per MF_5^- anion that are formed with imidazolium fragment: one bifurcated C–H$\cdots$F$_{ax}$(F$_{eq}$) bond and one sin-

Table S6. As in Table S5 but for the Ge compound (**2b**).

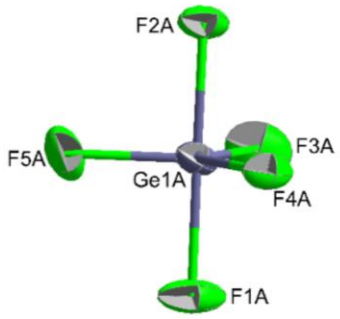
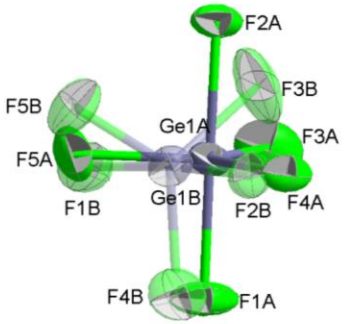
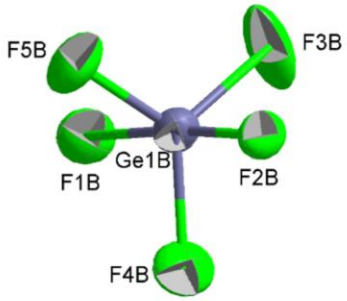
Domain A		**Anion as observed**		**Domain B**	
					
Bond length [Å] (calcd)	**Bond**	Bond length [Å] (expt)		**Bond**	Bond length [Å] (calcd)
		Domain A	Domain B		
1.818 [1.818]	**Ge1A—F1A**	1.759 (3)	1.776 (8)	**Ge1B—F1B**	1.808 [1.798]
1.808 [1.799]	**Ge1A—F2A**	1.759 (2)	1.734 (15)	**Ge1B—F2B**	1.817 [1.809]
1.777 [1.779]	**Ge1A—F3A**	1.716 (2)	1.727 (8)	**Ge1B—F3B**	1.780 [1.777]
1.784 [1.777]	**Ge1A—F4A**	1.726 (3)	1.700 (14)	**Ge1B—F4B**	1.785 [1.787]
1.779 [1.779]	**Ge1A—F5A**	1.702 (2)	1.663 (8)	**Ge1B—F5B**	1.777 [1.783]
Angle [°] (calcd)	**Angle**	Angle [°] (expt)		**Angle**	Angle [°] (calcd)
		Domain A	Domain B		
178.3 [179.1]	**F1A$_{ax}$—Ge1A—F2A$_{ax}$**	178.5 (2)	176.7 (9)	**F1B$_{ax}$—Ge1B—F2B$_{ax}$**	178.4 [177.9]
121.9 [119.0]	**F3A$_{eq}$—Ge1A—F4A$_{eq}$**	121.2 (2)	122.5 (7)	**F3B$_{eq}$—Ge1B—F4B$_{eq}$**	119.8 [119.5]
118.1 [121.9]	**F3A$_{eq}$—Ge1A—F5A$_{eq}$**	117.7 (1)	117.2 (6)	**F3B$_{eq}$—Ge1B—F5B$_{eq}$**	118.7 [118.2]
120.1 [119.1]	**F4A$_{eq}$—Ge1A—F5A$_{eq}$**	121.1 (2)	120.2 (6)	**F4B$_{eq}$—Ge1B—F5B$_{eq}$**	121.6 [122.3]

Table S7. Calculated M–F (M = Si, Ge) bond distances within the MF_5^- anion as given by various methods and basis sets (designated as "method/basis-set"). Experimental values for domain A are stated for comparison. Labels F_{ax} and F_{eq} stand for axial and equatorial F atoms, respectively, whereas label "pw" stand for the plane-wave basis set.

Bond type	Bond distance [Å]					
	PBE/pw[a] (domain A)	PBE/pw[b] (isolated)	PBE/ aug-cc-pVTZ[b]	B3LYP/ aug-cc-pVTZ[b]	MP2/ aug-cc-pVTZ[b]	Expt.[c] (domain A)
Si–F_{ax}	1.691, 1.703	1.693	1.696	1.682	1.679	1.623, 1.643
Si–F_{eq}	1.640, 1.645, 1.648	1.651	1.657	1.641	1.638	1.585, 1.592, 1.594
Ge–F_{ax}	1.808, 1.818	1.812	1.804	1.789	1.773	1.759, 1.759
Ge–F_{eq}	1.777, 1.779, 1.784	1.787	1.778	1.761	1.743	1.702. 1.716, 1.726

[a] From calculation of full-crystal structure with all MF_5^- anions in domain A.
[b] From calculation of isolated MF_5^- anion.
[c] For MF_5^- in domain A.

gular C–H$\cdots$F$_{ax}$ bond. In the domain A these are C2–H$\cdots$F1A$_{ax}$(F4A$_{eq}$) and C4–H$\cdots$F2A$_{ax}$, whereas for the domain B they are C2–H$\cdots$F2B$_{ax}$(F4B$_{eq}$) and C5–H$\cdots$F1B$_{ax}$. The criterion for the identification of H-bonds is the existence of electron charge accumulation lobe in between the H$\cdots$F atoms. The bifurcated H-bond is formed with one axial and

Table S8. PBE calculated and experimentally determined H-bond lengths and angles for [(L^{Dipp})H][SiF_5] and [(L^{Dipp})H][GeF_5] compounds (**2a**) and (**2b**); experimental values are stated in parentheses. Labels have the following meaning: d(H···F) ≡ distance between H and F atoms within the C–H···F; d(C···F) ≡ distance between C and F atoms within the C–H···F; a(C–H···F) ≡ C–H···F bond angle.

Bond type	Si compound			Ge compound		
	d(H···F) [Å]	d(C···F) [Å]	a(C–H···F) [°]	d(H···F) [Å]	d(C···F) [Å]	a(C–H···F) [°]
domain A						
C2–H···F1A_{ax}	2.04	3.07 (3.08)[a]	156 (149)[a]	2.02	3.05 (3.04)[a]	158 (154)[a]
C2–H···F4A_{eq}	2.39	3.30 (3.04)[a]	140 (149)[a]	2.43	3.28 (3.01)[a]	134 (138)[a]
C4–H···F2A_{ax}	2.21	3.03 (2.88)[a]	131 (123)[a]	2.27	3.00 (2.90)[a]	123 (124)[a]
domain B						
C2–H···F2B_{ax}	2.04	3.07 (3.00)[a]	157 (148)[a]	2.06	3.06 (3.07)[a]	153 (138)[a]
C2–H···F4B_{eq}	2.39	3.30 (2.97)[a]	140 (148)[a]	2.37	3.26 (2.93)[a]	139 (154)[a]
C5–H···F1B_{ax}	2.20	3.03 (2.91)[a]	132 (123)[a]	2.20	2.99 (2.90)[a]	128 (123)[a]

[a]Experimental value.

one equatorial F atom, yet the interaction with F_{ax} is stronger as clearly evidenced by considerably larger electron-charge accumulation lobe in between the H···F_{ax} as compared to H···F_{eq}, see Figure 4 in the main paper which shows the charge density difference for the Ge compound (**2a**) with the anion in the domain A; $\Delta\rho(\mathbf{r})$ plots are analogously similar for the domain B as well as for the Si compound (**2b**) for both domains (not shown for brevity). Also the distance between the H···F_{ax} (2 Å) is by about 0.4 Å shorter than the H···F_{eq} distance (2.4 Å)—see Table S8, which tabulates the PBE calculated and experimentally determined bond-lengths and angles of the identified H-bonds. From the tabulated distances we can infer that these H-bonds are relatively weak.

S2.4 Transition of MF_5^- Anions Between Domain A and B

Using the ^{19}F NMR spectroscopy (see Figure S2) we only observed a single signal instead of two signals for axial and equatorial fluorides. This observation can be explained by assuming that the lifetime of an anion in a given domain is very short, i.e., anions flip frequently between the two domains. To confirm this hypothesis we calculated the activation barrier for the transition of the GeF_5^- anion between the two domains. Both possible mechanisms were explored: rotation (R) and Berry pseudorotation mechanism (BM). The calculations were performed in such a way that only one anion per unit-cell undergoes transition (note that there are four anions per unit-cell). The PBE/pw calculated activation energies (E^*) for R and BM mechanisms in [(L^{Dipp})H][GeF_5] compound (**2b**) are almost degenerate and very small, 12 kJ/mol for A → B transition and 10 kJ/mol for the reverse B → A transition. This implies that both R and BM mechanisms are similarly probable. The "movie" snapshots of the two mechanisms are shown in Figure 2 in the main paper. These activation energies imply that at 300 K—temperature at which ^{19}F NMR was performed—the average lifetime (τ) of the GeF_5^- anion in a given position between the two flips is on the order of a 10^{-10} s, which is way shorter than the NMR time scale. The average lifetime of the anion in a given position was estimated as $\tau = \nu^{-1}\exp(E^*/(k_B T))$, where the value of 10^{12} s^{-1} was assumed for the frequency prefactor ν.

S2.5 Relative Stabilities of Anions: Bipyramidal GeF_5^- vs Octahedral GeF_6^{2-}

One of the reasons that GeF_5^- anion is so difficult to synthesize is due to its tendency to polymerize and form chains of octahedra. This indicates that the stability of bipyramidal GeF_5^- anion is inferior to that of octahedral GeF_6^{2-}. To substantiate this inference, we characterized the relative stabilities of the two anions computationally on the B3LYP/aug-cc-pVTZ level of theory. A word of caution is in place here, namely, it would be inappropriate to directly compare "GeF_5^- + F^-" to GeF_6^{2-}. If this is done then GeF_6^{2-} is found inferior to "GeF_5^- + F^-" by 164 kJ/mol. The reason is that GeF_6^{2-} is a relatively small object and it cannot efficiently "accomodate" the surplus of two-electrons—that this is so can be appreciated from its electron affinities (EA): the first calculated adiabatic EA of GeF_6 is huge, 899 kJ/mol (for GeF_6 + e^- → GeF_6^-), whereas the second adiabatic EA is way smaller, only 145 kJ/mol (for GeF_6^- + e^- → GeF_6^{2-}) and this value is smaller than the ionization potential of the most electropositive species. However, in reality the GeF_6^{2-} is "never" alone but is instead surrounded by cations for the reason of charge-neutrality. It is therefore stabilized considerably by the corresponding cation–anion interactions. A much more appropriate way to characterize the relative stability of the two anions is therefore to deduce it from stabilities of neutral "objects". We thus evaluated the relative stability of the two anions by considering the following two consecutive reaction steps (the B3LYP/aug-cc-pVTZ calculated energies of reactions, $\Delta E = E_{\text{products}} - E_{\text{reactants}}$, are also stated):

$$GeF_4 + NaF \rightarrow NaGeF_5, \quad \Delta E_5 = -181 \text{ kJ/mol} \quad \text{(S3a)}$$

$$NaGeF_5 + NaF \rightarrow Na_2GeF_6, \quad \Delta E_6 = -244 \text{ kJ/mol} \quad \text{(S3b)}$$

and

$$\Delta\Delta E_{65} = \Delta E_6 - \Delta E_5 = -63 \text{ kJ/mol}. \quad \text{(S3c)}$$

It can be seen from the Figure S7 that the point representing the ammonium case, reactions (S4a) and (S4b), lies on the Na^+ curve. This Figure suggests that for $R_\pm \gtrsim 4$ Å, the $\Delta\Delta E_{65}$ values become endothermic and correspondingly the GeF_6^{2-} anion inferior to GeF_5^- anion.

We also calculated the respective reaction steps for the bulky tetramethylammonium cation, $N(CH_3)_4^+$, for which the $R_\pm$ distance is about 4.2 Å (due to a symmetry, the $R_\pm$ is roughly given by the Ge–N distance). Similarly as for the ammonium cation, also this case lies very near the Na^+ curve. Notably, though, Figure S7 suggests that $N(CH_3)_4^+$ cation is large enough to stabilize the GeF_5^- against the GeF_6^{2-}, because the $\Delta\Delta E_{65} > 0$.

Although the above analysis was performed with small clusters instead of solids, we believe that it correctly captures the qualitative trend that thermodynamic preference of GeF_6^{2-} against GeF_5^- diminishes with increasing size of cation. We therefore believe that the above presented analysis clearly demonstrates that apart from the steric effects, bulky cations stabilize the GeF_5^- against the GeF_6^{2-} also due to electrostatic effects. But Figure S7 should not be taken too quantitatively, in the sense that GeF_5^- wins over GeF_6^{2-} if $R_\pm > 4$ Å. At what $R_\pm$ distance this happens (if at all) for specific case, depends on the actual crystal structures involved.

S2.6 Vibrational Characterization of SiF_5^- and GeF_5^- as well as SiF_6^{2-} and GeF_6^{2-} Anions

S2.6.1 Raman Spectra

The vibrations of the MF_5^- anions (M = Si, Ge) can be assigned based on D_{3h} symmetry. Three stretching vibrations (ν_1, ν_2, and ν_5) are Raman active. According to the literature, the strongest Raman active peak is the ν_1, which is found at 708 cm^{-1} for SiF_5^- [7] and at 665 cm^{-1} for GeF_5^-.[8] In the recorded Raman spectra of $[(L^{Dipp})H][MF_5]$, shown in Figure S8a, the peak at 709 cm^{-1} (Si) and 664 cm^{-1} (Ge) can be therefore confidently assigned to the ν_1 vibration of the trigonal-bipyramidal anion MF_5^-. Other less intense vibrations that could belong to the anion cannot be discerned due to strong masking vibrations of the cation. Raman spectra of the of $[(L^{Dipp})H][MF_5]$ were also recorded up to 4000 cm^{-1} (Figure S8b). The most intense vibration of the anion is marked by asterisk (*), whereas we assigned other peaks to the vibrations of the cation.

With the use of the Raman spectroscopy we checked the stability of the $[(L^{Dipp})H][MF_5]$ compounds (**2a**) and (**2b**) exposed to air. Raman spectra were taken in sealed capillary and on the sample that was exposed to the air and air moisture for 24 hours (Figure S9). According to the Raman spectroscopy, there is no differences in the position of the ν_1 vibrations of the MF_5^- anions (marked by asterisk) and cations. The compounds (**2a**) and (**2b**) are therefore stable on air at room temperature.

In contrast to trigonal-bipyramidal MF_5^- the vibrations of octahedral MF_6^{2-} anions (M = Si, Ge) can be assigned based on O_h symmetry. Three vibrations (ν_1, ν_2, ν_5) are Raman active and ν_1 is usually the strongest and found at 663 cm^{-1} for SiF_6^{2-} and 624 cm^{-1} for GeF_6^{2-}.[7]

Raman spectra of the $[(L^{Dipp})H][GeF_5]$ compound (**2b**) (blue line) and $[(L^{Dipp})H]_2[GeF_6]$ compound (**3b**) (black line) are presented in Figure S10a. The absence of the peak at 664 cm^{-1} in the Raman spectrum of compound (**3b**) proofs the absence of the trigonal-bipyramidal MF_5^- anions in the compound (**3b**). Unfortunately, the position of the ν_1 peak[7] of the GeF_6^{2-} at 624 cm^{-1} falls in the region of the cation vibrations and is therefore masked by them. The spectrum of the $[(L^{Dipp})H]_2[GeF_6]$ compound (**3b**) was also recorded up to 4000 cm^{-1} (Figure S10b.)

Table S9. PBE calculated vibrational frequencies of Raman active ν_1 (A'_1) normal mode of SiF_5^- and GeF_5^- anions. Labels "(crystal)" and "(isolated)" indicate the results obtain from the plane-wave calculation of full-crystal structure with all MF_5^- anions in domain A and from calculation of isolated MF_5^- anion, respectively. The $\Delta_{PBE/pw}$ column tabulates the difference in vibrational frequencies as obtained from "(crystal)" and "(isolated)" calculations.

Normal mode	PBE/pw (crystal)	PBE/pw (isolated)	$\Delta_{PBE/pw}$ (crystal – isolated)	PBE / aug-cc-pVTZ
ν_1 (SiF_5^-) [cm^{-1}]	653	644	9	652
ν_1 (GeF_5^-) [cm^{-1}]	599	588	11	598

S2.6.2 Vibrational Calculations

PBE underestimates vibrational frequencies, in particular it predicts 10% softer frequencies of Raman active ν_1 (A'_1) normal mode of MF_5^- anions compared to experimental values. The PBE/pw values for ν_1 frequencies, obtained from the full-crystal structure calculations, are 653 and 599 cm^{-1} for Si and Ge compounds (**2a**) and (**2b**), whereas experimental values are 709 and 664 cm^{-1}, respectively (cf. Figure S8). Yet the PBE/pw calculations allow to quantify the effect of surrounding crystal structure on the vibrations of MF_5^- anions. The PBE/pw calculations performed for isolated MF_5^- anion (i.e. MF_5^- enclosed in a big box with the compensating counter-charge background) give by about 10 cm^{-1} softer vibrational frequencies (Table S9). Interestingly, the crystal PBE/pw calculations give almost identical vibrational ν_1 frequency as the molecular PBE/aug-cc-pVTZ calculations (Table S9). Small quantified effect of the crystal-field on the ν_1 vibrational frequencies reassures that the ν_1 vibrations of MF_5^- anions can be characterized with molecular calculations. In Table S10 we compare the results for the B3LYP and MP2 calculated ν_1 frequencies for isolated bipyramidal MF_5^- and octahedral MF_6^{2-} anions (M = Si and Ge) to experimental values. For the sake of completeness, we also list in Table S11 all the vibrational frequencies along with IR intensities and Raman activities, calculated on the MP2/aug-cc-pVTZ level of theory. The resulting calculated IR and Raman spectra are presented in Figure S11, whereas normal mode displacement patterns are shown in Figure S12.

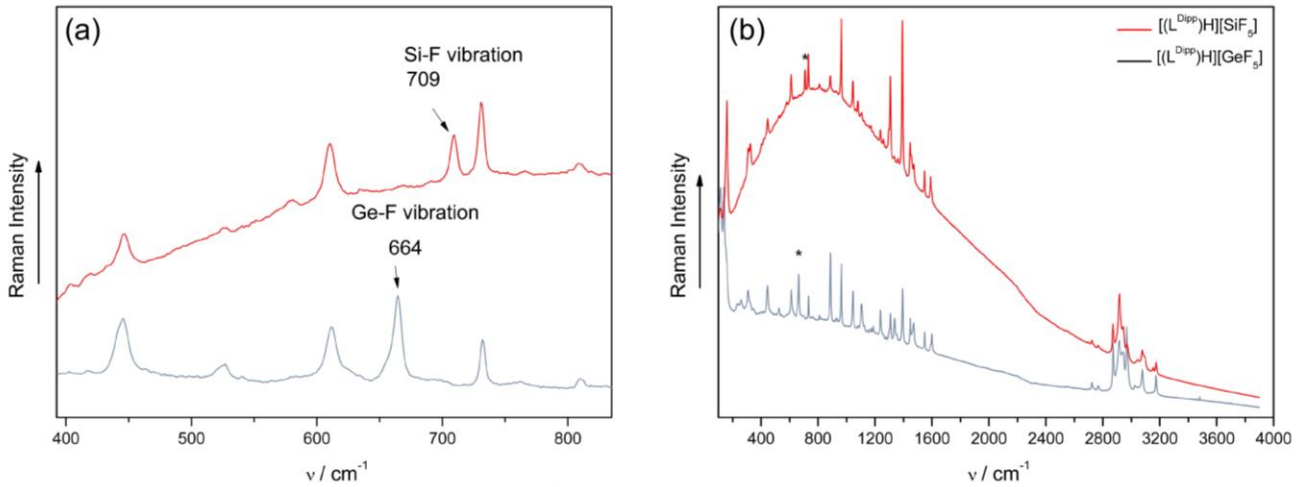


Figure S8. Raman spectra of $[(L^{Dipp})H][SiF_5]$ (**2a**) and $[(L^{Dipp})H][GeF_5]$ (**2b**). The most intense Raman peak, assigned to ν_1 vibrational mode of MF_5^- anion, is marked by asterisks (*).

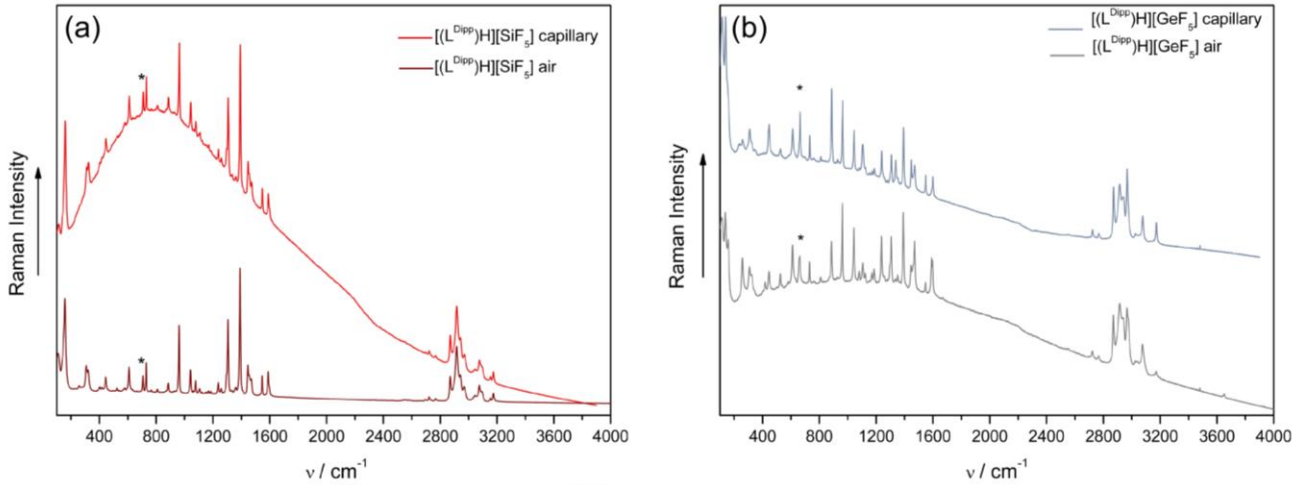


Figure S9. Raman spectra of $[(L^{Dipp})H][SiF_5]$ (**2a**) and $[(L^{Dipp})H][GeF_5]$ (**2b**) taken in sealed capillary and exposed on air after 24h.

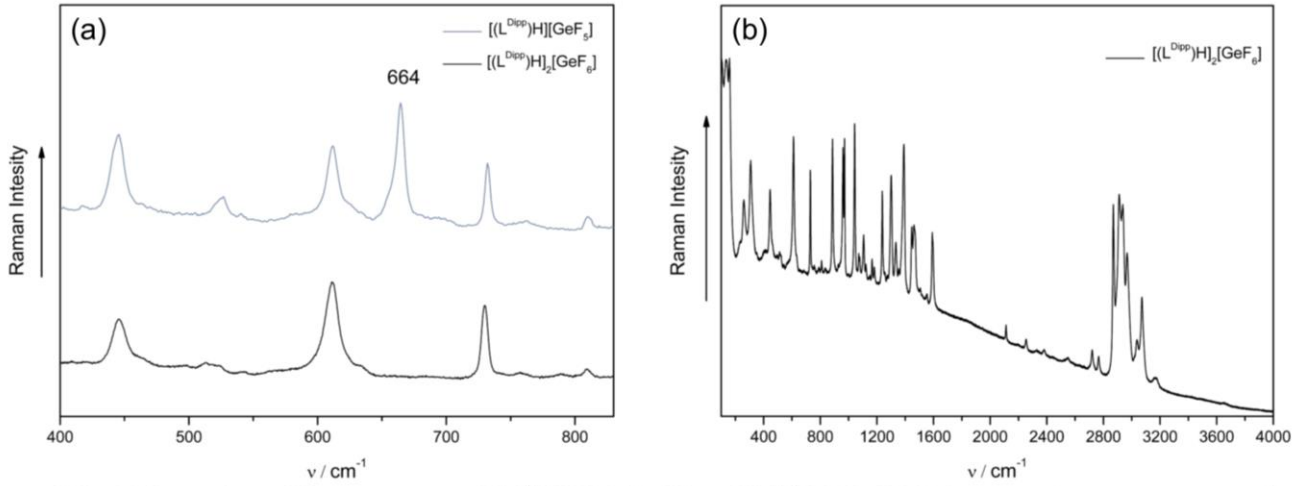


Figure S10. (a) Comparison of Raman spectra of $[(L^{Dipp})H][GeF_5]$ (**2b**) and $[(L^{Dipp})H]_2[GeF_6]$ (**3b**) in range from 400 to 850 cm^{-1}. (b) Raman spectrum of $[(L^{Dipp})H]_2[GeF_6]$ (**3b**) in range from 150 to 4000 cm^{-1}.

It can be seen from Table S10 that MP2 values of isolated bipyramidal SiF_5^- and GeF_5^- anions are very close to experimental values, whereas for the isolated octahedral MF_6^{2-} anions the agreement is not as good and the MP2 values are too soft by about 40 cm^{-1}. The reason is obviously due to neglect of the crystal field stabilization, which is much more important for bivalent MF_6^{2-} than for monovalent MF_5^- anions; for the latter the effect of crystal-field on ν_1 frequency

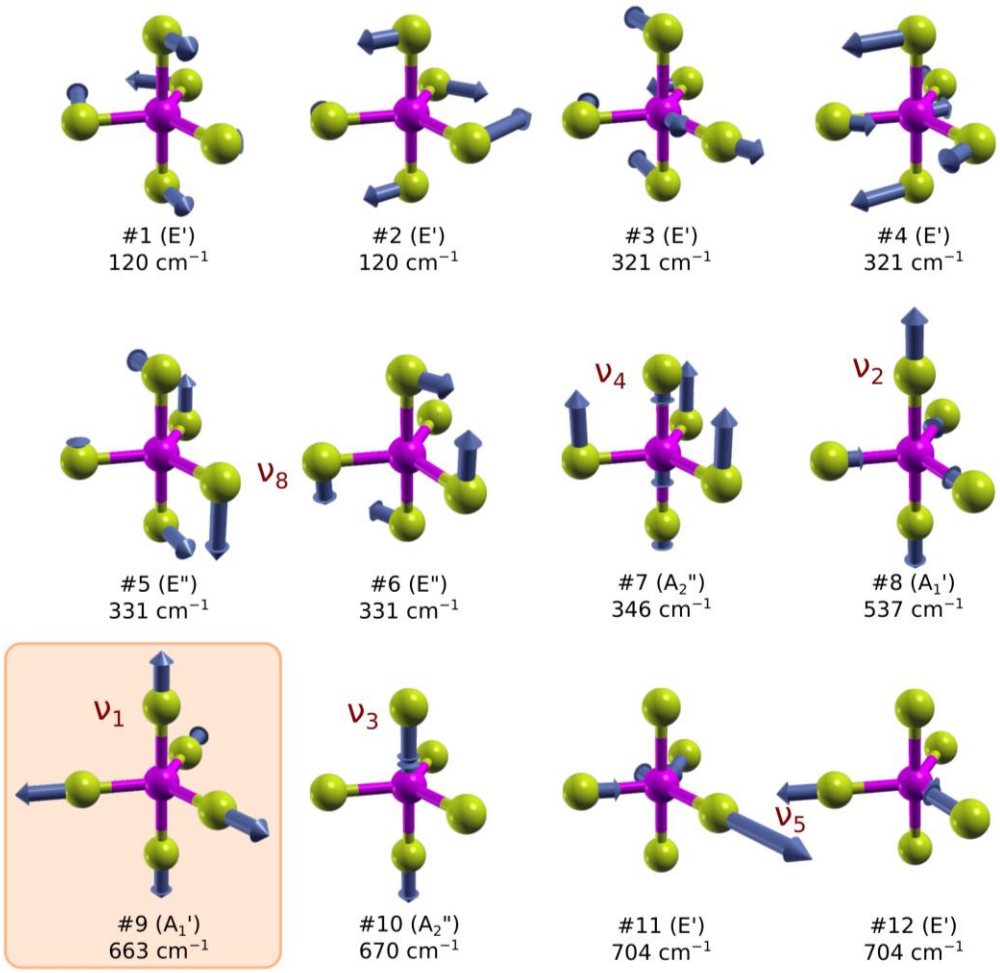


Figure S12. MP2/aug-cc-pVTZ calculated normal modes of GeF_5^- anion. Vibrational frequencies and normal mode symmetries are also reported below each snapshot. The Raman active ν_1 mode that was observed experimentally is highlighted.

[5] Wilson, A. K.; Woon, D. E.; Peterson, K. A.; Dunning Jr., T. H. Gaussian basis sets for use in correlated molecular calculations. IX. The atoms gallium through krypton, *J. Chem. Phys.* **1999,** *110,* 7667–7676.

[6] Gillespie, R. J.; Popelier, P. L. A. *Chemical Bonding and Molecular Geometry: From Lewis to Electron Densities;* Oxford University Press: New York, Oxford, USA, 2001.

[7] Nakamoto, K. *Infrared and Raman spectra of Inorganic and Coordibnation Compounds;* John Wiley and Sons: New York, USA, 5th ed.; 1997.

[8] Mallouk, T. E.; Desbat, B.; Bartlett, N. Structural studies of salts of cis and trans μ-fluoro-bridged polymers of pentafluorogermanate(1−) and of the pentafluorogermanate(1−) monomer, *Inorg. Chem.* **1984,** *23,* 3160–3166.

Chapter 8

Summary and Conclusions

In this chapter, we summarize the fundamental conclusions and achievements of this thesis. At the end, we give an outlook on the possibilities for future work.

The fundamental idea behind this thesis was to combine two fields of chemistry. On the one hand *N*-heterocyclic carbene chemistry and on the other one different fluoride substrates. Both types of used compounds are highly reactive and unstable on air. However, based on the slight of attention received, this combination of reagents is an interesting "mix" with a broad space to explore many possible basic and applicative ideas to take on the challenge of preparing soluble metal fluorides.

8.1 Summary

In the first part, we have managed to obtain a neutral complex of SbF_3 with NHC. However, the reactions of SbF_3 with NHC in acetonitrile or thf did not yield the desired neutral complex. Instead we observed a new imidazolium salt of $[(L^{Dipp})H]^+[SbF_4]^-$. The behaviour of the system showed that the proton responsible for $[(L^{Dipp})H]^+$ cation formation is abstracted from the solvent molecule. Additionally, we could observe that all three imidazolium protons are very labile and can easily undergo H/D exchange. To avoid the formation of the salt, we performed reactions in non-polar solvents (*i.e.* toluene and benzene) to avoid the proton abstraction from the solvent and formation of the $[(L^{Dipp})H]^+[SbF_4]^-$ salt. To do that, we had to first prepare a SbF_3tmen complex that acts as a SbF_3 synthon soluble in non-polar solvents. Subsequent reaction of SbF_3tmen complex with NHC in toluene or benzene forms a neutral NHC–SbF_3 complex stable in the solution. However, in the transition from the solution to the solid, additional auto-ionization reaction takes place and we obtain an interesting crystal structure of $[(L^{Dipp})_2SbF_2]^+[SbF_4]^-$. This product is a:

a) Rare example of SbF_3 auto-ionization that shows amphoteric nature of SbF_3.
b) First example of mesoionic carbene coordinated to any metal/metalloid fluoride substrate.
c) First example of carbon-based ligand coordinated to SbF_2 moiety.
d) First example of the reaction mechanism where NHC ligand facilitates the auto-ionization reaction.

Additionally, we have suggested the chemical mechanism of such conversion and determined that the formation of $[(L^{Dipp})_2SbF_2]^+[SbF_4]^-$ is not induced by the presence of

tmen base in the reaction mixture. The mechanism could be described as “ligand-assisted and heat-induced auto-ionization”.

In the second part, we have studied the reactivity of NHC with different HF sources. Initial reaction with a surplus of aHF resulted in the formation of imidazolium poly(hydrogen fluoride) product $[(L^{Dipp})H][F(HF)_2]$. This prompted the question if we could stabilize $[(L^{Dipp})H][F(HF)]$ and $[(L^{Dipp})H][F]$ compounds in 1:2 and 1:1 ratios of HF, respectively. $Et_3N{\times}3HF$ and KHF_2 reagents readily accomplished this task in stoichiometric quantities of HF. This way we have found an elegant solution for the formation of $[(L^{Dipp})H][F]$ that was analytically pure without water or other impurities usually present in analogous types of products. During the research and characterization we established that product $[(L^{Dipp})H][F]$ shows properties of a naked (free) fluoride reagent. Additionally, we observed that dissolution of a solid $[(L^{Dipp})H][F]$ in acetonitrile leads to the formation of $[(L^{Dipp})H][F(HF)_2]$ and free NHC (L^{Dipp}). This is the first example where imidazolium salt reacts with itself and produces free NHC – a type of process not observed before.

In the last part of our work we have tested the reactivity of $[(L^{Dipp})H][F]$ reagent and reacted it with SiF_4 and GeF_4 Lewis acids. Reaction yielded discrete, monomeric, trigonal bipyramidal SiF_5^- and GeF_5^- anions. With an additional equivalent of $[(L^{Dipp})H][F]$ the reaction yielded a GeF_6^{2-} anion which, surprisingly, showed lower stability than the GeF_5^- anion (visual assessment under the microscope). With the help of quantum-chemical calculations, we established that the large cations indeed stabilize the GeF_5^- anion against GeF_6^{2-} anion due to cation steric properties as well as electrostatic Coulomb interactions with the surrounding cations. Discrete GeF_5^- anion was structurally characterized for the first time. The anion in the crystal structure is disordered in two distinct positions and occupies two distinct positions. We tried to explain the disorder in the crystal structure terms of rotation (R) or the Berry pseudorotation mechanism (BM). Calculated activation energies for both mechanisms are comparable and small, which means both mechanisms are equally probable. Additionally, we have reported the first ^{19}F NMR spectra of GeF_5^- and GeF_6^{2-} in organic solvents (acetonitrile). Trigonal bipyramidal GeF_5^- anion has two magnetically inequivalent sets of fluorides (equatorial and axial) but NMR shows only one singlet at –136.60 ppm for GeF_5^- anion in acetonitrile. This observation can be explained by assuming that the lifetime of the anion in a single domain is very short which thus confirms BM, however R mechanism cannot be excluded.

8.2 Outlook

Combining NHC chemistry with fluorine chemistry shows bright perspective. We would still like to perform other reactions with the rest of PnX_3 (Pn = P, As and Bi) halides and analyse if they have the same reactivity or if we can observe something unexpected that could give insights on:

a) NHC modes of coordination – an aspect highly important in catalysis
b) effects of the central metal size on the system
c) different Lewis acidity effects
d) other unexpected phenomena

We have characterized and performed interesting chemistry with a novel naked fluoride reagent $[(L^{Dipp})H][F]$ that is only in preliminary stages. To understand and establish the full scope of utility and applicability of the $[(L^{Dipp})H][F]$, $[(L^{Dipp})H][F(HF)]$ and $[(L^{Dipp})H][F(HF)_2]$ reagents, they have to be tested in numerous different reaction systems and $[(L^{Dipp})H][F]$ with $[(L^{Dipp})H][F(HF)]$ is already showing promising results as a fluorination reagent of organic compounds [111].

8.3 Final Personal Remark

I would like to conclude this thesis with a thought: You can either be attracted or repulsed by fluorine, but never does this small element leave anything or anyone without a reaction (except maybe He and Ne – at least until now). One could say that, in all its forms, it has "a mind of its own". Its reactivity often does not behave according to the trends or predicted mechanisms and is thus a worthy moiety for research, because you never know when you will encounter the "next big thing" that will further push the boundaries of this fundamental science that is Chemistry.

Bibliography

Journal Articles

B. Alič, A. Štefančič, and G. Tavčar, "Small molecule activation: SbF3 auto-ionization supported by transfer and mesoionic NHC rearrangement," *Dalton Transactions*, vol. 46, pp. 3338-3346, 2017.

B. Alič and G. Tavčar, "Reaction of *N*-heterocyclic carbene (NHC) with different HF sources and ratios – A free fluoride reagent based on imidazolium fluoride," *Journal of Fluorine Chemistry,* vol. 192, pp. 141-146, 2016.

B. Alič, M. Tramšek, A. Kokalj, and G. Tavčar, "Discrete GeF5– Anion Structurally Characterized with a Readily Synthesized Imidazolium Based Naked Fluoride Reagent," *Inorganic Chemistry,* vol. 56, pp. 10070-10077, 2017/08/21 2017.

Conference Paper

B. Alič and G. Tavčar, "Indices of new free fluoride reagent derived from persistent *N*-heterocyclic carbene." in *Proceedings of the 22th Slovenian Chemical Days*, Portorož, Slovenia: Slovenian Chemical Society, 2016.

B. Alič and G. Tavčar, "Abnormal behaviour of *N*-heterocyclic carbenes with MF_3 compounds." in *Proceedings of the 10th Young researchers' day,* Ljubljana, Slovenia: Jožef Stefan Institut, 2016.

G. Tavčar, B. Alič, E. Goreshnik, "Reactivity of selected pnictogen trifluorides." In *PACIFICHEM 2015*, 2015 International Chemical Congress of Pacific Basin Societies, Honolulu, Hawaii, 2015.

B. Alič and G. Tavčar, "$(SbF_2)^+$ elusive cation" in *Book of abstract*, [21st International Symposium on Fluorine Chemistry jointly with the 6th International Symposim on Fluorous Technologies], 21st ISFC & ISoFT'15 2015, Como, Italy. Milano: Politecniico di Milano, 2015.

B. Alič and G. Tavčar, "Reactivity of SbF_3(TMEDA) in different organic solvents." in *Proceedings of the 9th Young researchers' day,* Ljubljana, Slovenia: Jožef Stefan Institut, 2015.

Biography

Blaž Ališ was born on June 13, 1988 in Brežice, Slovenia. His education started at primary school in Boštanj. Knowing chemistry was his passion, he continued his secondary school in Celje where he attended the Vocational and Technical, Electro and Chemical School at School Center Celje, where he obtained his high-school diploma from Chemistry in 2007.

In the same year, he enrolled in the Faculty of Chemistry and Chemical Technology, Ljubljana, in the university programme Chemistry where he further extended his knowledge of chemistry. He graduated at the cathedra of organic chemistry, under the supervision of Prof. Dr. Branko Stanovnik, earning him the title B.Sc in Chemistry (equivalent to M.Sc after the Bologna reform) in 2013. In parallel, during his B.Sc work, he was involved in academic research with Asst. Prof. Dr. Marjan Jereb for a period of 8 months, during which he was introduced to his future supervisor at the Jožef Stefan Institute.

After graduation, Blaž Ališ enrolled in postgraduate studies of Ecotechnology at the Jožef Stefan International Postgraduate School in the same year. During his postgraduate studies, Blaž Ališ was a young researcher at the Department of Inorganic Chemistry and Technology (K1) of the Jožef Stefan Institute, under the supervision of Asst. Prof. Dr. Gašper Tavčar. He took on the challenges of his early academic life with dedication, devotion and a high level of enthusiasm. He has proven himself as a hard working person with real interest in his research work. He was grateful to anyone that helped him on his path and always tried to maintain a healthy balance between striving for the greater good while trying to establish his individual accomplishments.

His research activities were focused on combining *N*-heterocyclic carbene chemistry with fluorine chemistry. The three scientific papers, published in distinguished international scientific journals, are collected in this doctoral thesis which represents the results of his work.

References

[1] E. Buchner and L. Feldmann, "Diazoessigester und Toluol," *Berichte der deutschen chemischen Gesellschaft,* vol. 36, pp. 3509-3517, 1903.

[2] H. Staudinger and O. Kupfer, "Über Reaktionen des Methylens. III. Diazomethan," *Berichte der deutschen chemischen Gesellschaft,* vol. 45, pp. 501-509, 1912.

[3] W. von E. Doering and A. K. Hoffmann, "The Addition of Dichlorocarbene to Olefins," *Journal of the American Chemical Society,* vol. 76, pp. 6162-6165, 1954.

[4] E. Fischer and A. Maasböl, "On the existence of a tungsten carbonyl carbene complex," *Angewandte Chemie International Edition in English,* vol. 3, pp. 580–581, 1964.

[5] K. Öfele, "1, 3-Dimethyl-4-imidazolinyliden-(2)-pentacarbonylchrom ein neuer Übergangsmetall-carben-komplex," *Journal of Organometallic Chemistry,* vol. 12, pp. P42–P43, 1968.

[6] H. W. Wanzlick and H. J. Schönherr, "Direct synthesis of a mercury salt-carbene complex," *Angewandte Chemie International Edition in English,* vol. 7, pp. 141–142, 1968.

[7] R. R. Schrock, "Alkylcarbene complex of tantalum by intramolecular .alpha.-hydrogen abstraction," *Journal of the American Chemical Society,* vol. 96, pp. 6796–6797, 1974.

[8] A. J. Arduengo III, R. L. Harlow, and M. Kline, "A stable crystalline carbene," *Journal of the American Chemical Society,* vol. 113, pp. 361–363, 1991.

[9] A. Nemirowski and P. R. Schreiner, "Electronic Stabilization of Ground State Triplet Carbenes," *The Journal of organic chemistry,* vol. 72, pp. 9533–9540, 2007.

[10] D. Bethell, "Structure and Mechanism in Carbene Chemistry," in *Advances in Physical Organic Chemistry*. vol. Volume 7, V. Gold, Ed., ed: Academic Press, 1969, pp. 153-209.

[11] I. Shavitt, "Geometry and singlet-triplet energy gap in methylene: a critical review of experimental and theoretical determinations," *Tetrahedron,* vol. 41, pp. 1531-1542, 1985.

[12] P. S. Skell and A. Y. Garner, "Reactions of Bivalent Carbon Compounds. Reactivities in Olefin-Dibromocarbene Reactions," *Journal of the American Chemical Society,* vol. 78, pp. 5430-5433, 1956.

[13] V. P. W. Böhm and W. A. Herrmann, "The “Wanzlick Equilibrium”," *Angewandte Chemie International Edition,* vol. 39, pp. 4036-4038, 2000.

[14] W. Kirmse, "Persistent Triplet Carbenes," *Angewandte Chemie International Edition,* vol. 42, pp. 2117-2119, 2003.

[15] I. Fernández, C. A. Dyker, A. DeHope, B. Donnadieu, G. Frenking, and G. Bertrand, "Exocyclic Delocalization at the Expense of Aromaticity in 3,5-bis(π-Donor) Substituted Pyrazolium Ions and Corresponding Cyclic Bent Allenes," *Journal of the American Chemical Society,* vol. 131, pp. 11875-11881, 2009.

[16] M. Soleilhavoup and G. Bertrand, "Cyclic (Alkyl)(Amino)Carbenes (CAACs): Stable Carbenes on the Rise," *Accounts of Chemical Research,* vol. 48, pp. 256-266, 2015.

[17] M. N. Hopkinson, C. Richter, M. Schedler, and F. Glorius, "An overview of N-heterocyclic carbenes," *Nature,* vol. 510, pp. 485–496, 2014.

[18] M. K. Denk, K. Hatano, and M. Ma, "Nucleophilic carbenes and the wanzlick equilibrium: A reinvestigation," *Tetrahedron Letters,* vol. 40, pp. 2057-2060, 1999.

[19] H. W. Wanzlick, "Aspects of Nucleophilic Carbene Chemistry," *Angewandte Chemie International Edition in English,* vol. 1, pp. 75-80, 1962.

[20] H.-W. Wanzlick and E. Schikora, "Ein nucleophiles Carben," *Chemische Berichte,* vol. 94, pp. 2389-2393, 1961.

[21] H. W. Wanzlick and E. Schikora, "Ein neuer Zugang zur Carben-Chemie," *Angewandte Chemie,* vol. 72, pp. 494-494, 1960.

[22] W. Kirmse, "The Beginnings of N-Heterocyclic Carbenes," *Angewandte Chemie International Edition,* vol. 49, pp. 8798-8801, 2010.

[23] A. J. Arduengo Iii, R. Krafczyk, R. Schmutzler, H. A. Craig, J. R. Goerlich, W. J. Marshall*, et al.*, "Imidazolylidenes, imidazolinylidenes and imidazolidines," *Tetrahedron,* vol. 55, pp. 14523-14534, 1999.

[24] A. J. Arduengo, H. V. R. Dias, R. L. Harlow, and M. Kline, "Electronic stabilization of nucleophilic carbenes," *Journal of the American Chemical Society,* vol. 114, pp. 5530-5534, 1992.

[25] A. J. Arduengo, F. Davidson, H. V. R. Dias, J. R. Goerlich, D. Khasnis, W. J. Marshall*, et al.*, "An Air Stable Carbene and Mixed Carbene “Dimers”," *Journal of the American Chemical Society,* vol. 119, pp. 12742-12749, 1997.

[26] F. Liu, X. Bugaut, M. Schedler, R. Fröhlich, and F. Glorius, "Designing N-Heterocyclic Carbenes: Simultaneous Enhancement of Reactivity and Enantioselectivity in the Asymmetric Hydroacylation of Cyclopropenes," *Angewandte Chemie International Edition,* vol. 50, pp. 12626-12630, 2011.

[27] F. Wang, L.-j. Liu, W. Wang, S. Li, and M. Shi, "Chiral NHC–metal-based asymmetric catalysis," *Coordination Chemistry Reviews,* vol. 256, pp. 804-853, 2012.

[28] A. Alexakis, C. L. Winn, F. Guillen, J. Pytkowicz, S. Roland, and P. Mangeney, "Asymmetric Synthesis with N-Heterocyclic Carbenes. Application to the Copper-Catalyzed Conjugate Addition," *Advanced Synthesis & Catalysis,* vol. 345, pp. 345-348, 2003.

[29] L. Hintermann, "Expedient syntheses of the N-heterocyclic carbene precursor imidazolium salts IPr · HCl, IMes · HCl and IXy · HCl," *Beilstein Journal of Organic Chemistry,* vol. 3, p. 22, 2007.

[30] L. Jafarpour, E. D. Stevens, and S. P. Nolan, "A sterically demanding nucleophilic carbene: 1,3-bis(2,6-diisopropylphenyl)imidazol-2-ylidene). Thermochemistry and catalytic application in olefin metathesis," *Journal of Organometallic Chemistry,* vol. 606, pp. 49-54, 2000.

[31] O. Kühl, *Functionalised N-Heterocyclic Carbene Complexes*: Wiley Online Library, 2010.

[32] C. Boehme and G. Frenking, "Electronic structure of stable carbenes, silylenes, and germylenes," *Journal of the American Chemical Society,* vol. 118, pp. 2039–2046, 1996.

[33] P. S. Skell and R. C. Woodworth, "STRUCTURE OF CARBENE, CH2," *Journal of the American Chemical Society,* vol. 78, pp. 4496-4497, 1956.

[34] C. Heinemann, T. Müller, Y. Apeloig, and H. Schwarz, "On the Question of Stability, Conjugation, and “Aromaticity” in Imidazol-2-ylidenes and Their Silicon Analogs†," *Journal of the American Chemical Society,* vol. 118, pp. 2023–2038, 1996.

[35] N. Marion, P. De Fremont, I. M. Puijk, E. C. Ecarnot, D. Amoroso, A. Bell, *et al.*, "N-Heterocyclic Carbene–Palladium Complexes [(NHC) Pd (acac) Cl]: Improved Synthesis and Catalytic Activity in Large-Scale Cross-Coupling Reactions," *Advanced Synthesis & Catalysis,* vol. 349, pp. 2380–2384, 2007.

[36] S. Ahrens, E. Herdtweck, S. Goutal, and T. Strassner, "Synthesis, Structure and Stability of New PtII–Bis (N-Heterocyclic Carbene) Complexes," *European journal of inorganic chemistry,* vol. 2006, pp. 1268–1274, 2006.

[37] D. Enders, H. Gielen, G. Raabe, J. Runsink, and J. H. Teles, "Synthesis and Stereochemistry of the First Chiral (Imidazolinylidene)-and (Triazolinylidene) palladium (ii) Complexes," *Chemische Berichte,* vol. 129, pp. 1483–1488, 1996.

[38] W. A. Herrmann, M. Elison, J. Fischer, C. Koecher, and G. R. J. Artus, "Metal Complexes of N-Heterocyclic Carbenes—A New Structural Principle for Catalysts in Homogeneous Catalysis," *Angewandte Chemie International Edition in English,* vol. 34, pp. 2371–2374, 1995.

[39] W. A. Herrmann and C. Koecher, "N-Heterocyclic Carbenes," *Angewandte Chemie International Edition in English,* vol. 36, pp. 2162–2187, 1997.

[40] I. J. B. Lin and C. S. Vasam, "Preparation and Application of N-heterocyclic Carbene Complexes of Ag (I)," *Coordination Chemistry Reviews,* vol. 251, pp. 642–670, 2007.

[41] C. Y. Liao, K. T. Chan, C. Y. Tu, Y. W. Chang, C. H. Hu, and H. M. Lee, "Robust and Electron-Rich cis-Palladium (II) Complexes with Phosphine and

Carbene Ligands as Catalytic Precursors in Suzuki Coupling Reactions," *Chemistry-A European Journal,* vol. 15, pp. 405–417, 2009.

[42] O. Winkelmann, C. Näther, and U. Lüning, "Bimacrocyclic NHC transition metal complexes," *Journal of Organometallic Chemistry,* vol. 693, pp. 923–932, 2008.

[43] C. Y. Liao, K. T. Chan, J. Y. Zeng, C. H. Hu, C. Y. Tu, and H. M. Lee, "Nonchelate and chelate complexes of palladium (II) with n-heterocyclic carbene ligands of amido functionality," *Organometallics,* vol. 26, pp. 1692–1702, 2007.

[44] C. Y. Liao, K. T. Chan, Y. C. Chang, C. Y. Chen, C. Y. Tu, C. H. Hu*, et al.*, "Unexpected Solvent-Induced Cis/Trans Isomerization and Catalytic Application of a Bis-bidentate Nickel (II) Complex with N-Heterocyclic Carbene and Amido Functionalities," *Organometallics,* vol. 26, pp. 5826–5833, 2007.

[45] J. M. Wilson, G. J. Sunley, H. Adams, and A. Haynes, "Oxidative addition of MeI to cationic Rh (I) carbonyl complexes with pyridyl bis (carbene) ligands," *Journal of organometallic chemistry,* vol. 690, pp. 6089–6095, 2005.

[46] A. E. Wang, J. H. Xie, L. X. Wang, and Q. L. Zhou, "Triaryl phosphine-functionalized< i> N</i>-heterocyclic carbene ligands for Heck reaction," *Tetrahedron,* vol. 61, pp. 259–266, 2005.

[47] E. Mas-Marzá, M. Sanaú, and E. Peris, "A new pyridine-bis-N-heterocyclic carbene ligand and its coordination to Rh: Synthesis and characterization," *Journal of organometallic chemistry,* vol. 690, pp. 5576–5580, 2005.

[48] C. Y. Legault, C. Kendall, and A. B. Charette, "Structure and reactivity of a new anionic N-heterocyclic carbene silver (I) complex," *Chemical Communications,* pp. 3826–3828, 2005.

[49] M. V. Baker, B. W. Skelton, A. H. White, and C. C. Williams, "Synthesis and Characterization of a Saddle-Shaped Nickel-Carbene Complex Derived from an Imidazolium-Linked m eta-Cyclophane," *Organometallics,* vol. 21, pp. 2674–2678, 2002.

[50] S. Gründemann, A. Kovacevic, M. Albrecht, J. W. Faller, and R. H. Crabtree, "Abnormal Ligand Binding and Reversible Ring Hydrogenation in the Reaction of Imidazolium Salts with IrH5(PPh3)2," *Journal of the American Chemical Society,* vol. 124, pp. 10473–10481, 2002.

[51] A. Kovacevic, S. Grundemann, J. R. Miecznikowski, E. Clot, O. Eisenstein, and R. H. Crabtree, "Counter-ion effects switch ligand binding from C-2 to C-5 in kinetic carbenes formed from an imidazolium salt and IrH5(PPh3)2," *Chemical Communications,* pp. 2580–2581, 2002.

[52] L. N. Appelhans, D. Zuccaccia, A. Kovacevic, A. R. Chianese, J. R. Miecznikowski, A. Macchioni*, et al.*, "An Anion-Dependent Switch in Selectivity Results from a Change of C−H Activation Mechanism in the Reaction of an Imidazolium Salt with IrH5(PPh3)2," *Journal of the American Chemical Society,* vol. 127, pp. 16299–16311, 2005.

[53] Y. Wang, Y. Xie, M. Y. Abraham, P. Wei, H. F. Schaefer, P. v. R. Schleyer, *et al.*, "A Viable Anionic N-Heterocyclic Dicarbene," *Journal of the American Chemical Society,* vol. 132, pp. 14370-14372, 2010.

[54] V. Lavallo, Y. Canac, C. Präsang, B. Donnadieu, and G. Bertrand, "Stable Cyclic (Alkyl)(Amino)Carbenes as Rigid or Flexible, Bulky, Electron-Rich Ligands for Transition-Metal Catalysts: A Quaternary Carbon Atom Makes the Difference," *Angewandte Chemie International Edition,* vol. 44, pp. 5705–5709, 2005.

[55] E. Tomás-Mendivil, M. M. Hansmann, C. M. Weinstein, R. Jazzar, M. Melaimi, and G. Bertrand, "Bicyclic (Alkyl)(amino)carbenes (BICAACs): Stable Carbenes More Ambiphilic than CAACs," *Journal of the American Chemical Society,* vol. 139, pp. 7753-7756, 2017.

[56] R. H. Crabtree, "Abnormal, mesoionic and remote N-heterocyclic carbene complexes," *Coordination Chemistry Reviews,* vol. 257, pp. 755–766, 2013.

[57] H. Lebel, M. K. Janes, A. B. Charette, and S. P. Nolan, "Structure and Reactivity of "Unusual" N-Heterocyclic Carbene (NHC) Palladium Complexes Synthesized from Imidazolium Salts," *Journal of the American Chemical Society,* vol. 126, pp. 5046–5047, 2004.

[58] A. M. Magill, K. J. Cavell, and B. F. Yates, "Basicity of Nucleophilic Carbenes in Aqueous and Nonaqueous SolventsTheoretical Predictions," *Journal of the American Chemical Society,* vol. 126, pp. 8717-8724, 2004.

[59] Y.-J. Kim and A. Streitwieser, "Basicity of a Stable Carbene, 1,3-Di-tert-butylimidazol-2-ylidene, in THF1," *Journal of the American Chemical Society,* vol. 124, pp. 5757-5761, 2002.

[60] A. M. Magill and B. F. Yates, "An Assessment of Theoretical Protocols for Calculation of the pKa Values of the Prototype Imidazolium Cation," *Australian Journal of Chemistry,* vol. 57, pp. 1205-1210, 2004.

[61] O. Schuster, L. Yang, H. G. Raubenheimer, and M. Albrecht, "Beyond Conventional N-Heterocyclic Carbenes: Abnormal, Remote, and Other Classes of NHC Ligands with Reduced Heteroatom Stabilization," *Chemical Reviews,* vol. 109, pp. 3445–3478, 2009.

[62] B. Eguillor, M. A. Esteruelas, M. Oliván, and M. Puerta, "Abnormal and Normal N-Heterocyclic Carbene Osmium Polyhydride Complexes Obtained by Direct Metalation of Imidazolium Salts," *Organometallics,* vol. 27, pp. 445-450, 2008.

[63] C. W. Bielawski and R. H. Grubbs, "Highly Efficient Ring-Opening Metathesis Polymerization (ROMP) Using New Ruthenium Catalysts Containing N-Heterocyclic Carbene Ligands," *Angewandte Chemie International Edition,* vol. 39, pp. 2903-2906, 2000.

[64] Y. Chauvin, "Olefin Metathesis: The Early Days (Nobel Lecture)," *Angewandte Chemie International Edition,* vol. 45, pp. 3740-3747, 2006.

[65] R. H. Grubbs, "Olefin-Metathesis Catalysts for the Preparation of Molecules and Materials (Nobel Lecture)," *Angewandte Chemie International Edition,* vol. 45, pp. 3760-3765, 2006.

[66] R. R. Schrock, "Multiple metal–carbon bonds for catalytic metathesis reactions (Nobel lecture)," *Angewandte Chemie International Edition,* vol. 45, pp. 3748-3759, 2006.

[67] A. T. Normand and K. J. Cavell, "Donor-Functionalised N-Heterocyclic Carbene Complexes of Group 9 and 10 Metals in Catalysis: Trends and Directions," *European Journal of Inorganic Chemistry,* vol. 2008, pp. 2781-2800, 2008.

[68] N. Marion and S. P. Nolan, "N-Heterocyclic carbenes in gold catalysis," *Chemical Society Reviews,* vol. 37, pp. 1776-1782, 2008.

[69] K. Chandra Mondal, S. Roy, and H. W. Roesky, "Silicon based radicals, radical ions, diradicals and diradicaloids," *Chemical Society Reviews,* vol. 45, pp. 1080-1111, 2016.

[70] C. D. Martin, M. Soleilhavoup, and G. Bertrand, "Carbene-stabilized main group radicals and radical ions," *Chemical Science,* vol. 4, pp. 3020-3030, 2013.

[71] Y. Wang and G. H. Robinson, "Carbene-stabilized main group diatomic allotropes," *Dalton Transactions,* vol. 41, pp. 337-345, 2012.

[72] D. Martin, M. Soleilhavoup, and G. Bertrand, "Stable singlet carbenes as mimics for transition metal centers," *Chemical Science,* vol. 2, pp. 389-399, 2011.

[73] E. L. Kolychev, T. Bannenberg, M. Freytag, C. G. Daniliuc, P. G. Jones, and M. Tamm, "Reactivity of a Frustrated Lewis Pair and Small-Molecule Activation by an Isolable Arduengo Carbene B{3,5-(CF3)2C6H3}3 Complex," *Chemistry – A European Journal,* vol. 18, pp. 16938-16946, 2012.

[74] D. Holschumacher, T. Bannenberg, C. G. Hrib, P. G. Jones, and M. Tamm, "Heterolytic Dihydrogen Activation by a Frustrated Carbene–Borane Lewis Pair," *Angewandte Chemie International Edition,* vol. 47, pp. 7428-7432, 2008.

[75] M. Shimizu and T. Hiyama, "Modern Synthetic Methods for Fluorine-Substituted Target Molecules," *Angewandte Chemie International Edition,* vol. 44, pp. 214-231, 2005.

[76] R. Berger, G. Resnati, P. Metrangolo, E. Weber, and J. Hulliger, "Organic fluorine compounds: a great opportunity for enhanced materials properties," *Chemical Society Reviews,* vol. 40, pp. 3496-3508, 2011.

[77] K. Reichenbacher, H. I. Suss, and J. Hulliger, "Fluorine in crystal engineering-"the little atom that could"," *Chemical Society Reviews,* vol. 34, pp. 22-30, 2005.

[78] K. O. Christe, E. C. Curtis, D. A. Dixon, H. P. A. Mercier, J. C. P. Sanders, G. J. Schrobilgen*, et al.*, "Heptacoordinated Main-Group Fluorides and Oxofluorides," in *Inorganic Fluorine Chemistry*. vol. 555, ed: American Chemical Society, 1994, pp. 66-89.

[79] K. Seppelt, "Main-Group Fluorides with Coordination Numbers Greater Than Six," in *Inorganic Fluorine Chemistry*. vol. 555, ed: American Chemical Society, 1994, pp. 56-65.

[80] J. Kvíčala, P. Mysík, and O. Paleta, "Tetrabutylammonium Butyldifluorodimethylsilicate and Difluorodimethylphenylsilicate, New Nucleophilic Fluorinating Reagents," *Synlett,* vol. 2001, pp. 0547-0549, 2001.

[81] C. B. McPake and G. Sandford, "Selective Continuous Flow Processes Using Fluorine Gas," *Organic Process Research & Development,* vol. 16, pp. 844-851, 2012.

[82] T. Liang, C. N. Neumann, and T. Ritter, "Introduction of Fluorine and Fluorine-Containing Functional Groups," *Angewandte Chemie International Edition,* vol. 52, pp. 8214-8264, 2013.

[83] C. N. Neumann and T. Ritter, "Late-Stage Fluorination: Fancy Novelty or Useful Tool?," *Angewandte Chemie International Edition,* vol. 54, pp. 3216-3221, 2015.

[84] A. Kornath, F. Neumann, and H. Oberhammer, "Tetramethylphosphonium Fluoride: “Naked” Fluoride and Phosphorane," *Inorganic Chemistry,* vol. 42, pp. 2894-2901, 2003.

[85] G. A. Olah, J. G. Shih, and G. K. S. Prakash, "Fluorine-containing reagents in organic synthesis," *Journal of Fluorine Chemistry,* vol. 33, pp. 377-396, 1986.

[86] J. H. Clark, "Fluoride ion as a base in organic synthesis," *Chemical Reviews,* vol. 80, pp. 429-452, 1980.

[87] W. J. Middleton, "New fluorinating reagents. Dialkylaminosulfur fluorides," *The Journal of Organic Chemistry,* vol. 40, pp. 574-578, 1975.

[88] G. S. Lal, G. P. Pez, R. J. Pesaresi, F. M. Prozonic, and H. Cheng, "Bis(2-methoxyethyl)aminosulfur Trifluoride: A New Broad-Spectrum Deoxofluorinating Agent with Enhanced Thermal Stability," *The Journal of Organic Chemistry,* vol. 64, pp. 7048-7054, 1999.

[89] F. Beaulieu, L.-P. Beauregard, G. Courchesne, M. Couturier, F. LaFlamme, and A. L'Heureux, "Aminodifluorosulfinium Tetrafluoroborate Salts as Stable and Crystalline Deoxofluorinating Reagents," *Organic Letters,* vol. 11, pp. 5050-5053, 2009.

[90] A. L'Heureux, F. Beaulieu, C. Bennett, D. R. Bill, S. Clayton, F. LaFlamme*, et al.*, "Aminodifluorosulfinium Salts: Selective Fluorination Reagents with Enhanced Thermal Stability and Ease of Handling," *The Journal of Organic Chemistry,* vol. 75, pp. 3401-3411, 2010.

[91] T. Umemoto, R. P. Singh, Y. Xu, and N. Saito, "Discovery of 4-tert-Butyl-2,6-dimethylphenylsulfur Trifluoride as a Deoxofluorinating Agent with High Thermal Stability as Well as Unusual Resistance to Aqueous Hydrolysis, and Its Diverse Fluorination Capabilities Including Deoxofluoro-Arylsulfinylation with High Stereoselectivity," *Journal of the American Chemical Society,* vol. 132, pp. 18199-18205, 2010.

[92] R. K. Sharma and J. L. Fry, "Instability of anhydrous tetra-n-alkylammonium fluorides," *The Journal of Organic Chemistry,* vol. 48, pp. 2112-2114, 1983.

[93] K. O. Christe, W. W. Wilson, R. D. Wilson, R. Bau, and J. A. Feng, "Syntheses, properties, and structures of anhydrous tetramethylammonium fluoride and its 1:1 adduct with trans-3-amino-2-butenenitrile," *Journal of the American Chemical Society,* vol. 112, pp. 7619-7625, 1990.

[94] R. Schwesinger, R. Link, G. Thiele, H. Rotter, D. Honert, H.-H. Limbach*, et al.*, "Stable Phosphazenium Ions in Synthesis—an Easily Accessible, Extremely Reactive "Naked" Fluoride Salt," *Angewandte Chemie International Edition,* vol. 30, pp. 1372-1375, 1991.

[95] A. R. Mahjoub, X. Zhang, and K. Seppelt, "Reactions of the "Naked" Fluoride Ion: Syntheses and Structures of SeF 62− and BrF 6−," *Chemistry – A European Journal,* vol. 1, pp. 261-265, 1995.

[96] R. Z. Gnann, R. I. Wagner, K. O. Christe, R. Bau, G. A. Olah, and W. W. Wilson, "Naked Fluoride Ion Sources: Synthesis, Characterization, and Coupling Reaction of 1-Methylhexamethylenetetramine Fluoride," *Journal of the American Chemical Society,* vol. 119, pp. 112-115, 1997.

[97] S. Bouvet, B. Pégot, J. Marrot, and E. Magnier, "Solvent free nucleophilic introduction of fluorine with [bmim][F]," *Tetrahedron Letters,* vol. 55, pp. 826-829, 2014.

[98] C. Hollingworth and V. Gouverneur, "Transition metal catalysis and nucleophilic fluorination," *Chemical Communications,* vol. 48, pp. 2929-2942, 2012.

[99] M. Gingras, "Tetrabutylammonium difluorotripheylstannate as a new anhydrous synthetic equivalent to TBAF," *Tetrahedron Letters,* vol. 32, pp. 7381-7384, 1991.

[100] W. A. Szarek, G. W. Hay, and B. Doboszewski, "Utility of tris(dimethylamino)sulphonium difluorotrimethylsilicate (TASF) for the rapid synthesis of deoxyfluoro sugars," *Journal of the Chemical Society, Chemical Communications,* pp. 663-664, 1985.

[101] H. Sun and S. G. DiMagno, "Anhydrous Tetrabutylammonium Fluoride," *Journal of the American Chemical Society,* vol. 127, pp. 2050-2051, 2005.

[102] D. W. Kim, H.-J. Jeong, S. T. Lim, and M.-H. Sohn, "Tetrabutylammonium Tetra(tert-Butyl Alcohol)-Coordinated Fluoride as a Facile Fluoride Source," *Angewandte Chemie International Edition,* vol. 47, pp. 8404-8406, 2008.

[103] P. Tang, W. Wang, and T. Ritter, "Deoxyfluorination of Phenols," *Journal of the American Chemical Society,* vol. 133, pp. 11482–11484, 2011.

[104] N. W. Goldberg, X. Shen, J. Li, and T. Ritter, "AlkylFluor: Deoxyfluorination of Alcohols," *Organic Letters,* vol. 18, pp. 6102-6104, 2016.

[105] T. Böttcher, S. Steinhauer, N. Allefeld, B. Hoge, B. Neumann, H. G. Stammler*, et al.*, "Carbene complexes of phosphorus(v) fluorides substituted with perfluoroalkyl-groups synthesized by oxidative addition. Cleavage of the complexes reveals a new synthetic protocol for ionic liquids," *Dalton Transactions,* vol. 43, pp. 2979–2987, 2014.

[106] T. Böttcher, O. Shyshkov, M. Bremer, B. S. Bassil, and G.-V. Röschenthaler, "Carbene Complexes of Phosphorus(V) Fluorides by Oxidative Addition of

2,2-Difluorobis(dialkylamines) to Phosphorus(III) Halides," *Organometallics,* vol. 31, pp. 1278–1280, 2011.

[107] T. T. Tidwell, "Wilhelm Schlenk: The Man Behind the Flask," *Angewandte Chemie International Edition,* vol. 40, pp. 331–337, 2001.

[108] M. S. (2013). *Tips and Tricks for the Lab: Air-Sensitive Techniques (1).* Available: http://www.chemistryviews.org/details/education/3728881/Tips_and_Tricks_for_the_Lab_Air-Sensitive_Techniques_1.html

[109] A. A. Danopoulos, N. Tsoureas, J. A. Wright, and M. E. Light, "N-Heterocyclic Pincer Dicarbene Complexes of Iron(II): C-2 and C-5 Metalated Carbenes on the Same Metal Center," *Organometallics,* vol. 23, pp. 166–168, 2004.

[110] A. L. Balch, V. J. Catalano, M. A. Chatfield, J. K. Nagle, M. M. Olmstead, and P. E. Reedy, "Binding of lead(II), antimony(III), and other isoelectronic main-group ions to iridium in the metallomacrocycle Ir2(CO)2Cl2{u-(Ph2PCH2)2AsPh}2," *Journal of the American Chemical Society,* vol. 113, pp. 1252–1258, 1991.

[111] S. S. Chitnis, N. Burford, and M. J. Ferguson, "2,2-Bipyridine Complexes of Antimony: Sequential Fluoride Ion Abstraction from SbF3 by Exploiting the Fluoride Ion Affinity of Me3Si+," *Angewandte Chemie International Edition,* vol. 52, pp. 2042–2045, 2013.

[112] H. Braunschweig, R. D. Dewhurst, F. Hupp, and J. Wolf, "Unprecedented Oxidative Addition and Metal-Only Lewis Pair Chemistry of Antimony Trihalides," *Chemistry – A European Journal,* vol. 21, pp. 1860–1862, 2015.

[111] J. Petrovič, B. Alič, G. Tavčar, and J. Iskra, "Evaluation of Imidazolium Fluoride Based Reagetns for Nucleophilic Fluorination of Organic Compounds," in *Cutting Edge 2017*, Ljubljana, Slovenia, 2017.